University of Nottingham
UK | CHINA | MALAYSIA

School of Veterinary Medicine & Science

Establishment of Horse blood-brain barrier model for the study of drug delivery to the brain

By Gaurav Gupta

Thesis submitted to the University of Nottingham
for the degree of Doctor of Philosophy
March, 2025

Supervisors:
Dr Stuart Paine, Professor of Veterinary Pharmacology
Dr Bob Robinson, Associate Professor of Reproductive Physiology & Pharmacology
Dr Cyril Rauch, Associate Professor of Physical Biology & Biophysics
All Faculty of Medicine & Health Sciences, University of Nottingham, UK.

Table of contents

List of figures

Chapter 1

Chapter-2

Chapter-3

Chapter-4

Chapter-5

List of tables

Chapter 2

Chapter-3

Chapter-4

Chapter-5

Abbreviations

× g	Gravity
°	Degree
µg	Microgram
µl	Microlitre
µM	Micromolar
A-B	Apical to basal
ABC	Adenosine triphosphate binding cassette
ACC	Astrocyte co-culture
ACM	Astrocyte conditioned media
ANOVA	Analysis of variance
AQP4	Aquaporin-4
ATP	Adenosine 5’-triphosphate
B2M	Beta-2-microglobulin
B-A	Basal to apical
BBB	Blood-brain barrier
BCRP	Breast cancer resistance protein
BEC	Brain endothelial cell
BMP	Basement membrane protein
BSA	Bovine serum albumin
C	Celsius
C<*t*>	Average system concentration
cAMP	3’5’-cyclic adenosine monophosphate
C_D	Concentration (donor)
CL	Clearance
cm	Centimetre
CNS	Central nervous system
CO_2	Carbon dioxide
CR	Concentration ratio
C_R	Concentration (receiver)
CSF	Cerebrospinal fluid
CYP	Cytochrome P450
Da	Daltons
DMEM	Dulbecco’s minimum essential medium

DMSO	Dimethyl sulfoxide
DNA	Deoxyribonucleic acid
ECGS	Endothelial cell growth supplement
ECM	Extracellular matrix
EDTA	Potassium ethylenediaminetetraacetic acid
EGM	Endothelial growth media
ER	Efflux ratio
EVOM	Endothelial voltmeter
FBS	Fetal bovine serum
FDA	Food & drug administration agency
FGF	Fibroblast growth factor
FITC	Fluorescein isothiocyanate
g	Gram
GDNF	Glial derived neurotrophic factor
GFAP	Glial fibrillary acidic protein
GGT	γ-glutamyl transpeptidase
HBEC	Horse brain endothelial cell
HBSS	Hank’s balanced salt solution
HUVECs	Human umbilical vein endothelial cells
Hz	Hertz
IgG	Immunoglobulin G
iPSCs	Induced pluripotent stem cells
JAM	Junctional adhesion molecule
L	Litre
LCMS/MS	Liquid chromatography- mass spectrometry/ mass spectrometry
m	Metres
M	Molar
MDCK	Madin-Darby canine kidney cells
MDR1	Multidrug resistance protein 1 (P-glycoprotein)
mg	Milligram
min	Minute
ml	Millilitre
mM	Millimolar
MRP1	Multidrug resistance-associated protein 1

MW	Molecular weight
NGS	Normal goat serum
NTC	No template control
NVU	Neurovascular unit
OATPs	Organic anion transporting polypeptides
OATs	Organic anion transporters
OCTs	Organic cation transporters
PAMPA	Parallel artificial membrane permeability assay
P_{app}	Apparent permeability
PBS	Phosphate buffered saline
PCR	Polymerase chain reaction
PET	Positron emission tomography
P_{exact}	Exact permeability
P-gp	P-glycoprotein (MDR1)
PS	Permeability surface area product
PVDF	Polyvinylidene fluoride
qPCR	Quantitative polymerase chain reaction
RMT	Receptor mediated transcytosis
RNA	Ribonucleic acid
RO-20-1734	4-(3-Butoxy-4-methoxybenzyl)-2-imidazlidinone
RPM	Revolutions per minute
RT	Room temperature
RT-PCR	Reverse transcription polymerase chain reaction
s	Seconds
SD	Standard deviation
SDS-PAGE	Sodium dodecyl sulphate polyacrylamide
SEM	Standard error of means
SEM	Scanning electron microscopy
SLC	Solute carrier
SPECT	Single photon emission computerised tomography
t	Time
TAE	Tris acetate EDTA
TEER	Transendothelial electrical resistance
T_m	Melting temperature
U	Units

UK	United Kingdom
US	United States of America
V	Volume
V_D	Volume in donor
V_R	Volume in receiver
V_U	Volume unbound
ZO	Zona occludens
Ω	Ohms

Abstract

The lack of a benchmark standard *in vitro* model of blood-brain barrier (BBB) is the principal reason behind high failure rates of central nervous system drugs in clinical trials during their development phase. In the last few decades, *in vitro* models of BBB have been developed using brain endothelial cells from various species like rat, mice, pig, and cattle However, no *in vitro* BBB model till date has been developed using horse brain endothelial cells. Hence, the main aim of this study was to establish an *in vitro* primary horse brain endothelial cell (HBEC) transwell model of BBB for determining the how much drugs are transported and handled by the BBB by measuring various pharmacokinetic parameters.

Phylogenetic analysis of multi-drug efflux molecules, evolutionary history was inferred by using the Maximum Likelihood method and JTT matrix-based model. Species having only 1:1 orthologue genes to these multi-drug efflux molecules were included. This study revealed that these molecules are phylogenetically closest to similar molecules of donkey and there the horse was divergent from other species.

The next step established and standardised a method to isolate HBECs from horse brains. Different conditions were optimised to ensure that near-pure population of HBECs were being cultured. For this, addition of 4µg/ml puromycin for first 3 days of culture yielded the highest purity. These HBECs were then characterised to confirm retention of BBB phenotype by using PCR, immunofluorescence and Western blot for various cell type biomarkers and key protein. It was determined that these HBECs had similar key features to the BBB. In addition, the application of scanning electron microscopy brought to light, for the first time, the detailed structure of cell-cell junctions in HBECs. Further characterisation revealed that the presence of astrocyte conditioned medium (ACM) and puromycin affected the expression of multi-drug efflux transporter protein, P-Glycoprotein (P-gp). Furthermore, presence of both ACM and puromycin significantly enhanced P-gp expression.

Transwell model of horse BBB was standardised for drug transport studies by culturing HBECs in presence of transport medium (in essence control) or ACM or astrocyte co-culture or in a combination of transport medium and ACM. The transwell model with ACM performed most optimally in terms of highest transendothelial electrical resistance assay (TEER) and FITC-dextran permeability assay. Drug transport studies were undertaken on this transwell model of the horse BBB. Eight drugs were selected which were substrate for three important multi-drug efflux molecules. The results of drug studies using the HBEC Transwell model did reveal that paracellular movement of drugs was likely to the main transport process taking place for several drug. This could be suggestive of leaky cell-cell junctions. This finding is also corroborated by low-to-moderate TEER values observed in these studies.

Therefore, the project has established and standardised a method for isolation and culture of primary HBECs. Also, for the first time this project has established methodology of novel transwell model of Horse BBB. Nevertheless, additional improvements will be required to establish this model as a candidate for use in drug development for central nervous system.

Covid-19 Statement

The research work for the submission of this thesis started on the 31st January, 2019. The Laboratories of School of Veterinary Medicine and Science became closed because of national Covid-19 lockdown on 13th March 2020. I was given back access to the lab in the month of September, 2020 that too on the basis of a roaster which allowed me access to the lab two days per week. This resulted in loss of 24 weeks of laboratory time. In addition to this, slaughter house remained inaccessible till January, 2021 resulting in non-availability of horse brain tissue for primary horse brain endothelial cell isolation during this period. Furthermore, to comply with social distancing laws, laboratory occupancy was tremendously restricted from September, 2020 to July 2021. In total this resulted in loss of around half of the available research hours to carry out this research project. Moreover, research work also suffered due to social distancing norms in place at Boots Building, School of Pharmacy, University Park Campus, University of Nottingham where the drug transport studies were carried out.

Numerous moderations were introduced to the project to overcome the loss of time and lack of access to laboratory facilities. Firstly, as slaughter house was not accessible till January, 2021, thought was given to buy primary horse or dog brain endothelial cells and for this various cell line agencies/companies were contacted. But primary horse brain endothelial cells were not available. Primary dog brain endothelial cells were available but they were very costly and were out of the budget of this project. So, to utilise this time Phylogenetic analysis of Drug Efflux Transporter molecules was carried out. Secondly, because of the scarcity of time left for development and standardisation of chip model of Horse blood-brain barrier, drug transport study was carried on the Transwell model of Horse blood-brain barrier. Thirdly, this Coivd-19 lockdown impacted my mental health severely. During the period of lockdown, I was diagnosed with clinical depression and delusional disorder. Since, then I am under treatment of a psychiatrist and continuously taking medications for the same.

In nut shell, the research work undertaken for the submission of this thesis has been very adversely affected by the Coivd-19 pandemic in countless ways. This resulted in the presentation of results which have been adjusted and adapted as an aftermath of the global unprecedented, unparalleled and exceptional circumstances.

Acknowledgements

I was very happy when I was got accepted for PhD by Dr. Stuart Paine. The next issue was to get a scholarship which can fund my PhD fees. I was at the top of the moon when I got selected by the Indian Council for Agricultural Research for International Fellowship. The next challenge was to shift to England for three years. Going England was like a dream come true. England is very beautiful and people are very welcoming and kind hearted.

Embarking on a PhD once looked like an impossible assignment and it is a work which I would not have been able to complete without many amazing people who have helped me during this voyage.

First of all, I would like to thank my supervisors at the University of Nottingham Dr. Stuart Paine, Dr. Bob Robinson and Dr. Cyril Rauchf or their constant academic support and feedback feedback throughout the PhD. All three of my supervisors are amazing human beings. I would also like to acknowledge the help and support provided by Chloe Whitehouse and Rakesh Jha. This PhD project would not have been possible without these excellent people.

I am also thankful to my lunch group friends at School of Veterinary Medicine and Science namely Meshach, Awatif, Adriano, Marie, Purba, Mohammed and Sophie. The time spent with you is permanently etched in my heart in golden words.

I am also thankful to my wife Bhawna, my daughter Smyra, my son Avyaan who were always there during the ups and downs of this degree. I would also like to express my gratitude to my mother, father, brother Navneet and Sister Anupam for their words of encouragement and love during this degree.

Finally, I would like to thank my funding agencies Indian Council of Agricultural Research and British Horse Racing Authority whose financial support made this degree possible.

Declaration

I declare that the work presented in this thesis was carried out in accordance with the requirements of The University of Nottingham regulations.

The work is original except as indicated by specific references in the text, and the work has not been submitted for any other academic award at The University of Nottingham or any other institutions.

Name: Gaurav Gupta

Date: 13 March, 2025

Signed: 

CHAPTER-1
INTRODUCTION

1.1 Project background

The blood brain barrier (BBB) is a physiological semipermeable and selective barrier which separates circulating blood from the brain extracellular fluid, in which the brain cells reside. It acts as both a barrier as well as having carrier functions. As a barrier, it blocks entry of many molecules and pathogens, thereby providing protection to the brain. At the same time, as carrier it facilitates the transport of important biochemicals (e.g. glucose) between blood and brain.

The BBB functions as a physical, metabolic as well as enzymatic barrier. As physical barrier, abundant tight junctions between adjacent endothelial cells prevent entry of small molecules by passive paracellular transport to brain. As chemical barrier, it has many transporter and efflux proteins which block the entry of large number of molecules to the brain. As enzymatic barrier, BBB metabolises many molecules during their transit from blood to the brain e.g. L-DOPA. Thus, the BBB has a very significant role in maintaining the homeostasis required for chemical and electrical signal communication between the neurons of the brain (Abbott, et al., 2006

So, the BBB will naturally act as a hindrance in the targeting of various brain diseases with drug therapies. There is a huge amount of research going in this field to bypass or somehow alter BBB so that therapeutic and diagnostic agents can reach brain in the required concentrations. Several approaches have been reported to bypass or alter the BBB like disrupting the BBB using osmotic solutions, using biochemical molecules like bradykinin, (Marcos-Contreras et al., 2016)(Marcos-Contreras et al., 2016)(Marcos-Contreras et al., 2016)intracerebral injections, use of nanoparticles and transporter proteins(Paris-Robidas et al., 2011; Wiley et al., 2013)(Paris-Robidas et al., 2011; Wiley et al., 2013)(Paris-Robidas et al., 2011; Wiley et al., 2013) exposure to high intensity focussed ultrasound (McDannold et al., 2008)(McDannold et al., 2008)(McDannold et al., 2008)

There are three major obstacles in the successful development of effective CNS drugs and these impediments are somewhat unique to the CNS. First

obstacle is the lack of availability of accurate *in vivo* and *in vitro* pharmacokinetic models which can mimic the blood-brain barrier (BBB) in terms of scale, architecture, cellular components and molecular physiology. Secondly, the inherent nature of the BBB which prevents therapeutic molecules from reaching the targets in the brain. Lastly, the incomplete understanding of the underlying mechanisms involved in the many CNS pathologies. Consequently, these three factors contribute to the higher failure rate of novel drugs targeting the CNS during drug development stage and clinical trials. In United States, FDA approval rates for CNS drugs is less than half in comparison to drugs targeting other body system (Pardridge, 2012)(Pardridge, 2012)(Pardridge, 2012)

The main impediment for drug's permeability into the CNS is the preventive nature of the BBB, which restricts the number of molecules that can enter the brain from blood depending on the size and structure of the molecules (Abbott et al., 2006)(Abbott et al., 2006)(Abbott et al., 2006). The BBB is mainly formed by the abundant tight junctions between the adjacent endothelial cells of blood capillaries in the brain which restricts the entry of molecules via paracellular diffusion and forces the molecules to pass through the transcellular pathway (Liu et al., 2012). In addition to restricted paracellular transport, presence of very high concentration of efflux pumps and metabolising enzymes in brain endothelial cells restricts the entry of around 98% of small molecules and 100% of all drug molecules if they do not have a transcellular transport mechanism (Pardridge, 2005). So, it is necessary for a novel drug candidate molecule to cross the BBB in the drug development process to become a successful CNS drug.

Many different *in vitro* models of BBB are used in the pharmaceutical industry which are often quite simple and cost effective (Wilhelm & Krizbai, 2014). However, the physiological relevance remains unanswered. In the recent years, many publications have demonstrated the intricate and dynamic nature of BBB which is dependent on the external signalling molecules (Abbott et al., 2006; Wang et al., 2020). This shows the importance of creating appropriate and physiologically relevant in vitro BBB models.

Like other animals horse also suffers from a range of CNS pathologies, which can be infectious (such as Trypanosomiasis, equine rabies and equine protozoal myeloencephalitis), congenital (such as juvenile epilepsy) and behavioural (such as depression (Fureix et al., 2012), anxiety (Hernández-Avalos et al., 2021) and cognitive dysfunction (Cellai et al., 2024)). In recent times, there is an increasing trend of prescribing human medicines to the horses to treat various pathologies also those related to the brain (Song et al., 2023). Most of the CNS active drugs are administered to horses by extrapolating the pharmacokinetic data available in other species, in particular, humans. Extrapolation of pharmacokinetic data between species needs prior understanding and knowledge of interspecies differences in terms drug transporters, enzyme kinetics, drug receptors which can influence the permeability and overall effect of the drug (Toutain et al., 2010). These poorly characterised inter-species differences often limit the effectiveness of human drugs used in the treatment of horse brain diseases.

Several *in vitro* BBB models of many species such as human (Stone et al., 2019), pig (Thomsen et al., 2015a)(Thomsen et al., 2015a)(Thomsen et al., 2015a), bovine (Helms & Brodin, 2014)(Helms & Brodin, 2014)(Helms & Brodin, 2014), rat (Abbott et al., 2012)(Abbott et al., 2012)(Abbott et al., 2012) and mouse (Shayan et al., 2011)(Shayan et al., 2011)(Shayan et al., 2011) have already been developed to study various aspects of physiology and pathology of BBB. However, to the best of my knowledge no *in vitro* model of horse BBB has been developed. Very few studies have been conducted on the pharmacokinetics of the CNS active drugs in horses and even these were based on costly and ethically contentious *in* vivo models of analysis (Casbeer & Knych, 2013; Grimsrud et al., 2015). Thus there is an urgent requirement for the development of *in vitro* BBB model of horse for the study of drug kinetics across the BBB. Pharmacokinetic data generated from this model will help in more rational and knowledge-driven treatment of CNS diseases of horse.In the last few decades, tissue/cellular engineering and latest microfluidic technological advances have led to the development of sophisticated and advanced microfluidic BBB-on-chip models (Modarres et al., 2018). These BBB-on-chip models could be utilised to assess the

permeability of various drugs across BBB. The biggest distinction between transwell model and BBB-on-chip model is that in BBB-on-chip model permeability of various drugs could be measured in real time by means of biosensors (Modarres et al., 2018; van der Helm et al., 2016). Contemporary advances in this discipline of BBB modelling is development of 3-dimensional printing of the chips and human induced pluripotent stem cells based BBB-on-chips (Wolff et al., 2015). Nevertheless the foremost difficulty with these models is associated to development of standardised methods and comparative assessment of results obtained from various cell types of microfluidic based BBB models (Wolff et al., 2015). Target identification, lead discovery and study of structure activity relationship, optimisation and toxicological profile is common in initial phases of drug research and during these phases static co-culture models of BBB are more utilised to study the binding affinity, transporter kinetics or signal transduction pathways (Garberg et al., 2005; He et al., 2014; Lippmann et al., 2013; Sakolish et al., 2016; Vastag & Keserű, 2009; Veszelka et al., 2011).

Though, the transwell model is not ideal for integrity studies of BBB as it does not satisfactorily represents the brain's operational and ionic conditions. Therefore, more comprehensive and physiologically relevant BBB models, like microfluidic and co-culture models are necessitated for integrity and permeability research on BBB (Hori et al., 2004; Toimela et al., 2004; Wilhelm & Krizbai, 2014). Microfluidic dynamic *in vitro* models of BBB facilitates growth of neurovascular unit cells in artificial capillary like mechanical supports (Bussolari et al., 1982; Cucullo et al., 2008). A pulsatile fluid propelling device with changeable pace delivers intraluminal flow that may be regulated to give intraluminal pressure or shear stress comparable to physiological shear stress (Bussolari et al., 1982). The component of shear stress makes this model of BBB beneficial for augmenting lead molecules in drug development studies (Cucullo, Marchi, et al., 2011). The microfluidic BBB-on-chip model have the benefits of both *in vitro* and *in vivo* models (Helms et al., 2015; Yeon et al., 2012). This model of BBB encompasses more precise measurements and geometries, subjecting the endothelium to real-time fluid flow to mimic *in vivo* conditions, facilitating BBB modelling in a

three dimensional physiological environment (Bhatia & Ingber, 2014; Booth & Kim, 2012; Griep et al., 2013; Naik & Cucullo, 2012). The other important feature of this BBB model is that it permits drug permeability testing and secondly it is has high throughput (Gomes et al., 2015; Helms et al., 2015).

The construction and surface adaptation of the micro device form the foundation of every organ-on-chip. Numerous bio harmonious raw materials are employed to construct these micro devices of which polymethyl siloxane elastomer is the most commonly used. The prediltection for polymethyl siloxane over other materials is due to its elasticity, high degree of firmness and pellucidity (Jagtiani et al., 2022). Cell cultures in BBB-on-chips are co-cultures and comprise of virtually every single variety of cell engaged in the creation and preservation of the BBB. The co-culture could be attained by seeding the brain microvascular endothelial cells and astrocytes on both side of the permeable membrane by means of flowing cell suspensions (Jagtiani et al., 2022).

The *in silico* extrapolation of BBB permeability of molecules/drugs is a cost effective, swift and high throughput screening implement. These computer tools are frequently created by means of *in vitro* and *in vivo* experimental data. Therefore, it is critical to the analytical capacity of assessments that the dataset selection method is accurate. Improved approaches have been instituted to increase the extrapolation ability of these computer based tools (Jagtiani et al., 2022).

Many innovations have taken place with BBB-on-chip like hypoxia induced BBB-on-chip (Park et al., 2019), Neonatal BBB-on-chip (Deosarkar et al., 2015) and induced pluripotent stem cell based BBB-on-chip (Workman & Svendsen, 2020). There are two main BBB-on-chip models commercially available. The two companies marketing these are Synvivo and Mimetas. These products have been used by various research studies on BBB by many researchers (Jagtiani et al., 2022).

It is clearly evident that new CNS-acting drugs are required for horses, however a common point in the pipeline, where candidate drugs fail, is due to inappropriate pharmacokinetics profile and impermeability into the brain.

This is, in part, hindered by the lack of *in vitro* BBB models in the horse. Hence, the development of a new, physiologically-relevant BBB model will help to address these challenges and this is a core component of this study.

This study thus investigated the transport of drugs which are substrates of different transporters across BBB constituted by equine brain endothelial cells using a Transwell-based culture system.

1.2 Evolution and discovery of BBB

With evolution, the nervous tissue of species kept on becoming larger and more centralised, providing them with more control over the body and limb movements and increased ability to interact with the surroundings. Larger and more centralised nervous system required a more efficient system of nutrient delivery and waste disposal. So to fulfil this requirement brain was evolved in annexation with a dense vascular system (Mastorakos & McGavern, 2019)(Mastorakos & McGavern, 2019)(Mastorakos & McGavern, 2019). As the surface area for the nutrient transport and waste clearance increased with evolution, surface area for diffusion of harmful molecules increased as well. Consequently, to decrease the exposure of harmful molecule to the brain the BBB came into existence with evolution.

The evolutionary function of blood brain barrier was to prevent the entry of pathogens into the brain. Indeed, only very few infectious agents like Group B *Streptococci, Toxoplasma gondii, Treponema pallidum* can cross the BBB (Nizet et al., 1997)(Nizet et al., 1997)(Nizet et al., 1997). If infectious agents enter the central nervous system, then this can become a very serious situation as antibodies and immune cells are not capable to penetrate the BBB and very few drugs cross BBB. The permeability of BBB will increase though during various conditions like neurological disorders like epilepsy, oedema, meningitis, brain trauma and systemic diseases like liver failure (Daneman & Prat, 2015).(Daneman & Prat, 2015).(Daneman & Prat, 2015).

It was Paul Ehrlich in 1885 who first demonstrated that there is compartmentalisation of brain (Ribatti et al., 2006).(Ribatti et al., 2006).(Ribatti et al., 2006). Ehrlich injected a dye in the bloodstream of animal and examined the distribution of dye throughout the body of the

animal. As expected the dye permeated through all the organs except the CNS. Edwin Goldman demonstrated that in 1909 that if the dye is injected in the cerebrospinal fluid (CSF) than it could permeate the brain without permeating the rest of the organs of the body (Pardridge, 1983)(Pardridge, 1983)(Pardridge, 1983). After these experiments, the concept of blood-brain barrier was recognised by the scientific world.

The BBB is present and fully functional from birth. This concept has been established after much research on the permeability of molecules with wide range of physico-chemical properties like glucose, amino acids, nucleosides, purines, choline in the neonate. All these studies showed that BBB of a new born is equally functional to adult BBB (Braun et al., 1980; Mallard et al., 2018; Schmitt et al., 2017).(Braun et al., 1980; Mallard et al., 2018; Schmitt et al., 2017).(Braun et al., 1980; Mallard et al., 2018; Schmitt et al., 2017).

1.3 Structure and function of BBB

The BBB allows entry of many lipophilic molecules such as barbiturates, gaseous molecules such as O_2, CO_2 and certain amino acids into the brain whereas it blocks the permeation of large hydrophilic molecules (> 500 Dalton). BBB allows passive diffusion of certain molecules like water whereas it actively transport certain biochemicals like glucose against the concentration gradient from blood to the brain via specific carrier molecules and transporters (e.g. GLUT1).(D. J. Begley & Brightman, 2003).(D. J. Begley & Brightman, 2003).(D. J. Begley & Brightman, 2003).

It is the endothelial cells within the BBB that are principally responsible for the barrier function. The potential difference across the membrane is reported as units of resistance (Ω) multiply by unit of surface area (cm^2) and is termed transendothelial electrical resistance (TEER) with units of $\Omega.cm^2$. TEER is the most frequently used parameter to assess the junctional grip in the brain endothelial cell monolayer (Wilhelm et al., 2011). One of the particular feature of these endothelial cells is high TEER (i.e. 300-2000 $\Omega.cm^2$) in comparison to capillary endothelial cells of other tissues (i.e. 3-33 $\Omega.cm^2$) (A. M. Butt et al., 1990; Crone & Christensen, 1981).(A. M. Butt et al., 1990; Crone & Christensen, 1981).(A. M. Butt et al., 1990; Crone &

Christensen, 1981). Indeed, high TEER reading is the most widely accepted marker of tight junction functionality in cell culture models of BBB

The BBB comprises of endothelial cells that form capillaries supplying the brain, alongside perivascular foot processes (PFPs) of astrocytes and pericytes. The PFPs surrounds the blood capillaries and pericytes are embedded inside the basement membrane (Ballabh et al., 2004)(Ballabh et al., 2004)(Ballabh et al., 2004). The most vital characteristic of BBB is the existence of tight junctions between adjacent endothelial cells with very minimal intercellular space (approx. 4Å) for paracellular transport (Daneman & Prat, 2015; Hawkins & Davis, 2005)(Daneman & Prat, 2015; Hawkins & Davis, 2005)(Daneman & Prat, 2015; Hawkins & Davis, 2005). Transmembrane proteins like occludins, claudins and junctional adhesion molecules provide the structural and functional integrity to the tight junctions. These transmembrane proteins are stitched to endothelial cells by zona occludens-1 (ZO-1) and other similar proteins (Stamatovic et al., 2008).(Stamatovic et al., 2008).(Stamatovic et al., 2008).

The main function of BBB is to control the transport of critical nutrients and waste products across the CNS and also to prevent the entry of harmful xenobiotics in the brain, so as to preserve an environment conducive for brain functioning and neuronal signalling. The BBB cardinally and primarily consists of a continuous monolayer of endothelial cells that lines the microvessels in the brain parenchyma. These endothelial cells exhibit efflux transporter proteins, metabolic enzymes and tight junction proteins. Endothelial cells and other supportive cells like perivascular astrocyte end feet processes, pericytes, neuronal processes and basement membrane together form the neurovascular unit. These supportive cells along with shear stress induce and maintain the unique characteristics of the BBB (Abbott et al., 2006).(Abbott et al., 2006).(Abbott et al., 2006).

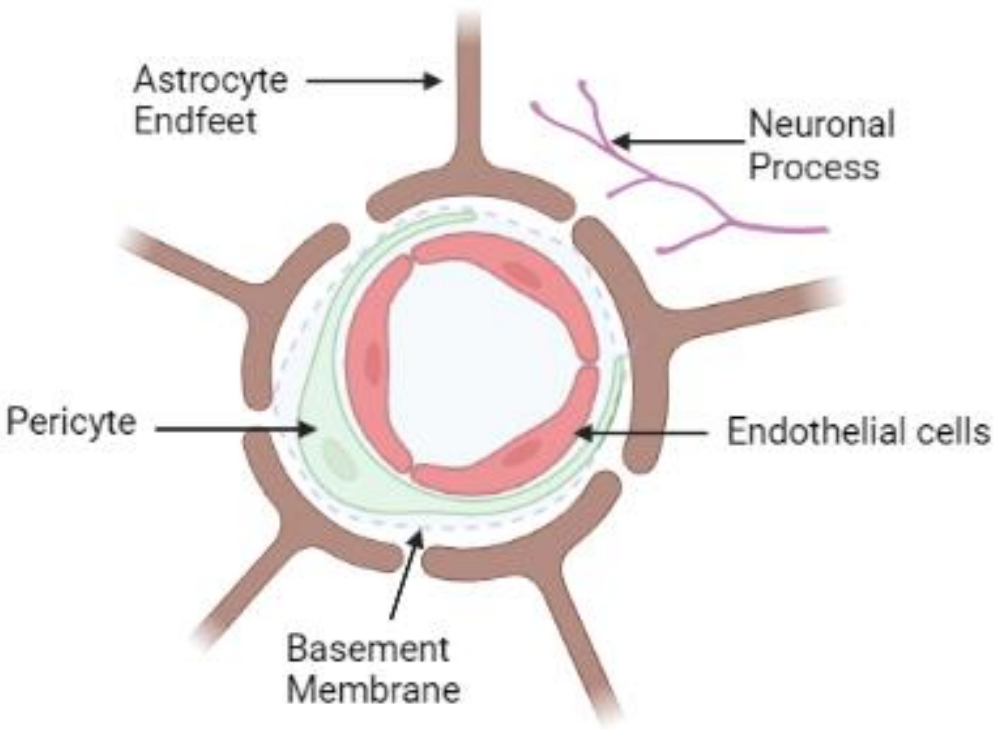

Fig. 1.1: An outline of the neurovascular unit within a cross section of a brain microvessel. The brain microvessel is composed of endothelial cells, encircled by pericytes, perivascular end feet processes of astrocytes and also in contact is neuronal processes. Basement membrane is shown by the blue dashed line. (This diagram was produced using Biorender software).

1.3.1 The neurovascular unit

Historically, it was considered that endothelial cells were the sole constituent of the functioning of BBB with some studies indicating that, astrocytic end feet processes do not contribute to the physical structure of BBB. A study in 1969 showed that horseradish peroxidase injected in brain capillaries was concentrated in the abluminal side of membrane of endothelial cells by diffusing through astrocytic end feet processes (Brightman & Reese, 1969)(Brightman & Reese, 1969)(Brightman & Reese, 1969) Similarly, using electron microscopy, it was observed that injected electron dense horseradish peroxidase was found in the endothelial cells of brain capillaries not in the astrocytic end feet processes or basement membrane of the capillaries (Reese & Karnovsky, 1967).However, later studies proved that cells other than capillary endothelial cells are also required for proper functioning of BBB.

The development, maintenance, and dynamic regulation of the BBB is regulated by multiple cellular and protein elements and signalling molecules, which act together to induce the BBB phenotype in brain endothelial cells. Brain endothelial cells and these individual supportive components together forms neurovascular unit (NVU). Astrocytes, pericytes and the basement membrane (BM) proteins are generally termed as the main supportive components of NVU and also neurons, microglia and other immune cells can also play important role in the functioning of BBB (Abbott et al., 2006). Fig. 1.1 depicts the schematic representation of the neurovascular unit components within the microvessel.

The brain endothelial cells, astrocytes and pericytes together constitute a continuous placation between blood and brain interstitial fluid and importantly these cells communicate with each other by chemical signals. In this way, they make an effectively intercalated working unit (Abbott, 2002). These chemical signals means that the different cell types are capable of altering their phenotype and thereby enabling them to adjust themselves to the altered micro-environment. These cells respond by changing the expression of tight junction proteins and by induction or expression of transporter proteins and enzymes (Abbott et al., 2006; Dauchy et al., 2008)

1.3.2 Brain capillary endothelial cells

Brain capillary endothelial cells are the principal component of the BBB. A key feature is the presence of tight junctions between adjacent endothelial cells. Transmembrane proteins (e.g. occludin and claudins) are responsible for binding the adjacent endothelial cells very closely to each other, leaving very less space for paracellular diffusion. This occurs to a greater extent in the BBB capillaries then in capillaries of other organs. Tight junction-associated proteins (e.g. ZO-1) bind the transmembrane proteins with the actin cytoskeleton of endothelial cells (Wolburg et al., 2009).

The brain endothelial cells are very rich in mitochondria both numerically as well as in terms of volume (Oldendorf et al., 1977). In contrast to other tissues, brain capillary endothelial cells have very limited capacity for transcytosis (Tuma & Hubbard, 2003). Endothelial cells permit transfer of

only a few essential molecules like albumin and low density lipoprotein by the process of transcytosis (Xiao & Gan, 2013). So, in this way these cells have enhanced barrier function which is essential for the BBB.

E-Selectin is a type of selectin cell adhesion molecule that is only expressed in endothelial cells, where it plays vital role in attracting leucocytes to an injury site. Intercellular adhesion molecule I (ICAM1) is a glycoprotein expressed by endothelial cells and assists in transmigration of leucocytes into the tissues (Yang et al., 2005). Unlike capillary endothelial cells in other organs, brain capillary endothelial cells do not express these leucocyte adhesion molecules (such as E-selectin and ICAM1) on their surface (Ransohoff & Engelhardt, 2012). So, immune cells present in blood cannot enter the brain tissue and by virtue of this, any antigen that enters into the brain will not stimulate an immune response (Muldoon et al., 2013).

There is a space between the endothelial cells of brain capillaries and brain tissue, which is called as Virchow-Robin space. This space is occupied by perivascular macrophages, which perform various immune functions (Abbott et al., 2010a).

1.3.3 Astrocytes

Astrocytes also called as astrocytic glial cells, are the most abundant glial cells in the brain. Astrocytes are star shaped and the processes of these cells make synapses with neurons and also participate in the transmission of the electrical impulses inside the brain. The end feet processes of astrocytes envelopes the brain capillary endothelial cells. The end feet processes of astrocytes perform important functions like regulating the blood-brain barrier (BBB), cerebral blood flow, nutrient uptake, and waste clearance (Díaz-Castro et al., 2023). Beyond the BBB, astrocytes also maintain the concentrations of neurotransmitters and electrolyte as well as water balance inside the brain (Wong et al., 2013). Astrocytes are not only required for development and support of barrier properties of BBB, they are also modulate the expression of transporter proteins on both the luminal and abluminal membranes of endothelial cells (Abbott, 2002; Rubin et al., 1991; Wolburg et al., 2009)

It is now recognised that astrocytes have an intricate and dynamic signalling network (Zonta et al., 2003). Calcium waves are propagated in the astrocytic network when the ionic and molecular changes occur due to neuronal signalling in the adjacent neurons (Abbott et al., 2006). Various molecules are released in response to these calcium waves at the perivascular endfeet processes. These signalling molecules include transforming growth factor β (TGF-β), glial derived neurotrophic factor (GDNF) and fibroblast growth factor 2 (FGF2) which increase and decrease the vascular permeability by controlling the expression of tight junction proteins (Cheslow & Alvarez, 2016).

The tightness of junctions of the BBB is not solely dependent on transcriptional changes, with cyclic AMP and phosphodiesterase inhibitors (i.e. RO-20-1724) resulting in the rapid and short-lived increase in the tightness of the tight junctions between brain endothelial cells. This tightness is increased by increasing the expression of tight junction protein claudin-5 via protein kinase A independent pathway (Ishizaki et al., 2003).

It is not that only astrocytes releases chemical signals which affect the functioning of brain endothelial cells. Rather the signalling between endothelial cells and astrocytes is mutual and bidirectional. For example, addition of endothelial conditioned medium resulted in altered cellular polarisation through expression of aquaporin-4 (AQP4) in a monoculture of astrocytes (Mader & Brimberg, 2019). Many studies have been conducted where addition of astrocytes or Astrocyte condition medium to a culture of brain endothelial cells resulted in change in expression of drug transporters including P-gp and GLUT1, tight junction proteins, and metabolic enzymes (Gaillard et al., 2000; Kuo & Lu, 2011; Siddharthan et al., 2007). Moreover, the presence of astrocyte conditioned media transformed leaky junctions between endothelial cells into functional tight junctions. (Abbott, 2002; Lee et al., 2003; Neuhaus et al., 1991) More recently, transformation of similar tight junction has been demonstrated using pericytes, and neurons conditioned media (Abbott et al., 2006; Nakagawa et al., 2009)

Most of the interaction between the astrocytes and endothelial cells occurs through soluble signalling molecules. Astrocyte-endothelial cell co-culture

can be mimicked by adding the astrocyte conditioned medium (ACM) to the endothelial cell monoculture, which decreased the BBB permeability in various *in vitro* studies (Nielsen et al., 2017). So, it is highly likely that the astrocytes are required for maintaining the proper phenotype and functioning of BBB.

1.3.4 Pericytes

Pericytes are the other essential component of BBB and they lie adjacent to neurons and astrocytes. In a functional BBB, the ratio of endothelial cells to pericytes is 3:1 (Shepro & Morel, 1993) Pericytes are required for both development, maturation and stabilisation of the BBB (Daneman et al., 2010). A key function of pericytes is to regulate cerebral blood flow by controlling the microvessel lumen diameter through contracting its actin filaments (Hamilton et al., 2010). Thus, unsurprisingly, the absence of pericytes adversely affects integrity of BBB as well as cerebral blood flow (Armulik et al., 2010)

Pericytes are heterogenous cell type, having a wide range of morphologies and roles in different type of tissues. All the microvessels within the brain are covered by pericytes. Brain has higher coverage of microvessel by pericytes than any other tissue in the body (Armulik et al., 2010). Pericytes and brain endothelial cells both expresses transforming growth factor-β (TGF-β) and its receptor TGFβ-R2. Activation of TGFβ-R2 receptor increased expression of tight junction proteins (Dohgu et al., 2005) demonstrating importance of pericyte-endothelial interactions.

1.3.5 Basement membrane (BM) proteins

On the abluminal (or basal) side of the endothelial cells, is the basement membrane of capillaries, which provide physical support to the endothelial cells. Basement membrane proteins), along with the interstitial matrix, form the extracellular matrix (ECM) around blood vessels in the CNS (Abbott et al., 2006). BECs, pericytes and astrocytes all contribute to the formation of the extracellular matrix, which mainly consists of structural proteins including fibronectin, heparan sulphate, laminin and collagen type IV (Zobel et al., 2016). The extracellular matrix both connects and functionally separates the

endothelial cells from the surrounding astrocytes and pericytes by acting as the interface for neurovascular signalling molecules. BM proteins can also govern gene transcription by directly interacting with the cell surface receptors (Abbott et al., 2010). Indeed, the addition of BM proteins to brain endothelial cells increases junctional adhesion and increased expression of metabolic enzymes *in vitro* (Zobel et al., 2016). Moreover, presence of ECM polarised astrocytes in vitro through altered AQP4 expression (Mader & Brimberg, 2019). Therefore, it can be considered as BM proteins are also an important component of the neurovascular unit and are required for proper functioning of BBB.

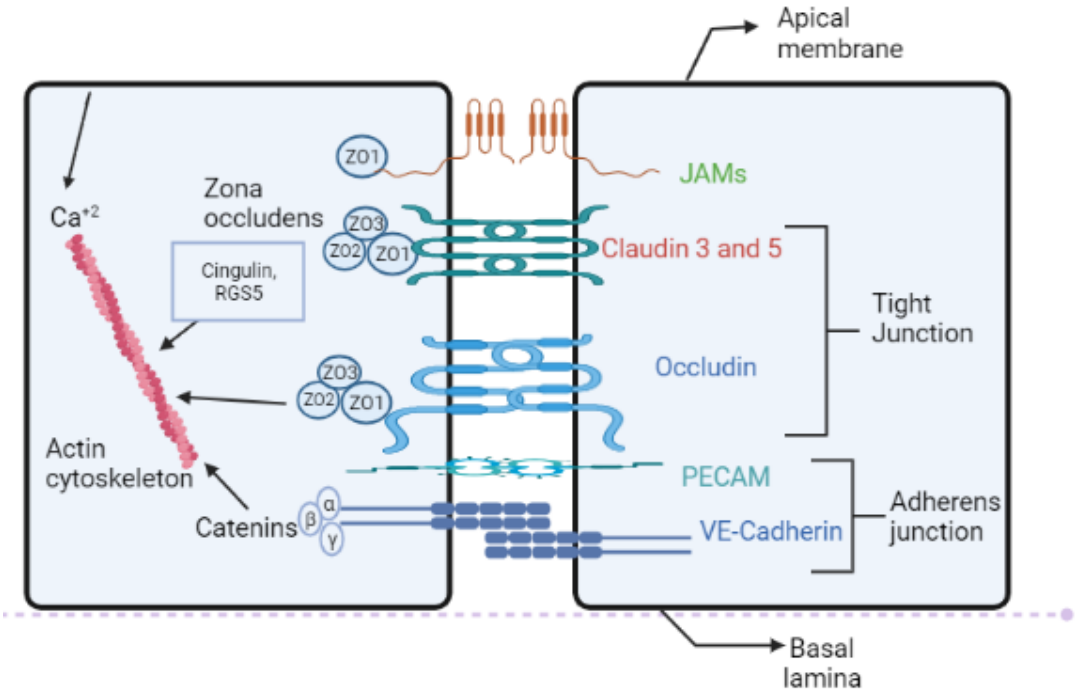

Fig. 1.2: A basic representation of the junctional adhesion proteins at the endothelial cell junctions of the blood-brain barrier. Tight junctions (claudins, occludin & JAMs) and adherens junctions (catenins, Platelet endothelial cell adhesion molecule (PECAM) & cadherins) are presented together with Zona occludens and actin cytoskeleton. The blck arrows indicate the interactions between Actin cytoskeleton and catenins, Zona occludens, Cingulin, RGS5. Also, the diagram indicates the basal lamina and the apical membrane. (This diagram was produced using Biorender software).

1.3.6 Junctional adhesion between endothelial cells

The tight junctions between the adjacent endothelial cells provides physical integrity to the BBB. These tight junctions restrict the entry of big and polarised molecules into the brain. BBB also restricts the movements of ions across the endothelial membrane, which creates the electrical potential

difference between the vascular compartment and the brain. In rats, the *in vivo* TEER values are between 1000 to 6000 $\Omega.cm^2$ (Butt et al., 1990).

There are mainly two groups of proteins that maintain junctional adhesion between adjacent brain endothelial cells namely 1) tight junctions and 2) adherens junctions. A basic representation of the junctional adhesion proteins at the endothelial cell junctions of the blood-brain barrier has been shown in Fig. 1.2.

The tight junction group of proteins comprises of claudins, occludin and junctional adhesion molecules (JAMs). Claudin proteins between adjacent endothelial cells form a primary tight junctional seal. Whereas occludin protein form heteropolymer with claudins and they have a major role in regulating tight junctions through the process of phosphorylation. All tight junction proteins namely claudins, occludin and JAMs are linked with the accessory zona occuldens proteins (i.e. ZO-1, ZO-2 and ZO-3) which connect these tight junction proteins to the actin cytoskeleton of the cell (Lochhead et al., 2020; Stamatovic et al., 2016).(Fig. 1.2)

The adherens junction of groups of protein is consists of cadherin-catenin complexes. The major adherens junction protein, VE-Cadherin binds with actin cytoskeleton within the cell through interactions with α and β catenins (Tietz & Engelhardt, 2015).

Various studies on the structure and functions of tight junctions have demonstrated that it is a highly functional and controlled structure with each of its molecular entities having specific functions. Transmembrane proteins called junctional adhesion molecule-1 (JAM1), occludin (OCLN) and claudins (CLDN) 1, 3 & 5, all form tight junctions between adjacent capillary endothelial cells in the brain. Cytoplasmic accessory proteins (e.g. zona occludens (ZO) -1 and -2, cingulin) act as a scaffold and bind these transmembrane proteins with endothelial cells. Both transmembrane proteins and cytoplasmic accessory proteins are required for structural and functional stability of tight junctions. The actin cytoskeleton of endothelial cells are cross-linked to claudins and occludins via these scaffold proteins (ZO-1, ZO-2 and cingulin) (Wolburg et al., 2009). Claudins, occludins and ZO-1 together

maintains tight junction while JAM1 increases barrier strength (Abbott et al., 2010; Bazzoni, 2006; Chen & Liu, 2012).The claudin family of proteins consist of 20 different proteins (CLDN1-20) (Mitic et al., 2000). Importantly, the loss of a single claudin isoform can result in loss of BBB integrity. For example, the loss of CLDN3 caused structural deformity of the BBB along with loss of certain barrier capabilities (Wolburg et al., 2003). While CLDN5 knockout mice have a dysfunctional BBB and a very short lifespan (Nitta et al., 2003). Not only the presence or absence of claudins and occludins can affect the integrity of the BBB but also the manner in which these proteins are interacted with each other also affects the tight junction functions of BBB (Hamm et al., 2004)

1.3.7 ATP-Binding cassette (ABC) transporters across the BBB

In vivo, many molecules exhibit much lower penetration into the brain parenchyma as would be predicted their logD value (logD is a log of partition coefficient of a chemical entity between the oil and aqueous phases (water:octanol) at a specific pH, normally pH 7.4 and indicates the lipophilicity of a molecule). The main reason for this anomaly is that, these molecules are effluxed out from the brain or the capillary endothelium by a family of transporters known as ATP-binding cassette (ABC) transporters (Begley, 2004). ABC transporters are omnipresent in all kingdoms of life (Szöllősi e.t al., 2018).

Compared to other endothelial cell types, brain endothelial cells express greater levels of ABC transporters. The principal role of ABC transporters is to protect the brain by pumping out all endogenous and exogenous lipid-soluble toxic and unwanted molecules from the brain back into the blood but at the cost of utilising ATP (Dallas et al., 2006; Locher, 2016). This means that the approach of making a drug more lipophilic to enhance its BBB penetration can be futile because the molecular changes inserted in the drug can make a more optimal substrate for ABC efflux transporters (F. Förster et al., 2008; Giri et al., 2008)

In humans, the ABC transporter superfamily has a total of 48 members and depending on the structural homology, these members are divided into 7 sub-families. (Dean, 2002) Out of these ABC transporters, the most significant to the BBB are P-gp, multidrug resistance associated proteins (ABCC1, 2, 3, 4 and 5) and BCRP (Dauchy et al., 2008; Kamiie et al., 2008) Some members of this family like ABCA1 and ABCG1 transport cholestrol and these are also expressed in the BBB. Another member, ABCA2 has some significance in drug resistance and is also expressed in brain (Dean et al., 2001).

So, functioning of ABC transporters needs to be considered when designing any BBB model, as any change in the expression level of these transporters can severely affect the drug penetration into the brain.

Among these, ABC transporters, P-gp is probably best characterised since many drugs (e.g. loperamide and colchicine) are its substrate. This transporter is expressed on the luminal side of the endothelial cell membrane and its major role is to pump out substrates from endothelial cell cytoplasm back into blood (Polli et al., 2009). The P-gp transporter activity is mainly exhibited by endothelial cells in the BBB, but some transporter activity has also been reported by pericytes (Shimizu et al., 2008) and astrocytes (Wolburg et al., 2009). It has been hypothesised that astrocytes and pericytes can serve as second line of defence in the assemble of BBB when the first line of defence (i.e. endothelial cells) is dysfunctional (REF)

P-gp was the first ABC transporter identified in brain endothelial cells (Miller, 2010). This transporter is very higly conserved across mammals and serves as an important safeguard mechanism in the CNS (Borst & Schinkel, 2013). There is report of 10-100 times accumulation of toxic compounds in the brain of P-gp knockout rodents in comparison to WT animals (Löscher & Potschka, 2005). P-gp can efflux numerous xenobiotics as it can bind with a wide range of molecules with no apparent similarity in structure (Gomez-Zepeda et al., 2020). A hypothesis named “oscillating transporter” hypothesis states that the transporter molecule fluctuates between open and closed state to randomly hold drugs and efflux them without relying much on the structure of the binding sites (Rauch, 2011). An alternative hypothesis proposes that the

structure of the substrate binding pocket of P-gp transporter keeps on changing and it allows the substrate to form its own binding site inside the substrate binding pocket of P-gp transporter (Esser et al., 2017).

Loperamide is an opioid derivative that is a gut anti-motility drug with no undesired CNS effects. As loperamide is a P-gp substrate, pharmacokinetic profile of loperamide clearly depicts the huge effect of P-gp on the permeability of drug across the CNS (Baker, 2007). PET studies have demonstrated that tariquidar (a P-gp inhibitor) when administered alongside loperamide, increased the CNS permeability of ^{11}C-N-desmethyl-loperamide. Likewise, a common scenario in opioid drug addicts in which doses of loperamide higher than the therapeutic doses causes activation of μ-opioid receptors in the brain. This happens because higher doses saturates the P-gp efflux transporters resulting in the successful permeation of the loperamide molecule in the brain (Kreisl et al., 2010). Therefore, P-gp transporter carries immense importance especially when studying pharmacokinetics of drugs across BBB. Thus P-gp is considered the main ABC transporter of interest in this project.

Breast Cancer resistance protein (BCRP) was first identified as an efflux transporter in the breast cancer cell line but now it has also been identified in BBB, placenta, intestine, liver and kidney (Miller, 2010). Although, the role of BCRP in terms of drug efflux transporter is not as defined as for P-gp but rodent gene knockout model studies have confirmed its role in permeability of many drugs (Morris et al., 2017). In addition, BCRP has some role to play in conditions like multidrug resistant cancers, epilepsy and neurodegenerative diseases (Iorio et al., 2016). BCRP can also be considered a major efflux transporter in the BBB.

Various transporters of the multidrug resistance protein family (MRPs) from MRP1 to MRP6 (ABC-C family) are expressed in mammalian brain capillaries from different species (Löscher & Potschka, 2005). Even though it is not clear that which location of brain expresses which subtype of MRP transporters, there is no doubt that ABC-C family transporters play some role in the efflux of a wide range of xenobiotics ranging from anticonvulsants to chemotherapeutics (Gomez-Zepeda et al., 2020). As various ABC drug

transporters have overlapping tissue distributions and overlapping substrates, it can be concluded that different ABC transporters work in tandem with each other to efflux a wide range of xenobiotics.

1.3.8 Solute carrier transporters

The presence of tight junctions between endothelial cells of BBB restricts the paracellular transport of water-soluble or polar molecules. This property inhibits the transport of essential molecules like amino acids and glucose which are essential for the maintenance and functioning of brain cells (Morris et al., 2017). To transport these molecules across the BBB, endothelial cells possess a large spectrum and abundance of solute carrier proteins (SLC). These SLCs are specific for solutes that they carry. Some SLCs are present only on the luminal side, some only on the abluminal side and some are present on both sides of the membrane of brain endothelial cells (Bernacki et al., 2008; Roberts et al., 2008). These transporters transport the solutes in one direction, it can be from blood to brain and *vice versa* depending on the location and orientation of the transporter.

To transport a solute totally across the BBB, the SLC is required to be present on both luminal and abluminal membranes of endothelial cells (Abbott et al., 2010b). For example, the transport of glucose across the BBB is facilitated SLC2A1 (previously know as GLUT1) transporter which is located both on luminal and abluminal side. SLC2A1 is orienated on both locations, in such a way that it tansport glucose facilitatively from blood to brain. In the same way, sodium dependent glucose transporter SLC5A1 (also known as SGLT1) is present on abluminal membrane of the endothelial cells and transports glucose from brain to the cytoplasm of endothelial cells (Begley, 2006; Dahlin et al., 2009)

The SLC superfamily has 65 families with 439 identified members, several of these play a role in the functioning of BBB (Morris et al., 2017). As ABC transporters are mainly involved in the efflux of molecules whereas the SLC transporters are mainly involved in the uptake of molecules across the membrane. Although SLC transporters can also be responsible for efflux or bidirectional transport (C. Hu et al., 2020). So, it can be concluded that SLC

transporters play an important role in the carrier mediated uptake of the drugs and efflux of certain compounds.

SLC transporter family members namely L-alpha amino acid transporters and mono carboxylate transporters transport neurotransmitter precursor compounds. The SLCO family comprises of organic anion transporters (OATs), organic anion transporting polypeptides (OATPs), and organic cation transporters. OATs and OATPs which are bidirectional transporters play important role in the efflux of CNS active drugs like bumetanide (Römermann et al., 2017).

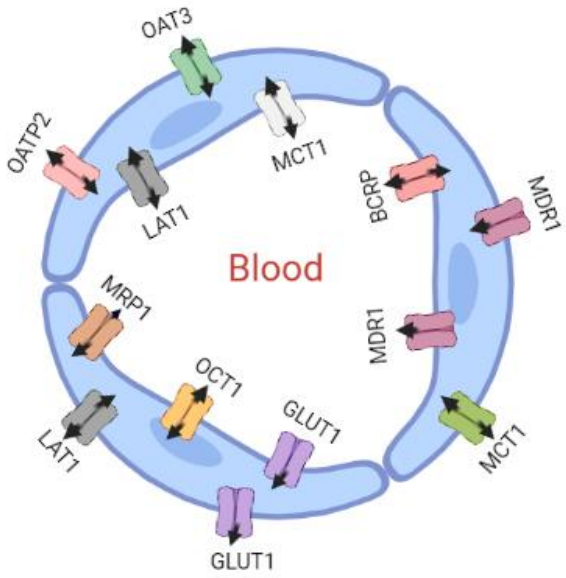

Fig. 1.3: A diagram depicting key ABC and SLC transporters expressed by brain endothelial cells, employing data from Morris et al., 2017. Key MDR1- multidrug resistance transporter 1 (P-glycoprotien, ABCB1), BCRP – breast cancer resistance protein (ABCG2), MRP1 – multidrug resistance protein 1 (ABCC1), OCT1- organic cation transporter 1 (SLC22A1), OAT3 – organic anion transporter 3 (SLC22A8), OATP2 – organic anion transporter protein 2 (SLCO1B1), LAT1 – L-alpha amino acid transporter 1 (SLC7A5), MCT1 – monocarboxylate transporter 1 (SLC161). (This diagram was produced using Biorender software).

1.3.9 Metabolic enzymes

Metabolic enzymes work in cooperation with tight junctions and efflux systems to block the entry of unwanted molecules into the brain (Decleves et al., 2011). Cytochrome P450 (CYP) enzyme superfamily play an important role in the metabolism of a wide range of endogenous compounds and xenobiotics. Most of the studies on CYPS has been performed in liver but

these enzymes are also present in non-hepatic tissues. Several studies have reported the presence of CYP enzymes in the brain micro-capillaries. Among various isoforms of CYPs, CYP1B1 and CYP2U1 isoforms are the most abundant in human brain microvasculature (Ghosh et al., 2011). Enzymes like γ-glutamyl transferase catalyzes the transfer of gamma-glutamyl functional groups from molecules such as glutathione to an acceptor that may be an amino acid, a peptide (Tate & Meister, 1985) and alkaline phosphatase hydrolyse phosphate esters, present in drug-like molecules in the BBB. In this way, several molecules are often polarised by the metabolic enzymes present in the BBB resulting in blockage of their transcellular transport across the BBB (Ghosh et al., 2010). Thus, a true representative BBB should express these efflux transporters and metabolic enzymes, as that it can fully represent the pharmacokinetics of different drugs across the BBB.

1.4 Drug transport across the BBB

Brain capillary endothelial cells are abundant in transporter proteins on both the luminal and basolateral/abluminal sides where they function as influx and/or efflux pumps. Influx pumps help transport nutrients to the brain whereas efflux pumps transport metabolic waste and unwanted molecules out of the brain into the blood for elimination. In addition to this, efflux pumps also block entry of undesired molecules in the brain by pumping these molecules back into the blood.

There are many processes by which molecules can penetrate and cross the BBB and these processes can be active or passive. There are various kinds of transporter proteins that can carry molecules across the BBB. Several macromolecules also cross BBB using the process of transcytosis. Whereas some cells cross BBB using the process of diapedesis. Trans-endothelial transport of molecules across the BBB can be divided into three main categories: passive diffusion, transcytosis and carrier mediated transport (Pardridge, 2005)

1.4.1 Passive diffusion

The movement of gases like oxygen and carbon dioxide dissolved in the blood occurs as per a concentration gradient from higher to lower concentration following the process of simple diffusion. As long as blood flow is maintained, this gradient also remain maintained and dissolved gases will continue move down their concentration gradient between blood and brain. Oxygen moves from blood to brain whereas carbon dioxide moves from brain to blood.

Lipid soluble molecules with molecular weight below 500 dalton can cross BBB passively. Factors like high polar surface area (more than 80 $Å^2$) and propensity to make more than six hydrogen bonds drastically decreases the capacity of a molecule to permeate the BBB passively (Clark, 2003). At physiological pH, molecules which are positively charged (i.e. bases) have a slightly increased capacity to cross BBB over negatively charged molecules due to their interaction with the negatively charged glycocalyx and phospholipids of the endothelial cells of BBB (Abbott et al., 2010). These same properties also apply for drug molecules (Pardridge, 2012).

Therefore, drugs that can't cross the BBB are more likely to be modified during the drug development phase by making them more lipophilic. But, in contrast, more lipophilic drugs have greater drug clearance because they can cross all biological membranes. Therefore, increased lipophilicity of drug can decreases the brain uptake because of more drug clearance (Pardridge, 2005). Moreover, any drug molecule that enters the endothelial cell for passive diffusion through transcellular pathway is subjected to efflux by the multidrug efflux transporters. The possible solution to this problem is to administer a multidrug efflux transporter inhibitor along with the main drug. So, that the main drug molecule can pass through the endothelial cell by passive diffusion without getting effluxed by the efflux transporters (Löscher & Potschka, 2005)

1.4.2 Transcytosis

The main route of entry of large molecules into CNS is transcytosis via the transendothelial pathway. In this process of transcytosis, large molecule are

engulfed in the endothelial membrane forming an intracellular vesicle, which then travels across the cytoplasm of the endothelial cell and finally adjoin the opposite membrane to then release its contents.

Larger molecules like peptides and proteins (including immunoglobulins) are generally blocked by BBB from entering into the brain but there are specific and some very specific transcytotic mechnism by which larger molecules are transported across BBB. The transcytotic mechanism consists of two general types: 1) Receptor mediated or 2) adsorptive mediated. In the case of receptor-mediated transcytosis, macromolecular ligands bind with the receptor present on the endothelial cellular surface and this binding initiates endocytosis. Both the macromolecule-receptor complex is then pinched off from the membrane, forming a vesicle which is then transported across the cytoplasm to the other side of the cell. Finally, the macomolecule is exocytosed from the other end of the cell (Sauer et al., 2005). For example, tumour necrosis factor is transported from blood to the brain through the process of receptor mediated transcytosis, although the exact identification of the receptor is still uncharecterised (Pan & Kastin, 2002). Similarly, iron-transferrin is transported from blood to the brain by receptor mediated transcytosis via binding to TfR receptor (Visser et al., 2004).

Adsorptive mediated transcytosis occurs only with positively charged molecules sufficiently charged to make the endothelial cell surface positively charged, this ionic interaction triggers a cascade of events resulting in endocytosis of the cationic macromolecule. Sequentially transcytosis occur and finally the molecule is exocytosed from the other end of the endothelial cell (Sauer et al., 2005). For example, highly positively charged molecules like the arginine-rich peptide, SynB5/pAnt-(43-58), are transported from blood to brain through non-specific and non-receptor-mediated adsorptive transcytotic process (Drin et al., 2003)

As large molecules like recombinant proteins, antibodies and gene therapies cannot enter the CNS via normal paracellular or transcellular pathway. Delivery of these molecules to CNS is possible by molecular Trojan horses. These types of large molecules when fused with Trojan horses can get access to CNS via receptor mediated transcytosis (Pardridge, 2007).

1.4.3 Carrier mediated transport (CMT)

The presence of tight junctions between endothelial cells of BBB restricts the paracellular transport of water-soluble or polar molecules. This property inhibits the transport of essential molecules like amino acids and glucose which are essential for the maintenance and functioning of brain cells. To transport these molecules across the BBB, endothelial cells possess a large spectrum and abundance of solute carrier proteins. These SLCs are specific for solutes that they carry.

Normally, SLC transporters are help in the influx of essential nutrients required by the brain but these transporters can be used to carry drug across BBB particularly if the structure of the drug mimics the nutrient (Morris et al., 2017). For example, pro-drug L-dopa and gabapentin cross the BBB with the help of LAT transporters. Likewise, OCT transporters help in the influx of lidocaine, imipramine and propranolol into the brain (Tsuji, 2005).

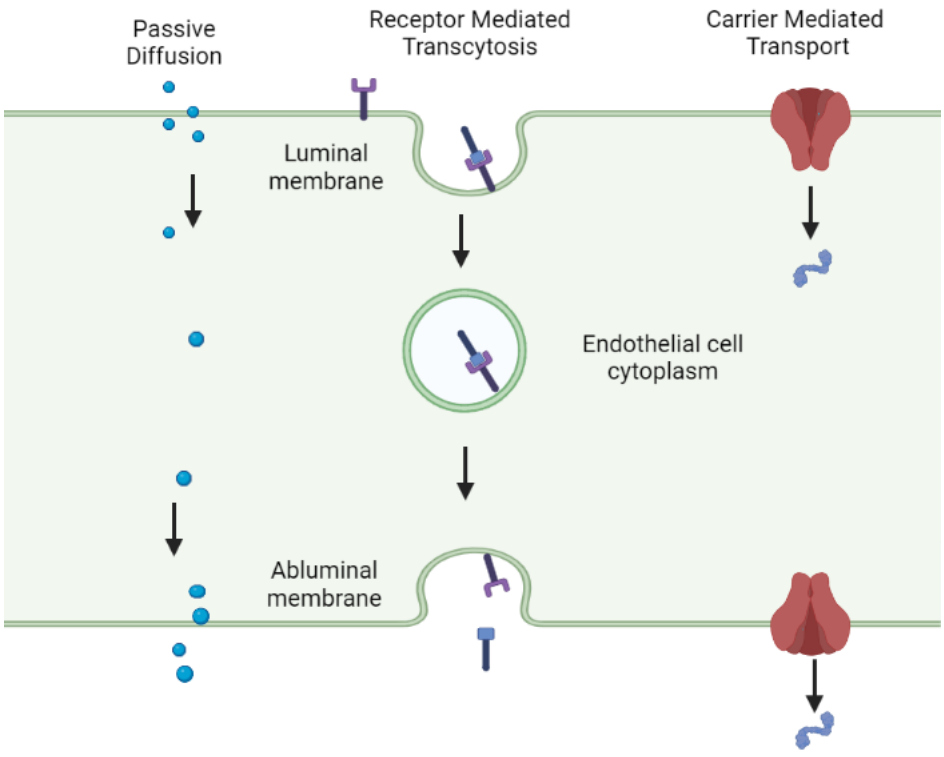

Fig. 1.4: A diagram depicting three types of drug transport across the blood-brain barrier: passive diffusion (for small lipophilic molecules), receptor mediated transcytosis (for large polar molecules), and carrier mediated transport (for small to mid-sized molecules). The diagram also specifies the luminal and abluminal membranes of the brain endothelial cells. (This diagram was produced using Biorender software).

1.4.4 Cellular movement across BBB

Mononuclear cells can reach the healthy brain from blood by the process of diapedesis via the cytoplasm of - endothelial cells and not through tight junctions or by paracellular transport (Engelhardt & Wolburg, 2004; Wolburg et al., 2005). The presence of tightly controlled BBB-immune cells interface, keep the neutrophil infiltration in brain very low as comapred to other organs (Scholz et al., 2007).

As paracellular transport is restricted at the BBB, processes like receptor and carrier mediated transport opens the door for more ways to cross the BBB. These processes can be further used and exploited to overcome the challenge of BBB permeability.

Collectively, this further strengthens the need for BBB models which exhibit all the characteristics like minimum passive perfusion, efflux pumps, SLC transporters and receptor and carrier mediated transcytosis.

1.5 Quantification of drug permeability at the BBB

Quantification of drug permeability across the BBB is required to measure the extent to which a drug can reach a target within the CNS and be freely available to bind. The most commonly used permeability values to describe drug penetration into the brain are apparent (Papp) and exact (Pexact) permeability values (Di et al., 2008; Loryan et al., 2013; Weidman et al., 2016).

1.5.1 Apparent and Exact permeability calculations

Apparent permeability (P_{app}) represents the rate of transport of a compound across the BBB. So, it shows the uptake or efflux of drugs via transporter mechanisms (Equation 1.1). But, this is only holds true when 1) drug transport is linear, 2) the total drug transported across the monolayer is less than 10% and 3) there is favourable mass balance and negligible backflow (Palumbo et al., 2008). Lately, a substitute measure of rate of drug transport has been derived which is known as P_{exact} (Equation 1.2).This measure provides a mathematical solution for the whole transport curve (Tran et al.,

2004). Moreover, P_{exact} remains accurate even when there are mass balance issues (Zhang et al., 2016).

Equation 1.1 $P_{app}\ (cm.s^{-1}) = (\Delta c/\Delta t).(V/AC_0)$

Δc/Δt = Change in receiver compartment concentration over time (mol. l^{-1}. s^{-1})

V = Volume in receiver compartment (cm^3)

A = Surface area of Transwell insert (cm^2)

C0 = Initial concentration of compound in donor compartment (mol. l^{-1})

Equation 1.2 $P_{exact} = -(V_R V_D/(V_R+V_D)At)\ln\{1-\langle C_R(t)\rangle/\langle C(t)\rangle\}$

V_D = Donor compartment volume (cm^3)

V_R = Receiver chamber volume (cm^3)

A = Surface area of the permeability barrier (cm^2)

t = Time of measurement (s)

$C_R(t)$ = Drug concentration in the receiver compartment (mol. l^{-1}) at time t

C(t)= Average system concentration of drug defined by Equation 1.3

Equation 1.3 $\langle C(t)\rangle = V_D C_D(t)+V_R C_R(t)/V_D+V_R$

$C_D(t)$ = Drug concentration in the donor compartment (mol. L-1) at time t

1.6 Current BBB models

Detailed understanding the anatomical, physiological and functional aspects of the BBB is required in the development of new CNS active drugs and also to understand various pathological conditions affecting the brain. So, in order to achieve this, various physiological models of BBB are required which can mimic the *in vivo* BBB as closely as possible and efforts to generate these *in vitro* BBB models have been in progress since early 1970s.

Assessment of drug's BBB permeability goes through high throughput *in vitro* testing during drug discovery followed by lower throughput whole system *in vivo* assays during drug development. High throughput *in vitro* assays are cost-effective, labour saving and fast but they can lack in accuracy whereas whole system *in vivo* assays demonstrate detailed analysis of pharmacodynamics and pharmacokinetic properties of the drug but these are not cost-effective and also require technical expertise. In this section the most commonly used *in vitro* and *in vivo* assays employed in the field of drug discovery and development will be discussed.

1.6.1 In vivo drug transport studies

The use of *in vivo* experiments in the pharmaceutical industry for testing the BBB permeability of new drug candidates is common (Pardridge, 2005). These *in vivo* experiments include: microdialysis, equilibrium dialysis and *in situ* perfusion. All these techniques are invasive and generally conducted in rodents to calculate BBB permeability values (Deguchi, 2002; Di & Chang, 2015). There are some non-invasive *in vivo* techniques as well like single photon computed tomography (SPECT) and positron emission tomography (PET) in which radiolabelled drugs are injected and BBB permeability is explored through dynamic scanning procedures (Bickel, 2005). *In vivo* techniques are considered as gold standard for estimation of BBB permeability as they employ tissue under physiological conditions and considered as reliable for estimating the BBB permeability of drugs that depend upon the transport mechanisms like carrier mediated transcytosis and receptor mediated transcytosis (Bickel, 2005).

Even though, *in vivo* experiments also have various drawbacks, invasive techniques require the sacrifice of the experimental animal and the data generated is species specific whereas the non-invasive technique do not allow analysis of the residual metabolites in the brain tissue (Heymans et al., 2018). The crux is that, *in vivo* experiments gives more physiologically relevant results but are low throughput, expensive, slow and require sophisticated equipment and specially trained human resource.

1.6.2 In vitro drug transport studies

There has been a large amount of advancement in the recent years in terms of development of new BBB models however still no single model is considered as the ideal model across the pharmaceutical industry (Wilhelm & Krizbai, 2014). The search for a standardised and valid BBB model is still on. But it is still considered that all currently available BBB models do not mimic the physiological *in vivo* BBB in terms of metabolic functions, transport and passive permeability (Bicker et al., 2014).

1.6.3. Non-cellular based in vitro models

These models are high throughput and cost-effective indicators of BBB permeability functions. The most commonly used non-cellular model is parallel artificial membrane permeability assay (PAMPA). This assay was first designed to assess the gastro-intestinal tract (GIT) absorption of orally administered drugs but now has been optimised for BBB permeability testing by developing PAMPA-BBB assays (Di et al., 2009). However, PAMPA assay is only capable of measuring passive diffusion of drugs through brain endothelial cell monolayer and it only measures the passive diffusion of lipophilic small molecule drugs which are not multidrug efflux transporter substrates. Likewise, PAMPA assay does not determine the permeability of drugs that are absorbed by RMT or CMT mechanisms.

1.6.4 *In silico* modelling of BBB

In silico modelling of BBB is also another non-cellular model for predicting the BBB permeability (Zhang et al., 2016). Computer based *in silico* models can build structure-activity relationships through analysis of commonalities in permeable compound structures and predict permeability depending upon the molecular weight, lipophilicity, and hydrogen bond forming ability (Wang et al., 2018). These *in silico* models are generally used in the initial phases of drug discovery process. These models can easily identify the molecules that are most probable of crossing the BBB via passive diffusion.

Although as discussed earlier, the binding of multidrug efflux transporters on the basis of structure of drug is very poorly defined. So, no *in silico* BBB

model can accurately predict whether a drug molecule would be able to permeate through the BBB or get effluxed.

These non-cell models are high throughput and cost-effective in comparison to cellular based models. But these non-cellular models cannot be used in isolation as they do not mimic the complex uptake, efflux and metabolic functions of *in vivo* BBB. Therefore, these non-cell models always require supportive data from cellular based models.

1.6.5Cellular based in vitro models

1.6.5.1 Models based on cells of non-brain origin

Initial *in vitro* BBB models were developed using endothelial or epithelial cells of non-brain origin. MDCK (Madin Darby Canine Kidney) cells were used in many initial *in vitro* BBB model studies. Although paracellular transport function of MDCK cells was similar to brain endothelial cells, there were some very major differences in the expression of junctional proteins. For example, CLDN1 is the main claudin in MDCK cells whereas in brain endothelial cells, it is CLDN5. Equally, ZO3 is main scaffold protein present in MDCK cells but is completely absent in brain endothelial cells (Nazer et al., 2008; Wang et al., 2005)

The subsequent model systems utilised human umbilical vein endothelial cells (HUVECs) as the cell source of BBB (Langford et al., 2005). The advantage of using cells of non-brain origin is that, they are more easily obtained, cultured and transfected. Some, modified versions of these cells were also developed, so that they more closely mimic brain-derived endothelial cells. However, while these models have provided some insight into the physiology and functioning of BBB but they had limited success as these models failed to mimic the brain barrier functions at molecular levels (e.g. presence of proteins like CLDN5, VE-Cadherin, Junctional adhesion molecule 1, β- and γ-catenins) and do not have brain endothelial transport functions (e.g. low permeability to inulin).

1.6.5.2 Models based on endothelial cells of brain origin

Many cell culture models have been developed by culturing brain endothelial cells alone or in combination with astrocytes and pericytes. Cultures with endothelial cells alone are called as mono-culture. However, when endothelial cells are cultured along with astrocytes and/or pericytes are called as co-culture models. If these two cell types are in physical, direct contact with each other, then it is contact co-culture otherwise non-contact co-culture. If along with endothelial cells and astrocytes, pericytes are also cultured, then this culture becomes triple co-culture which again can be contact and non-contact.

Models based on brain endothelial cells

The first significant step towards brain endothelial cell-based models was the isolation of brain capillaries (Joó & Karnushina, 1973) from which isolated endothelial cells were cultured (DeBault et al., 1979; Panula et al., 1978). Thereafter, these cells were cultured on semipermeable structures (Bowman et al., 1983). When the importance of astrocytes and pericytes in the functioning of BBB came to light, new *in vitro* models of BBB were developed in which astrocytes and/or pericytes were cultured along with brain endothelial cells (Laterra et al., 1990; Rubin et al., 1991; Tao-Cheng et al., 1987).

Primary cell culture based in vitro models

Most widely used primary brain endothelial cell cultures are from rodents (mice/rats), pigs and bovine species (Deli et al., 2005) Rodent cell-based cultures are more common in use because of their ready availability and the fact that genes and proteins in rodents are better characterised. In addition, transgenic and cloned rodent cells are also easily available. The main disadvantage with rodents is the very low yield of brain endothelial cells during isolation from each animal. This means that many animals are required to be euthanized for a single culture, which does not fulfil the 3R's remit of replace, reduce and refine. Whereas brains from pigs and cattle generate a much greater brain endothelial cell yield per animal but are less characterised at genetic and molecular levels. Use of human cells for

developing model of BBB is extremely limited because of restricted availability of human brain endothelial cells (Wilhelm et al., 2011).

Cell lines based in vitro models

The involvement of cumbersome surgical process, high costs and contentious ethical issues with the use of primary cells resulted in development of many *in vitro* models using continuous cell lines. Brain endothelial cells exhibit capability to form cell lines with minimum changes. Indeed several porcine and rodent cell lines (e.g. RBE4) can be maintained for up to 35-40 passages (DeBault et al., 1981)

The best characterised brain endothelial cell line is RBE4 which was obtained by transfecting brain endothelial cells of rats with a plasmid carrying the E1A adenovirus (Roux et al., 1994)This cell line retains many properties through passage like high alkaline phosphatase activity and gamma glutamyl transpeptidase activity (Roux et al., 1994) as well as high expression of P-glycoprotein (Regina et al., 1998) This cell line was used to study various aspects of BBB such as brain endothelial cell signalling (Fábián et al., 1998; Krizbai et al., 1995; Smith & Drewes, 2006; Y. Zhang et al., 2009), P-glycoprotein expression (Pilorget et al., 2007) and cell migration (Barakat et al., 2008)

Similarly, an immortalised rodent cell line GP8 was obtained from rat brain endothelial cells and is very commonly incorporated into *in vitro* BBB models (Greenwood et al., 1996). Pig (Neuhaus et al., 2006) and cow (Sobue et al., 1999) cell lines have also been developed but these are less frequently used as these species are less characterised at the molecular level.

The most studied human brain endothelial cell line is Hcmec/d3. This line express both typical BBB markers (e.g. CLDN5, VE-Cadherin, ZO-1, JAM-1, β- and γ-catenins) as well as transporter properties (e.g. functional expression of MDR-1, MRP-1 and BCRP; TEER < 300 $\Omega.cm^2$; paracellular tracers similar to primary brain endothelial cells (Weksler, Subileau, Perrière, Charneau, Holloway, Leveque, Tricoire-Leignel, et al., 2005). A new human cell line has been more recently developed by immortalising human brain endothelial cells with SV40-T antigen (Sano et al., 2010)which provided a

BBB model in which the morphology and physiology of endothelial cells was sustained through passages.

Co-cultures based in vitro models

It is important to recognise that other cells like astrocytes and pericytes also have a crucial role in the proper functioning of the BBB. So, *in vitro* models have been developed by co-culturing these cells and/or astrocyte-conditioned media along with brain endothelial cells (Deli et al., 2005). These studies again provide evidence that astrocytes chemical signalling is required for optimal functioning of BBB (DeBault & Cancilla, 1980). Newer models have been developed by co-culturing brain endothelial cells with astrocytes. Mostly primary cells have been used in these models but sometimes cell lines were also used. Astrocytes of G6 cell line are most commonly used cell line and have been extensively used to study gliomas (Hu et al., 2010)

In models, where both brain endothelial cells and astrocytes are from the same species, they are called as syngeneic models. Many syngeneic BBB co-culture models of rat (Veszelka et al., 2007) and mouse (Stamatovic et al., 2005) have been developed. These brain endothelial cell and astrocyte co-culture models exhibit high transendothelial electrical resistance (TEER) (500-600 Ω.cm2) reading and low permeability (Dehouck et al., 1990; Zysk et al., 2001). Similarly, bovine brain endothelial cells cultured in presence of astrocyte-conditioned media show high TEER (Rubin et al., 1991) and this is a crucial feature of any physiological BBB. More importantly, a BBB model of porcine brain with physical contact between endothelial cells and astrocytes produced high TEER values (i.e. >1000 Ω.cm2) whereas non-contact porcine BBB model of endothelial cells and astrocytes produced lower TEER values (i.e. 680 Ω .cm2) (Malina et al., 2009)

Physiologically, pericytes remain in contact with brain endothelial cells. Studies have also proved that co-culture of endothelial cells and pericytes showed high TEER in rat model (Hayashi et al., 2004) and pericytes induced expression of multidrug resistance-associated protein 6 (MRP6, an ABC transporter) in endothelial cells (Berezowski et al., 2004). In a later study,

triple co-culture of brain endothelial cells, pericytes and astrocytes also showed high TEER and low permeability (Nakagawa et al., 2009). Efforts are going on to develop human BBB co-culture models but there is limited availability of human brain tissue.

Stem cell based *in vitro* models of BBB

The stem cell originated BBB model can generate barrier properties like those present *in vivo* and is accessible source of cells. Main target of the patient specific *in vitro* models of the BBB is to ascertain fresh components so that mediators for the collapse of barrier function in neurological ailments could be determined. Genome editing methods such as CRISPR/Cas9 are expanding the kind of disease modelling prospects by propounding a process to produce pluripotent stem cells by the use of genome editing (Page et al., 2020). An isogenic human BBB model make up of Induced pluripotent stem cells originated brain microvascular endothelial cells, astrocytes and neurons was formulated. Furthermore, this co-culture give rise to continuous increase in TEER in comparison to previously developed models utilising neural cell sources as primary human neural progenitor cells and rat astrocytes (Canfield et al., 2017).

Microfluidic BBB-on-chip models

The microfluidic *in vitro BBB* models are helpful in research related to the drug permeability across the BBB. Assessment of various molecules of different molecular masses, lipophilic attributes and types of efflux transporters (Erdo & Krajcsi, 2019) has facilitated in establishment of permeability correlation of the *in vitro* data with human pharmacokinetic data. This is particularly necessary to calculate the efficacy of the drug delivery across the BBB (Boyer-Di Ponio et al., 2014; Weksler, Subileau, Perrière, Charneau, Holloway, Leveque, Tricoire-Leignel, et al., 2005).

Advances in the area of BBB modelling

There are few advances have been made in the field of BBB modelling like Neonatal BBB-on-chip (Deosarkar et al., 2015), Hypoxia induced BBB-on-chip (Park et al., 2019) and induced pluripotent stem cell (IPSC) based BBB-on-chip (Workman & Svendsen, 2020).

At present, mainly two BBB-on-chips models are available commercially. Synvivo and Mimetas are the two companies maketing them commercially. These commercially available BBB-on-chip models have been used by many researchers for different BBB research experiments (Jagtiani et al., 2022).

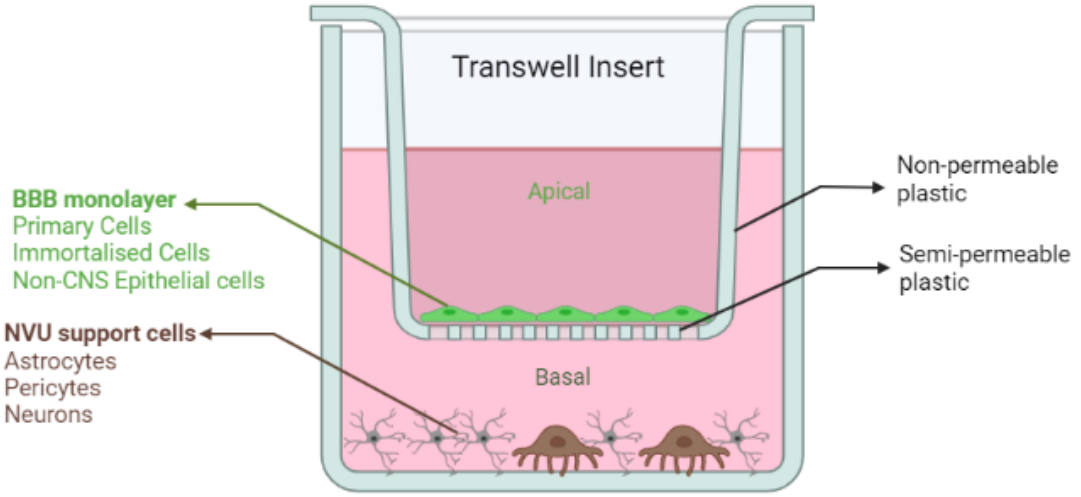

Fig. 1.5: A representation of Transwell model of BBB: the transwell insert is placed inside a multi-well culture plate and the BBB monolayer is of primary BECs, immortalised BECs, or non-CNS epithelial cells on the semi-permeable apical insert. Co-cultured neurovascular unit (NVU) cells like astrocytes, pericytes and neurons can be cultured on the bottom of the well. During transport studies, drugs are added to the apical compartment and permeability in to the basal compartment is assessed. (This diagram was produced using Biorender software).

1.7 The Transwell BBB model

One of the most commonly used cell-based *in vitro* model used for BBB research and for drug development is the Transwell model (Bicker et al., 2014). In this model, cell monolayer is suspended in a semipermeable insert inside a cell culture well. This creates two compartments apical and basal separated by a cell monolayer. Drug permeability can be quantified on this model by adding drug to the donor chamber and measuring the drug in the receiver chamber and for this the drug has to cross the monolayer of brain endothelial cells cultured over the semi-permeable insert (Oddo et al., 2019). The Transwell model of BBB is a very adaptable system as different cell types can be cultured in the apical and basal chamber of this model.

Primary brain endothelial cells have also demonstrated the expression of many uptake and efflux transporters (Nielsen et al., 2017). Nevertheless, these primary cells models are not used in the pharmaceutical industry as

these models are often not standardised for industrial use. Pharmaceutical industry mainly uses Transwell models which are based on immortalised non-CNS epithelial cells, which were created for testing the *in vitro* drug permeability across the gut (Hellinger et al., 2012)

Cell lines namely Madin-Darby canine kidney (MDCK) and Human colon adenocarcinoma (Caco-2) which were originally designed for gut permeability studies are now commonly used for BBB permeability studies (Lundquist & Renftel, 2002).

Many modifications of the cell lines have been evolved to enable high expression levels of transporters, including VB-Caco-2, a high P-gp expressing vinblastine treated Caco-2 cell line, and MDR1-MDCKII, which has increased P-gp expression (Hellinger et al., 2012). Some studies have demonstrated that these cell lines have a good resemblance with the *in vivo* BBB in terms of physiology but there are some important dissimilarities which may be due to differences with passive permeability and efflux transporter mechanism (Di et al., 2009). Another major drawback of using Transwell model with non-CNS epithelial cells is that these models can never be recognised as representative of metabolic or uptake functions of the BBB (Abbott, 2004).

Main benefit of Transwell model is that, monoculture of endothelial or epithelial cells can be easily cultured on the Transwell insert and drug permeability across the two chambers can be determined very readily. Another benefit of the transwell model is the ease with which endothelial cells can be cultured along with other supportive cells of neurovascular unit (Bicker et al., 2014). As earlier stated, astrocytes can induce BBB junctional properties through release of soluble signalling molecules. Inclusion of primary or immortalised astrocytes in non-contact co-culture with the endothelial cell type increased TEER and expression of efflux transporters (Abbott et al., 2006).

The major limitation of the Transwell model is that it lacks the component of haemodynamic flow and therefore inductive mechanical signalling pathways

from shear stress are not activated, which makes it a less representative model for the *in vivo* BBB (Cucullo et al., 2011).

Therefore, it is clear that, drug development process relies on both the labour effective and fast *in vitro* as well as costly and expertise oriented *in vivo* experiments to estimate the BBB drug permeability. But, a new generation *in vitro* model that precisely expresses tight junctions, passive diffusion, transport proteins, signalling of molecules along with remaining cost effective and easy to operate may offer a solution to this problem.

1.8 The lack of equine BBB models

Like other animals, horse also suffers from a range of CNS pathologies, which can be infectious (such as Trypanosomiasis, equine rabies and equine protozoal myeloencephalitis), congenital (such as juvenile epilepsy) and behavioural (such as depression, anxiety and cognitive dysfunction). In recent times, there is an increasing trend of prescribing human medicines to the horses to treat various pathologies especially those related to the brain. Most of the CNS active drugs are administered to horses by extrapolating the pharmacokinetic data available in other species, in particular, humans. Extrapolation of pharmacokinetic data between species needs prior understanding and knowledge of interspecies differences in terms drug transporters, enzyme kinetics, drug receptors which can influence the permeability and overall effect of the drug. These poorly characterised inter-species differences often limit the effectiveness of human drugs used in the treatment of horse brain diseases.

Several *in vitro* BBB models of many species such as human (Stone et al., 2019), pig (Thomsen et al., 2015a), bovine (Helms & Brodin, 2014), rat (Abbott et al., 2012) and mouse (Shayan et al., 2011) have already been developed to study various aspects of physiology and pathology of BBB. However, to the best of my knowledge no *in vitro* model of horse BBB has been developed. Very few studies have been conducted on the pharmacokinetics of the CNS active drugs in horses and even these were based on costly and ethically contentious *in vivo* models of analysis (Casbeer & Knych, 2013; Grimsrud et al., 2015). Thus, there is an urgent

requirement for the development of *in vitro* BBB model of horse to study drug kinetics across the BBB. Pharmacokinetic data generated from this model will help in more rational and knowledge-driven treatment of CNS diseases of horse.

1.9 Aims and hypothesis

The original aim of the project was to establish a dynamic model of Dynamic/fluidic Horse BBB on-a-chip but due to COVID-19 the aim need to be curtailed. The modified aim of the project is to establish a Transwell model of Primary Horse BBB and to study the permeability of selected test drugs across this BBB model.Transwell model is more commonly employed for studying the permeability of various drugs across the BBB because this model is adequate and optimal to study the transport kinetics of drugs and also to study the role of efflux transporters across the BBB. Secondly, to mimic the structural and physiological environment of the *in vivo* BBB, astrocytes/ACM was used during standardisation as well as during drug permability studies.

The first hypothesis of this study, was that presence of puromycin will eliminate most of the contaminating cells (i.e. astrocytes and pericytes) and a pure culture of brain capillary endothelial cells will be achieved. Also, it was hypothesised that the cultured cells will exhibit different biomarker molecules of brain capillary endothelial cells. Next, it was hypothesised that on culturing cryopreserved horse brain endothelial cells will grow in a similar manner to fresh horse brain endothelial cells. The follow-uphypotheis was that HBEC monolayer will demonstrate good barrier properties exhibited in the form of high TEER value and low permeability to the marker dye molecule i.e. FITC-dextran. For this study, a list of drugs was selected which are substrates for various multidrug efflux transporters like P-gp, BCRP and MRP1. The final hypothesis, was that these selected test drugs will be effluxed by the multidrug efflux transporters which will be reflected in the values of Apparent Permeabiltiy and Exact permeability of individual drugs

CHAPTER 2

MATERIALS AND METHODS

2.1 Materials

The sources for commonly-used reagents (Table 2.1) and equipment (Table 2.2) are below:

Table 2.1 List of frequently used reagents/chemicals

Reagent/chemical	Source	Product/ Catalogue number
Dulbecco's Modified Eagle Medium: Nutrient Mixture F-12 (DMEM/F12)	Lonza, CH	BE12-719F
Bovine Serum Albumin (BSA)	Sigma, UK	A9418
Normal Goat Serum (NGS)	Abcam, UK	Ab7481
Collagenase 2 (CLS2; 2000U/ml)	Worthington Biochemical Corporation, US	LS004176
DNase 1 (3400U/ml)	Sigma, UK	DN25
Dimethyl Sulphoxide (DMSO)	Sigma, UK	276855
Fetal Bovine Serum (FBS)	Sigma, UK	F7524
Bovine Fibronectin	Sigma, UK	F1141
Collagen from human plcenta Type IV	Sigma, UK	C5533
Antibiotic-Antimycotic solution 100x (containing penicillin (10,000U/ml), streptomycin (10mg/ml) and Amphotericin B (25µg/ml))	Sigma, UK	A5955
Heparin (15U/ml)	Sigma, UK	H3393
Puromycin	Sigma, UK	P8833
Astrocyte Conditioned Media (ACM)	Calteg Med Systems, Science Cell Research Labs	SC-1181
Endothelial cell growth supplement (ECGS)	Sigma, UK	E2759
RNAlater	Sigma, UK	R0901
Hank's Balanced Salt Solution (HBSS) (no calcium, no magnesium, no phenol red)	Corning, UK	HBS009
Fluorescein isothiocyanate dextran 4000 Da (FITC-Dextran)	Sigma, UK	46944
8-(4-chlorophenylthio) Adenosine 3' 5'-cyclic monophosphate sodium (cyclic AMP)	Sigma, UK	C3912
Hydrocortisone	Sigma, UK	H0135
RO-20-1724	Sigma, UK	557502
All other reagents used in this study were sourced from Sigma, UK unless otherwise indicated.		

Table 2.2 List of frequently used equipment

Equipment	Source	Product/ Catalogue number
Hand-held Homogeniser with Grinder Tube 100 ml (Kimble Dounce tissue grinder set)	Sigma, UK	D0189
Petri dish (90 mm diameter)	Tarsons, UK	460090
Millipore stretitop vacuum bottle top filter	Millipore, UK	S2GPT05RE
50 ml syringes	BD Medical, UK	AEC9271
50 ml tubes	Tarsons, UK	339652
0.22 µm Syringe Filter	Sartorius, UK	16532K
Culture Flask, Filtered (T-75cm^2, T-25cm^2)	ThermoFisher, UK	156499, 156367
Inverted Microscope	Leica, Germany	Leica DM IL
Digital Color Camera	Leica, Germany	Leica DFC490
Trans epithelial electrical resistance meter	World Precision Instruments, UK	EVOM2
EndOhm for 6mm culture cups	World Precision Instruments, UK	ENDOHM-6G
Corning 6.5 mm Transwell with 0.4 µm pore polyester membrane insert and plate (4 x 10^6 pores/cm$^{2)}$	Corning, US	3470
150 and 60 µm filter mesh	Plastok Associates Ltd., UK	03-150/38 and 03-60/32
1ml Cryovials	Tarsons, UK	523011
Mr. Frosty Freezing Container	ThermoFisher, UK	5100-0001

2.2 Isolation of horse brain endothelial cells (HBECs)

Total eighteen horse heads from Abattoir and three horse heads from knacker's yard were used in the present study. The animals were of the mixed gender. Isolation and culture of HBECs was performed based on methodology by Nielsen et al., 2017, but with some modifications. The skulls of healthy horses, aged 4-8 years, were collected at a commercial abattoir (F

Drury & Sons Ltd, Swindon) and transported back to SVMS on ice (approximately 3h journey). Using an oscillating saw, a square window of ~15cm × 15cm was made in the frontal bone of the skull. The anterior border of this window is hypothetical line that runs between posterior border of bony orbit and the posterior border is 2cm anterior to the nuchal crest. Lateral borders of this window are ~1cm medial to the sagittal crest. Brain was then removed and sealed in a plastic bag with 50ml ice-cold DMEM F-12 media with antibiotic-antimycotic solution and transported to the lab.

The horse brain was then washed in ice-cold PBS inside a class II biosafety cabinet and henceforth handled in an aseptic manner. All the meninges and outer blood vessels were then removed from the brain. The outer grey matter was then scraped away from the cerebrum and transferred to fresh DMEM/F-12 medium. The grey matter was then homogenised using a Dounce hand-held tissue grinder tube and pestle. The homogenised grey matter was then filtered successively through 150µm and 60µm nylon filter mesh. The blood capillary fragments that remained on the filter meshes were then transferred to 20ml of collagenase enzyme mix (containing 2000U/ml collagenase CLS2 (Worthington Biochemical Corporation, US), 3400U/ml (DNase-I and 2.5% trypsin EDTA in DMEM/F12; see appendix for details). The capillary fragments were enzymatically digested at 37^0C for 1h with gentle shaking intermittently every 10 minutes. After incubation, 1ml fetal bovine serum was added to stop the digest and followed by 10ml DMEM/F-12 prior to being transferred to a 50ml centrifuge tube. The digest was then centrifuged at 250 x g at 4ºC for 5 minutes. The supernatant was aspirated without disturbing the pellet. The cell pellet was re-suspended in fresh 10ml DMEM/F-12 medium. The process of centrifugation and resuspension was then repeated a further two times. This process of isolation of brain capillary endothelial cells has been taken from Whitehouse, 2022.

The isolated endothelial cells from a single brain were either cryopreserved or processed further for primary culture. In the case of primary culture, the final capillary pellet obtained from one horse brain was suspended in 1ml of endothelial cell growth media (ECGM) [containing 4µg/ml puromycin, 20µg/ml endothelial cell growth supplement, 1.5U/ml heparin, 10% fetal

bovine serum and 1×antibiotic-antimycotic solution in DMEM/F-12 medium; see appendix for details). From this, 160µl aliquot was plated into a fibronectin-coated well on a 12 well plate. Fibronectin coating was performed on the day prior to culture and involved adding bovine Fibronectin solution (Sigma) at 500 µl of 100µg/ml per well and the plate was placed in the CO_2 incubator at 37^0C with 5% CO_2 in air overnight.

In the case of cryopreservation for later use, the final cell pellet was re-suspended in 1ml of sterile 10% v/v DMSO in fetal bovine serum (called as freezing solution). This freezing solution containing the capillaries was then transferred to a cryovial. Cryovial was then placed in isopropyl alcohol containing freezing box at -80ºC overnight. On the next day, the cryovial was then transferred to liquid nitrogen for long term storage and subsequent usage.

2.3 Cultivation of primary horse brain endothelial cells

Day 0 (fibronectin coating)

Bovine fibronectin solution (500µl, 100µg/ml,) (Sigma) was added to each well of 12 well plate to provide a substrate for cell attachment. Uniform coverage of the well surface was ensured by tilting the plate on all sides. Plate was then placed in incubator at 37ºC overnight.

Day 1 (cell plating; day 0 of culture)

Before plating the capillaries, fibronectin solution was aspirated and each well was washed with 1ml PBS solution. The capillary pellet resuspended in ECGM was plated into a 12 well-plate such that one capillary pellet was sufficient for 6 wells of the plate. To these cells, 4µg/ml puromycin and ACM was added (optimised in Chapter 4). The cells were incubated at humidified incubator at 37^0C with 5% CO_2 in air.

Day 2 (day 1 of culture)

The media was aspirated, and cells were washed with PBS. Then, fresh ECGM with different treatments (see experimental chapter for details) were added to the cells and the plate was returned the incubator. The growth of the cells was observed under microscope every 24 hours and ECGM was

further changed every 24-48 hours depending upon the colour of the media and growth of the cells. Puromycin treatment was stopped after day 3 of the culture.

2.4 Cell Culture of HBECs from cryopreserved capillaries

Objective(s) – The objective of this experiment is to assess the viability and growth of HBEC culture obtained from cryopreserved capillaries of horse brain. An additional objective was to obtain cDNA for performing PCR for biomarker molecules of brain endothelial cells, astrocytes and pericytes. In each case, this was performed three times.

Coating flasks for primary horse brain endothelial cells

HBECs were seeded on a fibronectin-coated T-75cm^2 culture flasks. For fibronectin-coating, 10 ml of 100 µg/ml fibronectin solution was added to the flask and incubated for a minimum 4 hours to overnight at 37˚C and 5% CO_2.

Thawing and culturing isolated HBECs

For thawing the cells, cryovial was removed from the liquid nitrogen and immediately whirled in water bath kept at 37^{0}C. After the ice had completely melted, the vial was sprayed with 70% ethanol. Then, the vial was transferred the Class II cabinet and five drops (~50–60µl/drop, total 250-300µl) of pre-warmed endothelial cell growth media (Table 2.3) was added to the vial using Pasteur pipette. This suspension was then added to 10 ml of pre-warmed growth media and centrifuged at 300 ×g for 7 minutes. The supernatant was discarded, and the cell pellet was re-suspended in 10 ml of complete growth media. The suspension was added to the fibronectin-coated T-75cm^2 flask. After 24h, the spent media was removed, non-adherent cells were washed off with warm sterile PBS, and 20 ml of same endothelial cell growth media was replaced. Cells were grown to confluence for next 48 hours. Puromycin (4 µg/ml) was added for the initial 3 days to aid with culture purification, and after which media without puromycin was used.

Table 2.3 Composition of Endothelial cell growth media (ECGM) used for culturing primary horse brain endothelial cells

S. No.	Constituents	Concentration
1	Dulbecco's Modified Eagle Medium: Nutrient Mixture F-12 (DMEM/F12)	n/a
2	Endothelial cell growth supplement (ECGS)	20 µg/ml
3	Heparin	1.5 U/ml
4	Fetal bovine serum	10% (v/v)
5	Antibiotic-Antimycotic solution 100x (containing penicillin (10,000U/ml), streptomycin (10mg/ml) and Amphotericin B (25µg/ml))	1x (containing penicillin (100U/ml), streptomycin (100µg/ml) and Amphotericin B (0.25µg/ml))
6	Puromycin (for first three days only)	4 µg/ml
Puromycin concentration was standardised by initially testing puromycin at three different concentrations which are 0 µg/ml, 1 µg/ml and 4 µg/ml. The composition of endothelial cell growth media (ECGM) has been taken from Whitehouse, 2022.		

2.5 Sub-culturing of Horse brain endothelial cells

Once cells were confluent, the spent media was removed from the T-75cm^2 flask and the cells were washed twice with warm PBS. Then, pre-warmed TrypLE (20 ml) was added to the T-75cm^2 and incubated for 20 minutes at 37˚C. Next, the cells were observed under an inverted microscope to ensure that >90% of the cells were detached. The TrypLE cell suspension was then aspirated and centrifuged for 7 minutes at 300×g at 4˚C. The supernatant was discarded, and the pellet was resuspended in 3 ml of (ECGM) without puromycin (Table 2.3). This subculturing method has been taken from Whitehouse, 2022. Cells were counted using a haemocytometer and diluted in ECGM to a final concentration of 2.2 × 10^5 cells per ml before being plated on Transwell plates for permeability assay, TEER assay and drug transport studies.

2.6 Measurements of endothelial cells and capillaries

The size of the endothelial cells and capillaries were measured using calibrated Nikon NIS – Elements Image Analysis Software on the images taken under brightfield on inverted microscope (Leica, DE) with the 10x objective.

2.7 Histopathology

2.7.1 Preparation of horse brain tissue samples

A 4 cm section of horse cerebral cortex tissue was collected from the horse brain during dissection and washed in PBS in preparation for immunohistochemistry. The cerebral tissue was incubated in 4% paraformaldehyde (VWR International, US) for 48 hours, with the solution being changed after 24 hours. Once removed from the paraformaldehyde, the cerebral tissue was transferred to PBS with 30% sucrose solution for 3 days. The sample was then cut down into 2 cm × 1.5 cm × 0.5 cm blocks and loaded into sample holders and placed in a tissue processor for 16 hours (Leica, DE). The sample progressed through stages of 10% neutral buffered formalin (1 hour), through increasing concentrations of industrial methylated spirits (IMS) from 80% to 100% (6 hours in total), xylene and Histoclear (SLS, UK) (4.5 hours in total), followed by 100% molten paraffin wax (4.5 hours). After processing, the embedded tissue was sliced on a manual rotatory microtome (Leica, Germany) in 4 µm sections which were immediately submerged in a 45˚C water bath and placed on electrostatic adhesive microscope slides. Slides were left to dry for one hour before gentle heating on a hot plate to 60˚C. Sections were dewaxed in xylene twice for 2 minutes each, then rehydrated in a series of descending ethanol solutions before staining. Preparation of horse brain tissue samples for histopathology was done by Mel Hagarty, Histology Technician, School of Veterinary Medicine and Science, Univeristy of Nottingham, United Kingdom.

2.7.2 Haematoxylin and Eosin (H&E) staining of brain tissue samples

Haematoxylin and Eosin (H&E) staining was performed on brain tissue sections to identify key structures. Sections were treated with Harris's haematoxylin for 20 minutes and washed in tap water until sections were visibly blued. Sections were then submerged in 70% ethanol with 1% hydrochloric acid for 5 seconds to remove excess dye and rewashed in tap water. Sections were subsequently treated in an 1.5 % Eosin solution for 10 minutes and washed in tap water for 5 minutes. H&E-stained sections were dehydrated by submerging in Histoclear (SLS, UK), and then treated with xylene twice for 2 minutes. Following dehydration, slides were left to dry overnight in a fume hood and then mounted using Histomount (SLS, UK). Haematoxylin & Eosin staining of horse brain tissue samples was done by Mel Hagarty, Research Technician, School of Veterinary Medicine and Science, Univeristy of Nottingham.

2.8 Immunohistochemistry

Paraffin embedded brain sections (4µm) were incubated with 33% acetic acid and 67% ethanol for 10 minutes at -20˚C for fixation. Samples were incubated with 5% hydrogen peroxide (VWR International, US) in methanol for 10 minutes to block endogenous peroxidase activity. Slides were washed twice with PBS for 5 minutes, and blocked with 20% NGS in PBS and incubated at room temperature (RT) for 30 minutes. Primary antibodies were diluted in PBS with 2% NGS and 1% Triton X-100. Samples were incubated with the primary antibody overnight at 4˚C in a humidified chamber. The primary antibody was removed by washing with PBS twice for 5 minutes on a shaking plate. Biotinylated secondary antibodies (Table 2.3) were diluted in PBS with 2% NGS and incubated at RT for 60 minutes. During this time, avidin and biotin (AB) (Vector Labs, UK) were combined and incubated at RT for 30 minutes prior to incubation. The secondary antibody was removed by rinsing in PBS twice for 5 minutes. The AB complex was added to the slides and left to incubate at RT for 30 minutes. The AB complex was removed by washing twice in PBS for 5 minutes on a shaking plate. The DAB solution

(Vector Labs, UK) was added and left to develop for up to 5 minutes before rinsing in RO water for 10 minutes. Haematoxylin was added for 20 seconds to counterstain nuclei. Samples were dehydrated by incubating with 100% ethanol for 2 minutes, followed by xylene for 20 seconds, at RT and then mounted using Histomount. Staining was viewed using an upright microscope, images were captured using the attached digital camera and processed using Leica Image software.

2.9 Immunofluorescence (IF)

Horse brain endothelial cells were grown on fibronectin-coated glass coverslips (19mm) in a 12-well plate until 90% confluence was reached. Spent media was removed and cells were incubated in a 1:1 solution of acetone:methanol at 4°C for 10 minutes for fixation. Samples were incubated with 5% hydrogen peroxide in methanol for 10 minutes to block endogenous peroxidase activity. Cells were washed twice with PBS for 5 minutes on a shaking plate, and 4% Normal Goat Serum (NGS) or Normal Horse Serum (NHS) [depending on species in which secondary antibody was raised in] in PBS was added at RT and left for 30 minutes. After blocking, primary antibodies were diluted in PBS with 2% NGS (Table 2.4). For IF controls, cells were incubated with equivalent concentrations of rabbit or mouse IgG. Cells were incubated with the primary antibodies for 2 hours at RT. After incubation, the cells were rinsed by washing with PBS twice for 5 minutes on a shaking plate. Secondary antibodies (Table 2.4) were diluted in PBS with 2% NGS or NHS and incubated in the dark at RT for 1 hour. Coverslips were removed from each well using forceps and mounted upon slides using Vectashield mounting medium with DAPI counterstain (Vector Labs, UK). Samples were viewed using an upright microscope (Leica, Germany) under 10×, 40× 100× objective. Images were captured using the attached digital camera and processed using ImageJ software, version-J2, National Institutes of Health and the Laboratory for Optical and Computational Instrumentation, University of Wisconsin, USA. Blue fluorescent filter was used to detect DAPI, green for FITC and orange for Texas Red.

Table 2.4 List of Primary and Secondary antibodies used along with source and dilution used in Immunohistochemistry and Immunofluorescence

S. No.	Primary Antibody	Source	Secondary Antibody	Source
1	Rabbit anti-human ZO1 (1:100, 5.8µg/ml) [IHC] (Polyclonal)	Abcam [ab221547]	Goat anti-Rabbit IgG Peroxidase Antibody (1:1000) (Polyclonal)	Sigma [A9169]
2	Rabbit anti-human ZO1 (1:100, 5.8µg/ml) [IF] (Polyclonal)	Abcam [ab221547]	Goat anti-Rabbit IgG conjugated to Alexa Fluor 488 (1:1000, 2µg/ml) (Polyclonal)	Abcam [ab150077]
3	Mouse anti-P-gp (1:27, 2.5µg/ml) [IF] (Monoclonal)	Genetex [GTX23366]	Horse anti-mouse IgG Texas-Red (1:100, 15 µg/ml) (Polyclonal)	Vector Lab [TI-2000]
4	Mouse anti-Alpha SMA (1:800, 7µg/ml) [IF] (Monoclonal)	Sigma (A2547)	Horse anti-mouse IgG Texas-Red (1:100, 15 µg/ml) (Polyclonal)	Vector Lab [TI-2000]

2.10 Scanning electron microscopy of horse brain endothelial cells

Scanning electron microscopy (SEM) was used to assess the formation of tight junctions between HBECs in the confluent monolayer. Cells were grown to confluence on fibronectin-coated glass inserts in a 12-well cell culture plate. When cells had reached confluence, the medium was aspirated, and cell monolayers were rinsed twice with PBS. The cells were fixed in 0.1 M

sodium cacodylate buffer containing 0.1 M glutaraldehyde for 1 hour. The cells were then washed twice with sodium cacodylate buffer and dehydrated in an increasing concentration of ethanolic solutions (70%, 90%, & 100% ethanol for 30 minutes each). SEM studies were carried out by Nicola Weston at the University of Nottingham, Nanoscale, and Microscale Research Centre. In brief, the scanning electron microscope was a FEI Quanta 650 ESEM fitted with Peltier cooling stage. The sample was coated in platinum for 90 seconds at a 15-mA current and the dehydrated sample was imaged in high vacuum mode.

2.11 Western Blotting

2.11.1 Preparation of tissue and cell samples

Samples of cultured cells were collected once HBECs had reached 90% confluence by scraping cells. Cells were centrifuged and resuspended in ice-cold RIPA Lysis Buffer (Sigma, US) with protease inhibitor cocktail (Sigma, US, for use with mammalian cells [P8340]). The cell and capillary suspensions were incubated on ice for 30 minutes with occasional vortexing. Samples were centrifuged at 13,000 ×g for 10 minutes, and lysates in the supernatant were collected, aliquoted and stored at -80^{0}C. Protein concentration was determined using the Bradford assay (section 2.12.2).

Horse liver tissue (stored in -80^{0}C) sample was used for positive control in this experiment. For this, the samples (200 mg) were suspended in 1 ml of ice-cold RIPA lysis buffer with 10 µl of 100× commercial protease inhibitor (both Thermofisher, UK). Samples were homogenised using gentle MACS M-tubes in a gentle MACS Dissociator and centrifuged at 2000 ×g for 15 minutes.

2.11.2 Protein concentration determination using the Bradford assay

Protein concentration of tissue, capillary or cell samples was determined using the Bradford assay against a serial dilution of bovine serum albumin (BSA) standards (0-2000 µg/ml). BSA standards and a PBS blank were added to a 96-well plate in duplicate. Previously prepared samples were

diluted (1:10 [cells] and 1:100 [tissue]) in PBS and added to the 96-well plate in duplicate. Bradford solution (200 µl; Sigma) was added to each standard and sample well. The wells were gently mixed and left to develop for 30 minutes at RT. Absorbance was measured at 595 nm, using FLUOstar Optima, (BMG LabTech). The sample protein content was determined from the linear part of the BSA standard curve using Microsoft Excel.

2.11.3 Sodium dodecyl sulphate polyacrylamide gel electrophoresis

Protein separation by gel electrophoresis was performed using NuPAGE SDS-PAGE pre-cast 12% Bis-Tris protein gels (ThermoFisher, UK) in the SureLock XCell II electrophoresis chamber. The gels were allowed to equilibrate to RT, the comb and protective tape were removed, and the chamber was assembled. 200 ml of 1x MOPS SDS running buffer (ThermoFisher, UK) was added to the central chamber to the top of the gel. Samples were vortexed and the required volume for 6.2 µg of protein was aliquoted. The appropriate volume of SDS-lysis buffer (25 µl mercaptoethanol in 475 µl Laemmli buffer (Bio-Rad, UK)) was added to each sample such that the final volume was 24 µl. Samples used for β-Actin (house-keeping protein) detection were heated at 100˚C for 10 minutes while those used in P-gp detection were not boiled, as per manufacturers guidelines (ab170904, Abcam). Samples were loaded into the appropriate well and the gel was run at 200 Volts for 60 minutes at room temperature. A coloured protein ladder/marker was also added to one of the wells of the gel.

2.11.4 Trans-Blot Turbo protein transfer

The Bio-Rad Trans-Blot Turbo Transfer System (Bio-Rad, UK) was used for transfer of proteins from NuPAGE Gel (Invitrogen, US) to the PVDF membrane (Bio-Rad, US). The Trans-Blot Transfer System was run for 30 minutes at 25 Volts.

2.11.5 Immunoblotting

The membrane was incubated in blocking solution, 5% milk in PBS-Tween (PBS-T) for one hour on a shaking plate at 40 rpm. After blocking, the

membrane was submerged in blocking solution containing the appropriate dilution of primary antibody (Table 2.5) and incubated at 4˚C overnight. Then the membrane was washed five times in PBS-T for 10 minutes on a shaking plate at 40 rpm. Secondary antibodies were diluted in blocking solution (Table 2.5) and the membrane was incubated in the solution for 1 hour at RT with gentle agitation. The membrane was washed five times in PBS-T for 10 minutes on a shaking plate, and then rinsed twice in cold distilled water. The membrane was covered with ECL Prime (GE Healthcare, UK) for 5 minutes at RT. The membrane was drained of detection solution, wrapped in cling film, and imaged in ChemiDoc MP Imaging system (Bio-Rad, UK).

Table 2.5 Primary and Secondary antibodies (along with source and dilution) used in Immunoblotting

S.No.	Primary Antibody	Source	Secondary Antibody	Source
1	Rabbit Anti-human P-glycoprotein (1:1000) (Polyclonal)	Abcam [ab170904]	Goat anti-rabbit IgG Peroxidase (1:5000) (Polyclonal)	Sigma [A9169]
2	Rabbit Anti-human β-Actin (1:50000) (Polyclonal)	Genetex [GTX110564]	Goat anti-rabbit IgG Peroxidase (1:5000) (Polyclonal)	Sigma [A9169]

2.12 Primer designing and BLAST

Primers were designed by using the National Centre of Biotechnology Information (NCBI) website. Primer pair with lowest self-complementarity and that spanned exon-exon junctions were chosen. The product size was kept less than 200 base pair. Using the NCBI Basic Local Alignment Search Tool (BLAST) operation, primer pairs having only specific binding to the target equine gene of the intended species were chosen for this study (Table 2.6).

Table 2.6: Detail of primer pairs designed for housekeeping genes and marker of endothelial cells, astrocytes & pericytes in the horse

	Gene	Forward primer (5' to 3')	Reverse Primer (5' to 3')	Product size (bp)	Accession No.	Annealing Temperature (^{0}C)	Source
Housekeeping genes							
1	GAPDH	GTTTGTGATGGGCGTGAACC	TGCACTGTGGTCATGAGTCC	147	NM_001163856.1	60	Designed
2	β-Actin	CTTCCCTGGAGAAGAGCTACG	GGATTCCATGCCCAGGAAGG	113	NM_001081838.1	60	Designed
Endothelial cell markers							
1	ZO-1	GCGGGGACAAGATGAAGTACC	CCATTACTGTGTTCACAGCTTCC	119	XM_023651569.1	60	Designed
2	P-gp	GACTACGGCTGCCATCATCC	TGTAGGGCTGCCATTACTTGG	130	XM_014739171.2	60	Designed
3	VE-Cad	CTTGGACCGAGAGAGAACGC	TACTTGGTCTGGGTGAAGATGG	147	XM_001495895.5	60	Designed
4	BCRP	CCTCCACTGGCTGTGATACG	TGGAGAGATTCTGCGTTTCTTGG	139	XM_014738742.2	60	Designed
5	MRP1	AAAGCCAAAACTGCCTTGGG	ACCTGCCCCAACTTCTTTCC	88	NM_001081763.1	60	Designed
6	GLUT1	AGGTTTCAGCGTGGTGATCG	GAGTGTGGAGGGCAAGATGG	82	XM_005607003.3	60	Designed
7.	ZO-2	CTTCCGAGTGGTCGATACGC	GGCCATTTGTTCAGCTCTGC	118	XM_023627247.1	60	Designed
Astrocyte markers							
1	GFAP	AGACCTGCTCAATGTCAAGC	GGCTGGTTTCTCGGATCTGC	131	NM_001163861.1	60	Designed
2	Desmin	AACAATTTGGCTGCCTTCCG	AACAATTTGGCTGCCTTCCG	133	XM_001492002.6	60	Designed
3	RGS5	AGCCAGACTCTGCTATTGACC	TCATCCAGGGAGGGTTTCTGG	85	XM_001492029.5	60	Designed

4	ABCC9	TCTTTTGAAGCAACCAGAAGTAGG	GCATCTGTGACAGCTTTGTACC	143	XM_023635197.1	60	Designed
5	KCNJ8	ATGTCAGGTCTTTCACCTCTGC	TGATCAAACCCACAATGTTCTGC	138	XM_001502229.4	60	Designed
6	DLK1	GACCAATGCGTGACCTTTCC	CGGATGTCTAAGTCGCAGAGG	107	XM_005605449.2	60	Designed
7	Zic1	GCGACAAGCCCTATCTTTGC	CGTGGACCTTCATGTGTTTGC	81	XM_023621070.1	60	Designed
Pericyte markers							
1	PDGFR-beta	CAGCTACACCGACCTTGTGG	TCGGTGGACGCAATTCTTGG	82	XM_014730580.2	60	Designed
2	AAP	GCCCCTCAGAGTTCAACTACC	AGTATTCCTCCTGCTGTGTGC	75	XM_003363579.4	60	Designed
3	CSPG4	TCTTGCTGTAGCTGTATCTTTCG	GACCCAGAGACCTTTGTTCC	79	XM_005602901.3	60	Designed
4	ASMA	CAGACATCAGGGGGTGATGG	TCCCAGTTGGTGATGATGCC	126	XM_001503035.6	60	Designed
5	CD146	AGATAAACTCCCAGAAGAGATGGG	TTCTCTCCCTGGCTCTACCG	134	XM_023644990.1	60	Designed

GAPDH is glyceraldehyde 3-phosphate dehydrogenase; ZO-1 is zona occludens-1; P-gp is P-Glycoprotein; VE-Cad is vascular endothelial cadherin; BCRP is breast cancer resistance protein; MRP1 is multidrug resistance protein 1; GFAP is glial fibrillary acidic protein; RGS5 is regulator Of G protein signaling 5; ABCC9 is ATP binding cassette subfamily C member 9; KCNJ8 is potassium voltage-gated channel subfamily J member 8; DLK1 is delta like non-canonical notch ligand 1; Zic1 is zinc finger protein of cerebellum 1; AAP is alanyl aminopeptidase; CSPG4 is chondroitin sulphate proteoglycan-4; ASMA is alpha smooth muscle actin; CD146 is cluster of differentiation 146.

NB. Desmin is marker for both astrocytes and pericytes.

2.13 Polymerase Chain reaction (PCR)

1) Samples of horse brain (100mg from cerebral cortex) were collected during dissection and placed into RNAlater. Tissue was homogenised in a 1.5ml microcentrifuge tube using hand held micropestle and then centrifuged at 2000 ×g for 15 minutes.
2) Samples of horse brain endothelial cells were collected once the cells had reached confluence. Spent media was removed and replaced with ice-cold PBS; cells were removed from the bottom of the well using cell scrapper. The cell suspension was aspirated from the wells and transferred into a 1.5 ml Eppendorf tube for RNA isolation.

2.13.1 RNA Isolation

RNA was isolated using the NucleoSpin RNA kit (Machery-Nagel, Germany). In brief, cells were suspended in 1:10 β-mercaptoethanol: lysis buffer, and further homogenised using an Eppendorf micropestle. The lysate was filtered through a NucleoSpin filter tube by centrifugation at 11,000 ×g for 1 minute. Following filtration, 350µl of 70% ethanol was added and the sample was centrifuged at 11,000 ×g for 30 seconds. The silica membrane was desalted through the addition of 350 µl of membrane desalting buffer, and the samples were centrifuged at 11,000 ×g for 1 minute. DNA was digested through addition of 95µl of DNase reaction mix, which was incubated at RT for 15 minutes. The silica membrane was washed three times: firstly using 200µl of RAW2 and centrifuged at 11,000 ×g for 30 seconds, followed by a wash with 600µl of RA3 and centrifugation in the same conditions, and finally using 250µl of RA3 and centrifugation at 11,000 ×g for 2 minutes. The purified RNA was extracted by suspension in 30 µl of RNase-free water and centrifugation at 11,000 ×g for 1 minute.

2.13.2 Synthesis of cDNA

The RNA concentration and the A260:A280 ratio of the samples were quantified using a Nanodrop (ThermoFisher NanoDrop 8000). Samples were used for amplification if the A260:A280 ratio exceeded 1.8. Once quantified, 1 µg of RNA was added to a PCR tube with 1µl of Oligo (DT) 12-18 primer (Thermofisher, UK) and 1µl of deoxynucleotide mix (New England Biolabs,

UK). The volume for each sample was made up to 13µl with RNase-free water. The samples were heated in the Thermocycler (Life Touch, BioER) at 65˚C for 5 minutes and incubated on ice for 1 minute. Samples were centrifuged briefly, and 4µl of 5× first strand buffer, 1µl of 0.1M dithiothreitol, 1 µl of RNaseOUT Recombinant Ribonuclease Inhibitor and 1µl of SuperScript III reverse transcriptase were added (all reagents from ThermoFisher, UK). Samples were mixed thoroughly, incubated at 50˚C for 60 minutes and inactivated by heating to 70˚C for 15 minutes in the thermocycler.

2.13.3 Amplification

Amplification involved adding approximately 10ng of cDNA (calculated relative to the RNA concentration) to a PCR tube with 10µl of REDTaq ReadyMix PCR Reaction Mix, 1 µl of both forward and reverse primers (Table 2.6), and up to 7µl of RNase-free water (Table 2.7). No template control samples were made up by replacing the sample with 1 µl of RNase-free water. Samples were vortexed and amplified in the Thermocycler for 2 minutes at 94˚C, followed by 40 cycles of 94˚C for 30 seconds, 60˚C for 30 seconds (Table 2.7), and 72˚C for 2 minutes. Finally, samples were heated to 72˚C for 5 minutes and then remain on hold at 4^0C.

Table 2.7: Composition of the PCR reaction mixture for expression analysis of biomarker and transporter proteins of Horse brain endothelial cells

Reagent	**Volume**
Nuclease free water	Upto 7µl
Jumpstart REDTaq PCR master mix	10µl
Forward primer (10 nM)	1µl
Reverse primer (10 nM)	1µl
cDNA (approx. 10 ng reverse transcribed from RNA)	-
Total volume	20µl

2.13.4 Gel Electrophoresis

To make the gel, 2 g of Agarose was mixed with 100ml of 1x Tris Acetate-EDTA (TAE) buffer and heated until the agarose was fully dissolved. When slightly cooled, 3µl of ethidium bromide (ThermoFisher, UK) was added. The 2% agarose gel was placed in a gel electrophoresis tank filled with TAE buffer. The gel combs were removed and 3µl of 50 base pair DNA ladder (New England Biolabs, UK) was loaded into the first well, followed by 8µl of each PCR sample and negative control into subsequent wells. The gel was run at 100 Volts for 70 minutes. The bands of the amplified DNA were observed and photographed under UV light in Gel Documentation system (Chemi Doc^{TM} MP Imaging system, Bio-Rad Laboratories, USA).

2.14 TaqMan Reverse transcription polymerase chain reaction

Reverse transcription polymerase chain reaction was performed using TaqMan Gene Expression Assays (Applied Biosystems, UK). Predesigned primers and probes were procured ThermoFisher Scientific for P-Glycoprotein, GAPDH and β-Actin. Sample preparation, RNA isolation and cDNA synthesis was undertaken as described in section 2.14. TaqMan Gene Expression Assays were used for P-gp (ABCB1) (Ec03470342_m1,), alongside GAPDH (Ec03210916_gH,) and β-Actin (Ec04176172_gH) as the endogenous control assays. Amplification efficiency of these genes with predesigned primers and probes were tested by taking a pooled sample of cDNA to make serial 10-fold dilution from 1:10 to 1:100000. The TaqMan gene expression assays were thawed and resuspended by vortexing. For accuracy, 3 replicates of each cDNA sample were used per gene expression assay and a no template control was used for each gene. Each PCR reaction mix was prepared to 20µl total volume in a RNase-free PCR tube using 1 µl TaqMan Gene Expression Assay (20X), 10µl TaqMan gene expression assay master mix (4369016, ThermoFisher), 10 ng cDNA from samples, and 5µl of RNase-free water. Each reaction was vortexed and centrifuged briefly before samples were transferred to a 96-well real time PCR plate (Bio-Rad, UK). The PCR plate was centrifuged briefly before being loaded into the real time PCR machine (CFX Connect Real Time PCR System, Bio-Rad). The thermal

cycling conditions were as follows: hold at 50°C for 2 minutes, initial denaturation at 95°C for 2 minutes, before 40 subsequent cycles of 95°C for 3 seconds (Denaturation) and 60°C degrees for 30 seconds (Annealing/Extension). Real time PCR data was analysed using Bio-Rad CFX Maestro software. Delta-Delta Ct method (Livak and Schmittgen, 2001) was used to calculate the fold expression change of P-Glycoprotein.

2.15 Assessment of γ-glutamyl transferase activity

HBECs were grown on a fibronectin-coated 96-well plate (45µl of 100µg/ml fibronectin per well). When cells had reached confluence, cell medium was removed, and monolayers were washed twice in warm PBS. Following the washes, 275µl of 0.1 M Tris-HCl buffer containing 20mM glycylglycine and 1mM L-γ-glutamyl-p-nitroanilide was added to each well. The plate was incubated at 37°C in 5% CO_2 for 40 minutes. The reaction was stopped with the addition of 55µl of 1 N NaOH per well. The amount of p-nitroanilide product formed was measured spectrophotometrically using a plate reader (FLUOstar Omega, BMG Labtech) at 410 nm against a calibrated standard curve of known p-nitroanilide concentrations. Enzyme activity was calculated using Equation 2.1, where *B* is the concentration of p-nitroanilide generated between Tinitial (0 minutes) and Tfinal (40 minutes), *T* is the total reaction time, and *V* is the sample volume of the well.

Equation 2.1

$$\gamma\text{-}glutamyl\ transferase\ activity = (B \times dilution\ factor)/(T \times V)$$

The value for enzyme activity was normalised to the total cell protein (mg), which was calculated using a Bradford assay

2.16 Modelling the BBB

2.16.1 Transwell Monoculture of horse brain endothelial cells

Horse brain endothelial cells were cultured in T75 flasks until 80-90% confluent. This confluency was chosen as the maximum number of cells that could be used without contact inhibition being a detrimental factor in future growth. Transwell inserts (24-well plate, 6 mm diameter, Corning, US) were coated with fibronectin (100 µg/ml; 100 µl per insert) and collagen IV (500

µg/ml; 100 µl per insert) in PBS. Cells were passaged according to methodology detailed in Section 2.3. The coating solution was removed from the Transwell inserts and 250µl of cell suspension (containing 2.2×10^5 cells) was added to each insert. Then, 750µl of endothelial cell growth media (ECGM) without puromycin was added to the bottom compartment of the Transwell. Cell media was replaced with fresh ECGM after 24 hours.

After 48 hours, the cells were typically 100% confluent, cell medium was changed in both compartments to transport medium (Table 2.8). The media within the Transwell insert was refreshed every 48 hours subsequently, or 3 hours before every TEER measurement.

Table 2.8: Constituents of transport media (TM) constituents for Transwell insert culture

Constituent	**Concentration**
Dulbecco's Modified Eagle Medium: Nutrient Mixture F-12 (DMEM/F12)	N/A
Fetal bovine serum	10% (v/v)
Heparin	1.5 U/ml
Antibiotic-Antimycotic solution 100x (containing penicillin (10,000U/ml), streptomycin (10mg/ml) and Amphotericin B (25µg/ml))	1x
8-(4-chlorophenylthio) Adenosine 3' 5'-cyclic monophosphate sodium (Cyclic AMP analogue)	250 µM
Hydrocortisone	550 µM
RO 20-1724	17.5 µM

The composition of transport media has been taken from (Whitehouse, 2022). cAMP analogue was added to increase the BBB tightness by increasing the formation and function of tight junctions between endothelial cells, mainly be controlling the expression and localisation of tight junctions protein like claudin-5. Claudin-5 is vital for maintenance of BBB integrity (Ishizaki et al., 2003). Hydrocortisone increases BBB tightness by upregulating the expression of tight junction proteins, mainly occludin (Schrot et al., 2005). RO 20-1724 is a cell permeable selective inhibitor of cAMP specific phosphodiesterase. This phosphodiesterase causes destruction of cAMP. Therefore, cAMP, hydrocortisone and RO 20-1724 were added to the transport media to increase the BBB tightness.

2.16.2 Horse brain endothelial cell co-culture with astrocytes on Transwell inserts

The immortalised rat astrocyte cell line, CTX-TNA2, was purchased from the European Collection of Authenticated Cell Cultures (ECACC, UK). The ECACC guidelines were followed for the culture of astrocytes, with cells cultured on fibronectin (5 µg/cm^2) coated cell culture flasks. Media was DMEM with L-glutamine and sodium pyruvate (Lonza, Switzerland), supplemented with 10% FBS. Cells were at passage number 6 upon receipt from ECACC and were subsequently passaged when cells reached 70-80% confluence and were used until passage number 14.

Astrocytes were passaged onto the bottom of the Transwell plates 24 hours prior to the end point assay or start of TEER measurements, as indicated in Fig. 2.1 Astrocytes were passaged according to the methodology for horse brain endothelial cells (Section 2.5), and 0.5 × 10^4 cells/cm^2 (0.95 x 10^4 per bottom) were plated in each bottom of the 24-well Transwell plate. During non-contact co-culture, the spent astrocyte media was changed every 48 hours.

HBEC co-culture with astrocyte conditioned media (ACM)

As per Section 2.17.1, spent medium was removed and collected from CTX-TNA2 astrocyte culture, after 48 hours in culture. This was stored as ACM at -20°C for a maximum of 1 month before use. During Transwell culture of HBECs which were subjected to ACM treatment, ACM was thawed, and cAMP, hydrocortisone, and RO 20-1724 were added as for transport media (Table 2.8). For ACM treated Transwells, the transport media in the bottom half of the Transwell was replaced with fresh ACM every 48 hours.

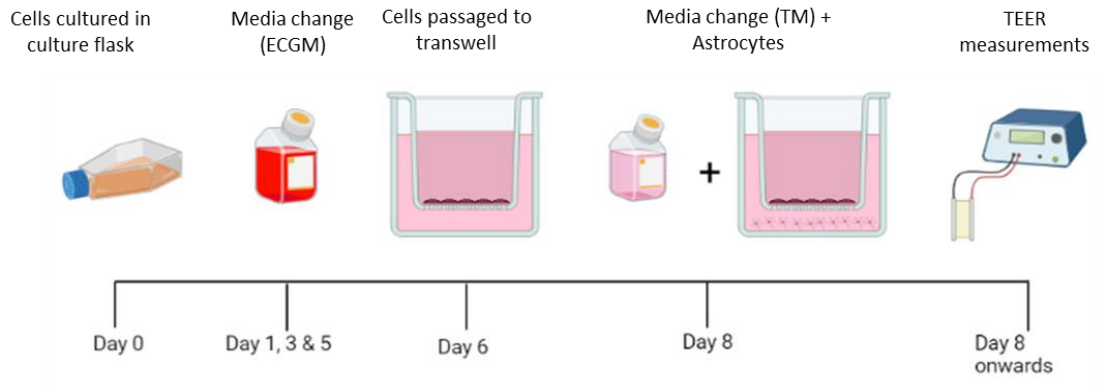

Fig. 2.1: Illustration of timeline for seeding of HBECs on the Transwell inserts. ECGM: endothelial cell growth medium (Table 2.3), and TM: transport media (Table 2.8). TEER: transendothelial electrical resistance. (This diagram was produced using Biorender software).

2.17 TEER measurements in Transwell culture

HBECs were cultured and passaged onto Transwell inserts (Section 2.17.1). Prior to TEER measurements being recorded, the media in the Transwell inserts was changed and replaced with fresh transport media (Table 2.8). Cells were re-incubated for 3 hours to recover from the media change. TEER was measured using a 6mm Cell Culture Cup Chamber and EVOM2 Epithelial Volt/Ohm Meter. The cup electrode was sterilised using 70% ethanol and equilibrated for 30 minutes in 4ml of pre-warmed DMEM/F12 before use. TEER values were measured by placing each insert into the electrode cup (containing 3ml of fresh warm DMEM/F12) and measuring resistance in triplicate. The resistance of a no-cell control was obtained in triplicate as reference for the resistance of the Transwell insert per se.

The average of triplicates were used to calculate resistance values, after subtracting the baseline resistance values from the inserts. TEER was calculated by multiplying the resistance of the monolayer by the surface area of the membrane (0.33 cm^2).

2.18 FITC-Dextran permeability measurements in Transwell culture

HBECs were cultured and passaged onto Transwell inserts. On the measurement day, the media in the Transwell inserts was changed and replaced with fresh transport media. The cells were then left for a minimum of

3 hours in the incubator to recover from the media change. FITC-Dextran (molecular weight 4 kDa; 0.5 mg/ml) was dissolved in Hank's Balanced Salt Solution (HBSS) without calcium, magnesium, or phenol red (ThermoFisher, UK). Prior to the permeability assay, the cells were rinsed twice with warm HBSS. The FITC-dextran solution was added to the apical insert (100µl) and warm HBSS was added to the basolateral plate (600µl) compartment. No-cell controls were prepared in the same manner. Once prepared, the Transwell plate was incubated at 37^0C in 5% CO_2 for 1 hour. After which, a 100µl sample was taken from both the apical and basal compartments of each well. Sample fluorescence was analysed with excitation filter 485 nm and emission filter 535 nm (FLUOstar Omega, BMG Labtech). Amount of FITC-dextran present in each sample was determined using a standard curve of known concentrations using linear regression analysis in Microsoft Excel. As apical (donor) chamber of each well of the transwell plate received equal amount (0.05 mg i.e. 100 µl of 0.5 mg/ml) of FITC-dextran. The percentage permeability of any well with HBEC monolayer (in comparison to NCC well) was determined by the dividing the amount of FITC-dextran present in the basal (recipient) chamber of that well with HBEC monolayer by the FITC-dextran present in the basal (recipient) chamber of the NCC well multiplied by 100%.

2.19 Analysis of drug transport in Transwell

2.19.1 Selection of test drugs

Criteria for selection of drug targets were as follows:

1) a molecular weight < 600 Da;
2) covering a range of values for lipophilicity (-1.8 to 5.4);
3) known uptake/efflux transporter interactions and
4) contained both CNS and non-CNS targets.

Eight drugs were selected for Transwell drug permeability studies namely: chlorpromazine Hydrochloride, lamotrigine, mitoxantrone Dihydrochloride, camptothecin, etoposide, methotrexate, loperamide Hydrochloride, topiramate.

The following drugs are substrate forefflux proteins as follows (Reference and species in which efflux activity has been reported for the corresponding efflux pump is given in parenthesis):

- P-gp substrate: loperamide (Zoghbi et al., 2008)(monkey), chlorpromazine (J. S. Wang et al., 2006)(mouse), lamotrigine (Potschka et al., 2002)(rats) and topiramate (Luna-Tortós et al., 2009)(human).
- BCRP substrate: mitoxantrone (Miyake et al., 1999)(human), camptothecin (Maliepaard et al., 2001; Kawabata et al., 2001)(human)
- MRP1 substrate: methotrexate (Cole, 2014)(Human), etoposide (Sakamoto et al., 1998)(human or mice)

2.19.2 Preparation of test drugs

A stock solution (10mM) of each drug was made in DMSO and stored at -20°C. Immediately prior to experimentation, a working solution (1 µM) of the drug was freshly prepared by dilution of the 10 mM stock in HBSS (no magnesium, no calcium, no phenol red). The final DMSO concentrations in all test drug concentrations was 0.03% (v/v).

Table 2.9 : The aqueous solubilty of the test drugs (in mg/ml) along with the source of solubility

Sr. No.	Name of the drug	Aqueous solubility (in mg/ml)	Source (Reference)
1.	loperamide	0.00086	ALOGPS (Tetko et al., 2005)
2.	chlorpromazine	0.00417	ALOGPS (Tetko et al., 2005)
3	lamotrigine	0.488	ALOGPS (Tetko et al., 2005)
4	topiramate	6.8	ALOGPS (Tetko et al., 2005)
5	mitoxantrone	0.734	ALOGPS (Tetko et al., 2005)
6	camptothecin	0.511	ALOGPS (Tetko et al., 2005)
7	methotrexate	0.0819	ALOGPS (Tetko et al., 2005)
8	etoposide	0.978	ALOGPS (Tetko et al., 2005)

2.19.3 Measuring permeability of drugs in Horse Transwell model

Transport assays were conducted using the HBEC Transwell model. The permeability of the test drugs was assessed bi-directionally by measuring

apical (A) to basal (B) (A-B) and B-A transport. To assess cell monolayer integrity, TEER measurements were performed at the start (Section 2.18). All test drugs were assayed in triplicate across three different experiments to accommodate variability in the HBEC monolayers. On the day of study, HBEC monolayers were equilibrated for at least 1 hour after TEER analysis. After this period, HBEC monolayers were carefully washed with HBSS twice and equilibrated in HBSS for 30 minutes at 37°C, after which, cells were incubated with 1 µM of test drug in HBSS in the donor compartment (100 µl in apical or 600 µl in basal compartments). The Transwell plates were incubated at 37°C in 5%CO_2. Samples (100µl) were taken at 30, 60 and 120 minute time points from the apical and basal compartments. A separate Transwell insert was used for each time point replicate. Samples were stored in -20^{0}C until analysed using liquid chromatography mass spectrometry (LC-MS/MS)

2.19.4 Analysis of test drugs samples using liquid chromatography-mass spectrometry

Sample analysis was performed at Boots Building, School of Pharmacy, University of Nottingham, UK. Dilutions of each drug from the 10 mM stock were made using 1:1 methanol: HBSS yielding the following concentrations: 1, 10, 25, 50, 100, 250, 500, 1000 nM. Where a higher concentration calibration line was required, the following concentrations were used: 1, 10, 25, 50, 100, 250, 500, 1000, 10000 nM.

Samples (1µl) were injected into ACE Excel 2 C18 column (50 x 2.1 mm id) operated at 50^{0}C, which was split by an accurate splitter to deliver an initial flow rate of 2ml.min^{-1} to the mass spectrometer. Gradient elution of each analyte was attained over a runtime of 6 minutes. Liquid Chromatography gradient conditions are given in Table 2.9.

Solvent A was water with 2mM ammonium acetate and 0.1% formic acid and solvent B was acetonitrile with 0.1% formic acid. All drugs were analysed using ESI in positive ion mode except topiramate which was analysed in negative ion mode. Lansoprazole drug was kept as internal standard at the concentration of 1µM. Samples (in triplicate) were analysed by LC-MS/MS on AB Sciex 4000 QTRAP system (Sciex, US) linked to Multiquant 3.0.3 software

for processing. The percent coefficient of variation for each drug is given in Chapter 6, Table 6.4.

Table 2.10: Gradient conditions for liquid chromatography as performed on Acquity UPLC BEH C8 column.

Time (mins)	Flow (ml.min^{-1})	Solvent A (%)	Solvent B (%)
0.10	0.4	100	0
1.00	0.4	70	30
5.00	0.4	10	90
6.00	0.4	100	0

Standard curves for different test drugs are given in Appendix 2. These standard curves were used to determine the concentration of each sample using the MultiQuant 3.0.3 software. This was also manually checked with linear regression in Microsoft Excel

Table 2.11: Molecular weights, LogP and mass transitions of drugs with Mass Spectrometer (LC-MS-MS)

S. no.	Drug	Molecular weight (Da)	LogP	Mass Transition with Mass Spec
1	camptothecin	348.35	1.74	**349.2** > 305.3, 220.2, 248.2
2	chlorpromazine	318.86	5.18	**319.1** > 86.2, 58.1
3	loperamide	477.00	4.77	**477.2** > 266.1, 210.0
4	etoposide	588.56	0.60	**589.2** > 229.2, 185.0
5	lamotrigine	256.10	2.57	**256.1** > 43.4, 211.0, 157.1
6	methotrexate	454.40	-1.85	**455.1** > 308.2, 175.0, 134.1
7	topiramate	339.36	0.13	**338.2** > 78.0, 95.7
8	mitoxantrone	444.48	-3.10	**445.2** > 88.2, 358.1

1. LogP is defined as the partition coefficient of a molecule between aqueous and lipophilic phases usually considered as octanol and water. It indicates which drugs have significant binding to plastic in the Transwell system.

2. All drugs except topiramate are in positive ion spray mode. topiramate is in negative ion spray mode. The mass of parent ion is one more than the molecular mass due to the addition of one proton. In case of topiramate the mass of parent ion is one less than the molecular mass due to the loss of one proton.

3. For mass transition, parent ion is in bold followed by daughter ions.

Table 2.12: Retention time (RT) and lower limit of detection (LLOD) of drugs on LC-MS-MS (QTRAP4000)

S.No.	Name of drug	RT	LLOD
1	camptothecin	3.01	10nM
2	chlorpromazine	3.09	10nM
3	loperamide	3.34	1nM
4	etoposide	2.99	250nM
5	lamotrigine	2.37	10nM
6	methotrexate	2.21	10nM
7	topiramate	3.13	25nM
8	mitoxantrone	2.23	25nM

Retention time (RT) is a measure of the time taken for a solute to pass through a chromatography column. It is the interval between the injection of a sample and the detection of substances in that sample.

Lower limit of detection (LLOD) is the lowest concentration of the particular drug that can be detected by the LC-MS-MS. This LLOD was determined by feeding the LC-MS-MS with samples of cocktail of drugs at different concentrations. The lowest concentration that can be detected by LC-MS-MS will be taken/termed as LLOD.

2.20 Statistical analysis and Ethical statement

Statistical analyses were performed using GraphPad Prism 8, treatment groups were compared by one-way ANOVA or two-way ANOVA as stated. Post-hoc tests were used for multiple comparisons; Tukey's multiple comparisons test was used for one-way ANOVA whereas Sidak's multiple comparisons test was used for two-way ANOVA. Values presented on table and figures are Mean ± SEM unless otherwise indicated. All experiments using animal tissue were conducted according to ethical approval by the University of Nottingham School of Veterinary Medicine and Science Ethics Committee.

Chapter 3

Isolation and characterisation of primary horse brain endothelial cells

3.1 Background

Brain endothelial cells (BECs) which are the main component of the blood-brain barrier (BBB) have various structural and functional differences in their drug transport mechanism compared to the peripheral endothelial cells. For example, the intercellular space between the peripheral endothelial cells is 6-7nm, which is sufficient to allow some passage of circulating molecules from the blood to the tissue (Gomes et al., 2015). There is also increased expression of tight junction proteins in the BECs enabling in stronger cell-cell connection. This decreases paracellular permeability of circulating molecules from the blood to the brain tissue (Sharif et al., 2018). In addition, transcellular transport of low molecular weight lipophilic molecules into the brain tissue through the BECs is also restricted through the presence of multidrug efflux transporters and various drug metabolising enzymes present inside the BECs (Morris et al., 2017). Collectively, this means that any physiologically relevant model of the BBB would ideally express these qualities for it to be valid.

Recently, different source of endothelial cells have been used to create *in vitro* models of the BBB. The endothelial cell type chosen for the development of the BBB determines the workability, performance, cost-effectiveness and output of the model developed (Sivandzade & Cucullo, 2018). The gold standard BBB model utilises primary BECs, as these cells abundantly express tight junction proteins and multidrug efflux transporters which are vital for the physiological functioning of the BBB (Patabendige, Skinner, Morgan, et al., 2013). In comparison to primary BECs, BBB models developed using immortalised cell lines regularly exhibit leaky tight junctions and inconsistent expression of multidrug efflux transporters (Oddo et al., 2019; Rahman et al., 2016). While the use of primary BECs in development of BBB models has many merits but there are few challenges associated with the use of primary BECs. These include low cell yield, requirement of specialised technical and methodical skills for isolation and culture of BECs, safeguarding the purity of cell culture post-isolation and repeatability among individual cultures.

The biggest challenge with primary BECs is the high level of variability linked with primary cell isolation and culture. Thus, it is essential to carefully evaluate the phenotype of the isolated primary cell cultures in terms of the molecular

and functional BBB characteristics across different cultures (Nielsen et al., 2017a). Consequently, this Chapter describes the development of modified procedures for the isolation and characterisation of primary horse brain endothelial cells (HBECs). Furthermore, the BBB phenotype of the isolated and successively cultured primary HBECs will be characterised by the authenticating 1) the purity of the isolated and cultured cell cultures 2) the expression of tight junctions and 3) the expression and function of drug metabolising enzymes and multidrug efflux transporters, using polymerase chain reaction (PCR), immunofluorescence (IF), Western blotting (WB), transendothelial electrical resistance (TEER) fluorescein isothiocyanate (FITC) permeability assays.

3.2 Methods

For specific methodology, please refer to Chapter 2, For methodology of histology and immunofluorescence please refer to the section 2.8 and 2.9, respectively. For methodology of scanning electron microscopy and Western blotting see section 2.10 and 2.11, respectively. For methodology of PCR and quantitative PCR see section 2.12 and 2.13, respectively. For methodology of GGT assay and FITC-dextran permeability assay see section 2.15 and 2.18, respectively.

3.3 Results

3.3.1 Identification of BBB in equine brain *ex vivo*

Immunohistochemistry (IHC) was performed on fixed horse cerebrum for ZO-1 to confirm the presence and localisation of the BBB inside the microvessels of the brain. ZO-1 was used as the BEC marker because it is an integral tight junction protein that is expressed at higher levels in the BBB than any other brain cell types (Howarth et al., 1992).

ZO-1 staining (green) was very apparent through the cerebral tissue in localised areas that resembled blood vessels. The cells were counterstained with DAPI and all cell nuclei were stained blue.

3.3.2 Isolation of primary equine cerebral microvessels

Horse brains were used for isolation of the microvessels as this was the target species. Additionally, the volume of brain and presence of grey matter per animal is higher than in rodents meaning that fewer animals were required for each experiment. For isolation of microvessels, an established method that incorporated the use of mechanical homogenisation and physical isolation of whole cerebral microvessels was used (Nielsen et al., 2017b). In this Chapter found that this method was very reliable in terms of yield and was also cost-effective. Capillaries isolated from one horse brain were collected into a single cryovial which could be cryopreserved in liquid nitrogen. One cryovial of isolated capillaries was then adequate to make confluent monolayer of cells in one T75 cell culture flask in six days.

3.4 Establishment of culture protocols for HBECs

This experiment was performed with freshly isolated endothelial capillaries (Table 3.1). The objective of this experiment was to monitor the morphology and growth of HBECs over time and to determine the purity of the HBEC isolation using immunofluorescence, Polymerase chain reaction, and Western blotting. This assessment was conducted once the HBEC had formed a confluent monolayer in at least some treatments. ‘In addition, the effect of adding puromycin (0, 1 and 4µg/ml) for the first 3 days of culture on the growth and appearance of HBECs was tested. Puromycin is added to remove contaminating non-endothelial cells (eg. pericytes) since endothelial cells are capable of pumping out puromycin while other mammalian cell types are not (Calabria et al., 2006; Dylewski et al., 2020). Finally, it was determined whether astrocyte-conditioned media (ACM) promoted HBEC growth and expression of key transporters like P-glycoprotein using real time PCR.

Table 3.1: The plate layout of a 12 well plate where HBECs were culture in at different puromycin concentrations and in presence / absence of astrocyte condition media (ACM).

	1	**2**	**3**	**4**
A	2ml ECGM with 4µg/ml puromycin	2ml ECGM with 4µg/ml puromycin	1.5ml ECGM with 4µg/ml puromycin + 0.5ml ACM	1.5ml ECGM with 4µg/ml puromycin + 0.5ml ACM
B	2ml ECGM with 1µg/ml puromycin	2ml ECGM with 1µg/ml puromycin	1.5ml ECGM with 1µg/ml puromycin + 0.5ml ACM	1.5ml ECGM with 1µg/ml puromycin + 0.5ml ACM
C	2ml ECGM without puromycin	2ml ECGM without puromycin	1.5ml ECGM without puromycin + 0.5ml ACM	1.5ml ECGM without puromycin + 0.5ml ACM

1. Wells in columns 1 & 3 had 19mm coverslips inserted while wells of columns 2 & 4 were without coverslips.
2. After three days, no puromycin was added to all wells.

ECGM is endothelial cell growth media; ACM is astrocyte-conditioned media

On a daily basis, all cells were microscopically observed and photographs were taken. On the sixth day of culture, cells in columns 2 and 4 were scraped and collected in RNAlater and stored at -80°C for subsequent PCR studies. Cells on coverslips (columns 1 and 3) were fixed with ice-cold acetone:methanol (1:1 v/v) solution and then stored in PBS at 4°C for immunofluorescence analysis.

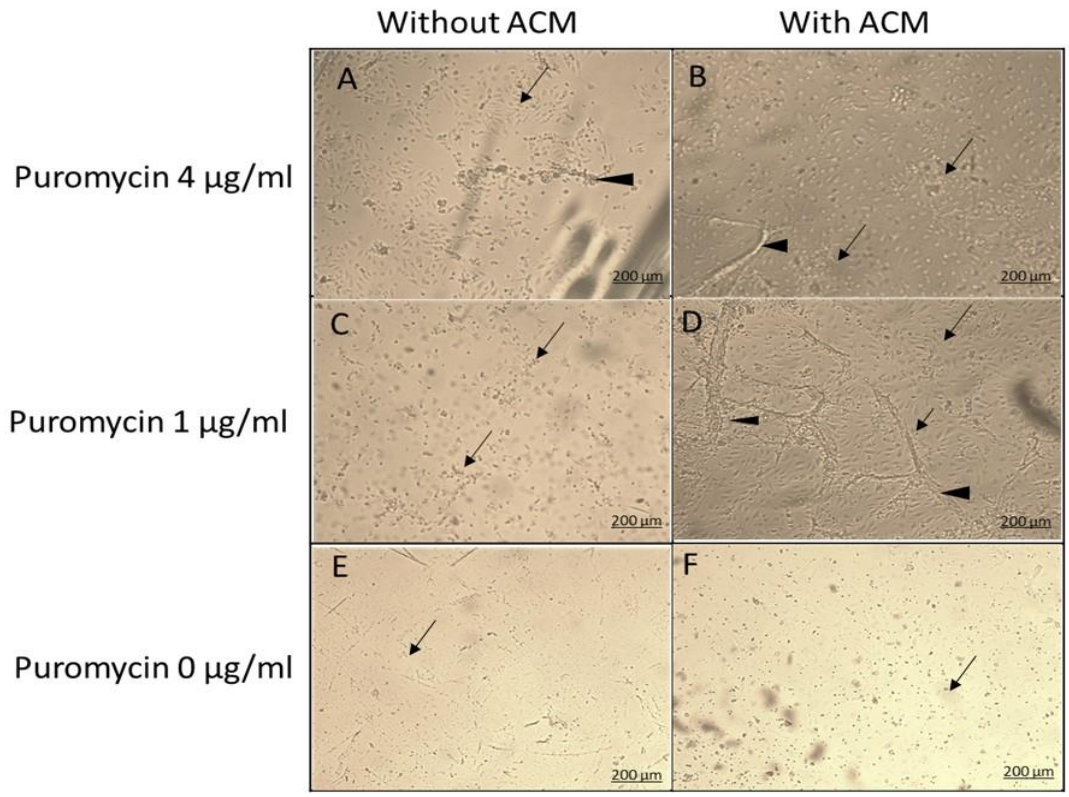

Fig 3.1: The growth of equine brain endothelial cells treated with puromycin and astrocyte-conditioned media (ACM) on day 3 of culture. Representative images are shown of cells treated with 4µg/ml (A & B), 1µg/ml (C & D) and 0µg/ml (E & F) puromycin. (A, C, E) show cells treated in the absence of ACM while (B, D, F) show cells cultured in the presence of ACM. Presumptive endothelial cells are indicated by arrows, while capillary fragments are indicated by arrowheads. Scale bar = 200µm

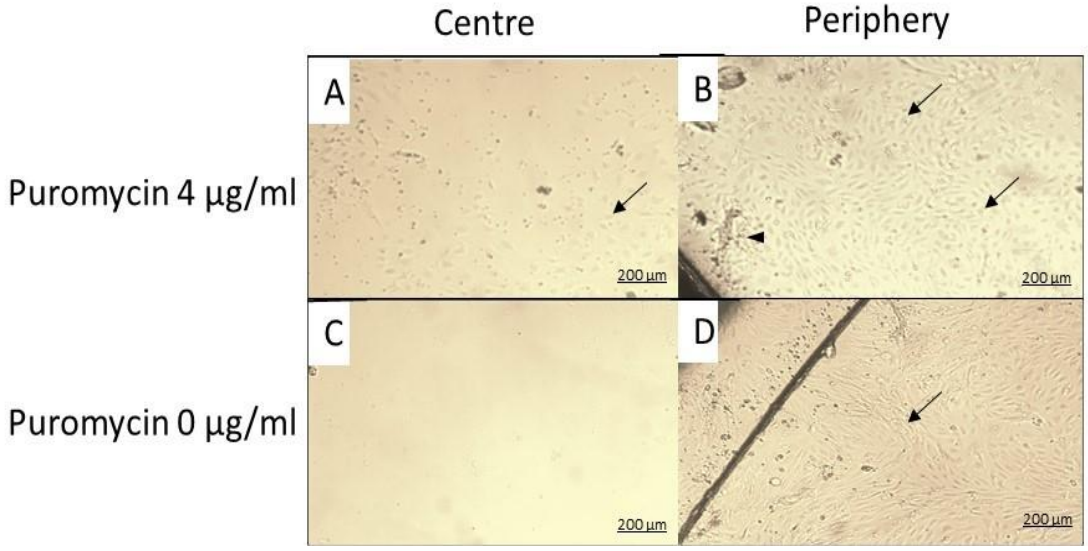

Fig. 3.2: The comparison of growth of equine brain endothelial cells in the centre and periphery of the wells of 12 well plate. Representative images are shown of cells treated with 4µg/ml (A & B) and 0µg/ml (C & D) puromycin. Presumptive endothelial cells are indicated by arrows, while capillary fragments are indicated by arrow heads. Scale bar = 200µm

3.4.1 Morphological appearance of horse brain endothelial cells in culture

The morphology of the HBECs was observed using an upright light microscope (Leica DM5000) on daily basis in the culture. On the day of seeding, the isolated capillaries appeared as tubule-like structures with frequent branches. The micro-capillaries attached to the surface within six hours of seeding and did not detach by the 24-hour post-seeding PBS wash. This PBS wash was performed to remove all the unattached cellular debris from the culture.

At 48 hours post-seeding, cells started to radiate out from the micro-capillaries and formed a confluent monolayer around the micro-capillary fragment. By 72 hours post-seeding, the culture became around 50-60 percent confluent (Fig. 3.1). By sixth day post-seeding the cell monolayer was 85-90 percent confluent. The cells that formed the confluent monolayer were characteristically spindle-shaped, slightly stretched out and tapering on both ends. This is the typical morphology of endothelial cells. This morphology and growth pattern of cells was consistent between the different batches of isolations. Moreover, the cells also exhibited similar morphology and growth pattern whether they cultured fresh or were cultured after cryopreservation. Microscopic observations performed on the third day of the culture revealed that cells grow more extensively on the plastic base of the well than on a glass cover slips. Also, cells grew more towards the periphery of the well than in the centre of the well (Fig. 3.2).

Puromycin was maintained in the growth media for the first three days of the culture in order to create a pure culture of brain endothelial cells as puromycin induces apoptosis in contaminating cell types like pericytes. Cell growth at 1 and 4 µg/ml concentration of puromycin appeared to be very similar. Conversely, cellular growth was visibly less when puromycin was absent. Cellular growth appeared to be slightly higher in the presence of ACM than in its absence.

3.4.2 Selection of HBECs in the primary cell culture

As the isolation of brain endothelial cells is performed from whole brain tissue, it is feasible that there is the presence of other contaminating cells in the culture. The most suitable method for obtaining a pure culture of brain endothelial cells is to keep the cell culture in the presence of low concentrations of puromycin for the initial three days of culture (Perriere et al., 2005).

3.4.3 Measurement of horse brain endothelial cells and capillaries

Measurement of dimensions of equine brain endothelial cells and capillaries was collected using Nikon NIS-Elements Image Analysis Software on the brightfield photographs captured on day six of culture. The values of length, width and area of endothelial cells and capillaries are given in Table 3.2.

Table 3.2 Measurement of horse brain endothelial cells and capillaries

	Length (µm)	Width (µm)	Area (μm^2)
Endothelial cells	23.4 – 80.0	8.70 – 17.0	256.0 –1440.0
Capillaries	610.0 – 938.0	34.0 – 278.0	4940.0 –53400.0

3.4.4 Validation of PCR primers in equine brain tissue

RNA was extracted from equine brain and liver tissues and used to prepare cDNA. The yield and quality parameters of both RNA and cDNA from both samples were within acceptable limits (Table 3.3).

Table 3.3: Quantitation of extracted RNA obtained from equine liver and brain

Tissue	**Yield (ng/µl)**	**%CV**	**Ratio 260/280**
Brain	213.4	3.9	2.16
Liver	649.8	10.7	2.10
Quantitation was performed in duplicate %CV is % Coefficient of variation			

Initially, PCRs were performed using cDNA from equine brain tissue for GAPDH, β-Actin, ZO-1, P-glycoprotein, VE-Cadherin, BCRP and their respective non-template controls (NTC). The annealing temperature was set to 60^{o}C and 35 amplification cycles were performed. The primers for GAPDH (147bp), β-Actin (293bp) and VE-cadherin (147bp) yielded a single PCR product at the correct size (Fig 4.4). Their respective NTC were blank. However, the primers of ZO-1, P-glycoprotein, BCRP failed to yield any band (Fig 3.3).

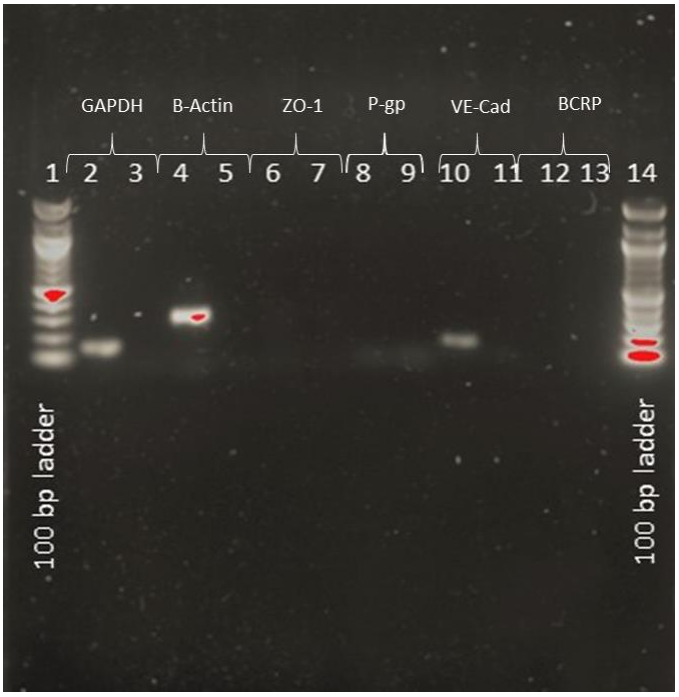

Fig. 3.3: Agarose gel depicting PCR products of primers of various endothelial cell markers and housekeeping genes. PCR products are shown for GAPDH (lane 2), β-Actin (lane 4), ZO-1 (lane 6), P-gp (lane 8), VE-Cad (lane 10) and BCRP (lane 12). The respective non-template control (NTC) of each gene is shown in adjacent lane (lanes 3, 5, 7, 9, 11 and 13).

3.4.5 Gradient PCR to check the optimal annealing temperature of primer pairs

Gradient PCR was performed using horse liver cDNA for primer pairs of endothelial cell, astrocyte and pericyte markers. Different annealing temperatures chosen were as follows: 57°C, 58°C, 58.8°C, 59.8°C, 60.9°C, 62°C, 62.8°C and 64°C. For the endothelial cell marker, MRP1, there was a band of product size 359bp at six annealing temperatures except 62.8°C and 64.0°C (Fig 3.4B). Primer pair for VE-Cadherin yielded a single band of product size (147bp) at all annealing temperatures (Fig 3.5D) but primer pair for ZO-1, P-gp & BCRP again failed to yield band at any of the annealing temperature (Fig 3.4A).

For the astrocyte markers, primers for RGS5 & KCNJ8 yielded single band of product size 312 and 595bp, respectively at all annealing temperatures but GFAP, ABCC9, DLK1 & Zic1 failed to yield band at any of the annealing temperature (Fig 3.4 and 3.5). Desmin (astrocyte and pericyte marker) yielded single band of product size 262bp at all annealing temperatures (Fig 3.4C and 3.4D). For the pericyte markers, ASMA yielded single band (538bp) at all

annealing temperatures but AAP, CSPG4 & CD146 failed to yield band at any of the annealing temperature (Fig 3.5).

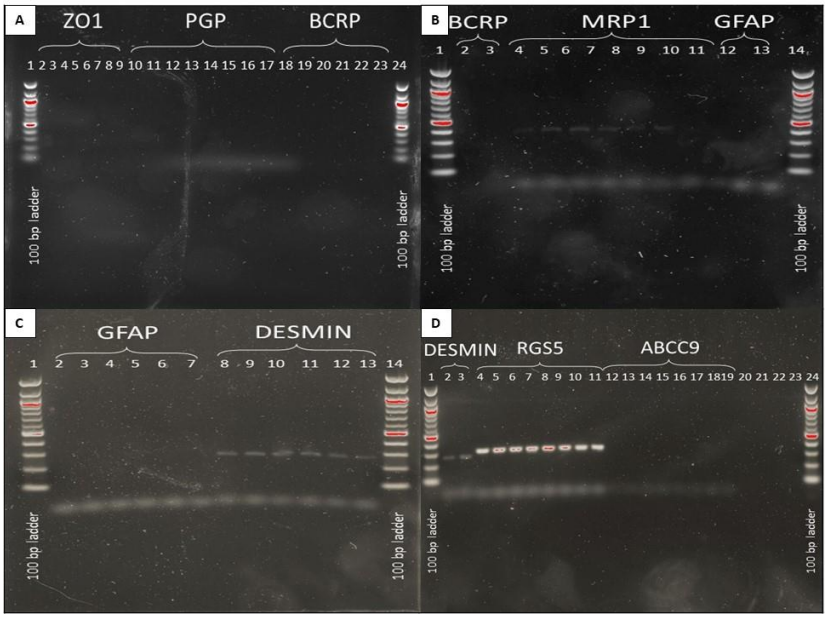

Fig. 3.4: Images of agarose gel for different primers in a gradient PCR with different annealing temperatures. (A) shows ZO1, PGP and BCRP; (B) shows BCRP, MRP1 and GFAP; (C) shows GFAP and Desmin; (D) shows Desmin, RGS5 and ABCC9. Desmin and RGS5 genes yielded single band whereas ZO1, PGP, BCRP, GFAP and ABCC9 yielded no band. Any bands below the first strand of the ladder were considered as primer dimers.

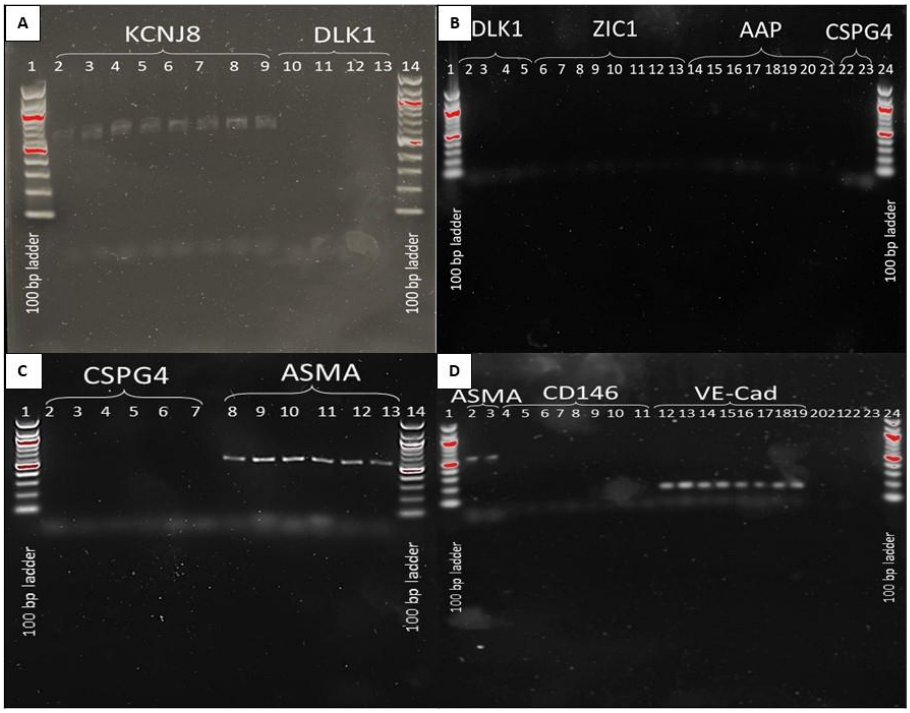

Fig. 3.5: Images of agarose gel of different primers in a gradient PCR with different annealing temperatures. (A) shows KCNJ8 and DLK1; (B) shows DLK1, ZIC1, AAP and CSPG4; (C) shows CSPG4 and ASMA (D) ASMA, CD146 and VE-Cad. KCNJ8, ASMA and VE-Cad genes yielded band whereas DLK1, ZIC1, AAP, CSPG4 and CD146 yielded no band. The bands below the first strand of the ladder are primer dimers.

3.4.6 Validation of new primer pairs (product size <150 bp) for biomarkers

A number of the primer pairs failed to give a specific amplified PCR product. Thus, new primer pairs were re-designed to ensure that the product size was less than 150 bp. The biomarker molecules for which the new primers were designed were: ZO-1, P-glycoprotein, VE-Cadherin, RGS5, ABCC9, Desmin, BCRP, MRP1, KCNJ8 and DLK1. The reaction mixture composition and thermocycle conditions were kept the same (Section 2.13.3 and Table 2.7). These primer pairs yielded a clear single band on gel electrophoresis and no band in non-template control (NTC) (Fig 3.6). The exception was BCRP which yielded two bands (i.e. one intense and one weak) at similar product size but there no band in NTC.

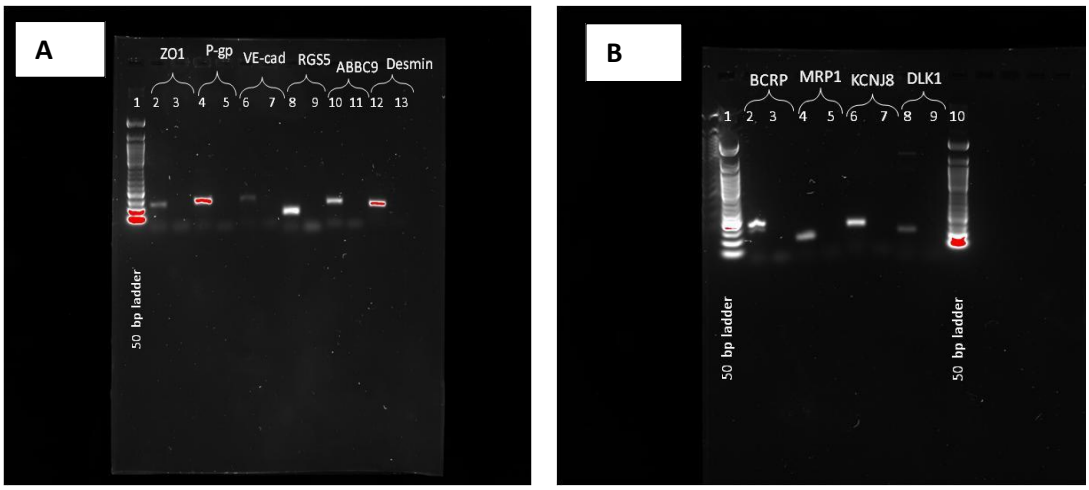

Fig. 3.6: Images of agarose gel of new primer pairs (product size <150 bp) for biomarkers. (A) shows ZO-1, P-gp, VE-Cad, RGS5, ABCC9 and Desmin, while (B) show BCRP, MRP1, KCNJ8 and DLK1.The respective non-template controls (NTC) of each gene are shown in adjacent lane. The bands below the first strand of the ladder are primer dimers.

3.4.7 PCR for biomarker molecules of the brain endothelial cells, drug transporters, astrocytes and pericytes

RNA was extracted from HBECs cultured with different concentrations of puromycin (0-4µg/ml) and in presence or absence of astrocyte condition media (ACM). The yields and quality parameters of RNA from the samples were within acceptable limits (Table 3.4). The 260/280 absorbance ratios were calculated to assess the purity of RNA extracted from cultured primary

equine endothelial cells. For RNA, 260/280 absorbance ratios of around 2.0 are considered as good and RNA is considered as free from contamination (Chong et al., 2020).

Table 3.4: Quantitation of RNA extracted from primary equine endothelial cells grown in different concentrations of puromycin (0-4µg/ml) and in presence or absence of astrocyte condition media (ACM).

Sample	260/280 ratio	RNA yield (ng/µl)
Endothelial cell growth medium with Puromycin at 4µg/ml	2.17	32.5
Endothelial cell growth medium +ACM with Puromycin at 4µg/ml	2.42	8.36
Endothelial cell growth medium with Puromycin at 1µg/ml	2.16	131.2
Endothelial cell growth medium +ACM with Puromycin at 1µg/ml	2.19	34.1
Endothelial cell growth medium with no Puromycin	2.21	47.8
Endothelial cell growth medium +ACM with no Puromycin	2.23	45.7

3.4.8 PCR to detect the quality of cDNA synthesised from endothelial cells

The PCR was performed by using cDNA at three different amounts 5ng, 10ng and 20ng per reaction. Housekeeping gene (i.e. GAPDH) were used in this experiment as a reference sample. A positive tissue control was also run using cDNA from horse brain tissue (1ng per reaction). cDNA extracted from cultured endothelial cells produced band for GAPDH at all three cDNA amounts . Positive tissue control also yielded a clear band at same size and no band was observed in NTC (Fig. 3.7). This confirm the quality of the cDNA was satisfactory and could be used for further experiments.

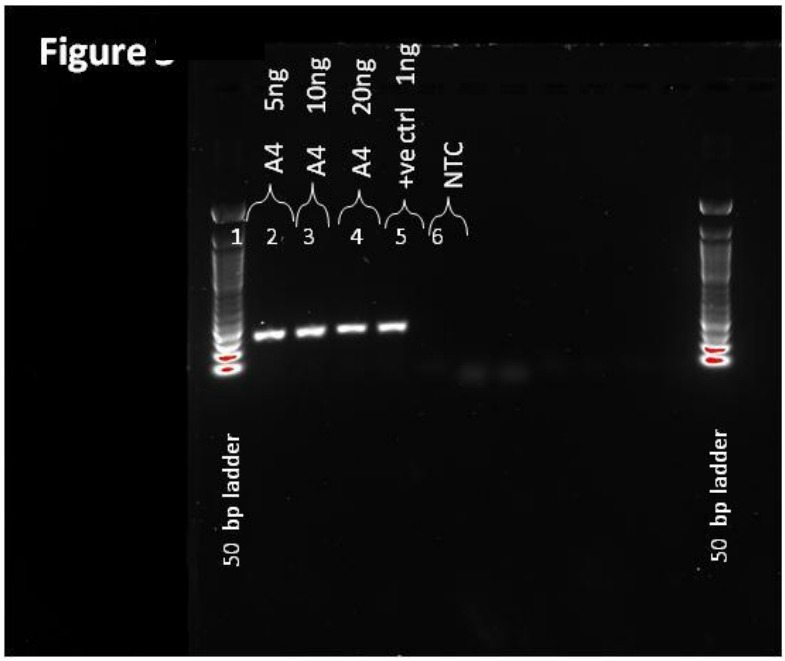

Fig. 3.7: Agarose gel showing PCR products of housekeeping gene (GAPDH) primers at different amounts of cDNA per reaction. The order of wells (left to right) is lane 1: 50 bp ladder, lane 2:5ng cDNA, lane 3: 10ng cDNA and lane 4: 20ng cDNA, lane 5 is 1ng c DNA from horse brain tissue (positive control) and lane 6 is non-template control (NTC).

3.4.9 PCR for cell type biomarkers and drug transporters using cDNA from cultured HBECs

The cultured primary equine brain endothelial cells expressed a number of different endothelial cell biomarkers including Zona Occludens-1 (ZO-1), VE-Cadherin and transporter proteins like P-Glycoprotein (P-gp), Glucose transporter 1 (GLUT1) (Fig 3.8 and 3.9). These cells also expressed the drug transporters: Breast Cancer Resistance Protein (BCRP) and Multidrug resistance-associated protein 1 (MRP1), (Fig. 3.10). These biomarkers were expressed at different concentration of puromycin (0, 1 and 4µg/ml) and both in presence and absence of ACM. □

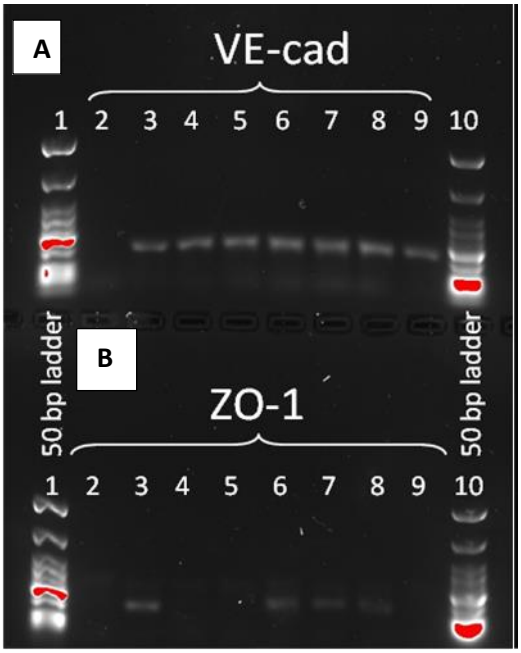

Fig 3.8: Images of PCR gels showing expression of endothelial cell biomarkers in HBECs. A) shows VE-cadherin, B) shows ZO-1. . The order (left to right) of wells for each biomarker is 1) 50 bp ladder, 2) NTC3)positive control from equine brain tissue, 4) 4 µg/ml puromycin without ACM, 5) 4 µg/ml puromycin with ACM, 6) 1 µg/ml puromycin without ACM, 7) 1 µg/ml puromycin with ACM, 8) no puromycin without ACM, 9) no puromycin with ACM, respectively. Any bands below the first strand of the ladder were considered as primer dimers. NTC stands for non template control.

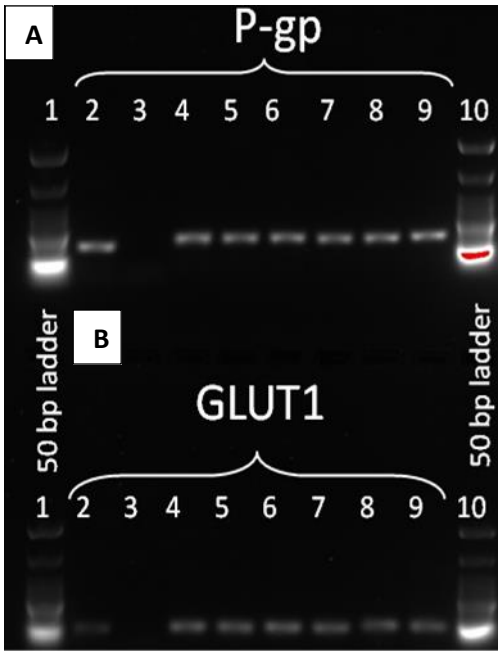

Fig 3.9: Images of PCR gels showing expression of drug transporter molecules in HBECs. A) shows P-glycoprotein B) shows GLUT1. The order (left to right) of wells for each biomarker is 1) 50 bp ladder, 2) positive control from equine brain tissue 3) NTC 4) 4 µg/ml puromycin without ACM, 5) 4 µg/ml puromycin with ACM, 6) 1 µg/ml puromycin without ACM, 7) 1 µg/ml puromycin with ACM, 8) no puromycin without ACM, 9) no puromycin with ACM, respectively. Any bands below the first strand of the ladder were considered as primer dimers. NTC stands for non template control.

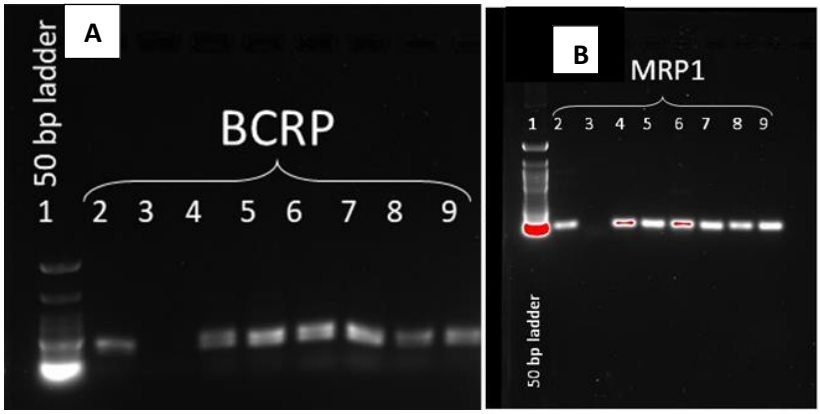

Fig 3.10: Images of PCR gels showing expression of key drug transporters in HBECs. (A) shows BCRP and (B) shows MRP1. The order (left to right) of wells for each biomarker is (1) 50 bp ladder, (2) positive control from equine brain tissue, (3) NTC, (4) 4 µg/ml puromycin without ACM, (5) 4 µg/ml puromycin with ACM, (6) 1 µg/ml puromycin without ACM, (7) 1 µg/ml puromycin with ACM, (8) no puromycin without ACM, (9) no puromycin with ACM, respectively. Any bands below the first strand of the ladder were considered as primer dimers. NTC stands for non template control.

3.4.10 PCR for biomarker of Astrocytes

PCRs were performed for biomarker of potential contaminating cells like astrocytes using specific primer for desmin. This was performed to determine the purity of horse brain endothelial cells and whether they were devoid of other contaminating cells. PCR was done using cDNA from HBECs cultured in different puromycin concentrations and in presence or absence of ACM.

A single band was detected for desmin in all samples except non template control (NTC). There were indications that the intensity of the band was different across the samples but this was not quantified (Fig 3.11).

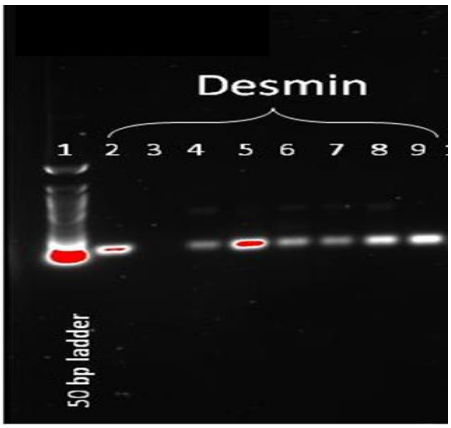

Fig 3.11: Image of PCR gel showing expression of desmin which is a biomarker of astrocyte in HBECs.. The order (left to right) of wells for each biomarker is (1) 50 bp ladder, (2) positive control from equine brain tissue, (3) NTC, (4) 4 µg/ml puromycin without ACM, (5) 4 µg/ml puromycin with ACM, (6) 1 µg/ml puromycin without ACM, (7) 1 µg/ml puromycin with ACM, (8) no puromycin without ACM, (9) no puromycin with ACM, respectively. Any bands below the first strand of the ladder were considered as primer dimers. NTC stands for non template control.

3.4.11 PCR for biomarker of Pericytes

PCR was performed for biomarker (PDGFR-β) to determine if there were any potential contaminating cells like pericytes. PCR was performed on cells cultured in under different puromycin concentrations, and in presence or absence of Astrocyte condition medium (ACM). Single PCR product bands for PDGFR-β were observed in all lanes including those from cells treated with puromycin (Fig. 3.12). This indicated that puromycin had minimal effect on the presence of pericytes.

Fig 3.12: Image of PCR gel showing expression of PDGFR-β which is a biomarker of pericytes in HBECs. The order (left to right) of wells for each biomarker is (1) 50 bp ladder, (2) positive control from equine brain tissue, (3) NTC, (4) 4 µg/ml puromycin without ACM, (5) 4 µg/ml puromycin with ACM,(6) 1 µg/ml puromycin without ACM, (7) 1 µg/ml puromycin with ACM, (8) no puromycin without ACM, (9) no puromycin with ACM, (10) 50 bp ladder, respectively. Any bands below the first strand of the ladder were considered as primer dimers. NTC stands for non template control.

3.4.12 Immunofluorescence for contaminating cells

To further examine the potential presence of pericytes in HBECs, immunofluorescence for αSMA was performed on HBECs cultured in presence and absence of puromycin. Cells were grown for 72 hours either in presence or absence of 4µg/ml puromycin, before being fixed. In the absence of puromycin, there was a significant number of positively stained cells and these cells were observed to have a dendritic morphology appearance. In contrast, in the presence of puromycin very few cells were observed with a dendritic morphology and moreover, there was very limited positive α-SMA immunostaining in the HBEC (Fig 3.13). This suggested that exposure of HBECs to puromycin did reduced the number of pericytes present in the HBEC culture.

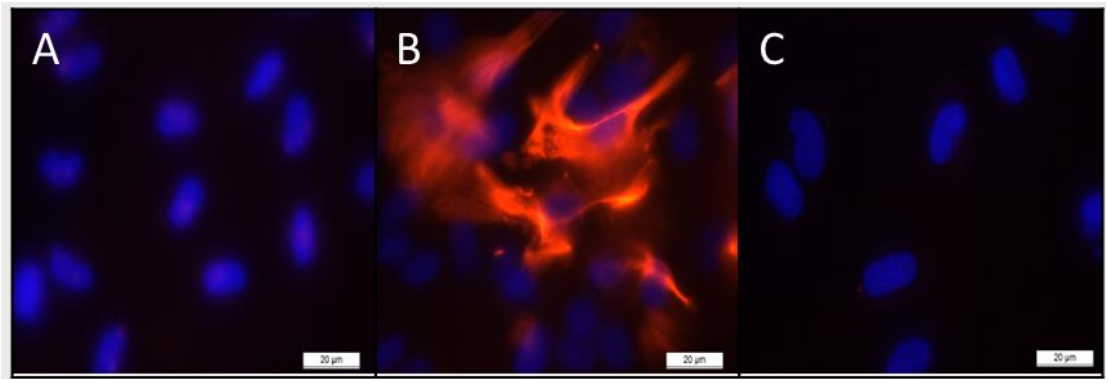

Fig 3.13: Representative immunofluorescence images showing whether pericytes were present in the culture of horse brain endothelial cells. α-SMA was used a pericyte marker. Cells in (A) were treated with puromycin at 4 µg/ml while cells in (B & C) were treated with no puromycin. Cells in A & B were stained with mouse anti-α-SMA antibody (red) whereas cells in C were treated with mouse IgG. Cells were counterstained with DAPI (blue) and the scale bar represents 20µm.

3.5 Identification of tight junctions between HBECs

The presence of tight junctions in primary HBECs was evaluated using PCR, Western blotting, immunofluorescence and Scanning Electron Microscopy (SEM) imaging. Moreover, transendothelial electrical resistance (TEER) experiments were also conducted as a functional measure of the dynamic junctional physiology, alongside FITC-dextran permeability assays to confirm the constraint to the passage of large molecules by these tight junctions. HBECs were cultured for maximum upto nine days for these experiments.

3.5.1 PCR for tight junction associated proteins in HBECs

Expression of VE-Cadherin (component of adherens junction) and zona occludens-1 (ZO-1, component of tight junction) was evaluated using PCR in HBEC treated with different concentrations of puromycin and in presence or absence of ACM. Single bands at correct product size were observed for VE-Cadherin and ZO-1 in cells grown in presence of different puromycin concentrations as well as in presence and absence of ACM. This clearly indicated that adherens junctions and tight junctions are present in the HBECs (Fig 3.8).

3.5.2 Western blot for presence of key transporter molecule, P-Glycoprotein in HBECs

Western blots showed that HBECs treated with ACM expressed P-Glycoprotein and β-Actin (house keeping protein). In contrast, HBECs cultured without ACM failed to express both P-Glycoprotein and β-Actin. This indicates that there was an issue with this sample (ie they were either destroyed or denatured completely). Protein extracted from horse liver were used as positive control for the Western blot experiment. This shows that the cells treated with ACM expressed multidrug efflux transporter protein P-Glycoprotein and also housekeeping gene β-Actin. But it cannot be concluded that cells not treated with ACM failed to express P-Glycoprotein as these cells also failed to express housekeeping gene β-Actin (Fig. 3.14)

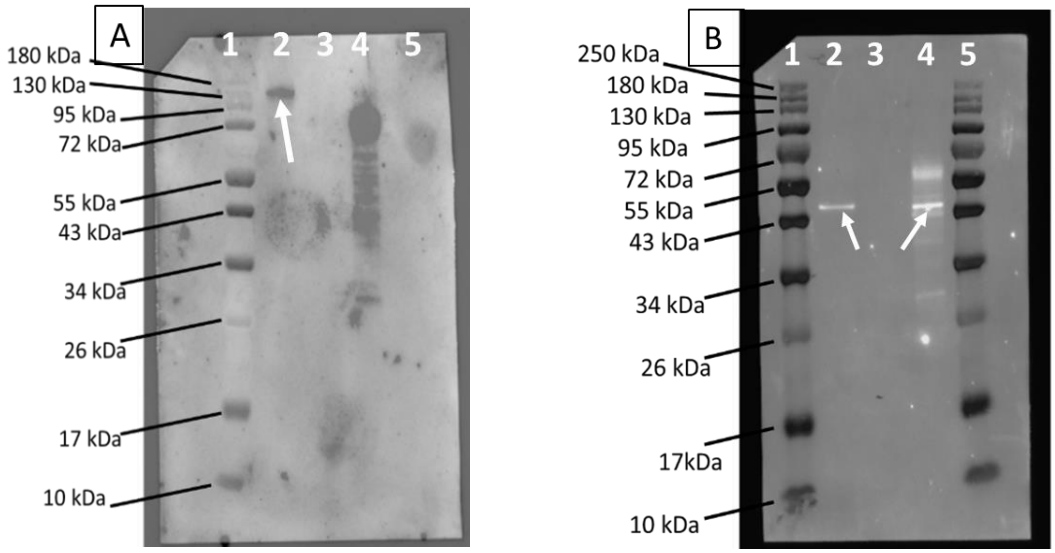

Fig 3.14: Western blot images for (A) P-glycoprotein (141 KDa) and (B) β-actin. In each case: lane 1 and 5 show protein markers, 2) HBECs treated with astrocyte condition medium, 3) HBECs culture without astrocyte condition medium 4) Horse liver tissue (positive control). (A) shows the presence of PGP (150 kDa), while B) shows the detection of β-actin in all samples except the HBECs not treated with astrocyte condition medium. The band appeared as white instead of black for β-actin when capturing the image. The reason for this is unknown but the band was present at the correct size. Images (A) and (B) are two separate blots.

Prior to western blot experiment protein quantification of the cultured endothelial cells samples was done using Bradford assay by plotting a standard curve. Each well received equal amount of protein. Western blot experiment was done using anti P-glycoprotein antibody (ab170904, Host

spp.-rabbit, predicted mol. Wt.-141 KDa, dilution 1:1000) and Anti-β-Actin antibody (GTX110564, Host spp.-rabbit, predicted mol. wt.-42 KDa, dilution 1:50000). Goat anti-rabbit IgG (A9169, dilution 1:5000) was used as secondary antibody.

3.5.3 Immunofluorescence for tight junction protein ZO-1 in HBEC culture

ZO-1 is a vital component of tight junctions and exists at the cellular boundary of all endothelial cells in a confluent monolayer.

The primary HBECs formed a continuous monolayer with cobblestone morphology Immunofluorescent staining for ZO-1 clearly showed that ZO-1 was localised to the cell membrane. This strongly indicated that tight junctions were present between all HBECs. Furthermore, this clearly showed that ZO1-positive cells were the most abundant across the confluent monolayer of HBECs (Fig. 3.15)

After this, cells were exposed to different concentrations of puromycin (4, 1 and 0µg/ml) both in absence and presence of ACM. Cells which were exposed to 4 µg/ml puromycin (both with and without ACM) and cells which were exposed to 1 µg/ml puromycin in presence of ACM exhibit confluent layer of cells and there is abundant presence of ZO-1 staining. In this experiment, no growth of cells was observed in those cells which were exposed to 1 µg/ml puromycin without ACM. Hence, there was no ZO-1 staining in the cells exposed to 1 µg/ml puromycin without ACM. Scanty growth of cells was observed in the well in which no puromycin without ACM treatment was given. In this, no puromycin, no ACM well, cells (scanty) that were present exhibited the presence of ZO-1 staining. Cells exposed to no puromycin but with ACM exhibited more growth (in comparison to the well with no puromycin and no ACM) but showed minimal ZO-1 staining (Fig. 3.16 and 3.17).

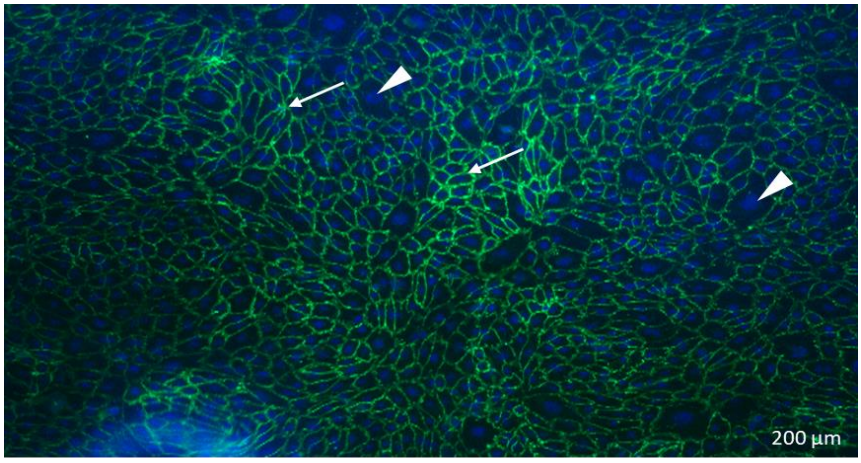

Fig. 3.15: Representative image showing ZO-1 protein localisation in the plasma membrane of horse brain endothelial cells in culture. ZO-1 protein (green) is indicated by arrows while the nucleus (blue, DAPI). Scale bar = 200µm.

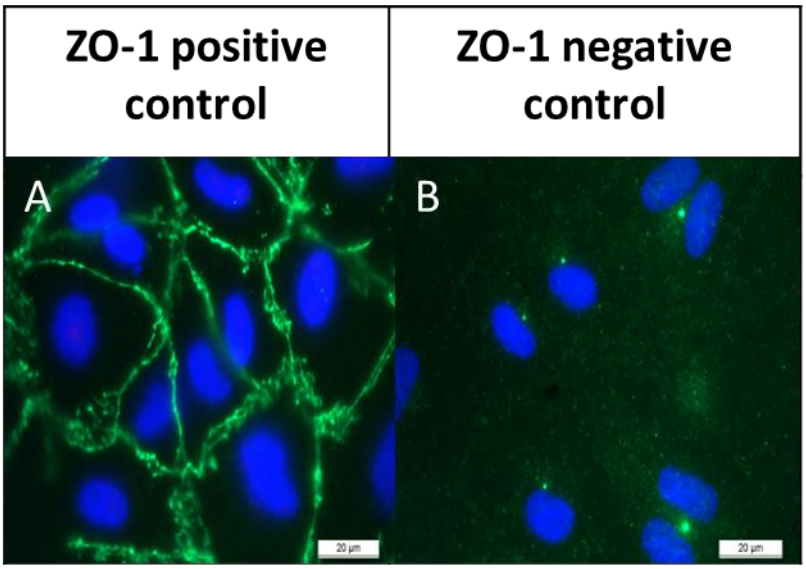

Fig 3.16: Representative immunofluorescence images showing the specificity of the anti ZO-1 primary antibody in horse brain endothelial cells. A) shows cells have been treated with rabbit anti-human ZO-1 primary antibody whereas B) shows cells incubated with equivalent concentrations of rabbit IgG negative control. Green staining indicates positive ZO1 staining localised to the membrane while the blue shows cell nuclei stained with DAPI. Scale bars are 20µm.

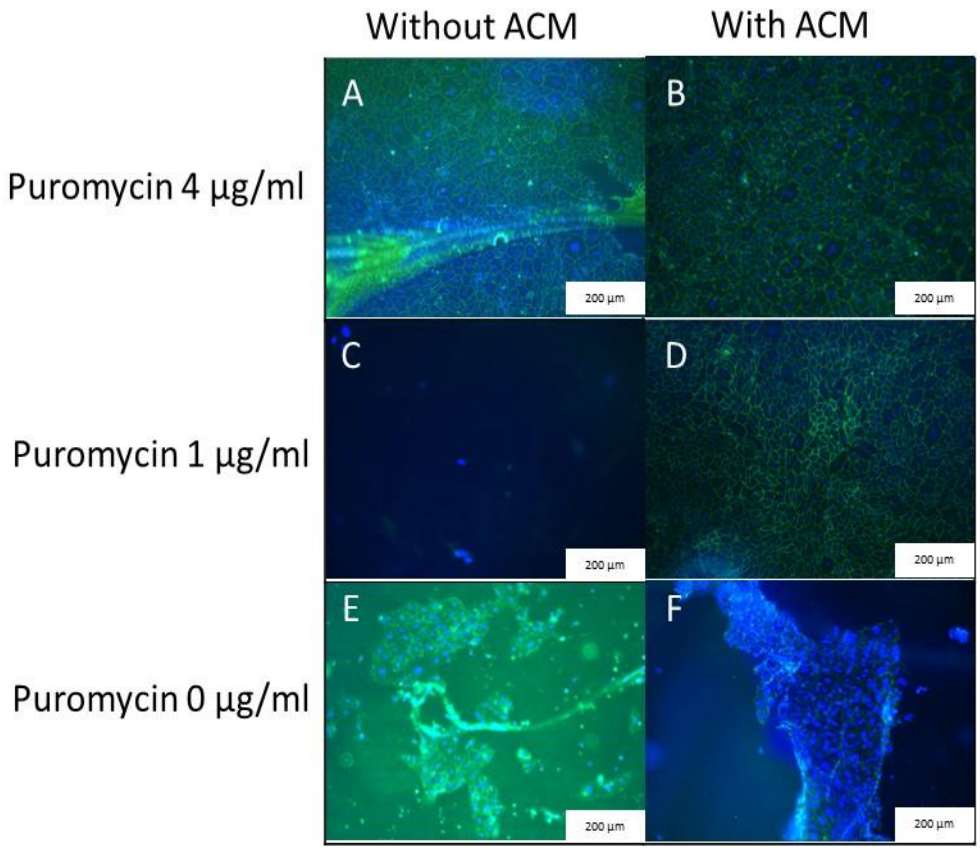

Fig. 3.17: Representative images showing ZO-1 protein localisation in equine brain endothelial cells treated with puromycin and astrocyte-conditioned media (ACM). Representative images are shown of cell treated with 4µg/ml (A & B), 1µg/ml (C & D) and 0µg/ml (E & F) puromycin. (A, C, E) show cells treated in the absence of ACM while (B, D, F) show cells cultured in the presence of ACM. Scale bar = 200µm

3.5.4 Scanning Electron Microscopy images of tight junctions in HBECs

Detailed surface structure of the HBECs was examined using scanning electron microscopy (SEM) imaging.

The surface structure of HBECs in culture exhibited definite, elevated and shoulder to shoulder areas at the cell borders. These features persuasively proposed the formation of tight junctions between the cells. This type of cell architecture was present across the whole well and was consistent between all cells. This supports the findings of the ZO1 immunofluorescence and PCR. Collectively, this strongly suggests the presence of tight junctions between the adjacent cells of the confluent monolayer of HBECs (Fig. 3.18)

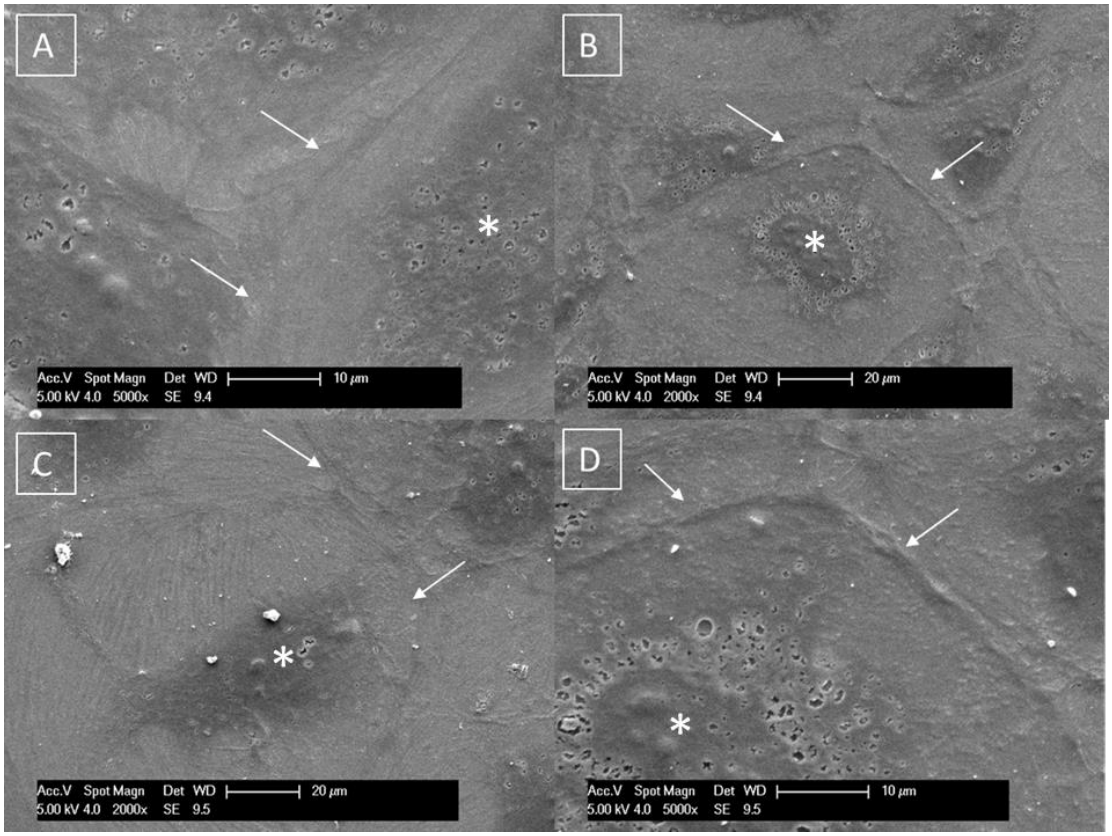

Fig. 3.18: Scanning Electron Microscopy (SEM) images of primary equine brain endothelial cells, following fixation, dehydration and platinum coating. White arrows show the presence of tight junctions in the endothelial cell culture. The asterisk in the images denotes the nucleus. Parameters for microscopy are indicated individually on each image and scale bar represent 10 µm (image A & D) and 20 µm (image B & C) respectively. The holes (largely around nucleus) present in the image are artefacts developed during the processing of the cells.

Cells grown both in presence or absence of puromycin were examined by SEM. The cells treated with puromycin clearly exhibited the presence of one cell type only. All these cells had a cobblestone-like appearance. In stark contrast, the cells cultured in absence of puromycin exhibited a much more mixed phenotype of cells with the presence of astrocytes, pericytes and neurons alongside endothelial-appearing cells. Astrocytes were easily distinguished by their star-like outline (Fig 3.19). Similarly, neurons were easily distinguished by their unique and distintive shape (Fig 3.20). These results suggest exposure to puromycin reduced the growth of other cell types.

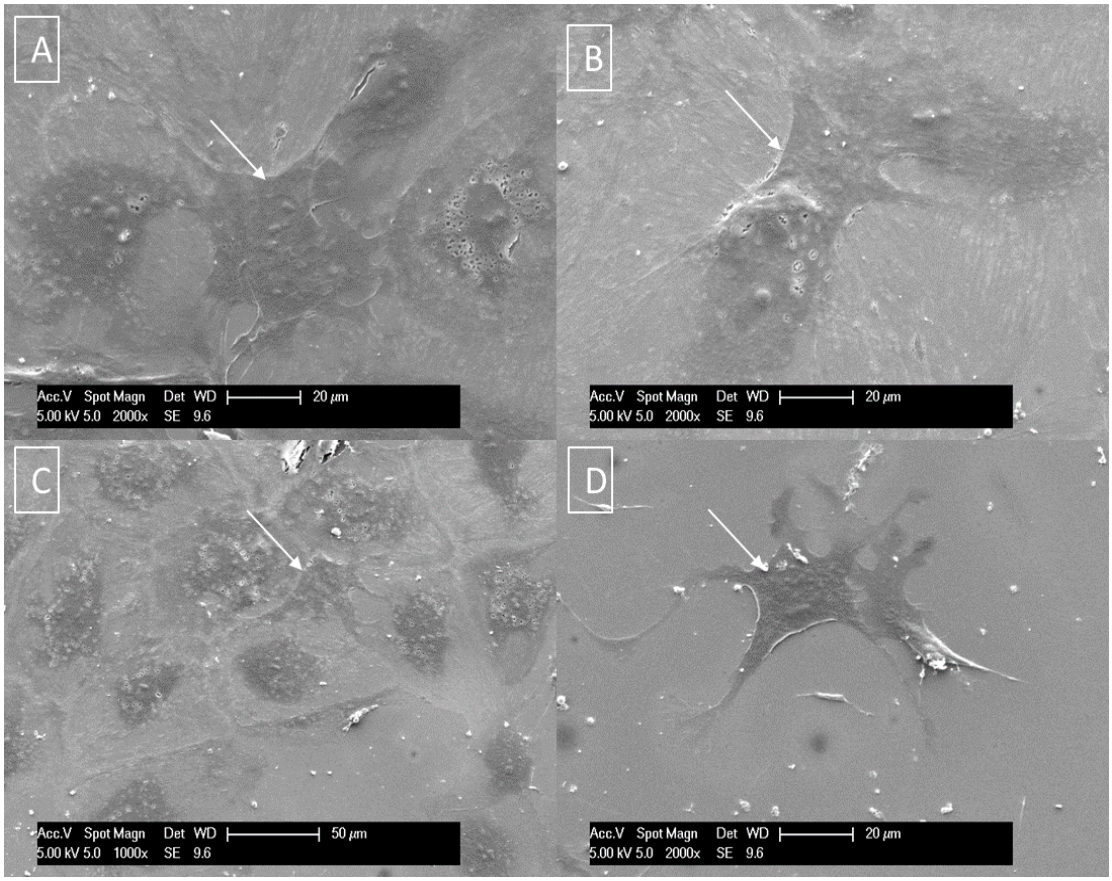

Fig. 3.19: Scanning Electron Microscopy (SEM) images of primary equine brain endothelial cells cultured in absence of puromycin. White arrows indicate presence of astrocytes in the culture of brain endothelial cells. Parameters for microscopy are indicated individually on each image and scale bar represent 20 µm (image A, B & D) and 50 µm (image C).

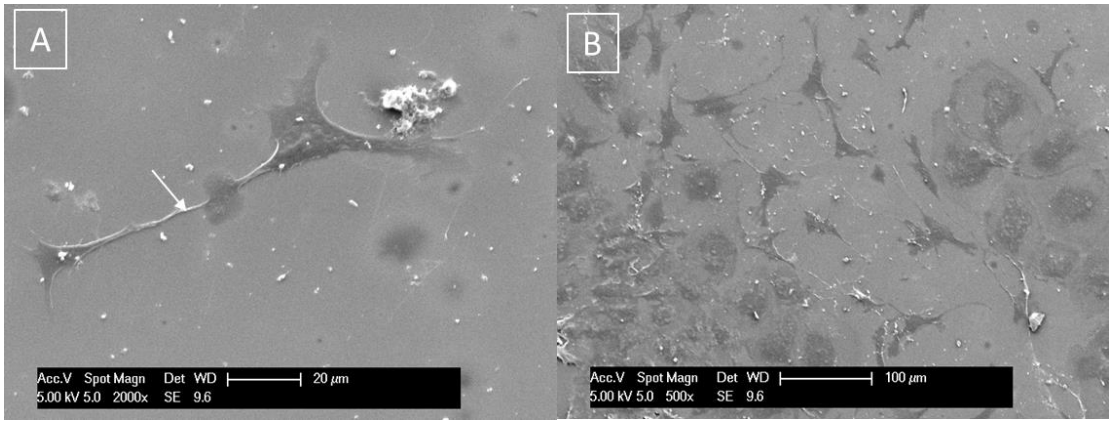

Fig. 3.20: Scanning Electron Microscopy (SEM) images of primary equine brain endothelial cells cultured in absence of puromycin. White arrows indicate presence of neurons in the image A. Image B represents the presence of neurons and pericytes in between the endothelial cell culture grown in absence of puromycin. Parameters for microscopy are indicated individually on each image and scale bar represent 20 µm (image A) and 100 µm (image B)

3.5.5 Transendothelial electrical resistance (TEER) in Transwell cultures of HBECs

TEER values indicate the electrical resistance exhibited by the cell monolayer to the passage of an alternating current. It shows the junctional adhesion between cells and also signifies the ability of the cells to make a tight monolayer of cells (Elbrecht et al., 2016). HBECs were cultured to 85-90% confluence before the cells were transferred to Transwell culture inserts. TEER values were assessed using the EVOM2 voltmeter and ENDOHM-6 voltmeter cup every day for 9 days. TEER values were taken in triplicate.

HBECs were grown in the presence or absence of ACM on the transwell culture plates. Cells treated with ACM exhibited peak TEER value on day 1 (178.3 ± 18.8 Ω.cm^2) which then reduced approximately 4-fold to 46.3 ± 10.3 Ω.cm^2 by day 4. Whereas, the cells cultured in absence of ACM, had peak TEER value on day 2 (219.8 ± 38.2 Ω.cm^2) and similar TEER values on day 3 but thereafter TEER reduced to 90.3 ± 7.4 Ω.cm^2 by day 4. TEER values remained static from day 4 to 9 both for cells treated with and without ACM.. These results suggested that the functional junctional adhesion was greater in the cells grown in the absence of ACM than in the presence of ACM. Additionally, these measurement strongly indicate that early time points were when cells exhibited optimal junctional adhesion for drug transport assays (Fig. 3.21)

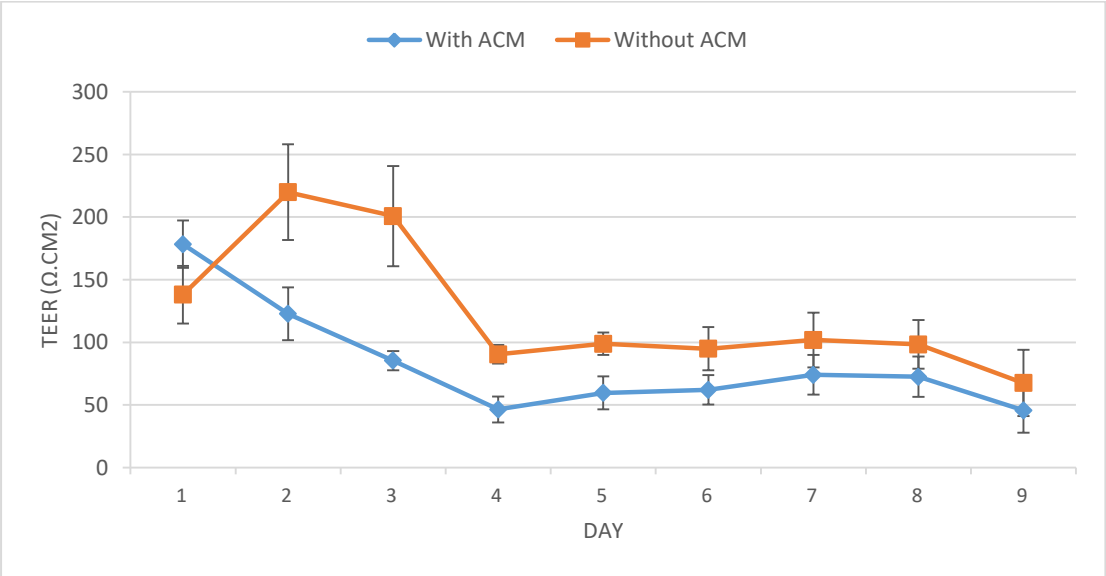

Fig. 3.21: TEER values over time in culture in HBECs treated with or without ACM. Values are Mean ± Standard Deviation from 2 independent cultures. Day means the day after plating the HBECs on the Transwell.

3.5.6 Measurement of FITC-dextran permeability in Transwell cultures of HBECs

The barrier function of the HBEC monolayer was additionally assessed through FITC-conjugated dextran permeability assays. FITC-dextran permeability studies were performed from apical to basal (A-B) chamber of the Transwell plate for a duration of one hour. The transport of FITC-dextran across the HBEC barrier is depicted as a percentage of the no cell control which denotes free diffusion between these Transwell compartments. Cell treated with ACM showed 23.8% permeability of that compared no cell control. Whereas cells without ACM showed 11.8% permeability. FITC-dextran permeability value of cells cultured with ACM is significantly higher (unpaired t-test, $p<0.05$) as compared to cells cultutred without ACM (Table 3.5) This indicated that the HBEC monolayer was restricting the flow of FITC-dextran to a certain but not full extent. These results also supported TEER assay observations, in that the junctional adhesion appeared greater in absence of ACM (Fig. 3.22).

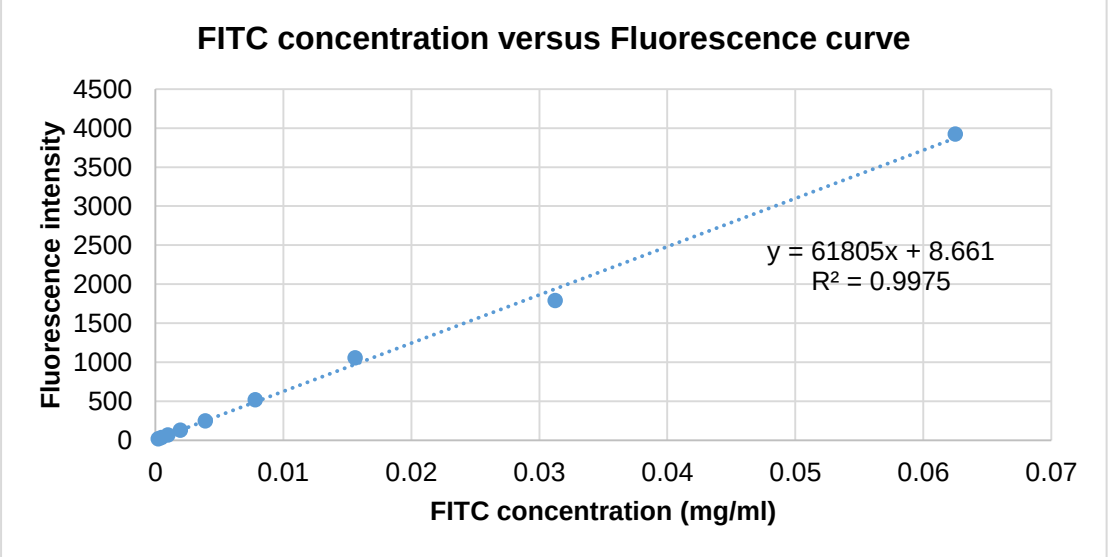

Fig. 3.22: Standard curve of FITC dextran concentration against fluorescence intensity

Table 3.5: Depicting the percentage permeability of FITC-dextran in Transwell cultures of HBECs cultured with ACM and without ACM. n = 4. Values (in third column) are mean ± standard deviation. Permeability values bearing different superscript differ significantly ($p<0.05$) in unpaired t-test.

Sr. No.	Treatment	Permeability of FITC-dextran in comparison to no cell control	Percentage coefficient of variation
1.	Cells cultured in transwells with ACM	23.8 ± 3.6^{a}	15.1
2.	Cells cultured in transwells without ACM	11.8 ± 3.6^{b}	30.3

3.6 Identification of multidrug efflux transporters in HBECs

ABC transporter like P-glycoprotein (P-gp) is accountable for the efflux of large number of drugs (Mahringer & Fricker, 2016). PCR and Western blot analysis were employed to verify the expression of this vital transporter in isolated HBECs.

3.7 qPCR for P-glycoprotein efflux transporter expression in HBECs

The expression of multidrug efflux transporter, P-gp (ABCB1) was analysed using qPCR TaqMan gene expression assay in HBECs in presence or absence of puromycin (4µg/ml) as well as in presence or absence of ACM. GAPDH and β-Actin were used as housekeeping/reference gene and reference gene stability test was conducted on these. Both housekeeping genes were found to be stable across different treatment groups of this qPCR assay (Fig. 3.23 and Table 3.6). The amplification efficiency for P-gp, GAPDH and β-Actin was 98%, 113% and 143% respectively. qPCR showed that the presence of both puromycin and ACM increased the expression of P-glycoprotein ($P>0.05$, Fig 3.24). Whereas treatment with puromycin or ACM alone did not produce change in P-gp expression ($P>0.05$).

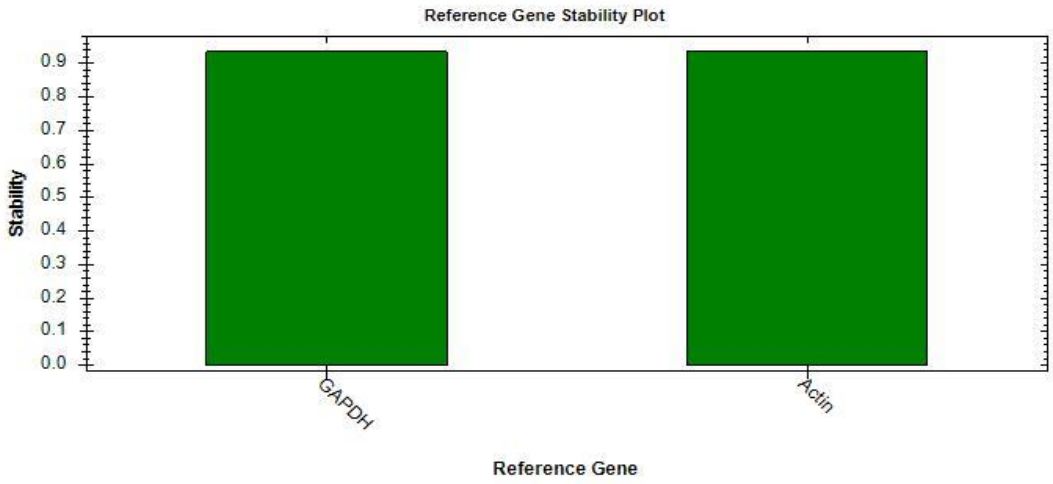

Fig. 3.23: Reference gene stability plot of GAPDH and β-Actin across the different treatment groups of the qPCR assay.

Table 3.6: Showing stability of the housekeeping genes namely GAPDH and β-Actin across the different treatment groups of the qPCR assay.

Order	Gene Name	Evaluation	Avg M Value	Stability (Ln(1/AvgM))	# Samples
1	GAPDH	Ideal	0.392	0.935	3
2	β-Actin	Ideal	0.392	0.935	3

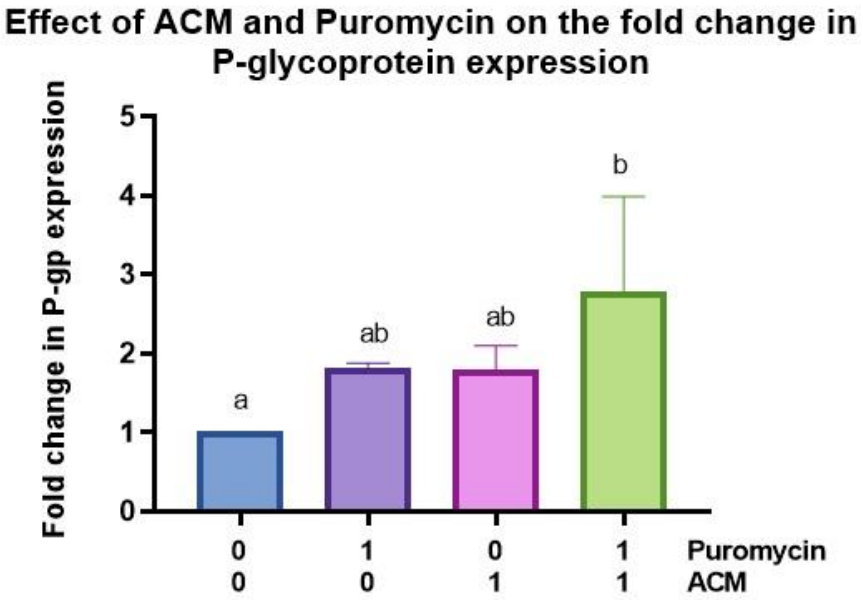

Fig. 3.24: Effect of puromycin and ACM on the fold change expression of P-glycoprotein. n=3, Bars are mean ± std. error of means. Bars having no superscript in common differs significantly (p≤0.05) in one-way ANOVA followed by Tukey's multiple comparisons post-hoc test.

3.8 Assessment of Ÿ-glutamyl transferase (GGT) activity in HBECs

The GGT activity was assessed in HBECs in the presence or absence of puromycin (4 µg/ml) and in the presence or absence of ACM by calculating the amount of p-nitroanilide substrate produced from Ÿ-glutamyl-p-nitroanilide precursor added to the HBEC cell culture in a 96 well plate. Results of this study showed that, all cultures of HBECs yielded a steady amount of p-nitroanilide per unit time per mg protein. Cultured HBECs exhibited maximum GGT activity per min per mg protein when both puromycin and ACM were present. Minimum GGT activity was exhibited by those cells which were cultured in the presence of puromycin but no ACM (Table 3.7)

Table 3.7: The γ-Glutamayl transferase (GGT) activity of HBECs grown in 96 well plate under different treatments. Data are mean. Two replicates were taken from one culture but from different wells. The individual replicates have been written in parenthesis.

Treatment	Amount of P-Nitroaniline generated (µg/ml)	GGT activity ($pmol.min^{-1}$)	Protein concentration (mg/ml)	GGT activity ($pmol.min^{-1}.mg\ protein^{-1}$)
Puromycin+ACM	2.41 (3.51 and 1.31)	0.182 (0.266 and 0.098	0.102 (0.108 and 0.095)	8.536 (12.439 and 4.632)
Puromycin+NO ACM	1.21 (1.16 and 1.26)	0.091 (0.087 and 0.095)	0.166 (0.163 and 0.169)	2.623 (2.515 and 2.730)
NO Puromycin + ACM	1.45 (1.60 and 1.30)	0.110 (0.121 and 0.099)	0.128 (0.141 and 0.116)	4.093 (4.510 and 3.675)
NO Puromycin + NO ACM	1.33 (1.45 and 1.21)	0.101 (0.110 and 0.092)	0.157 (0.173 and 0.142)	3.050 (3.333 and 2.766)

3.9 Discussion

The main emphasis of this Chapter was to establish a consistent, dependable and realistic method to culture HBECs, by determining the purity of the cell cultures at different concentrations of puromycin and to characterise the BBB phenotype of the isolated cells when cultured *in vitro*.

In the present study, the cultured primary HBECs expressed key efflux transporters, endothelial cell markers and produced tight intercellular junctions. This means that this system can be used to explore the transport of drugs across the BBB.

3.9.1 Isolation and culture of HBECs

Most isolation methods use one of two primary isolation techniques for brain endothelial cells. The methods described by (Abbott et al., 1992; Rosas-Hernandez et al., 2018) were primary focussed on homogenising the cerebral tissue in an enzyme digest, and this was followed by a density dependent centrifugation to separate the endothelial cells from myelinated cells. But, a subsequent method, developed by (Nielsen et al., 2017b), used filtration to separate the brain microvessels from the brain homogenate. The isolated capillaries are then exposed to an enzyme digest before plating or before being cryopreserved. This method reliably resulted in production of good yield of capillaries, high cell viability with good cell purity and was time and cost efficient. All cultures used in this study utilised this method

3.9.2 Purification of HBEC culture

To avoid growth of these contaminating cells like astrocytes and pericytes, puromycin was added for first 72 hours, to remove these contaminating cell types (Nielsen et al., 2017b; Perrière et al., 2005). Puromycin is a substrate for P-glycoprotein, an ABC transporter highly expressed in brain endothelial cells. Therefore, puromycin at this concentration will be effluxed out from the brain endothelial cells but will cause apoptosis of other cell types (astrocytes and pericytes) which do not express P-glycoprotein at these higher levels. However, on examination it was concluded from PCR for biomarkers of astrocytes (desmin) and pericytes (PDGFR-β) that puromycin failed to completely remove all contaminating cell types. To further investigate, immunofluorescence (IF) was performed to see the localisation of α-SMA (a pericyte biomarker) in HBEC cultures. Results of this, revealed that a good

number of α-SMA positive cells were present in HBECs without puromycin but no α-SMA positive cells were present in HBECs with puromycin. Thus, it can be hypothesised that puromycin eliminates possible contaminating cells like astrocytes and pericytes but the mRNA of these biomarker molecules were still present and detected due to the high sensitivity of PCR.

3.9.3 Characterisation of HBEC culture

This Chapter has clearly showed that the cultured HBECs expressed both tight junction and adherens junction at the mRNA and protein level. IF staining of HBEC cultures for ZO-1 noticeably depicts the localisation of ZO-1 at the cellular margins/periphery, which is agreement other previous studies (Cantrill et al., 2012; Nielsen et al., 2017b). The presence of VE-cadherin expression from PCR provide clear evidence that adherens junctions are also present in the HBECs. Scanning Electron Microscopy (SEM) of HBECs revealed that tight junctions between the cells appeared like elevated overlapping junctions. SEM investigation also showed that cells not exposed to puromycin exhibited the presence of other contaminating cells like astrocytes, pericytes and neurons. Whereas HBECs exposed to puromycin apparently appeared to be a near pure culture of endothelial cells with no contaminating cells.

3.9.4 TEER and FITC-dextran permeability assay

TEER is the most frequently used parameter to assess the junctional grip in the brain endothelial cell monolayer (Wilhelm et al., 2011). Earlier reports state that, the physiological value of TEER of the BBB *in vivo* can reach 6000 $\Omega.cm^2$ (Srinivasan et al., 2015). On the other hand, contemporary BBB models differ widely in TEER values, with human induced pluripotent stem cells reported values of greater than 4000 $\Omega.cm^2$, with primary cell culture models typically between 100-2000 $\Omega.cm^2$ and immortalised cell lines showing lower values around 30 $\Omega.cm^2$ (Czupalla et al., 2014; Y. I. Wang et al., 2017). The protocol developed by Nielsen et al., 2017 reported that Pig brain endothelial cells (PBECs) alone reached TEER values between 500-2000 $\Omega.cm^2$. In the culture with ACM, TEER value reached its maximum on day 1, which was 178.3 $\Omega.cm^2$and then declines on day 2 onwards. Whereas in the culture without ACM, TEER reached its maximum on day 2 at 219.8 $\Omega.cm^2$ and then declined on day 3 onwards. These TEER readings are similar to the other studies where primary cells were isolated for *in vitro* BBB modelling

(Patabendige et al., 2013). But, TEER values of >1000 Ω.cm^2 was regularly observed in the primary cells which followed the similar isolation technique (Nielsen et al., 2017a). However, the lower TEER values of 100-900 Ω.cm^2 were observed with inexperienced handling of cells during the initial phase of practising the technique (Nielsen et al., 2017b).

In published literature, TEER results are usually reinforced by tracer molecule permeability studies. The most common molecules are dextran, lucifer yellow, mannitol, sucrose (Thomsen et al., 2015b; Y. Zhang et al., 2006). In the present study, the permeability of 4 kDa Fluorescein isothiocyanate (FITC) conjugated dextran was measured through the HBEC monolayer on the Transwell system. Transwell with ACM showed higher permeability in comparison to transwell without ACM.. Contrary to expectations, this indicated that the presence of ACM increased the permeability of the HBEC monolayer. This was unexpected but it could be attributed to the presence of factors like vascular endothelial growth factor A (VEGFA), angiopoietin-1, fibroblast growth factor 2 (FGF2), glial cell line-derived neurotrophic factor (GDNF) in the ACM (Alvarez et al., 2013; Wong et al., 2013). Critically, these factors are all known to increase the permeability of the endothelial cell monolayer (Bates, 2010; Seghezzi et al., 1998).

Even though, it was clear that the cell monolayer was restricting the permeability of the FITC-dextran between the apical and basal chambers of the transwell system, the permeability was higher than the commonly accepted value for permeability studies. For example, the standardised acceptable permeability value for tracer compound is 3% through Caco-2 cell monolayer for high-integrity studies (Yamashita et al., 2000). Moreover, Gericke et al., 2020 reported the permeability of the tracer mannitol as 3% per hour in PBECs. That said, Gericke et al., 2020, reported 10-fold higher TEER values than the TEER values reported in this chapter. Therefore, it is suggested that in this study HBECs were not forming a complete barrier on the transwell system. It is possible that it could also be attributed to a species difference. But still, higher TEER values and lower tracer molecule permeability were achieved with co-culturing PBECs with CTX-TNA2 astrocytes brain endothelial cells. Therefore, further optimisation of the isolation and culture procedures/practices for BBB modelling and permeability assessment are scrutinised in the next Chapter.

3.9.5 P-glycoprotein expression and GGT assay

P-glycoprotein expression was analysed using Western blotting which showed a single band (at the predicted size) for P-gp in HBECs cultured in presence of ACM but no band was observed in the HBECs cultured in the absence of ACM. In the latter set of cells, no housekeeping gene β-Actin band was observed. So, this was assumed that there can be some contamination of proteases in this protein sample resulting in no bands being detected by Western blotting.

Ÿ-Glutamyl transferase (GGT) is a metabolic enzyme which is highly expressed in the brain endothelial cells and is quite commonly used a brain endothelial cell marker. Cultured horse brain endothelial cells exhibited maximum GGT activity when both puromycin and ACM were present and minimum GGT activity was observed in HBECs cultured in the presence of puromycin but without ACM.

3.9.6 Conclusion

In conclusion, these results endorse that a reliable procedure has been established to isolate healthy cultures of horse BECs from horse cerebral tissue. The benefits of this method is that it is inexpensive, trustworthy and can used to repetitively generate a high yield of HBECs. Various molecular and microscopic techniques were employed to verify the presence of mRNA and protein for important BBB phenotype markers: drug transporters, P-gp, GLUT1, BCRP, MRP1 and tight junction proteins, ZO-1, VE-cadherin and enzyme, GGT. TEER measurements and FITC-dextran permeability assays showed that HBECs also exhibited some but limited permeability across the BEC monolayer. Although the TEER values were lower than aimed for and FITC-dextran permeability is not as reported but it is important to remember that this was the first attempt to develop an *in vitro* BBB model using horse BECs. Nevertheless, the presence of key markers of adherens junctions, tight junctions and transporter molecules implies that HBEC culture do possess BBB phenotype and this model can be a suitable candidate for drug permeability studies across BBB monolayer with some more refinements.

Chapter 4

Establishing transwell models of the blood-brain barrier using primary HBECs

4.1 Introduction

In the previous chapter, a reliable method to isolate and culture primary horse brain endothelial cells (HBECs) from horse brain tissue was developed. In this chapter, the progress made in the further development of transwell culture models of HBECs and its application for drug permeability studies will be discussed.

(Gericke et al., 2020; Patabendige, Skinner, & Abbott, 2013; Thomsen et al., 2015a)The main advantage of the transwell system is capability to culture BECs in non-contact co-culture with other cells of NVU like astrocytes (Bicker et al., 2014). Earlier studies showed that addition of astrocytes to the transwell model of BECs affected the expression of tight junction proteins, metabolic enzymes and drug transporters like P-gp and GLUT1 (Cantrill et al., 2012; Gaillard et al., 2000; Toth et al., 2018). As most of the astrocyte-endothelial cell communications are facilitated through soluble signalling molecules, addition of astrocyte-conditioned media (ACM) to BECs culture can imitate several benefits of astrocyte co-culture with BECs. But addition of ACM has also decreased the BBB permeability *in vitro* (Nielsen et al., 2017b; Puech et al., 2018).

Transwell plates were not put on shaking incubator during the permeability studies (i.e. FITC dextran permeability studies and test drugs permeability studies) and as it was observed during the preliminary experiments that shaking disrupts the confluency of the endothelial cell monolayer. This loss of confluency has direct relation to the permabiltiy of monolayer. Therefore, transwell plated were kept static inside the CO_2 incubator during the permeability studies.

4.1.1 Generation of junctional adhesion by astrocyte co-culture and astrocyte conditioned medium

The number of astrocytes in the brain is 10 times higher than the number of neurons. Also astrocytes play countless roles in controlling the micro milieu of the neuron by sending different chemical signals to BECs and by regulating BBB permeability (Abbott et al., 2006; Zonta et al., 2003). It is very difficult to

isolate primary astrocytes because only the astrocytes collected from neonatal mammals readily propagate and grow *in vitro* (Schildge et al., 2013). This is the main reason behind the use of immortalised astrocytes cell lines like CTX-TNA2 in various BBB models (Wilhelm & Krizbai, 2014). This CTX-TNA2 cell line was established from primary astrocytes isolated from brain frontal cortex tissue of one day old Sprague-Dawley rats (Cantrill et al., 2012). Also, the spent media from primary or immortalised astrocytes (called as astrocyte conditioned media) can enhance the junctional adhesion and reduce the permeability of BEC monolayer (Puech et al., 2018). This chapter will evaluate the impact of co-culture of CTX-TNA2 immortalised cell line or astrocyte conditioned media on the TEER values and FITC –dextran permeability of primary HBEC monolayer.

The main objective of this chapter was to set up a transwell model of BBB using primary HBECs to examine the impact of the addition of astrocyte co-culture and astrocyte conditioned medium (ACM) on the BBB properties of the HBEC monolayer. However, this model, nor any other transwell model has been published using primary horse BECs.

4.2 Methods

4.2.1. Experiment 1: Assessment of HBEC monolayer tightness (TEER) using four different treatments

Transwell experiments were performed with cultured HBECs under various treatment conditions. HBECs were cultured in either transport medium in both apical and basal chambers, ACM in basal chamber and transport medium in apical chamber, transport medium in apical chamber and astrocytes cultured in the basal chamber, three quarters transport medium and 1/4th ACM in both apical and basal chambers. In the astrocyte co-culture wells, astrocytes of CTX-TNA2 cell line were seeded in non-contact co-culture in the basal chamber of the transwell plate and HBECs cultured on the porous semi-permeable insert of the apical chamber (Fig 4.1). In the astrocyte co-culture wells, transport medium was added in the basal wells in which the astrocytes were seeded. TEER was assessed in duplicate using the same procedure for a period of five days.

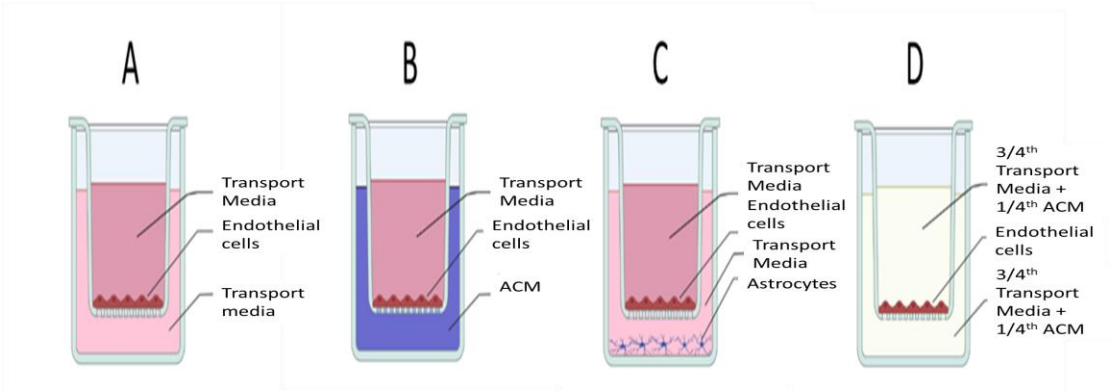

Fig. 4.1: Schematic representation of growth of endothelial cells on transwell inserts. Fig. A depicts the growth of endothelial cells with transport medium in both upper and lower chambers Fig. B depicts the growth of endothelial cells with transport medium in upper chamber and Astrocyte Conditioned Medium in lower chamber Fig C depicts the growth of endothelial cells with transport medium in both chambers plus astrocytes (i.e. CTX/TNA2) in the lower chamber. Fig D depicts the growth of endothelial cells in presence of 3/4th transport medium and 1/4th astrocyte conditioned medium in both upper and lower chambers.

The composition of transport medium is shown in Table 2.8 while the plate layout for the different treatments are shown in Table 4.1.

Table 4.1: Depicts the layout of transwell plate experiment with four treatments were given to HBEC monolayer over period of five days.

	1	2	3	4
A	**TM+TM** **Insert** (250µl TM) ---------- **Well** (800µl TM)	**TM+ACM** **Insert** (250µl TM) ---------- **Well** (800µl ACM)	**TM+Astrocytes** **Insert** **(**250µl TM) ---------- **Well** (800µl TM with astrocytes in the well)	**3/4TM+1/4ACM** **Insert** (187.5µl TM+62.5ul ACM) ---------- **Well** (600µl TM+ 200µl ACM)
B	**TM+TM** **Insert** (250µl TM) ---------- **Well** (800µl TM)	**TM+ACM** **Insert** (250µl TM) ---------- **Well** (800µl ACM)	**TM+Astrocytes** **Insert** **(**250µl TM) ---------- **Well** (800µl TM with astrocytes in the well)	**3/4TM+1/4ACM** **Insert** (187.5µl TM+62.5µl ACM) ---------- **Well** (600µl TM+ 200µl ACM)

TM+TM means Transport medium in both apical and basal chambers; TM+ACM means Transport medium in apical chamber and ACM in basal chamber; TM+Astro means Transport medium in both apical and basal chambers with astrocytes (i.e. CTX-TNA2) cultured on the bottom of basal chamber; 3/4th TM+1/4th ACM means 3/4th volume of Transport medium and 1/4th volume of ACM in both apical and basal chambers. Each treatment was given in two individual transwells.

Then, on each day (up to day 5 of culture), the medium was replaced and the cells were kept continuously in the presence of transport factors (i.e. 250µM cAMP, 550nM hydrocortisone and 17.5µM RO-20-1724).

4.2.2 Experiment 2: Assessment of HBEC monolayer tightness using two selected treatments

Previous transwell experiment in HBECs was repeated to determine which two treatment conditions yielded the optimal results in TEER assay and FITC dextran permeability assay. Namely, HBECs were cultured in either transport medium in both apical and basal chambers or transport medium in apical chamber with ACM in basal chamber (Table 4.2). TEER was assessed in duplicate using the same procedure for a total of four days.

Table 4.2: The layout of transwell plate experiment in which two selected treatments were given to HBEC monolayer over four days.

	1	2
A	**TM+TM** **Insert** (250µl TM) ---------- **Well** (800µl TM)	**TM+ACM** **Insert** (250µl TM ---------- **Well** (800µl ACM)
B	**TM+TM** **Insert** (250µl TM) ---------- **Well** (800µl TM)	**TM+ACM** **Insert** (250µl TM) ---------- **Well** (800µl ACM)

TM+TM: Transport medium in both apical and basal chamber; TM+ACM: Transport medium in apical chamber and ACM in basal chamber. Each treatment was given in duplicate.

4.3 Results

4.3.1. Experiment 1: Assessment of HBEC monolayer tightness (TEER) in four different treatments

Fig. 5.2 shows that all treatments have their highest TEER recorded on day 2, with the numerically highest recorded TEER values measured for Transport media in both chambers at 133.7±53.5 Ω.cm^2. This was followed by ¾ Transport medium and ¼ ACM in both chambers (133.3±31.9 Ω.cm^2), then transport media in apical chamber and ACM in lower chamber (128.3±23.7 Ω.cm^2) and finally astrocyte co-culture with HBECs (88.2±7.7 Ω.cm^2; Table 4.3 and Fig. 4.2). It appeared that addition of astrocytes (i.e. CTX-TNA2) to HBEC co-culture decreased tight junction integrity and exhibited lower TEER values.

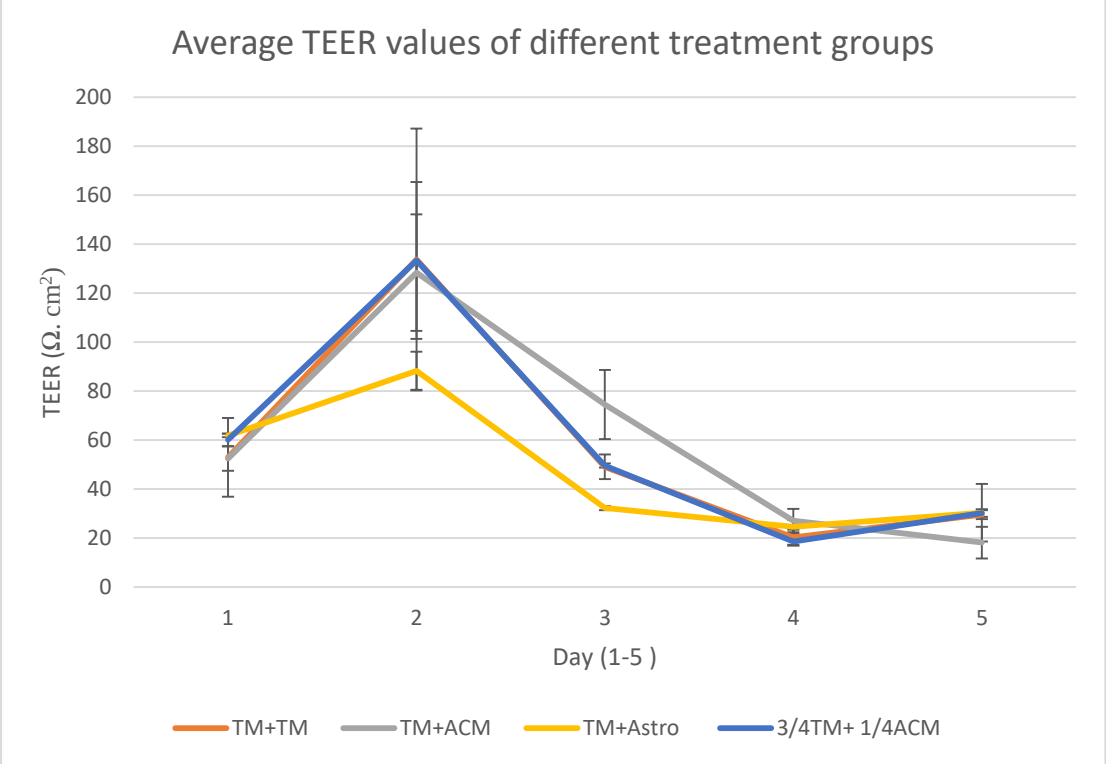

Fig. 4.2: Depicts the TEER over time in cells of different treatment groups over a time course of five days. Values are Mean TEER ± Standard Deviation. n = 6 measurements across two wells. TM+TM: transport medium in both apical and basal chambers; TM+ACM: Transport medium in apical chamber and ACM in basal chamber; TM+Astro: Transport medium in both apical and basal chambers with astrocytes (CTX-TNA2) cultured in the basal chamber; ¾ TM + ¼ ACM means 75% Transport medium and 25% ACM in both apical and basal chambers..

Table 4.3: The average TEER values on the transwell experiment with four treatments over a time period of five days. Values are Mean ± Std. Deviation. n = 6 measurements across two wells.

	Average TEER values (in ohm.cm^2)			
Time points	**TM+TM**	**TM+ACM**	**TM+Astro**	**¾ TM+ ¼ ACM**
Day 1	52.9 ± 16.1	52.4 ± 4.9	61.9 ± 0.6	60.1 ± 2.5
Day 2	133.7 ± 53.5	128.3 ± 23.7	88.2 ± 7.7	133.3 ± 31.9
Day 3	49.0 ± 5.0	74.5 ± 14.1	32.2 ± 0.8	49.6 ± 0.8
Day 4	20.3 ± 3.0	27.1 ± 4.7	24.5 ± 2.7	18.6 ± 1.7
Day 5	29.5 ± 1.7	18.1 ± 6.5	30.4 ± 11.7	30.2 ± 1.5

TM+TM: transport medium in both apical and basal chambers; TM+ACM: Transport medium in apical chamber and ACM in basal chamber; TM+Astro: Transport medium in both apical and basal chambers with astrocytes (CTX-TNA2) cultured in the basal chamber; ¾ TM + ¼ ACM means 75% Transport medium and 25% ACM in both apical and basal chambers

4.3.2 Permeability of FITC-Dextran in HBEC monolayer with four different treatments

To further investigate the effect of the different treatments on the tight junction function, FITC-dextran permeability studies were conducted on day 2 when TEER values were at their peak. The same treatment groups were as mentioned in section 4.2.1 The permeability of the FITC dextran from the apical to basal chamber was calculated as in methods section.

HBECs with transport media in both apical and basal chamber showed 15.7±2.5% permeability, while those with transport media in the apical chamber and ACM in the basal chamber had lower permeability (6.2±1.7%; $p<0.05$). HBECs cultured with transport media in the upper chamber and astrocytes in the lower chamber had similar permeability (16.0 ± 4.6%, $p>0.05$) to the controls. Likewise, HBECs cultured with ¾ transport media and ¼ ACM in both chamber were not different (21.3±3.6%; Table 4.4).

Table 4.4: The average FITC-Dextran permeability values on the transwell inserts at the time of peak TEER values (Day 2) in comparison to the no cell control group. Values are Mean ± SD

Treatment	**FITC dextran permeability (%)**
TM+TM	15.7 ± 2.5[a]
TM+ACM	6.2 ±1.7[b]
TM+Astro	16.0 ± 4.6[a]
3/4TM+ 1/4ACM	21.3 ± 3.6[a]

TM+TM: Transport medium in both apical and basal chambers; TM+ACM: Transport medium in apical chamber and ACM in basal chamber; TM+Astro: Transport medium in both apical and basal chambers with astrocytes (CTX-TNA2) cultured in basal chamber; ¾ TM+¼ ACM: 75% Transport medium and 25% ACM in both apical and basal chambers.n= 4 meaurements across two inserts. a<b; P<0.05

Therefore, this FITC-permeability study demonstrated that transport media in the apical chamber with ACM in the basal chamber was the most effective at intensifying the junctional tightness across the HBEC monolayer.

4.3.3 Experiment 2: Assessment of HBEC monolayer tightness using two selected treatments

In both treatments, the highest TEER was again recorded on day 2 of culture (Fig. 4.3). Numerically, the highest recorded TEER was when there was transport media in the apical chamber and ACM in the basal chamber at 122.7 ± 6.4 Ω.cm^2. In contrast, the TEER transport media in both apical and basal chamber was approximately 25% lower at 94.1 ± 22.6 Ω.cm^2 (Table 4.5). This suggested exposure of the HBEC monolayer to ACM increased tight junction integrity and thus exhibited higher TEER values than the controls.

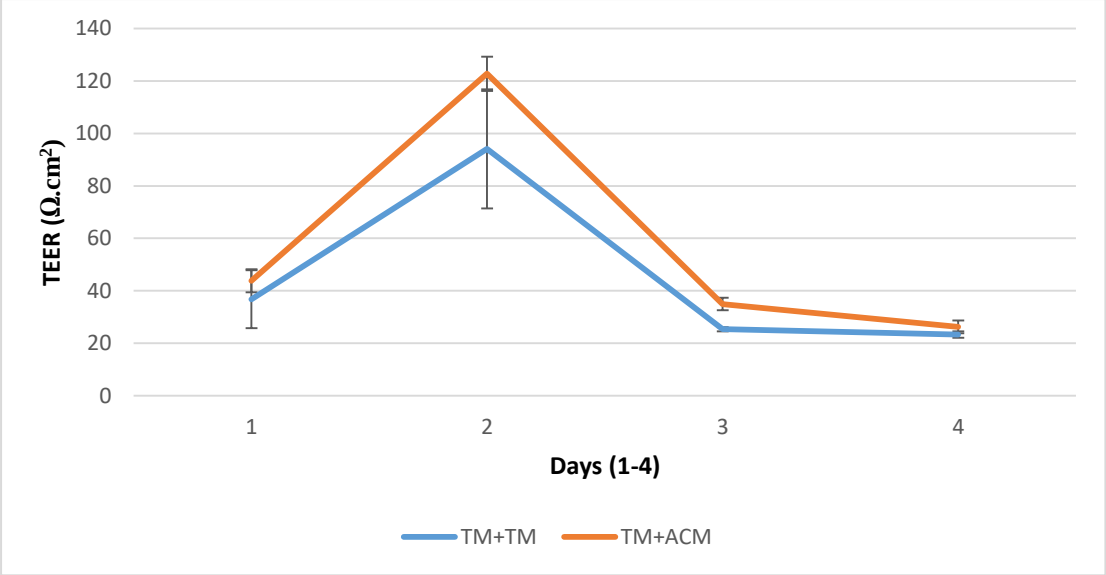

Fig. 4.3: Effect of ACM on the TEER in HBECs in transwells over a time course of 4 days. First treatment was transport medium in both apical and basal chambers and second treatment group was transport medium in apical chamber and ACM in basal chamber.n = 6 measurements aross 2 wells. Values are Mean ± SD.

Table 4.5: The average TEER values on the transwell experiment with two treatments over a time period of four days. Values are Mean ± SD.

	TEER values (in ohm.cm^2)	
Time points	**TM+TM**	**TM+ACM**
Day 1	36.7 ± 11.0	43.8 ± 4.4
Day 2	94.1 ± 22.6	122.7 ± 6.4
Day 3	25.3 ± 0.7	34.9 ± 2.3
Day 4	23.3 ± 1.2	26.2 ± 2.4

TM+TM: Transport medium in both apical and basal chamber; TM+ACM:Transport medium in apical chamber and ACM in basal chamber. n =6 measurements across 2 wells.

4.3.4 Permeability of FITC-Dextran in HBEC monolayer with two selected treatments at the peak of TEER value (i.e. Day 2)

To further investigate the effect of ACM upon the function of the tight junctions, FITC-dextran permeability studies were conducted on day 2 of

culture when TEER was at its peak. Two treatment groups were used as mentioned in the previous section. The permeability percentages of the groups were in comparison to the no cell controls.

HBECs cultured with transport media in both apical and basal chambers showed 6.94% permeability which was very similar to that observed for HBECs cultured with ACM in the basal chamber (6.86% permeability) (Table 4.6). The permeability values were clearly lower than those observed in Section 4.3.2.

Table 4.6: The FITC-Dextran permeability on the transwell inserts at the time of peak TEER values (Day 2) in comparison to the no cell controls. Values are Mean ± SD.

Treatment	FITC dextran permeability (%)
TM+TM	6.94 ± 3.46
TM+ACM	6.86 ± 1.49

TM+TM: Transport medium in both apical and basal chambers; TM+ACM: Transport medium in apical chamber and ACM in basal chamber. n = 4 measurements across two inserts.

The recovery for FTIC-dextran was similar across all groups at 73-82%.

The results of this experiment indicates that presence of ACM did not decrease the FITC dextran permeability of the HBEC monolayer.

4.3.5 Permeability of FITC-Dextran in HBEC monolayer with two selected treatments after passing of the peak of TEER value (Day 4)

FITC-dextran permeability studies were repeated but on day 4 of culture when TEER values had passed their peak and were declining. Two treatment groups were used as mentioned in the previous section. Both these permeability percentages of the treatment groups are in comparison to the no cell control group.

Both treatments showed higher permeability than observed on day 2 of culture. HBECS cultured with transport media in both apical and basal

chambers showed 11.66% permeability while those with ACM in the basal chamber showed 19.22% permeability (Table 4.7).

Table 4.7: FITC-Dextran permeability in transwell inserts after passing the time of peak TEER values (Day 4) in comparison to the no cell control group. Values are Mean ±SD.

Treatment	FITC dextran permeability (%)
TM+TM	11.66 ± 3.36
TM+ACM	19.22 ± 0.41

TM+TM: Transport medium in both apical and basal chambers; TM+ACM: Transport medium in apical chamber and ACM in basal chamber. n = 4 measurements acroos 2 wells.

For this experiment, FITC-dextran recoveries were lower and around 51-56%

Results of this experiment showed that on day 4 of culture, the FITC-dextran permeability in HBECs culture with transport media only was higher than those where ACM in the basal chamber. This was different to that observed on day 2 of culture when TEER was at its peak. This indicate that HBECs exposed to ACM in the basal chamber might loses their tightness faster than the TM+TM cells.

4.3.6 Correlation between TEER and FITC-dextran permeability

The correlation between the TEER values and FITC-dextran permeability on the same day was performed using Pearson's regression.

The correlation was -0.84 indicating a very strong negative relationship between the TEER values and FITC-dextran permeability. Specifically, this meant as the TEER increased FITC-dextran permeability decreased and vice-versa (Fig. 4.4).

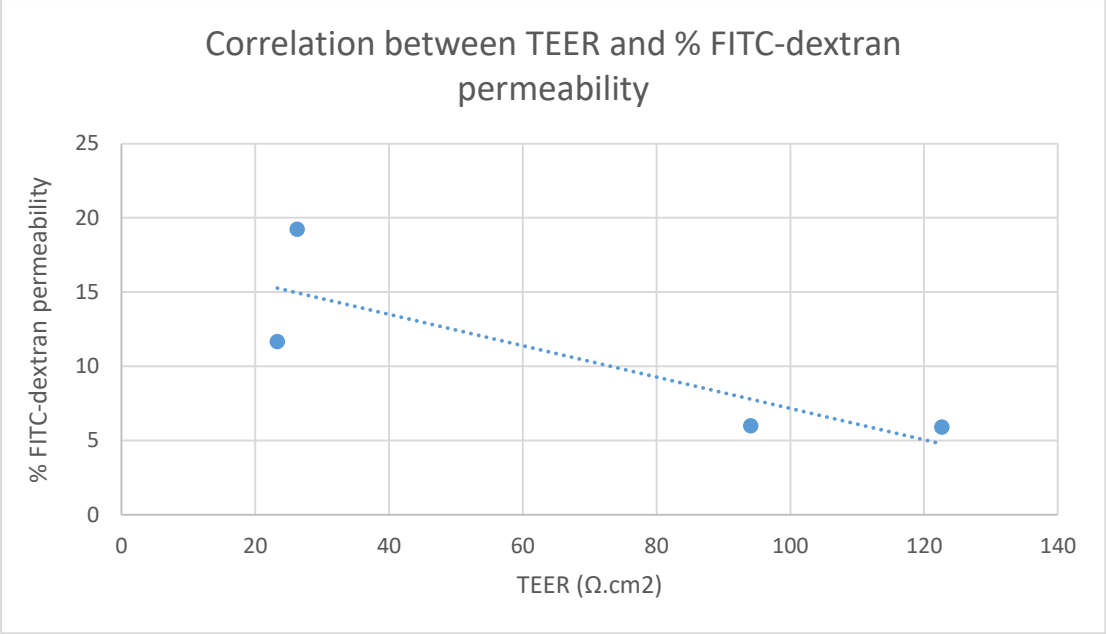

Fig. 4.4: The correlation between the TEER (Ω.cm2) and percentage dextran permeability. The Pearson's R-Square value for correlation between TEER (Ω.cm2) and percentage dextran permeability is -0.84 (n=4).

4.4 Discussion

The main objective of this chapter was to set up a transwell model of the BBB using primary HBECs and also to ascertain the effect of different treatments like exposure to ACM and astrocyte co-culture on the BBB properties like permeability and TEER. It is quite evident that co-culture of astrocytes (CTX-TNA2 cell line) along with HBECs failed to enhance the tight junction integrity of HBEC monolayer.

For the establishment of a transwell model of the BBB, HBECs were cultured upon 24 well semi-permeable transwell membrane inserts (6mm diameter). This transwell model of BBB was maintained by the addition of a supplemented media. Previously using a transwell model of brain endothelial cell culture that certain signalling factors are required for the HBEC monolayer to achieve the best possible TEER values (Cantrill et al., 2012). This supplemented media contained cyclic adenosine monophosphate (cAMP), hydrocortisone and RO 20-1724. Also signalling induced by cAMP enhanced the expression of the tight junction protein, claudin-5 and also supported the tight junction functions in the BBB (Ishizaki et al., 2003).

The presence of hydrocortisone also can enhance tightness in the junctional adhesion between the BECs and upregulates claudin-5 and occludin

expression in the BECs (C. Förster et al., 2008). RO20-1724 was added to the supplemented media as a selective inhibitor of cAMP-specific phosphodiesterase and thus increases intracellular cAMP. It has been proposed that mechanism of astrocyte-endothelial cell signalling require increased cellular availability of cAMP and hydrocortisone (Abbott, 2002). Vascular endothelial growth factor A (VEGFA) was not added to the supplemented media as its can diminish tight junction adhesion and promote vascular permeability (W. Wang et al., 2001).

In this present study, TEER was considered as the indicator of barrier resistance for the HBEC monolayer transwell model of BBB. Documented *in vivo* evidence showed TEER values for the BBB ranging from 1000 to 6000 $\Omega.cm^2$ in rats (Howarth et al., 1992). Results from this chapter have exhibited that much lower TEER values in transwell model of HBECs 94.1-122.7 $\Omega.cm^2$ at the peak. There was evidence that the addition of ACM increased TEER by 25%. But, these results were not repeated in a second experiment. The barrier resistance data obtained from TEER measurements is also corroborated by the permeability data for the diffusion of 4kD FITC-dextran across the HBEC monolayer. In this experiment, the permeability of the HBEC monolayer exposed to ACM was significantly lower than the HBEC monolayer not exposed to ACM on the day when the TEER was at its peak. The tight junctions present between the HBECs should restrict the paracellular transport of large molecules (>500 Da), therefore limiting the permeability of the FITC-dextran to permeate through the transcellular pathway.

The current study demonstrated that addition of ACM increased the functional tight junction formation in the transwell model of BBB. Similar findings from other studies on the transwell models of BBB also supports the concept that astrocyte signalling encourages the BBB characteristics of the BECs and also strengthens barrier tightness of the BEC monolayer (Cantrill et al., 2012; Nielsen et al., 2017b; Puech et al., 2018). The ACM used in this study was produced using primary human astrocyte culture. So, the findings of this study are in agreement with others which states that the signalling molecules from astrocytes of one species can stimulate the BBB characteristics of BECs from another species. Namely, astrocytes of rat origin induced barrier properties in chick BECs (Janzer & Raff, 1987). Similarly, in porcine BECs there was no

difference in the function of barrier tightness in their co-culture with astrocytes from rats or pigs (Cantrill et al., 2012). This suggests that there is some conservation of BEC-astrocyte signalling molecules between various species. That said, the effects were smaller than expected and it is feasible than the signalling molecules have lower efficacy in the horse. The exact mechanism of action of astrocyte signalling with the BECs has not yet fully been clarified. However, some reports state the Wnt signalling pathway and upregulation of alkaline phosphatase have important function in induction of barrier tightness in the BECs (Liebner & Plate, 2010; Meyer et al., 1991). It also have been proposed that the astrocyte signalling can increase intracellular cAMP. The basal transport medium contained signalling molecule that replicated cAMP function and this could explain the lower than expected response to ACM.

In the present study, co-culture with immortalised astrocyte cell line (CTX-TNA2) failed to stimulate barrier properties of the HBEC monolayer but the addition of ACM obtained from primary astrocytes augmented barrier properties in HBEC monolayer. This is, in contrast, to a previous study where no difference was observed when co-cultured using primary or immortalised astrocytes (Cantrill et al., 2012). It has been hypothesised that astrocytes in culture may undergo genotypic and phenotypic change (Cuiping et al., 2009). So, it can be hypothesised, that in the present study astrocyte CTX-TNA2 cell line used in transwell model of co-culture with HBECs may have acquired a molecular phenotype entirely changed from the original primary cells..

The present study showed that TEER value consistently reaches its maximum on day 2 of culture (after the transfer of HBECs from culture flask to the transwell). The time to reach peak TEER value was consistent across various independent HBEC cultures and was unaffected by treatment. In the present study, the time taken for HBECs reach their maximum TEER value was much shorter than that stated by other similar studies. For example, the highest TEER value was achieved after 6 days of transfer in transwell culture (Cantrill et al., 2012; Gericke et al., 2020; Y. Zhang et al., 2006). Similarly, in some other studies BECs were cultured for up to 2 weeks before the commencement of TEER assay (Thomsen et al., 2015a). Whereas in this present study, maximum TEER value and lowest FITC-dextran permeability were achieved two days after of the transfer of cells in the transwell system.

This longer time taken to achieve peak TEER values may be due to the difference in the seeding density of the HBECs on the transwell inserts. In the present study 8 X 10^4 horse brain endothelial cells were passaged to each transwell insert with a culture area of 0.33cm^2 equivalent to 24 X 10^4 cells per cm^2. Other studies used of lower seeding density per cm^2 of culture area and as a result more time was taken to make the monolayer confluent. This also explains early decline in the TEER values in the present study as HBECs may have become over confluent in less time and possibly leading to multi layering, pre-mature death and detachment of cells. This is the first study on the *in vitro* BBB in which primary BECs of horse origin has been employed. Cellular physiology and cellular processes can totally vary between species. Although further research is required to be carried out using confocal microscopy to ascertain the effect of seeding density on the TEER value and degree of confluence achieved.

It has also been observed in this study that, HBECs exposed to ACM might have lost their junctional tightness faster than the control-treated HBECs. This can be explained by ACM might have stimulated over confluence and multi layering of BECs resulting in more cellular death and detachment eventually leading to increased FITC-dextran permeability. This warrants further investigation.

In summary, this Chapter has characterised how HBECs behave in transwell culture and how they will behave in drug permeability studies. It was evident that day 2 of culture yielded in peak TEER and that this was the optimal day for drug permeability testing. While, there was no definite evidence for the best supplements to maximise TEER and minimise permeability, the most appropriate regime would be to include ACM. There was a couple of reasons for this: 1) ACM improved the barrier function of HBECs on occasion and 2) horse endothelial cells in the BBB are continuously exposed to astrocyte signalling so this feels more physiologically relevant.

Chapter 5:

Assessment of drug transport in the transwell model of Horse BBB

5.1 Background

Absence of a robust, trustworthy and well-characterised model of blood-brain barrier (BBB) is the main impediment in the development of new drugs that act on brain (Bicker et al., 2014). Out of the Transwell models characterised in the previous chapter, the model in which ACM was added in the lower chamber exhibited highest TEER and lowest permeability. Therefore, this transwell model of BBB was used for specific drug transport studies. In this chapter, the transport of selected drugs across the transwell model of horse BBB developed using HBECs will be discussed.

Eight test drugs were carefully chosen for drug permeability studies in the horse Transwell model of BBB. These test drugs were selected based on molecular weight, lipophilicity and for known drug-transporter interactions.

Several *in vitro* methods are available to determine the permeability of a new drug and its communications with various drug efflux pumps and drug transporters at the level of BBB. Apparent permeability (P_{app}) is an established parameter for quantitative assessment of the rate of permeability of a drug across cell barrier layer P_{app} is calculated using Equation 1.3, which remains accurate while drug transport between *in vitro* compartments is 1) linear; 2) <10% of the drug has passed between the compartments; 3) when there is insignificant backflow between the compartments and 4) a good mass balance ((Tran et al., 2004). A substitute to P_{app}, is P_{exact} (calculated using equation 1.1 & 1.2), has been subsequently derived to provide a mathematical explanation for the entire curve of the drug transport process and when there are mass balance issues (Tran et al., 2004). In this chapter, both P_{app} and P_{exact} were calculated for some selected test drugs to observe the rate of permeability of these across the Transwell model of horse BBB. It also examined the role of any drug efflux pump/drug transporter in the transport of these selected drugs across the Transwell model of horse BBB.

Thus, results presented in this chapter estimate the rate of permeability of these selected test drugs across the Transwell model of Horse BBB are an indication of drug-drug transporter interaction.

5.2 Methods

For methodology part of the analysis of drug transport in Transwell see section 2.19 for details. The criteria on selection of test drugs are detailed in section 2.19.1. Briefly, to select the most appropriate drugs for use in transport studies, a drug database of permeability parameters for various centrally and non-centrally acting drugs was created. Published literature was used as the basis of this database. The data obtained for each drug/compound were as follows: LogP, molecular weight, drug target, known BBB transporter interactions (Table 5.1). Test drugs were selected to cover different multidrug efflux transporters, LogP values, lipophilicity and molecular weights.

Table 5.1 Selected test drugs and their characteristic properties

S. No.	Drug	Target	Log P	Log D at assay pH	MW (g/mol)	Transporter	Lipophilicity	Ionisation at physiological pH
1	loperamide	Non-CNS	5.13	3.61 (Rana et al., 2020)	477.0	MDR1 substrate (Zoghbi et al., 2008)	High	Ionised
2	chlorpromazine	CNS	5.41	3.24 (Rana et al., 2020)	318.9	MDR1 substrate (J. S. Wang et al., 2006)	High	Ionised
3	lamotrigine	CNS	1.93	1.24 (Rana et al., 2020)	256.1	MDR1 substrate (Potschka et al., 2002)	High	Un-ionised
4	topiramate	CNS	0.13	2.15 (Rana et al., 2020)	339.4	MDR1 substrate (Luna-Tortós et al., 2009)	High	Un-ionised

5	mitoxantrone	Non-CNS	-3.1	-1.58 (Rana et al., 2020)	444.5	BCRP substrate (Miyake et al., 1999)	Medium	Ionised
6	camptothecin	Non-CNS	1.74	-1.74	348.4	BCRP substrate (Maliepaard et al., 2001; Kawabata et al., 2001)	High	Un-ionised
7	methotrexate	Non-CNS	-1.85	-5.10 (Rana et al., 2020)	454.4	MRP1 substrate (Cole, 2014)	Poor	Ionised
8	etoposide	Non-CNS	0.6	0.27 (Rana et al., 2020)	588.6	MRP1 substrate (Sakamoto et al., 1998)	High	Un-ionised

1. LogP is defined as the partition coefficient of a molecule between aqueous and lipophilic phases usually considered as octanol and water. It indicates which drugs will have significant binding to plastic in the transwell system.

2. LogD is distribution co-efficient of octanol and water measured at specific pH. But unlike LogP which only describes the lipophilicity of unionised compounds. LogD changes with pH and also takes into account all species of a compound at specific pH like ionzed, unionized and partially ionized. Therefore, it provides a better understanding of a compounds lipophlicity at various pH.

3. Assay pH means the pH of the transwell contents at the time of drug permeability studies. As both the apical and basal chambers were having Hank's Balanced Salt Solution (HBSS) and pH of HBSS used in this study was 7.4.

All the eight selected drugs were chosen based on a defined selection criteria which was as follows:

1) to ensure that there is no or limited non-specific binding by highly lipophilic drugs, all drugs had a logP value of <+5.5.

2) loperamide, chlorpromazine, lamotrigine and topiramate are all substrates of MDR1/P-gp which mean that these drugs are actively effluxed from the brain to the blood compartment by the MDR1/P-gp efflux pump.

3) mitoxantrone and camptothecin are substrate for BCRP efflux transporter molecule.

4) methotrexate and etoposide are substrate for MPR1 efflux pump (Table 6.1).

For experimental design of the assessment of drug transport and methodology of measuring permeability of drugs please refer to section 2.20.3.

For methodology of analysis of test drug samples using liquid chromatography-mass spectrometry (LC-MS), see section 2.20.4. for details. Briefly, sample analysis was performed at Boots Building, School of Pharmacy, University of Nottingham, UK. Dilutions of each drug from10 mM stock was made using 1:1 methanol: HBSS yielding the following concentrations: 1, 10, 25, 50, 100, 250, 500, 1000 nM. Where a higher concentration calibration line was required, the following concentrations were used: 1, 10, 25, 50, 100, 250, 500, 1000, 10000 nM.

For this analysis Solvent A was water with 2mM ammonium acetate and 0.1% formic acid while solvent B was acetonitrile with 0.1% formic acid. All drugs were analysed using ESI in positive ion mode except topiramate which was analysed in negative ion mode. Lansoprazole drug was kept as internal standard at the concentration of 1µM. The standard curves are shown in Appendix 2 and the concentration of each drug determined by linear regression using the Multiquant 3.0.3 software. This was verified using Excel. Each sample was analysed in triplicate.

The characteristics of each selected drug and their mass transitions are shown in Table 5.2

Table 5.2: Molecular weights, LogP and mass transitions of drugs with mass spectrometer (LC-MS-MS)

S.no.	Drug	Molecular weight (Da)	LogP	Mass Transition with Mass Spec
1	camptothecin	348.35	1.74	**349.2** > 305.3, 220.2, 248.2
2	chlorpromazine	318.86	5.18	**319.1** > 86.2, 58.1
3	loperamide	477.00	4.77	**477.2** > 266.1, 210.0
4	etoposide	588.56	0.60	**589.2** > 229.2, 185.0
5	lamotrigine	256.10	2.57	**256.1** > 43.4, 211.0, 157.1
6	methotrexate	454.40	-1.85	**455.1** > 308.2, 175.0, 134.1
7	topiramate	339.36	0.13	**338.2** > 78.0, 95.7
8	mitoxantrone	444.48	-3.10	**445.2** > 88.2, 358.1

1. *LogP is defined as the partition coefficient of a molecule between aqueous and lipophilic phases usually considered as octanol and water. It indicates which drugs have significant binding to plastic in the transwell system.*
2. *All drugs except topiramate are in positive ion spray mode. topiramate is in negative ion spray mode. The mass of parent ion is one more than the molecular mass due to the addition of one proton. In case of topiramate the mass of parent ion is one less than the molecular mass due to the loss of one proton.*
3. *For mass transition, parent ion is in bold followed by daughter ions.*

The retention time and lower limit of detection for each drug are shown in Table 5.3. For most drugs, the lower limit was 10nM but for 3 drugs it was higher, notably for etoposide (250nM).

Table 5.3: Retention time (RT) and lower limit of detection (LLOD) of drugs on LC-MS-MS (QTRAP4000)

S.No.	Name of drug	RT[1]	LLOD[2]
1	camptothecin	3.01	10nM
2	chlorpromazine	3.09	10nM
3	loperamide	3.34	1nM
4	etoposide	2.99	250nM
5	lamotrigine	2.37	10nM
6	methotrexate	2.21	10nM
7	topiramate	3.13	25nM
8	mitoxantrone	2.23	25nM

[1]Retention time (RT) is a measure of the time taken for a solute to pass through a chromatography column. It is the interval between the injection of a sample and the detection of substances in that sample.

[2]Lower limit of detection (LLOD) is the lowest concentration of the drug that can be detected by the LC-MS-MS. This LLOD was determined by feeding the LC-MS-MS with samples of cocktail of drugs at different concentrations. The lowest concentration that can be detected by LC-MS-MS will be taken/termed as LLOD.

5.3 Results

5.3.1 Assessment of quality control of the mass spectrometry (MS) for each drug

To check the precision (measurement repeatability) of the mass spectrometer sixteen injections of a mixture of eight drugs were analysed by MS. Standard deviations and % coefficient of variations (CV) were calculated from the results of the MS for sixteen injections of the same mixture of eight drugs. %CV was satisfactory (<15%) for most drugs (Table 5.4) except topiramate (81.7%), miloxantrone (26.9%) and etoposide (20.8%). Thus, all data regarding topiramate should be viewed with caution.

Table 5.4 Percent coefficient of variation of individual test drugs when 16 same injections of mixture of 8 test drugs analysed by Mass Spectrometry

S.No.	Name of the drug	Percent coefficient of variation
1	loperamide	12.7
2	chlorpromazine	13.1
3	lamotrigine	9.7
4	topiramate	81.7
5	mitoxantrone	26.9
6	camptothecin	9.07
7	methotrexate	9.84
8	etoposide	20.8

5.3.2 Observations from the no cell controls.

A no cell control experiment was performed on empty transwell plates in which the movement of drug was estimated from apical to basal chamber (A-B) and basal to apical (B-A) chamber at different time points (30, 60 and 120 minutes). For most drugs, the recoveries for each drug were between 88 – 244% at 30 minute time point. Likewise, the recoveries for each drug were between 61 – 214% at 60 minute time point. For most drugs, the recoveries for each drug were between 66- 193% at 120 minute time point. The recovery for chlorpromazine at all the three time points was higher than this but was felt valid to continue as the studies are predominantly focused on relative concentrations.(Appendix A3, Table A3.1 to A3.24 and Table A3.49 to A3.51),

Apparent permeability (P_{app}), Exact Permeability (P_{exact}) and efflux ratios at different time points were calculated. (Appendix 5, Table A5.1 to A5.4) (Fig. 5.1-5.6).

5.3.2.1 Apparent permeability of the test drugs in no cell control (NCC) studies performed on empty Transwell Plates

Drug transport studies were performed across no cell control as well as with HBEC. P_{app} was significantly higher in HBECs than NCC for drugs like loperamide, chlorpromazine and mitoxantrone at all the three time points in both A-B and B-A directions. Whereas for drugs like lamotrigine and camptothecin, P_{app} remained significantly higher in HBECs than NCC at 30 minutes in A-B direction, but P_{app} remained the same for both lamotrigine and camptothecin at all the three time points in B-A direction. P_{app} remained statistically same for drugs like topiramate, methotrexate and etoposide at all three time points in both A-B and B-A directions. (Appendix 5, Table A5.1) (Fig. 5.1 and 5.2)

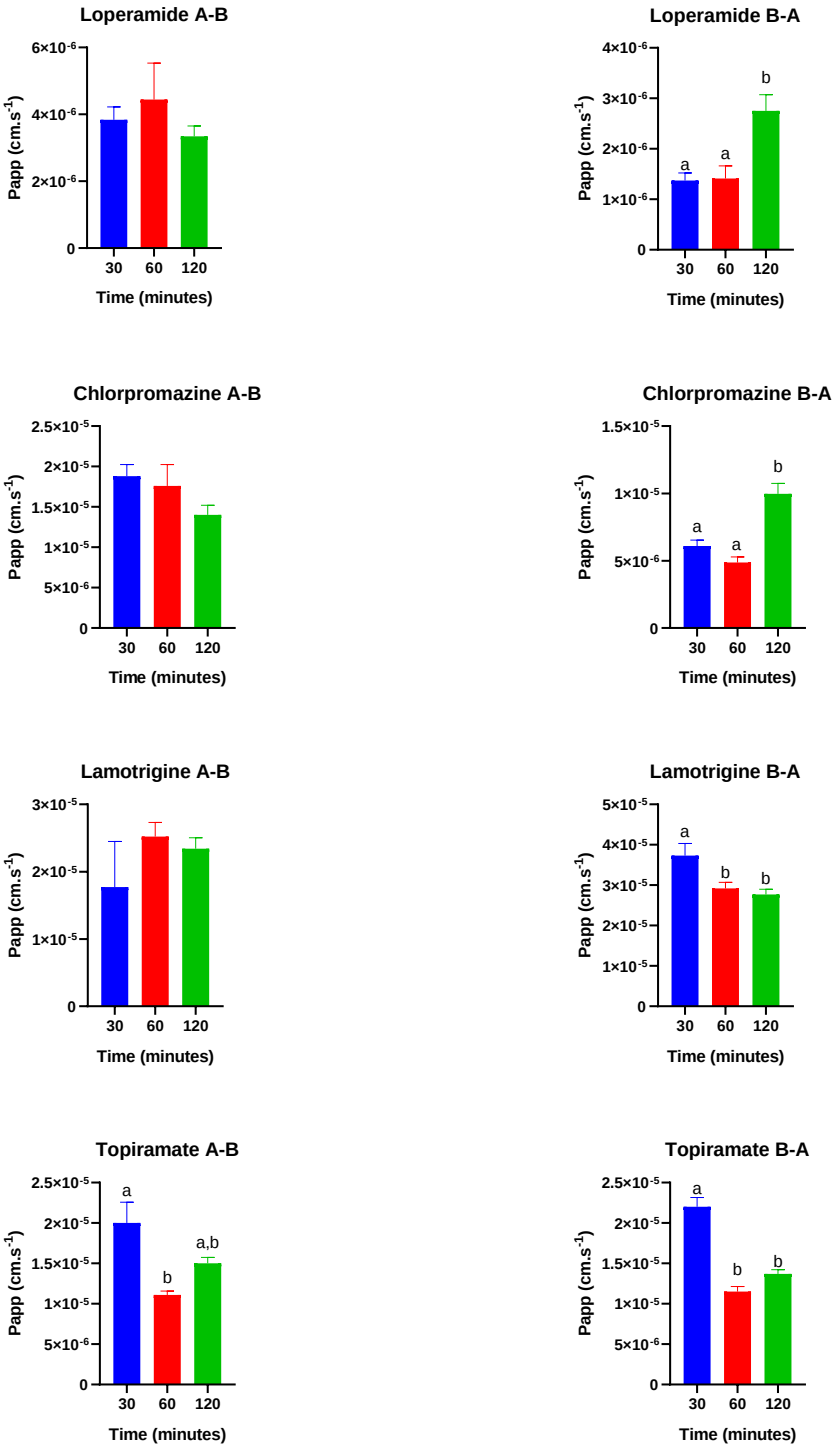

Fig. 5.1: Apparent permeability (P_{app}) values of various drugs (loperamide, chlorpromazine, lamotrigine and topiramate) from the no cell control studies in apical-to-basal (A-B) and basal-to-apical (B-A) directions at 30-, 60- and 120-minute time points. Bars shown are mean ± SEM for n=6 replicates for each drug and time point. Six replicates mean six different wells were used. Bars bearing different superscript differ ($P<0.05$) in one-way ANOVA followed by Tukey's multiple comparison post-hoc test. Further Apparent permeability calculations and concentrations of no cell control studies are in Appendix 3.

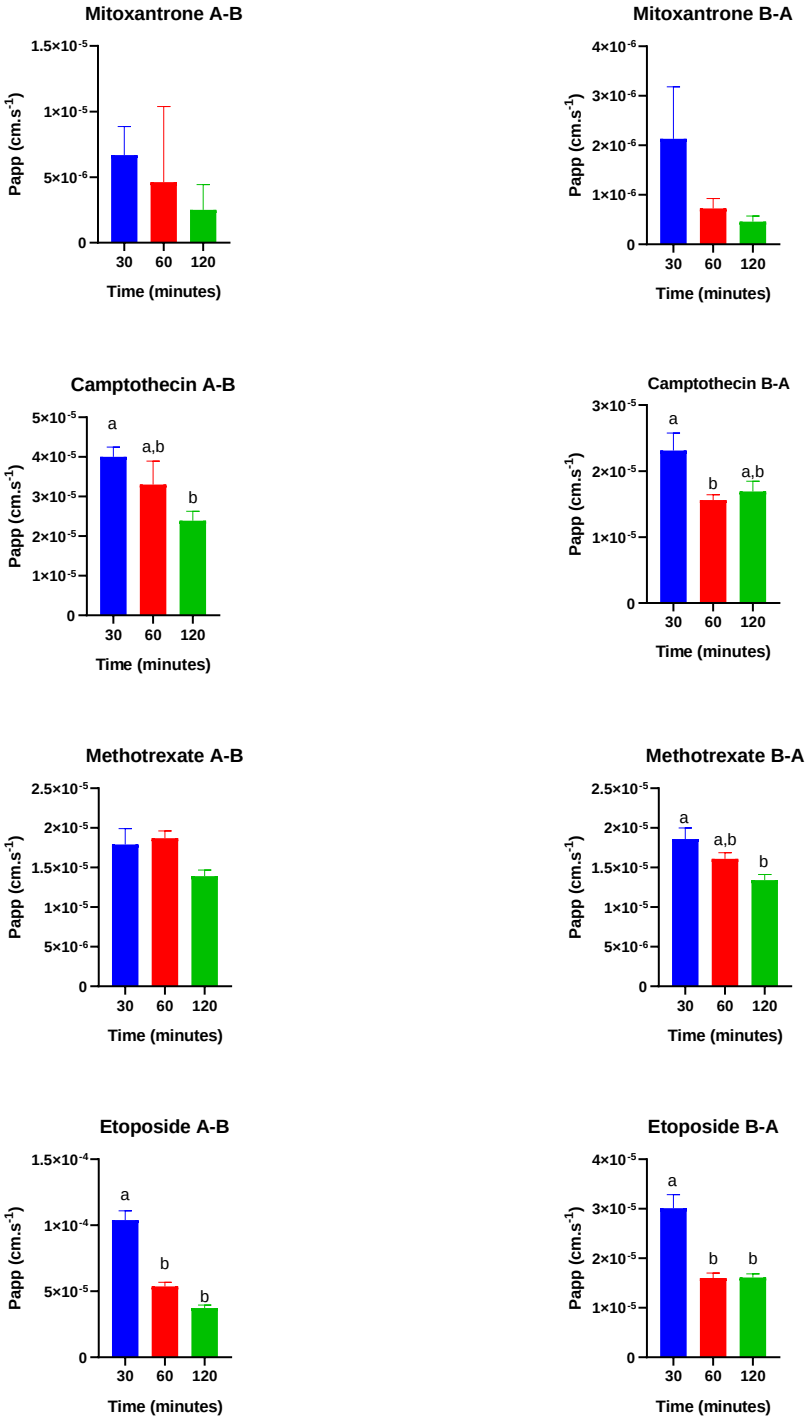

Fig. 5.2: Apparent permeability (P_{app}) values of various drugs (mitoxantrone, camptothecin, methotrexate and etoposide) from the no cell control studies in apical-to-basal (A-B) and basal-to-apical (B-A) directions at 30-, 60- and 120-minute time points. Bars shown are mean ± SEM for n=6 replicates for each drug and time point. Six replicates mean six different wells were used. Bars bearing different superscript differ ($P<0.05$) in one-way ANOVA followed by Tukey's multiple comparison post-hoc test. Further Apparent permeability calculations and concentrations of no cell control studies are in Appendix 3.

5.3.2.2 Exact permeability of the test drugs in no cell control studies performed on empty Transwell Plates

As mentioned earlier, drug transport studies were performed across no cell control as well as HBEC on transwell system of BBB. P_{exact} was significantly higher in case HBEC than NCC for drugs like chlorpromazine and mitoxantrone at all the three time points in both A-B and B-A directions. For loperamide, P_{exact} value remained significantly higher for HBEC than for NCC at all the three time points in A-B direction but P_{exact} value for loperamide remained statistically similar in both HBEC and NCC at 60 and 120 minutes in B-A direction. Although, P_{exact} value for loperamide at 30 minutes remained statistically higher for HBEC than NCC in B-A direction. For lamotrigine and camptothecin, P_{exact} value of HBEC is significantly higher than NCC at 30 minutes in A-B direction but P_{exact} value remained similar between HBEC and NCC for lamotrigine and camptothecin at all the three time points in B-A direction. Likewise, for topiramate, P_{exact} for HBEC was higher for HBEC than for NCC at 30 minutes in B-A direction but were similar between HBEC and NCC across all the three time points in A-B direction (Appendix 5, Table A5.2 and A5.6) (Fig. 5.17 and 5.18)

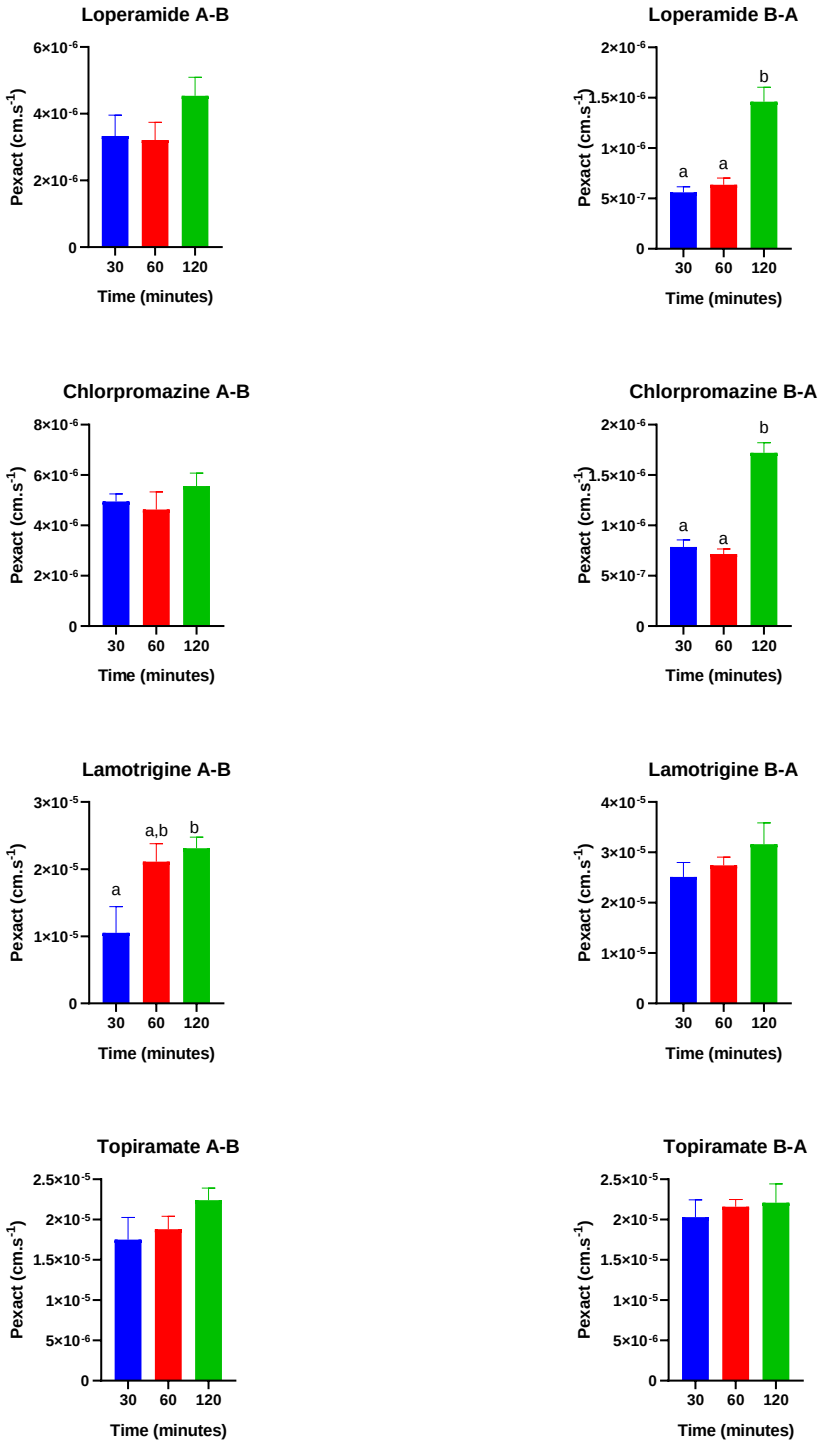

Fig. 5.3: Exact permeability (P_{exact}) values of various drugs (loperamide, chlorpromazine, lamotrigine and topiramate) from the no cell control studies in apical-to-basal (A-B) and basal-to-apical (B-A) directions at 30-, 60- and 120-minute time points. Bars shown are mean ± SEM for n=6 replicates for each drug and time point. Six replicates mean six different wells were used. Bars bearing different superscript differ (P<0.05) in one-way ANOVA followed by Tukey's multiple comparison post-hoc test. Further Exact permeability calculations and concentrations of no cell control studies are in Appendix 3.

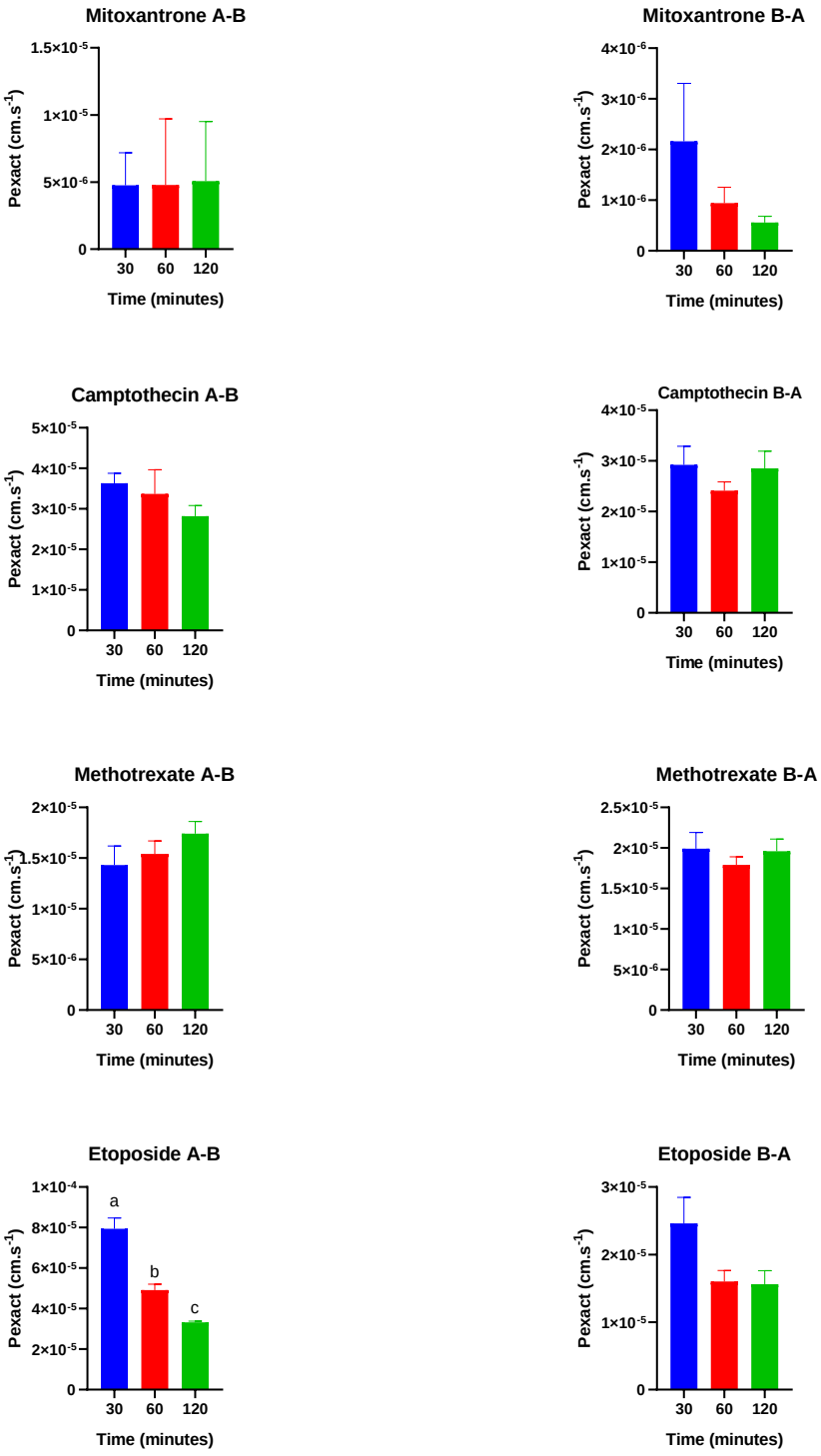

Fig. 5.4: Exact permeability (P_{exact}) values of various drugs (mitoxantrone, camptothecin, methotrexate and etoposide) from the no cell control studies in apical-to-basal (A-B) and basal-to-apical (B-A) directions at 30-, 60- and 120-minute time points. Bars shown are mean ± SEM for n=6 replicates for each drug and time point. Six replicates mean six different wells were used. Bars bearing different superscript differ (P<0.05) in one-way ANOVA followed by Tukey's multiple comparison post-hoc test. Further Exact permeability calculations and concentrations of no cell control studies are in Appendix 3.

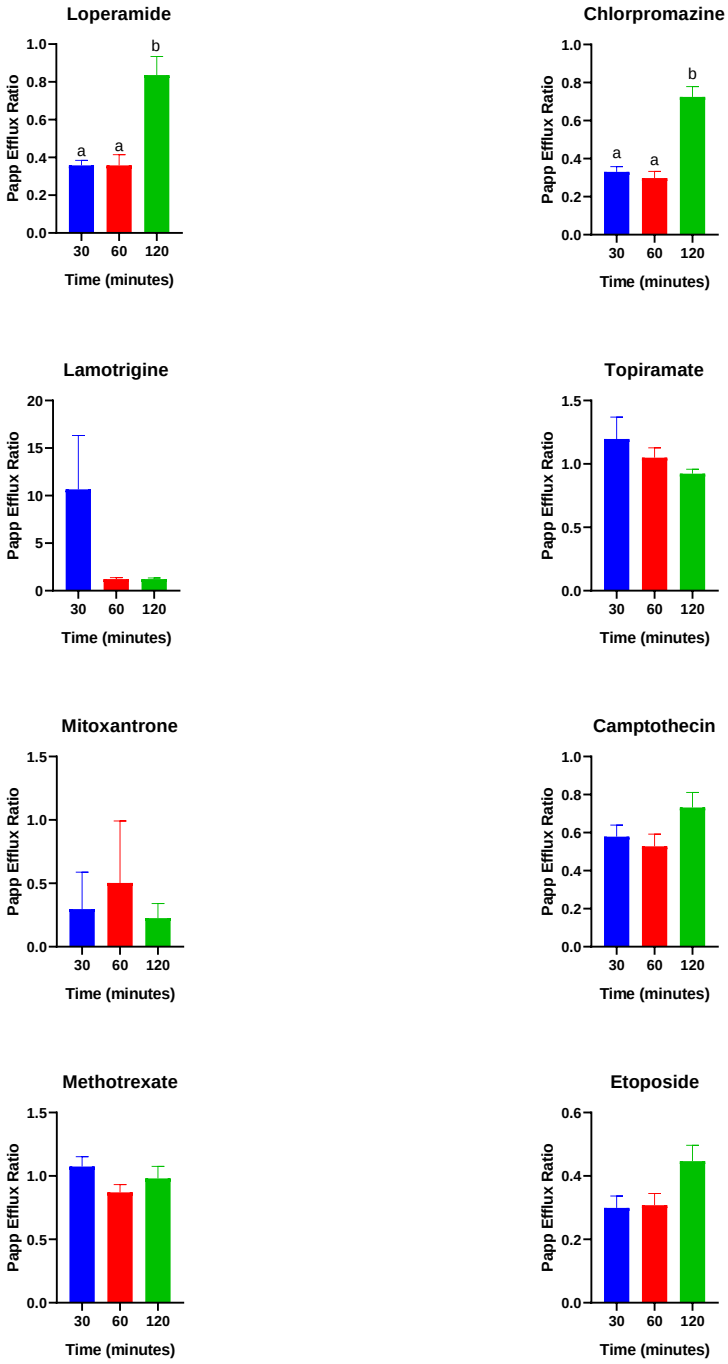

Fig. 5.5: Efflux ratio from apparent permeability (P_{app}) of test drugs from the no cell controls in apical-to-basal (A-B) and basal-to-apical (B-A) directions performed on transwell plates at 30-, 60- and 120-minute time points. Bars shown are mean ± SEM for n=6 replicates for each drug and time point. Six replicates mean six different wells were used. Bars with different superscripts differ (P<0.05) in one-way ANOVA followed by Tukey's multiple comparison post-hoc test. Further Efflux ratio from apparent permeability (P_{app}) calculations of no cell control studies are in Appendix 3.

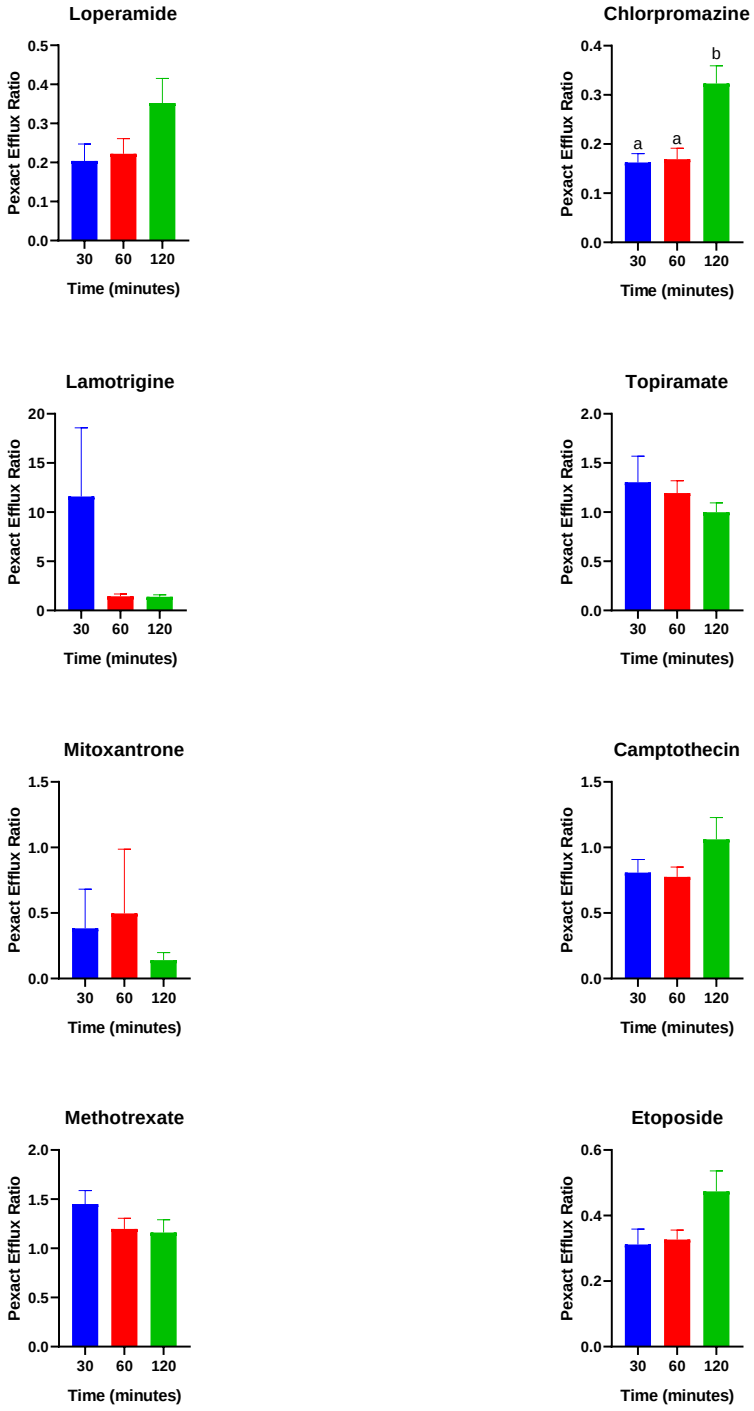

Fig. 5.6: Efflux ratio from exact permeability (P_{exact}) of test drugs from the no cell controls in apical-to-basal (A-B) and basal-to-apical (B-A) directions performed on transwell plates at 30-, 60- and 120-minute time points. Bars shown are mean ± SEM for n=6 replicates for each drug and time point. Six replicates mean six different wells were used. Bars with different superscripts differ (P<0.05) in one-way ANOVA followed by Tukey's multiple comparison post-hoc test. Further Efflux ratio from exact permeability (P_{exact}) calculations of no cell control studies are in Appendix 3.

5.3.3 Drug Transport studies

Transport studies were conducted in Transwell model of cultured primary HBECs in presence of culture media and ACM employing different concentrations of these eight selected drugs. Permeability was assessed in triplicate for each drug individually. Permeability studies were conducted both from apical-to-basal (A-B) and basal-to-apical (B-A) directions. Transwell cultures of HBECs were incubated with each drug separately by employing experiments separately for 30-, 60- and 120-minutes. Drug permeability parameters were calculated using equations 1.1, 1.2 and 1.3 given in Chapter 1. Standard curves used to calculate drug concentrations are available in Appendix 2.

As previously mentioned, apparent permeability (P_{app}) and exact permeability (P_{exact}) values symbolises the rate of drug transport across the cell monolayer between two compartments. P_{app} and P_{exact} values were calculated for all the eight selected test drugs at 30 minutes, 60 minutes and 120 minutes intervals in both apical-to-basal (A-B) and basal-to-apical (B-A) directions (Appendix 5, Table A5.5 and A5.6) (Fig. 5.7, to 5.12). Similarly, Efflux Ratios were derived from P_{app} and P_{exact} for each test drug (Appendix 5, Table A5.7 and A5.8) (Fig. 5.13 and 5.14)

5.3.3.1 Apparent permeability of the test drugs across Transwell model of Horse blood-brain barrier

Apparent permeability (P_{app}) and Exact permeability (P_{exact}) symbolise the rate of drug transport across a monolayer. P_{app} values were significantly different in both directions and across time points for some drugs. P_{app} was higher for loperamide at 30 minutes than at 60 and 120 minutes in A-B direction whereas it was similar at all time points in B-A direction. P_{app} for chlorpromazine was highest at 30 minutes, decreased at 60 minute and was lowest at 120 minutes in both A-B and B-A directions. For mitoxantrone, P_{app} was higher at 30 minutes than at 60 and 120 minutes in both A-B and B-A directions. For etoposide, P_{app} remained same in A-B direction across all the three time points whereas in B-A direction P_{app} was higher at 30 minutes than at 120 minute (Appendix 5, Table A5.5) (Fig. 5.7, 5.8 and 5.9). There was no difference over time for the remaining drugs.

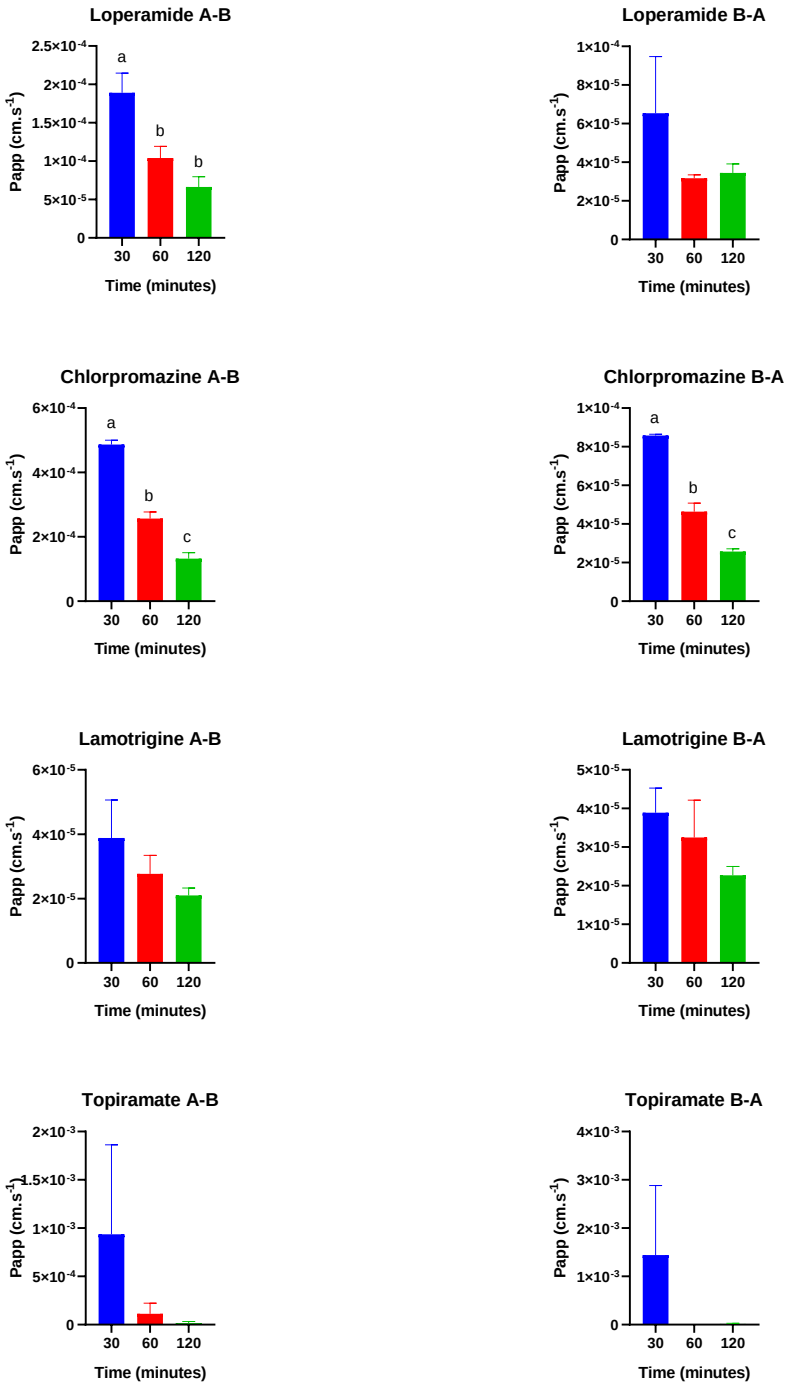

Fig. 5.7: Apparent permeability (P_{app}) values of various drugs (loperamide, chlorpromazine, lamotrigine and topiramate) conducted on transwell model of horse BBB in apical-to-basal (A-B) and basal-to-apical (B-A) directions at 30-, 60- and 120-minute time points. Bars shown are mean ± SEM for n=3 replicates for each drug and time point. Three replicates mean three independent experiments were carried out with three different animals. Bars bearing different superscript differ (P<0.05) in one-way ANOVA followed by Tukey's multiple comparison post-hoc test. Further Apparent permeability calculations and concentrations of transwell model of horse BBB studies are in Appendix 4.

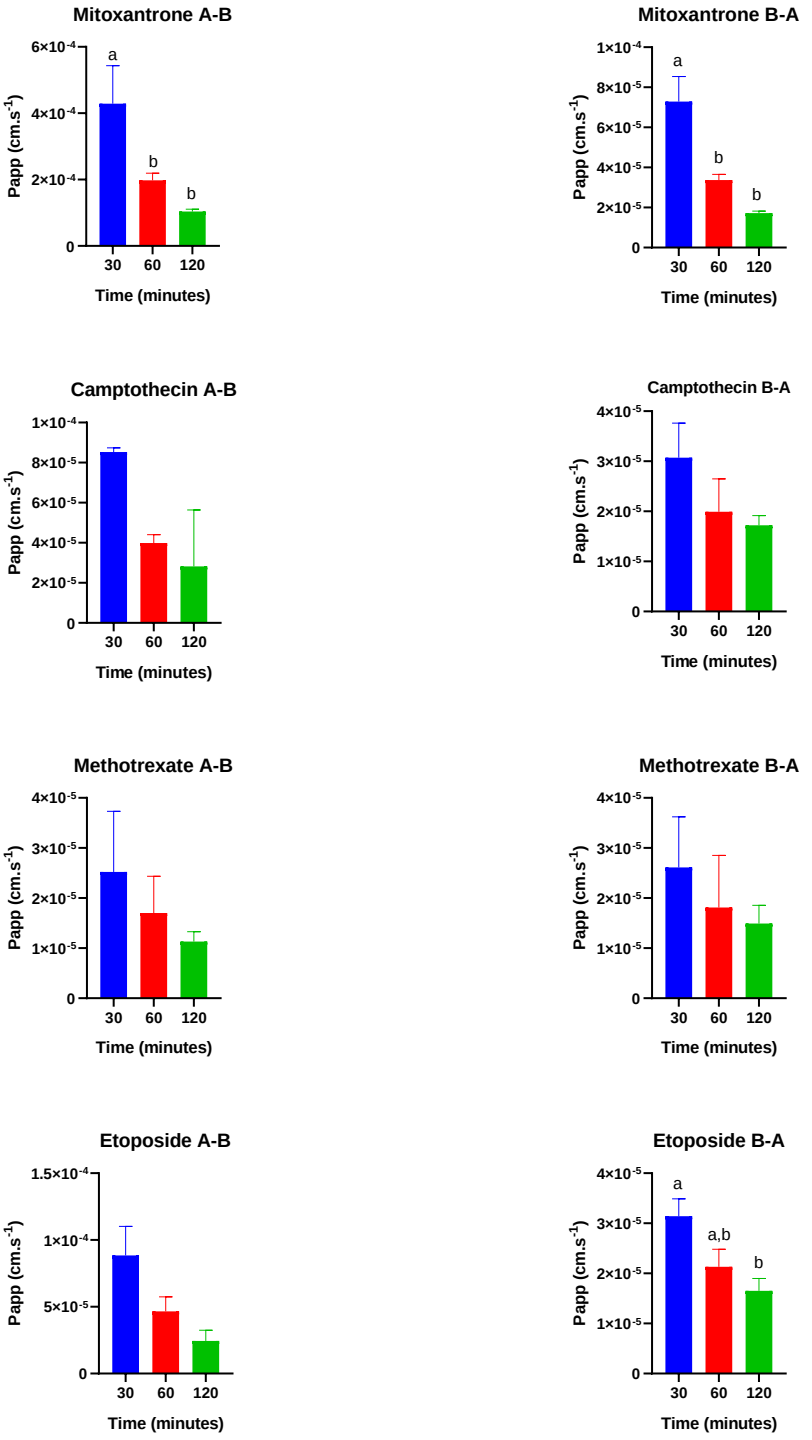

Fig. 5.8: Apparent permeability (P_{app}) values of various drugs (mitoxantrone, camptothecin, methotrexate and etoposide) conducted on transwell model of horse BBB in apical-to-basal (A-B) and basal-to-apical (B-A) directions at 30-, 60- and 120-minute time points. Bars shown are mean ± SEM for n=3 replicates for each drug and time point. Three replicates mean three independent experiments were carried out with three different animals. Bars bearing different superscript differ (P<0.05) in one-way ANOVA followed by Tukey's multiple comparison post-hoc test. Further Apparent permeability calculations and concentrations of transwell model of horse BBB studies are in Appendix 4.

Fig. 5.9: Apparent permeability (P_{app}) values of drug loperamide 10x conducted on transwell model of horse BBB in apical-to-basal (A-B) and basal-to-apical (B-A) directions at 30-, 60- and 120-minute time points. Bars shown are mean ± SEM for n=3 replicates for each drug and time point. Three replicates mean three independent experiments were carried out with three different animals. Bars bearing different superscript differ (P<0.05) in one-way ANOVA followed by Tukey's multiple comparison post-hoc test. Further Apparent permeability calculations and concentrations of transwell model of horse BBB studies are in Appendix 4.

5.3.3.2 Exact permeability of the test drugs across Transwell model of Horse blood-brain barrier

Exact permeability (P_{exact}) symbolises the rate of drug transport across a monolayer. P_{exact} values were calculated for each drug at three time points i.e. 30-minute, 60 minute and 120 minutes, in both apical-to-basal (A-B) and basal-to-apical (B-A) directions. P_{exact} values are significantly different in both directions and across time points for the same drug. Like P_{exact} for chlorpromazine is significantly higher at 30 minutes, lower at 60 minutes and significantly lower at 120 minutes in both A-B and B-A directions. For drugs like loperamide, camptothecin and etoposide, P_{exact} value is significantly higher at 30 minutes than at 120 minutes in A-B direction whereas P_{exact} value remained for these same drugs across all the three time points in B-A direction. For mitoxantrone, P_{exact} was significantly higher at 30 minutes at 120 minutes both in A-B and B-A directions. For lamotrigine, topiramate, methotrexate and loperamide 10x, P_{exact} value remained statistically same at all the three time points in both A-B and B-A directions. (Appendix 5, Table A5.6) (Fig. 5.10, 5.11 and 5.12)

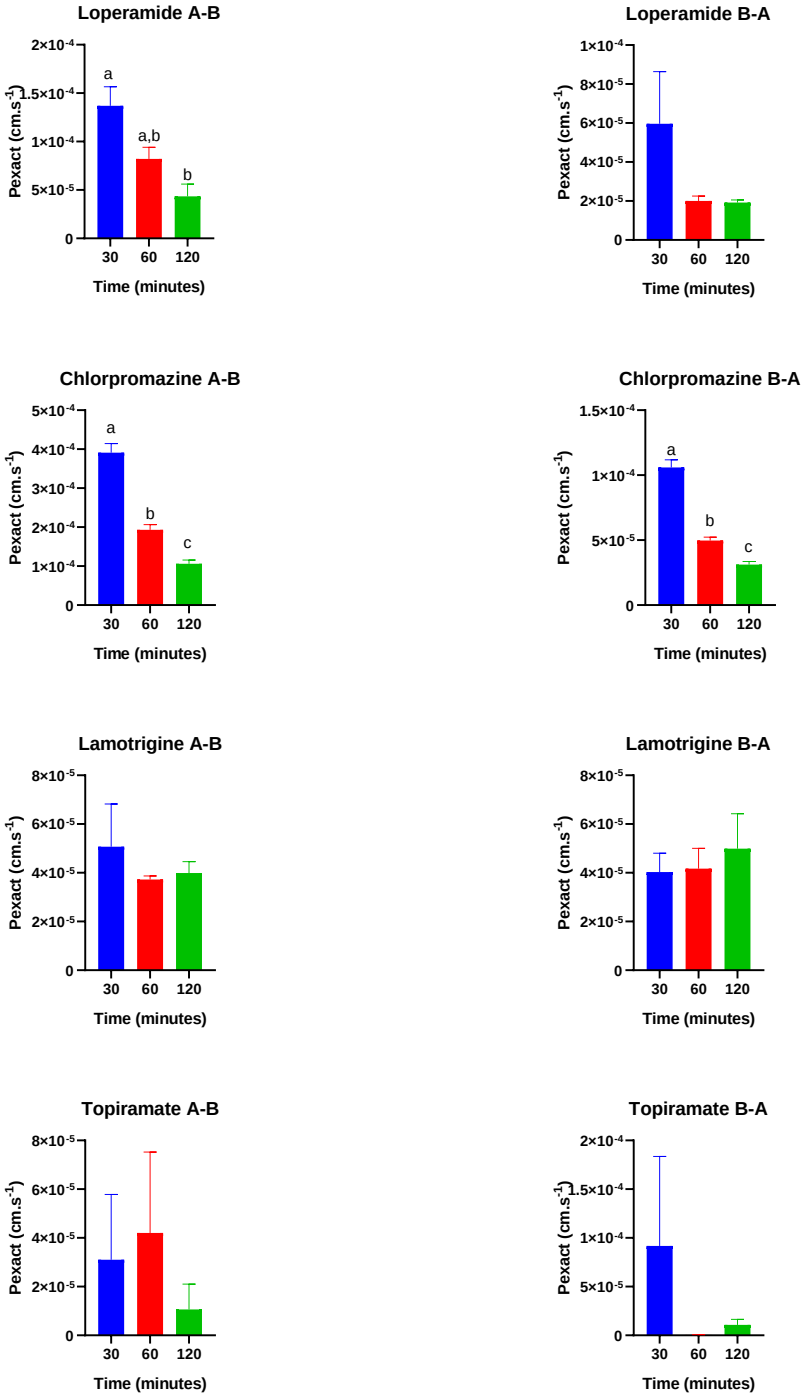

Fig. 5.10: Exact permeability (P_{exact}) values of various drugs (loperamide, chlorpromazine, lamotrigine and topiramate) conducted on transwell model of horse BBB in apical-to-basal (A-B) and basal-to-apical (B-A) directions at 30-, 60- and 120-minute time points. Bars shown are mean ± SEM for n=3 replicates for each drug and time point. Three replicates mean three independent experiments were carried out with three different animals. Bars bearing different superscript differ ($P<0.05$) in one-way ANOVA followed by Tukey's multiple comparison post-hoc test. Further Exact permeability calculations and concentrations of transwell model of horse BBB studies are in Appendix 4.

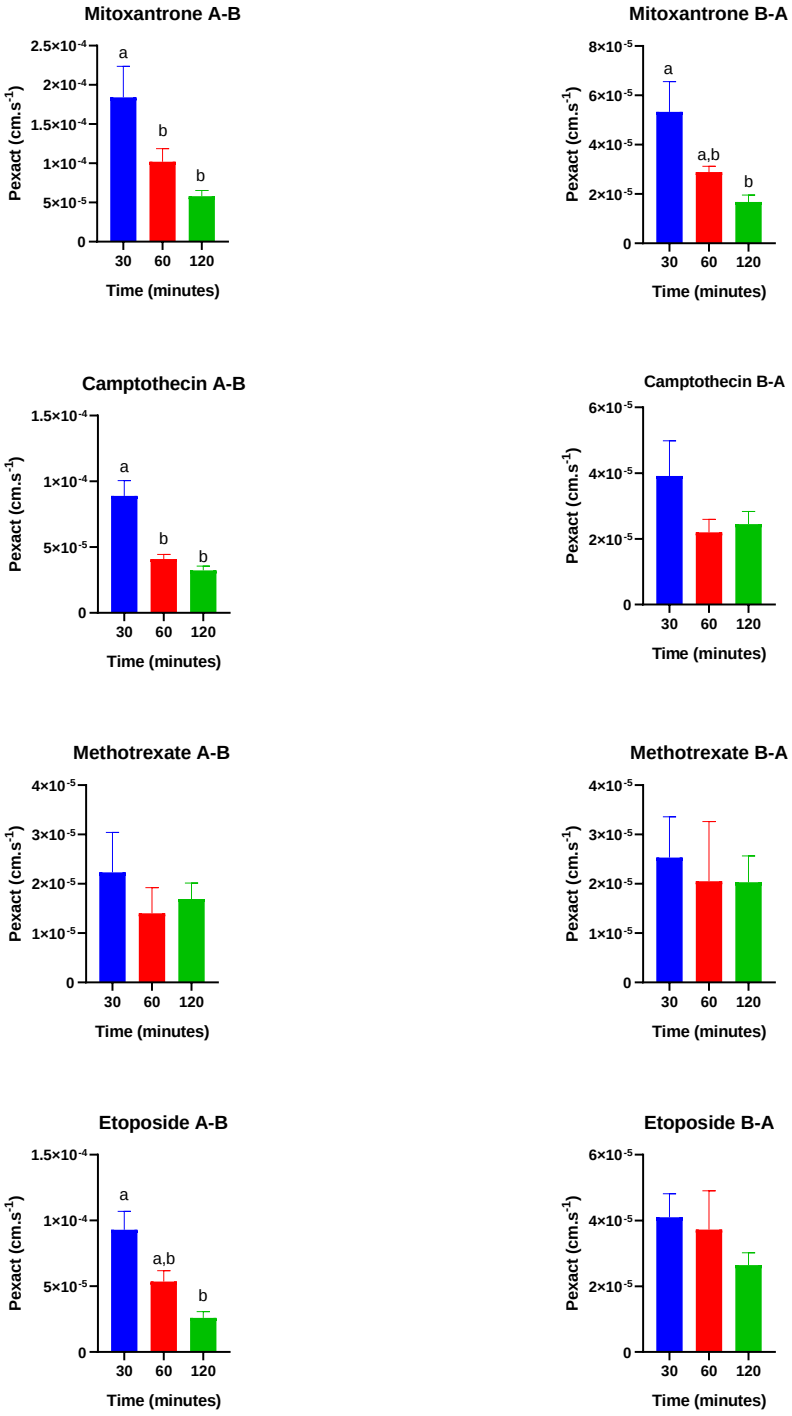

Fig. 5.11: Exact permeability (P_{exact}) values of various drugs (mitoxantrone, camptothecin, methotrexate and etoposide) conducted on transwell model of horse BBB in apical-to-basal (A-B) and basal-to-apical (B-A) directions at 30-, 60- and 120-minute time points. Bars shown are mean ± SEM for n=3 replicates for each drug and time point. Three replicates mean three independent experiments were carried out with three different animals. Bars bearing different superscript differ (P<0.05) in one-way ANOVA followed by Tukey's multiple comparison post-hoc test. Further Exact permeability calculations and concentrations of transwell model of horse BBB studies are in Appendix 4.

Fig. 5.12: Exact permeability (P_{exact}) values of drug loperamide 10x conducted on transwell model of horse BBB in apical-to-basal (A-B) and basal-to-apical (B-A) directions at 30-, 60- and 120-minute time points. Bars shown are mean ± SEM for n=3 replicates for each drug and time point. Three replicates mean three independent experiments were carried out with three different animals. Bars bearing different superscript differ (P<0.05) in one-way ANOVA followed by Tukey's multiple comparison post-hoc test. Further Exact permeability calculations and concentrations of transwell model of horse BBB studies are in Appendix 4.

5.3.3.3 P_{app} Efflux Ratio of test drugs across HBEC Transwell model of BBB

P_{app} Efflux Ratio is calculated by dividing the P_{app} in B-A direction with P_{app} of same drug in A-B direction. One thing that is common for all the drugs is that P_{app} Efflux Ratio remained similar across all time points. P_{app} Efflux Ratio for chlorpromazine and mitoxantrone remained below 0.5 for all time points which means that P_{app} value in A-B direction is at least 2-fold higher than P_{app} value in B-A direction across. Conversely, P_{app} Efflux Ratio remained between 0.5 to 1.5 for lamotrigine and loperamide 10x across (Appendix 5, Table A5.7) (Fig. 5.13).

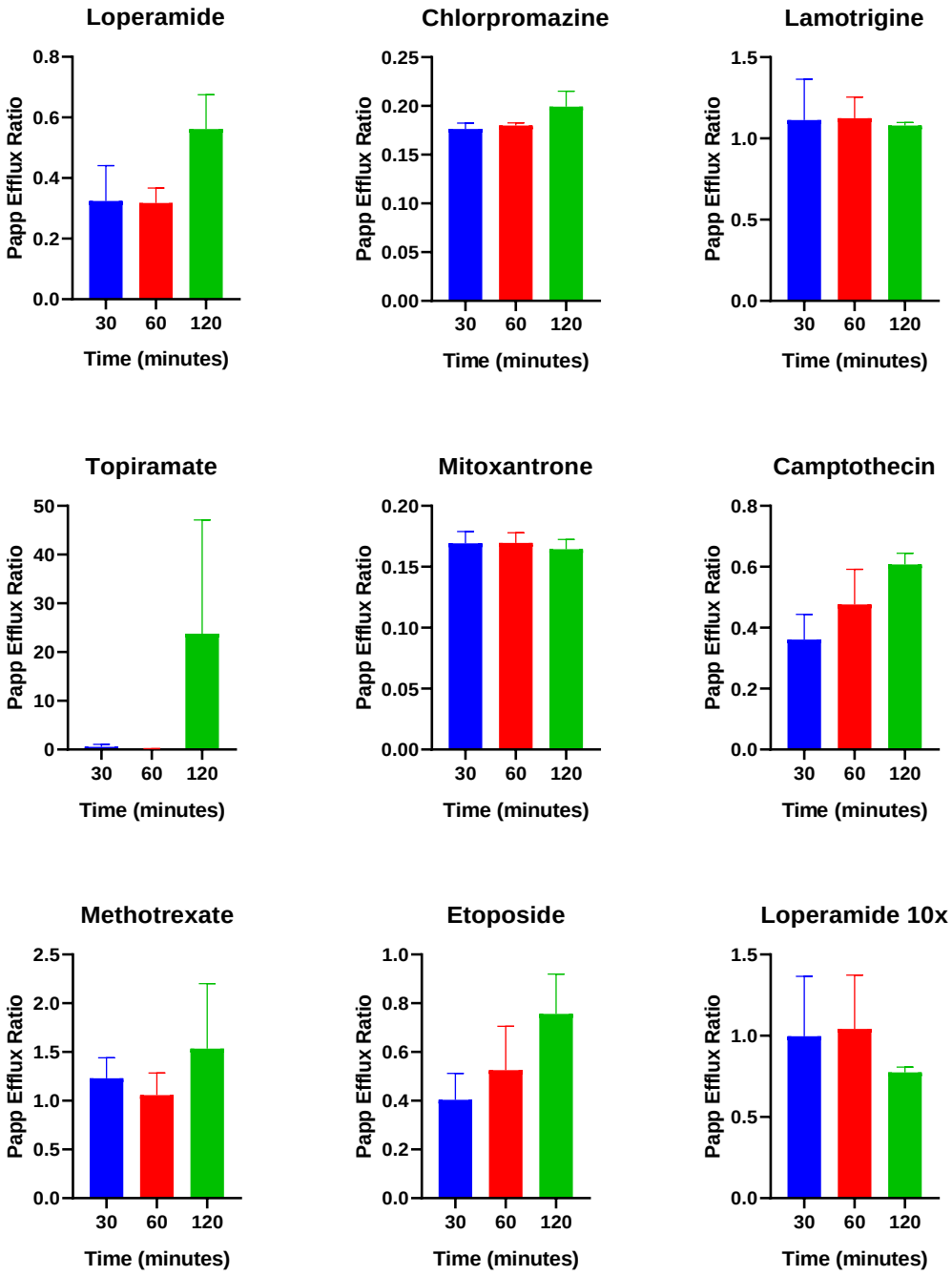

Fig. 5.13: Efflux ratio from apparent permeability (P_{app}) of selected test drugs namely loperamide, chlorpromazine, lamotrigine, topiramate, mitoxantrone, camptothecin, methotrexate, etoposide and loperamide 10x from drug transport studies in apical-to-basal (A-B) and basal-to-apical (B-A) directions carried out on transwell model of horse BBB at 30 minute, 60 minute and 120 minute time points. Bars shown are mean ± SEM for n=3 replicates for each drug and time point. Three replicates mean three independent experiments were carried out with three different animals. Bars bearing no superscript in a graph do not differ significantly ($P<0.05$) in one-way ANOVA followed by Tukey's multiple comparison post-hoc test. Further Efflux ratio from apparent permeability (P_{app}) calculations of drug transport studies conducted on transwell model of horse BBB can be found in detail in Appendix 4.

5.3.3.4 P_{exact} Efflux Ratio of test drugs across HBEC Transwell model of BBB

P_{exact} Efflux Ratio of a drug is calculated by dividing the P_{exact} of a drug in B-A direction with P_{exact} of the drug in A-B direction. So, value of P_{exact} Efflux ratio of any drug is directly proportional to P_{exact} of a drug in B-A direction and inversely proportional to P_{exact} of the drug in A-B direction. One common thing for all drugs in this study is that P_{exact} Efflux Ratio remained similar across all the three time points for any drug. P_{exact} Efflux Ratio of chlorpromazine and mitoxantrone remained below 0.33 at all the three time points which means that P_{exact} value for these drugs in A-B direction is at least three times higher than P_{exact} value of these drugs in B-A direction across all the three time points. For drugs like chlorpromazine, lamotrigine, camptothecin, methotrexate, etoposide and loperamide 10x, P_{exact} Efflux Ratio remained between 0.33 and 0.5 at all the three time points. At 60 minutes, P_{exact} Efflux Ratio for loperamide was 0.25 $\pm$ 0.04. (Appendix 5, Table A5.8) (Fig. 5.14)

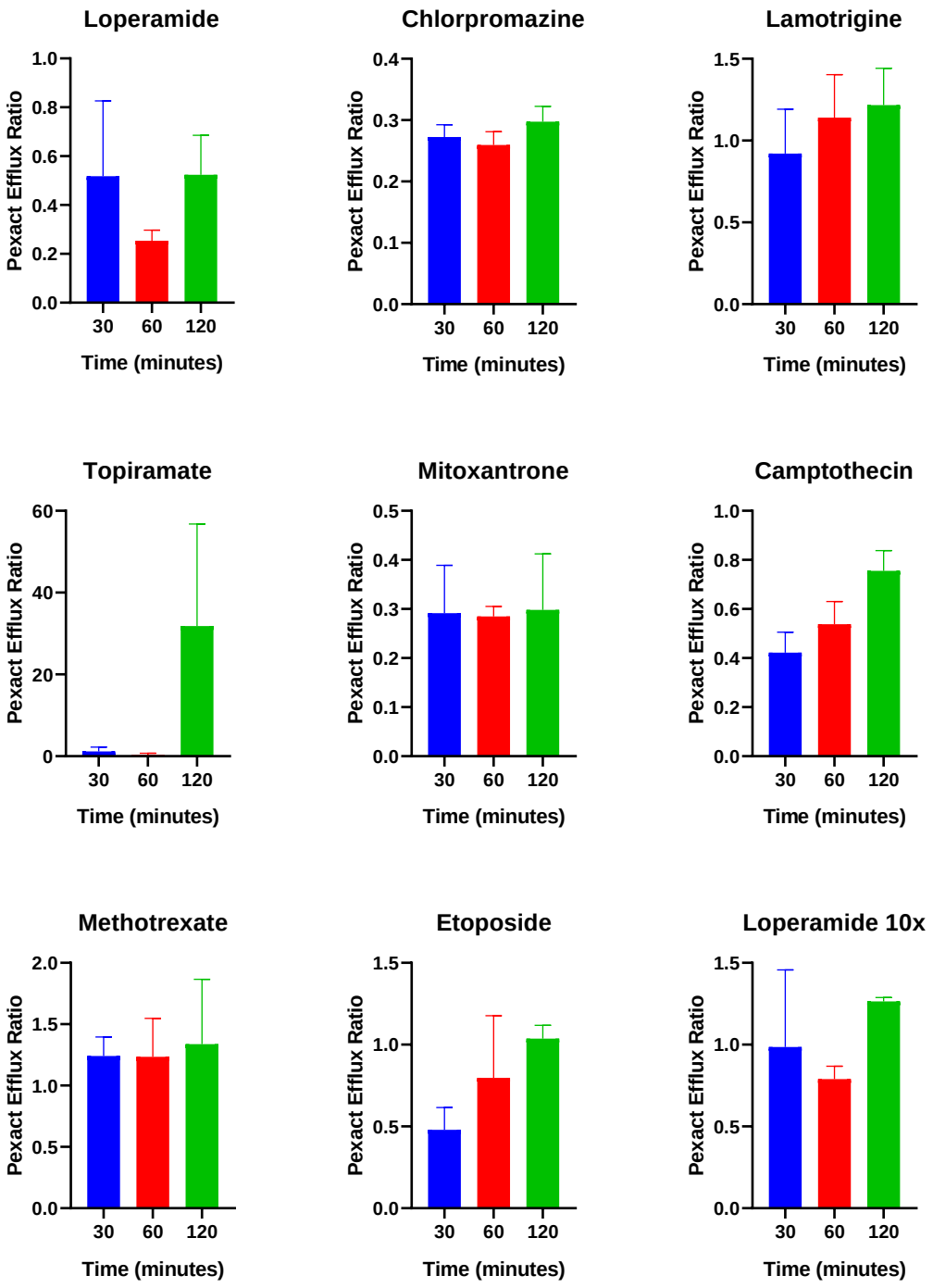

Fig. 5.14: Efflux ratio from Exact permeability (P_{exact}) of selected test namely loperamide, chlorpromazine, lamotrigine, topiramate, mitoxantrone, camptothecin, methotrexate, etoposide and loperamide 10x from drug transport studies in apical-to-basal (A-B) and basal-to-apical (B-A) directions carried out on transwell model of horse BBB at 30 minute, 60 minute and 120 minute time points. Bars shown are mean ± SEM for n=3 replicates for each drug and time point. Three replicates mean three independent experiments were carried out with three different animals. Bars bearing no superscript in a graph do not differ significantly ($P<0.05$) in one-way ANOVA followed by Tukey's multiple comparison post-hoc test. Further Efflux ratio from Exact permeability (P_{exact}) calculations of drug transport studies conducted on transwell model of horse BBB can be found in detail in Appendix 4.

5.3.3.5 Comparison between apparent permeability of drugs (P_{app}) between NCC and HBECs

Drugs like loperamide, chlorpromazine and mitoxantrone have higher P_{app} on HBECs in comparison to NCC in both apical-to-basal and basal-to-apical direction at all the three time points. lamotrigine and camptothecin have higher P_{app} in HBECs than NCC in apical-to-basal direction at 30-minute time point but no difference is recorded in 60 and 120 minute and in basal-to-apical direction. All other drugs have no difference in the P_{app} between NCC and HBECs (Fig. 5.15 and 5.16)

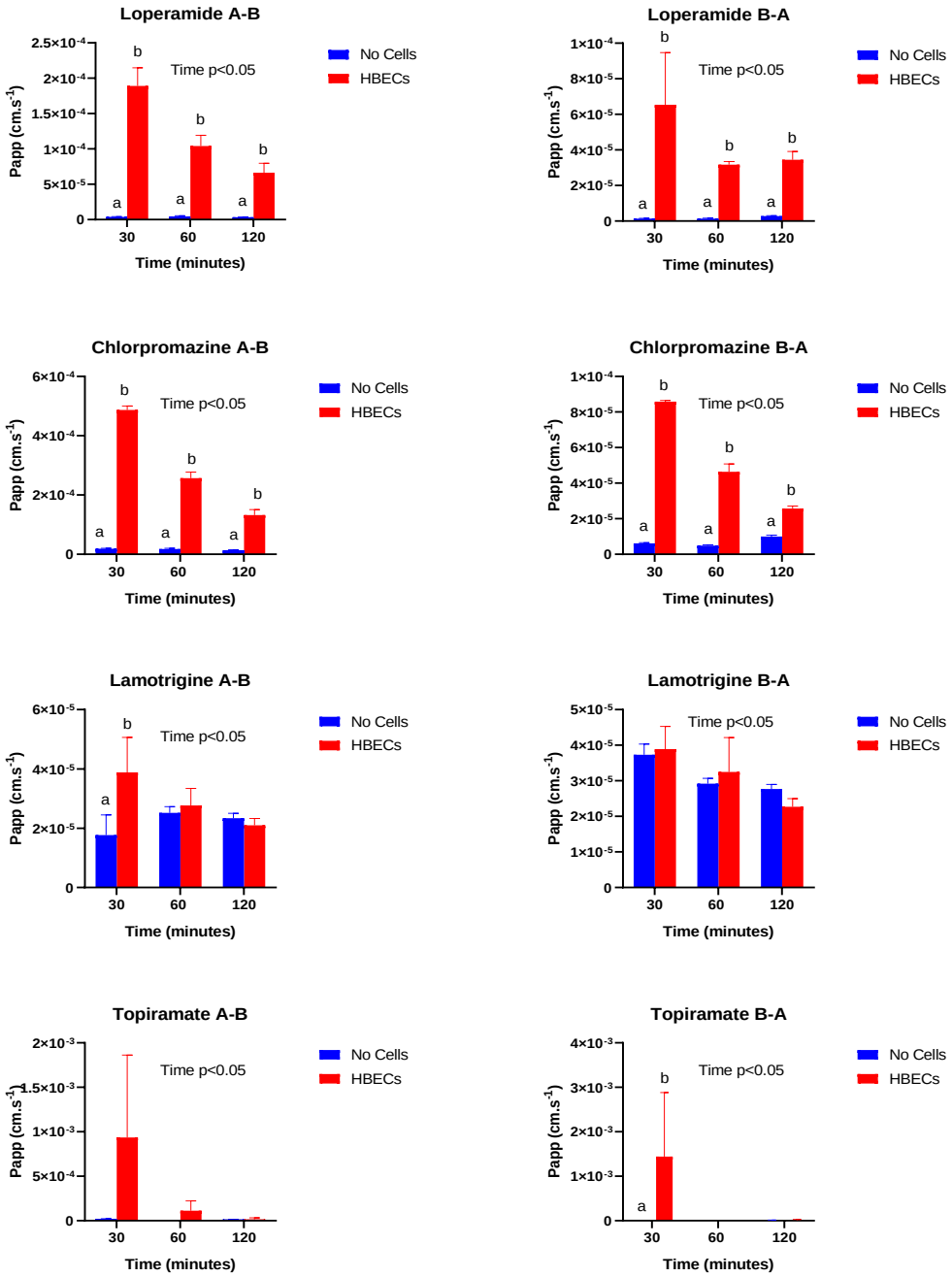

Fig. 5.15: Apparent permeability (P_{app}) of individual selected test drugs namely loperamide, chlorpromazine, lamotrigine, topiramate across transwell inserts with no cells and Horse Brain Endothelial Cell transwell models of BBB (HBEC) in apical-to-basal (A-B) and basal-to-apical (B-A) directions at 30-, 60- and 120-minute time points. Bars are mean ± SEM where n=6 for no cells (six replicates mean six wells were used) and n=3 for HBEC (three replicates mean three independent experiments were carried out with three different animals) for each drug and time point. Bars with different superscripts indicate a difference (P<0.05) between no cells and HBECs using 2-way ANOVA followed by Sidak's multiple comparison post-hoc test. Further Apparent permeability (P_{app}) calculations and concentrations of drug transport studies conducted on NCC and HBEC are in Appendix 3 and 4 respectively.

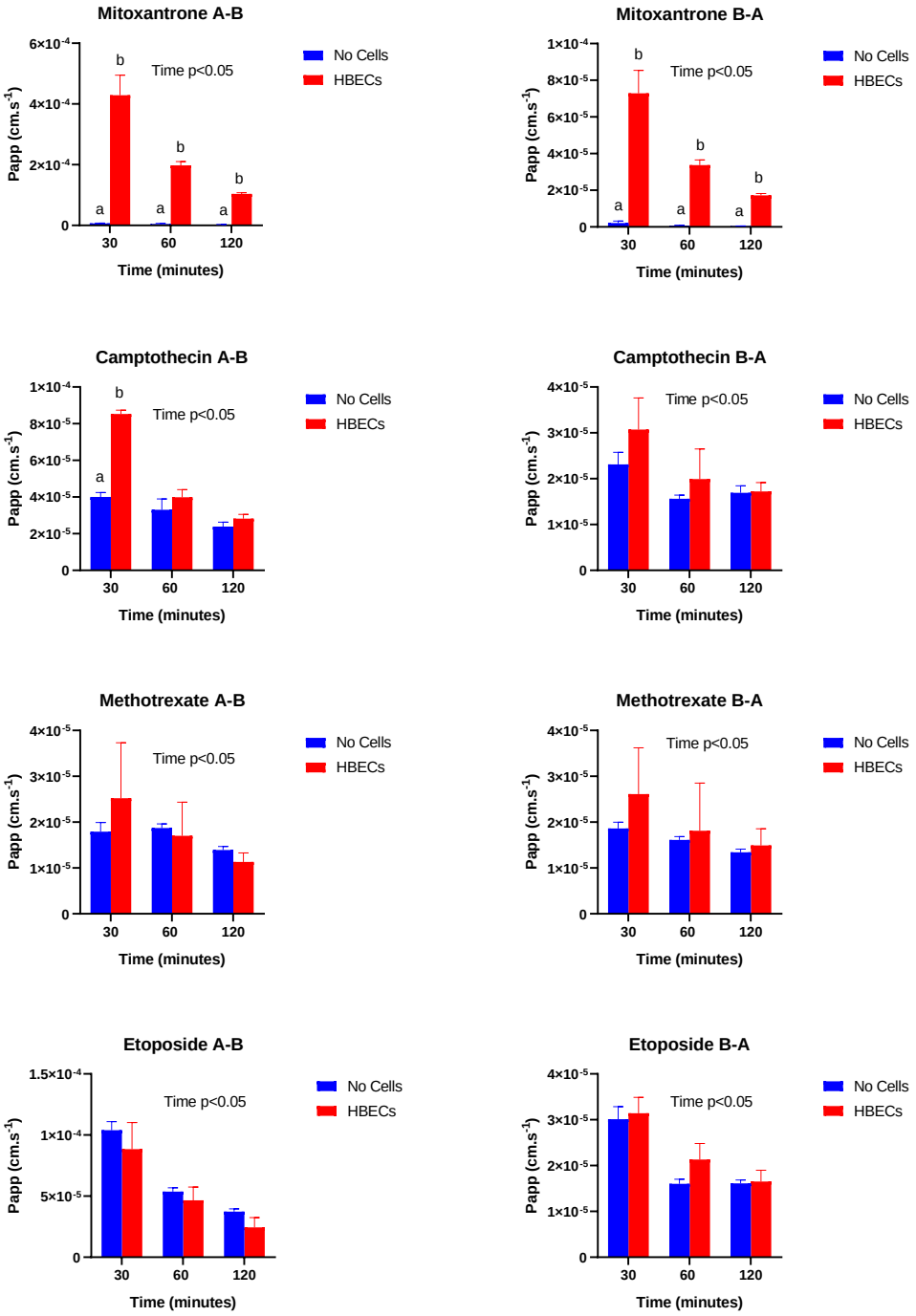

Fig. 5.16: Apparent permeability (P_{app}) of individual selected test drugs namely mitoxantrone, camptothecin, methotrexate and etoposide across transwell inserts with no cells (NCC) and Horse Brain Endothelial Cell transwell models of BBB (HBEC) in apical-to-basal (A-B) and basal-to-apical (B-A) directions at 30-minute, 60 minute and 120 minute time points. Bars shown are mean ± SEM where n=6 for NCC (six replicates mean six wells were used) and n=3 for HBEC (three replicates mean three independent experiments were carried out with three different animals) for each drug and time point. Bars bearing different superscript at one time point in a graph differ significantly (P<0.05) in Two-way ANOVA followed by Sidak's multiple comparison post-hoc test. Further Apparent permeability (P_{app}) calculations and concentrations of drug transport studies conducted on NCC and HBEC can be found in detail in Appendix 3 and 4 respectively.

5.3.3.6 Comparison between Exact permeability of drugs (P_{exact}) between NCC and HBECs

Drugs like chlorpromazine and mitoxantrone have higher P_{exact} on HBECs in comparison to NCC in both apical-to-basal and basal-to-apical direction at all time points. Loperamide has higher P_{exact} on HBECs than on NCC in apical-to-basal direction at the three time points but only at 30-minute time point in basal-to-apical direction. Lamotrigine and camptothecin have higher P_{exact} on HBECs than on NCC in apical-to-basal direction at 30-minute time point but no difference is recorded in 60 and 120 minute and in basal-to-apical direction (Fig. 5.17 and 5.18).

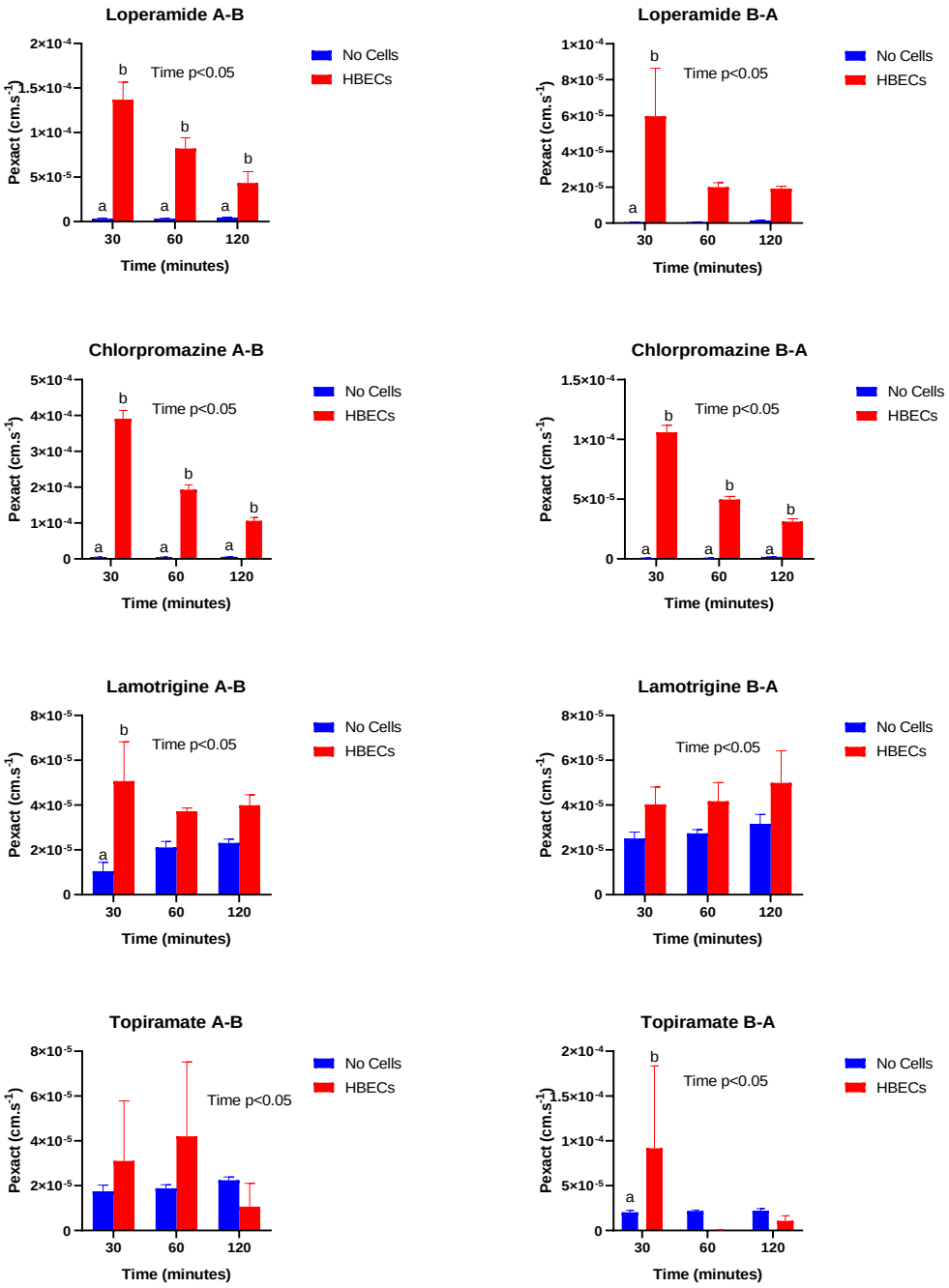

Fig. 5.17: Exact permeability (P_{exact}) of individual selected test drugs namely loperamide, chlorpromazine, lamotrigine and topiramate across transwell inserts with no cells (NCC) and Horse Brain Endothelial Cell transwell models of BBB (HBEC) in apical-to-basal (A-B) and basal-to-apical (B-A) directions at 30-minute, 60 minute and 120 minute time points. Bars shown are mean ± SEM where n=6 for NCC (six replicates mean six wells were used) and n=3 (three replicates mean three independent experiments were carried out with three different animals) for HBEC for each drug and time point. Bars bearing different superscript at one time point in a graph differ significantly (P<0.05) in Two-way ANOVA followed by Sidak's multiple comparison post-hoc test. Further Exact permeability (P_{exact}) calculations and concentrations of drug transport studies conducted on NCC and HBEC can be found in detail in Appendix 3 and 4 respectively.

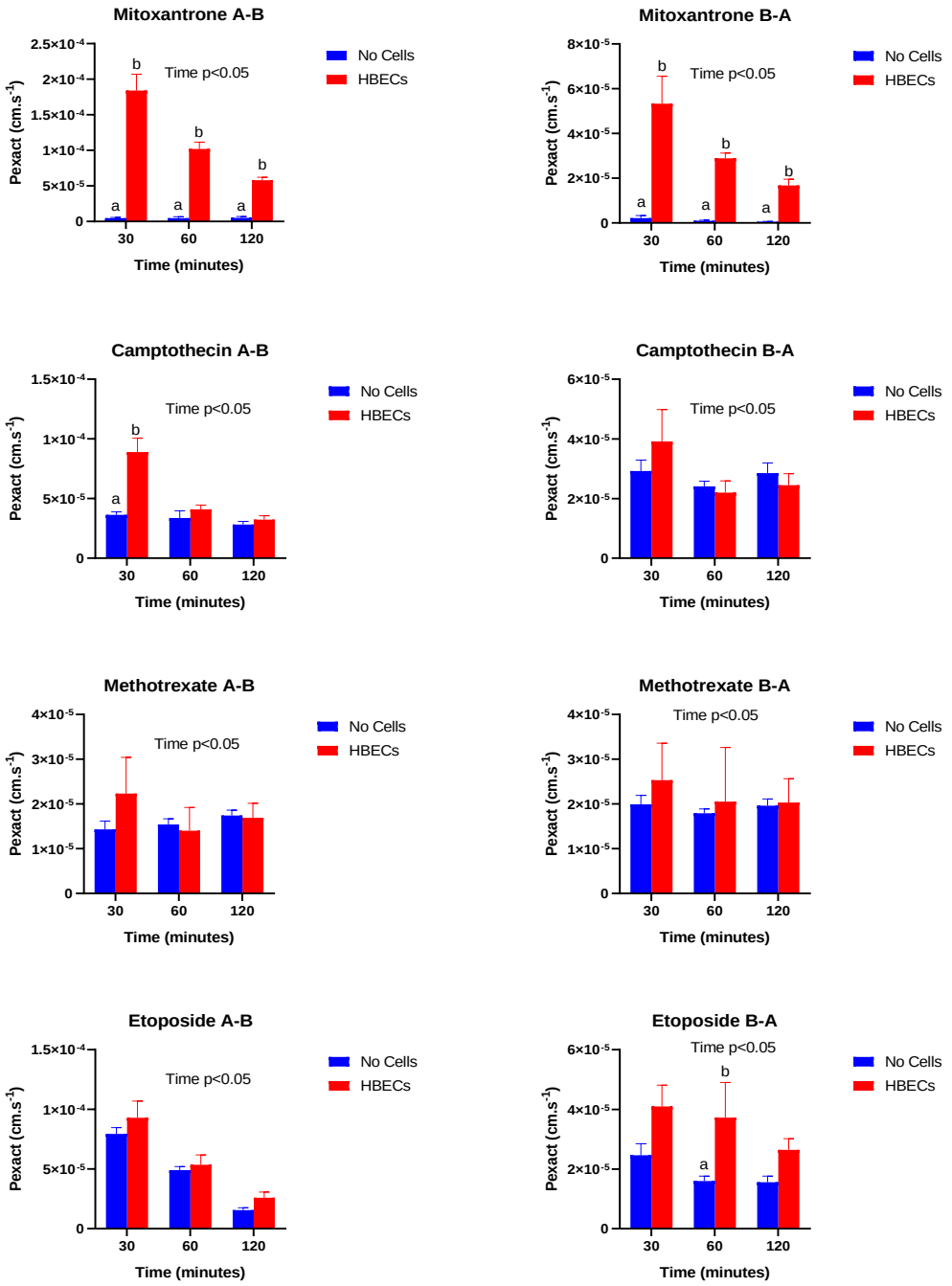

Fig. 5.18: Exact permeability (P_{exact}) of individual selected test drugs namely mitoxantrone, camptothecin, methotrexate and etoposide across transwell inserts with no cells (NCC) and Horse Brain Endothelial Cell transwell models of BBB (HBEC) in apical-to-basal (A-B) and basal-to-apical (B-A) directions at 30-minute, 60 minute and 120 minute time points. Bars shown are mean ± SEM where n=6 for NCC (six replicates mean six wells were used) and n=3 for HBEC (three replicates mean three independent experiments were carried out with three different animals) for each drug and time point. Bars bearing different superscript at one time point in a graph differ significantly (P<0.05) in Two-way ANOVA followed by Sidak's multiple comparison post-hoc test. Further Exact permeability (P_{exact}) calculations and concentrations of drug transport studies conducted on NCC and HBEC can be found in detail in Appendix 3 and 4 respectively.

5.3.3.7 Comparison of P_{app} Efflux Ratio of test drugs between no cell control and HBEC on transwell model of BBB

P_{app} Efflux Ratio of each drug was compared at each time point between NCC and HBEC on transwell model of BBB. Except chlorpromazine and etoposide, P_{app} Efflux Ratio of all other drugs were similar between NCC and HBECS For chlorpromazine, at 120-minute P_{app} Efflux Ratio of HBEC was lower than NCC. On the contrary, for etoposide at 120-minute P_{app} Efflux Ratio of HBEC was significantly than NCC. At 30- and 60-minute time points, both chlorpromazine and etoposide exhibited P_{app} Efflux Ratio similar between NCC and HBEC. (Appendix 5 Table A5.3 and A5.7) (Fig. 5.19)

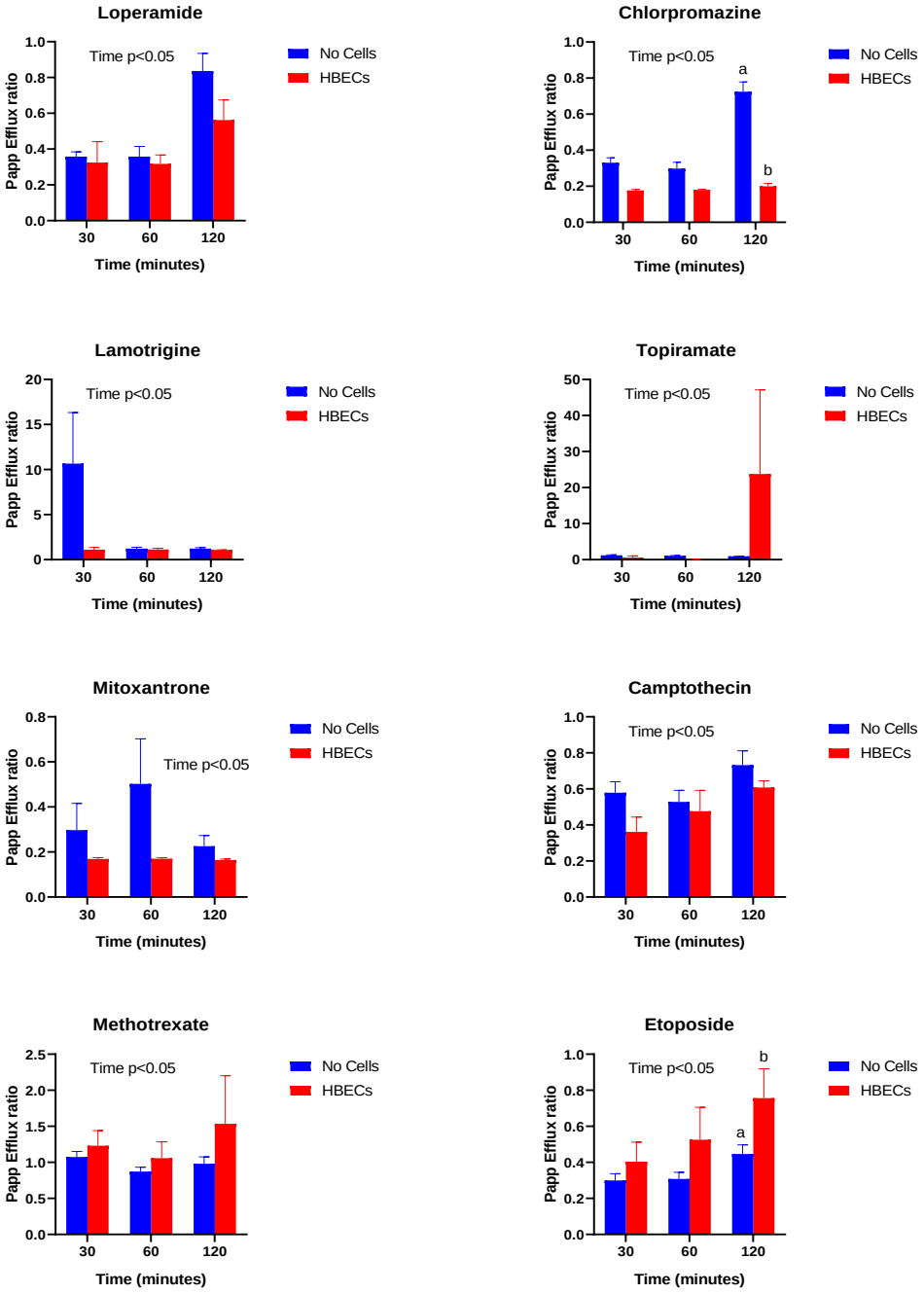

Fig. 5.19: Efflux Ratio of Apparent permeability (P_{app}) of individual selected test drugs namely loperamide, chlorpromazine, lamotrigine, topiramate, mitoxantrone, camptothecin, methotrexate and etoposide across transwell inserts with no cells (NCC) and Horse Brain Endothelial Cell transwell models of BBB (HBEC) at 30-minute, 60 minute and 120 minute time points. Bars shown are mean ± SEM where n=6 for NCC (six replicates mean six wells were used) and n=3 for HBEC (three replicates mean three independent experiments were carried out with three different animals) for each drug and time point. Bars bearing different superscript at one time point in a graph differ significantly (P<0.05) in Two-way ANOVA followed by Sidak's multiple comparison post-hoc test. Further P_{app} Efflux Ratio calculations and concentrations of drug transport studies conducted on NCC and HBEC can be found in detail in Appendix 3 and 4 respectively.

5.3.3.8 Comparison of P_{exact} Efflux Ratio of test drugs between no cell control (NCC) and HBEC on transwell model of BBB

P_{exact} Efflux Ratio of each drug was compared at each time point between NCC and HBEC on transwell model of BBB. For chlorpromazine at 30-minutes, P_{exact} Efflux Ratio was significantly higher than NCC. Likewise, for topiramate at 120 minutes, P_{exact} Efflux Ratio was significantly higher in HBEC as compared to NCC. For etoposide, at 60- and 120-minute time points, P_{exact} Efflux Ratio was significantly higher in HBEC as compared to NCC (Appendix 5, Table A5.4 and A5.8) (Fig. 5.20).

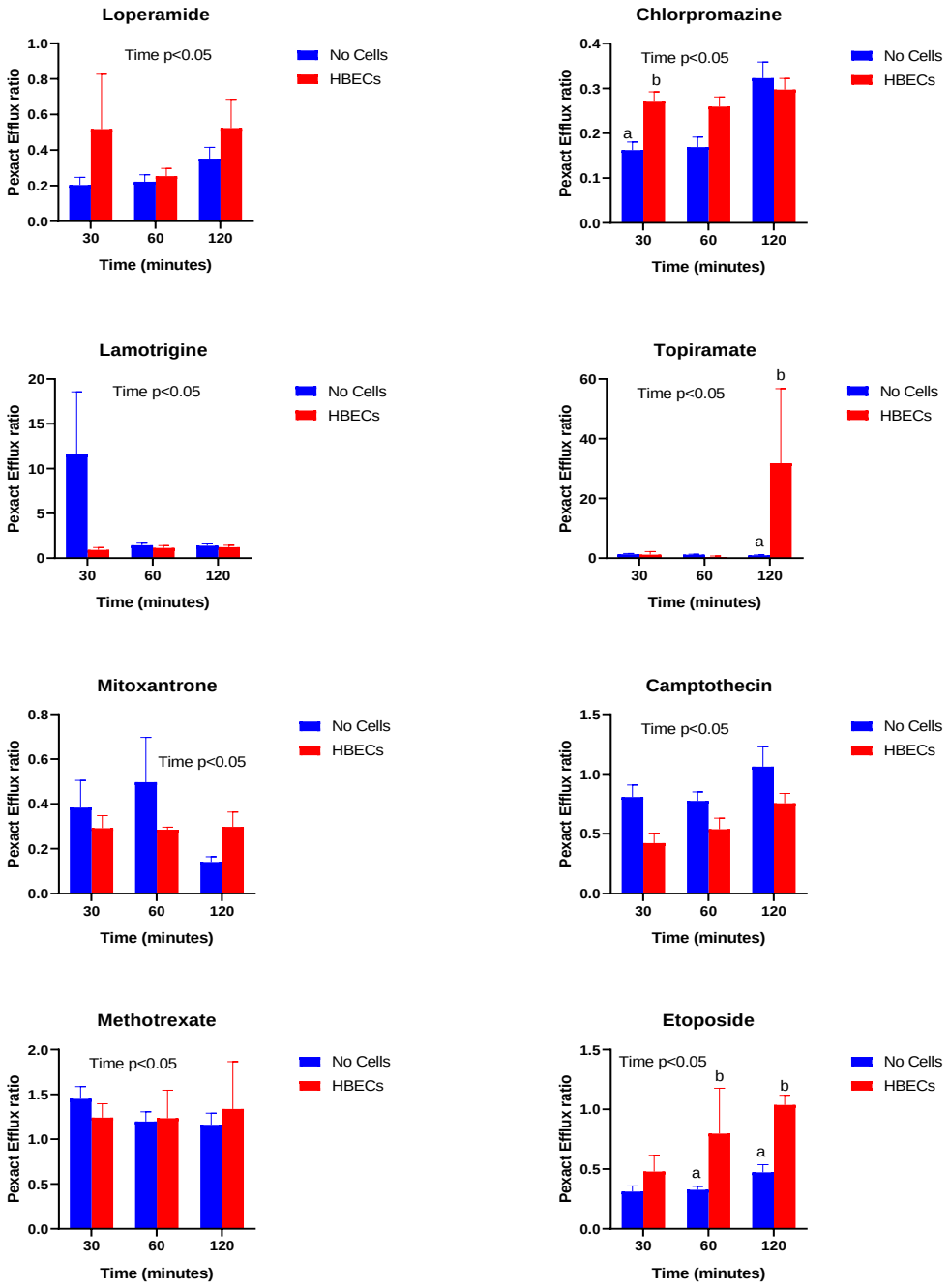

Fig. 5.20: Efflux Ratio of Exact permeability (P_{exact}) of individual selected test drugs namely loperamide, chlorpromazine, lamotrigine, topiramate, mitoxantrone, camptothecin, methotrexate and etoposide across transwell inserts with no cells (NCC) and Horse Brain Endothelial Cell transwell models of BBB (HBEC) at 30 minute, 60 minute and 120 minute time points. Bars shown are mean ± SEM where n=6 for NCC (six replicates mean six wells were used) and n=3 for HBEC (three replicates mean three independent experiments were carried out with three different animals) for each drug and time point. Bars bearing different superscript at one time point in a graph differ significantly (P<0.05) in Two-way ANOVA followed by Sidak's multiple comparison post-hoc test. Further P_{exact} Efflux Ratio calculations and concentrations of drug transport studies conducted on NCC and HBEC can be found in detail in Appendix 3 and 4 respectively.

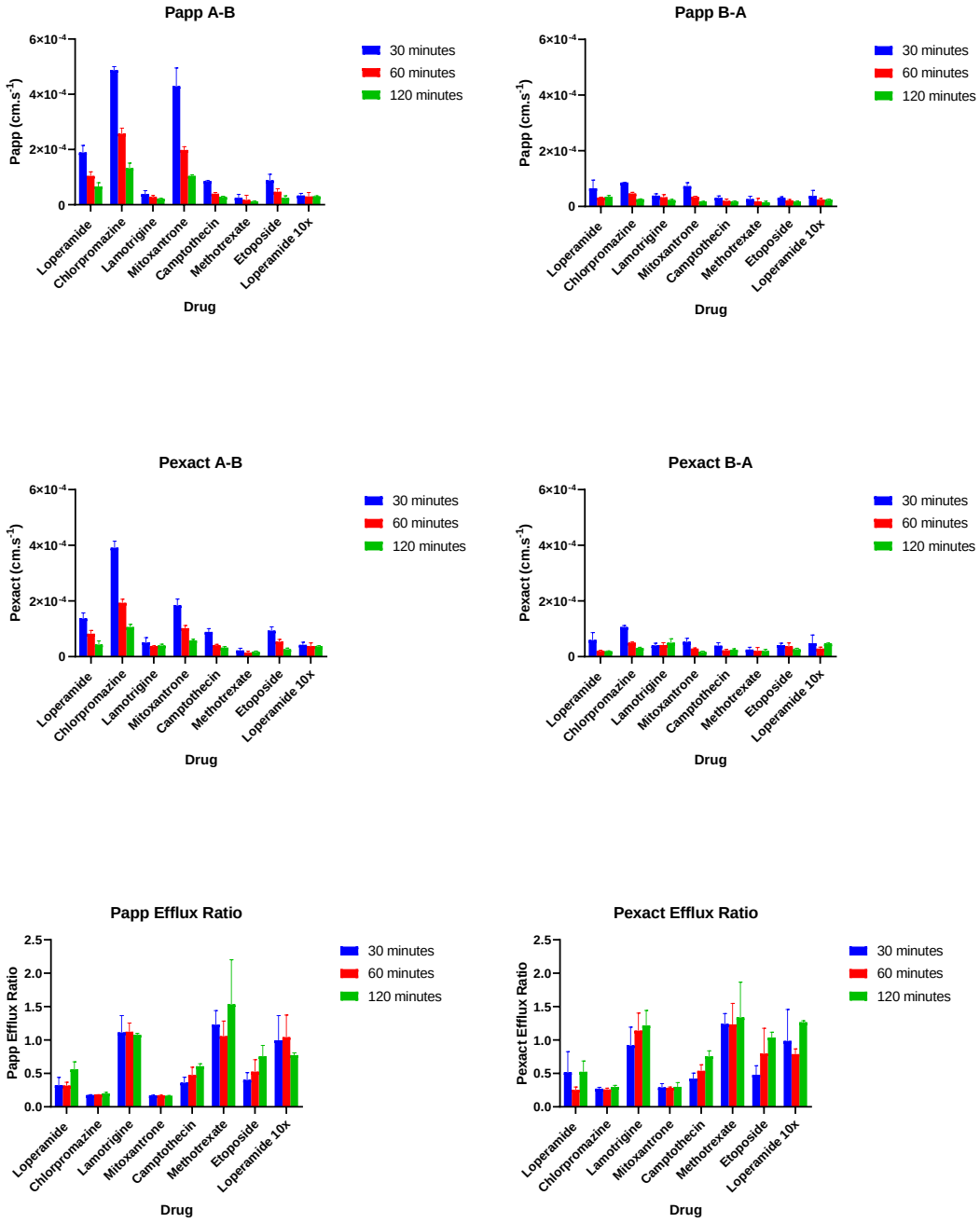

Fig. 5.21: Comparison of Apparent Permeability (P_{app}), Exact Permeability (P_{exact}), P_{app} Efflux Ratio and P_{exact} Efflux ratio of individual selected test drugs namely loperamide, chlorpromazine, lamotrigine, mitoxantrone, camptothecin, methotrexate, etoposide and loperamide 10x across Horse Brain Endothelial Cell transwell models of BBB (HBEC) at 30-minute, 60 minute and 120-minute time points. Bars shown are mean ± SEM where n=3 for each drug and time point. Three replicates mean three independent experiments were carried out with three different animals. Further Apparent Permeability (P_{app}), Exact Permeability (P_{exact}), P_{app} Efflux Ratio and P_{exact} Efflux ratio calculations and concentrations of drug transport studies conducted on HBEC transwell model can be found in detail in Appendix 4.

5.3.3.9 Comparison between permeability/transport of loperamide at 1 µM (loperamide) and loperamide at 10 µM (loperamide 10x) across transwell model of Horse BBB

Permeability of loperamide was studied at two concentrations (1 and 10 µM) using HBECs to determine the rate of flow and efflux ratio of loperamide at 10 times higher concentration. The hypothesis behind this was that the P-gp will get saturated at this 10x concentration and efflux ratio will be lower for loperamide 10x in comparison to loperamide. P_{app} for loperamide 10x was lower than loperamide at 30 and 60 minutes in A-B direction whereas P_{app} value was similar between loperamide and loperamide 10x across all time points in B-A direction. Similarly, P_{exact} for loperamide 10x was lower than loperamide at 30 minutes in A-B direction whereas P_{exact} value was similar between loperamide and loperamide 10x across all time points in B-A direction. P_{app} Efflux Ratio and P_{exact} Efflux Ratio remained similar between loperamide and loperamide 10x across all time points (Fig. 5.22).

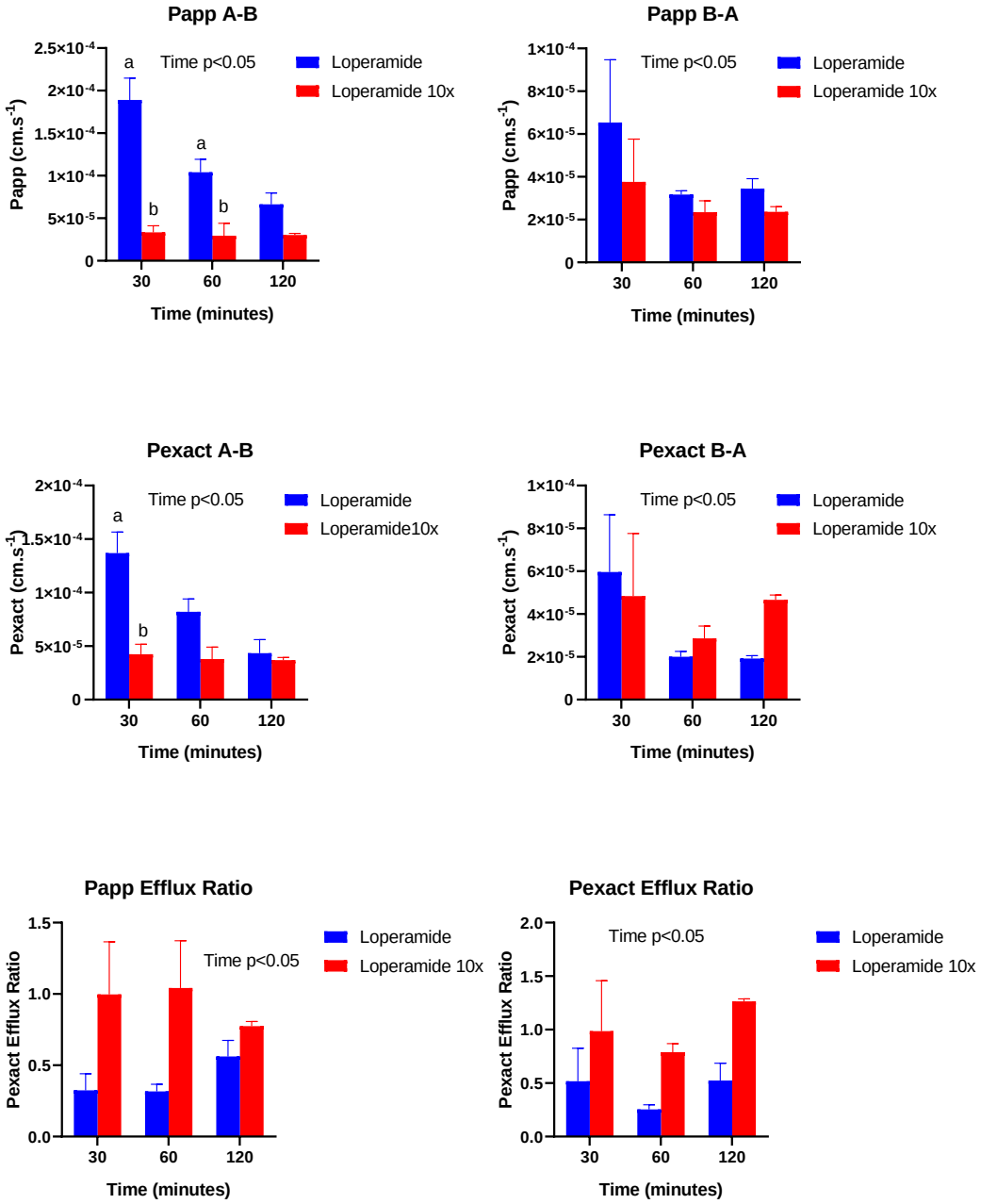

Fig. 5.22: Comparison between Apparent Permeability (P_{app}), Exact Permeability (P_{exact}), Efflux Ratio of Apparent Permeability and Exact permeability of loperamide and loperamide 10x across Horse Brain Endothelial Cell transwell models of BBB (HBEC) at 30-minute, 60 minute and 120-minute time points. Bars shown are mean ± SEM where n=3 for both drugs and time point. Three replicates mean three independent experiments were carried out with three different animals. Bars bearing same superscript at one time point in a graph do not differ significantly (P<0.05) in Two-way ANOVA followed by Sidak's multiple comparison post-hoc test. Further, P_{app}, P_{exact} and Efflux Ratios calculations and concentrations of drug transport studies conducted on HBEC can be found in detail in Appendix 4.

5.3.3.10 Correlation of Apparent permeability (P_{app}) and Exact Permeability (P_{exact}) with TEER values

TEER value of each *in vitro* HBEC Transwell model was recorded before drug transport studies at each time point to confirm that TEER was >85 Ω.cm^2. The mean TEER value was then compared to the P_{app} and P_{exact} for the respective Transwell in both A-B and B-A directions. This was conducted to confirm negative correlation between TEER & P_{app} and P_{exact}.

Table 5.5: Pearson's correlation coefficient (r value) of TEER value against Apparent Permeability (P_{app}) and Exact Permeability (P_{exact}) in both A-B and B-A directions, respectively at 120 minute time point. Negative r value indicates negative correlation between TEER & P_{app} and TEER & $P_{exact,}$ respectively.

S. no.	**Compound**	Pearson's Correlation Coefficient (r value)			
		TEER vs P_{app} (A-B)	TEER vs P_{app} (B-A)	TEER vs P_{exact} (A-B)	TEER vs P_{exact} (B-A)
1	loperamide	-0.73	-0.54	-0.98	-0.99
2.	chlorpromazine	-0.99	-0.88	-0.84	-0.92
3.	lamotrigine	-0.99	-0.99	-0.90	-0.56
4.	mitoxantrone	-0.97	-0.81	-0.99	-0.87
5.	camptothecin	-0.86	-0.85	-0.90	-0.88
6.	methotrexate	-0.96	-1.00	-0.68	-0.99
7.	etoposide	-0.51	-0.99	-0.91	-0.96

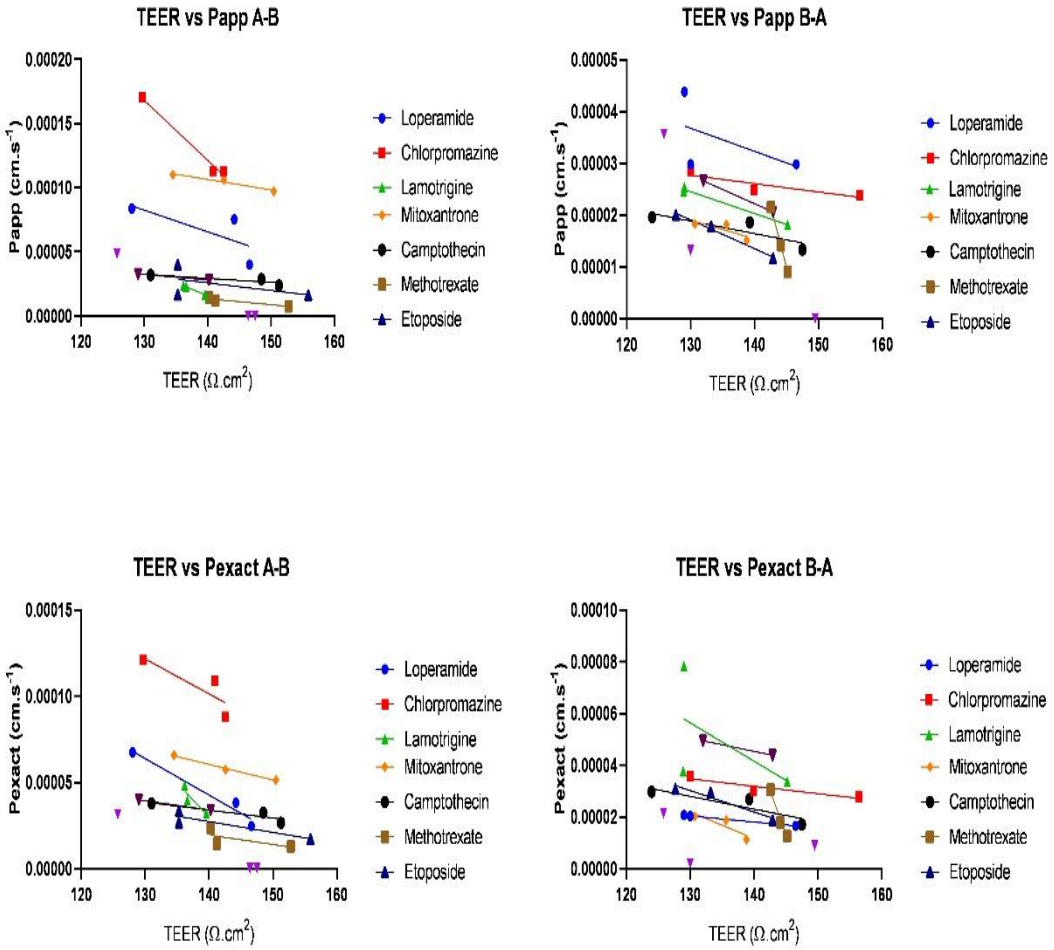

Fig. 5.23: Correlation plots of Transendothelial Electrical Resistance (TEER) values of Transwell model of HBECs against P_{app} and P_{exact} in both apical-to-basal (A-B) and (B-A) basal-to-apical (B-A) direction for all the selected drugs except topiramate at 120 minute time point. Best fit lines for each drug were generated separately using linear regression.

As confirmed by the best fit line and Pearson's Product Moment Correlation Coefficient (r value), there is a strong negative correlation (r value between -0.8 to -1.0) between TEER value & P_{app} and TEER value and P_{exact} in both A-B and B-A directions for most of the drugs in this study. The TEER vs P_{app} experiment for A-B direction had wells with TEER values ranging between 89.1 $\Omega.cm^2$ to 178.86 $\Omega.cm^2$. Similarly, TEER vs P_{app} experiment for B-A direction had wells with TEER values ranging between 86.46 $\Omega.cm^2$ to 173.25 $\Omega.cm^2$. (Table 5.5) (Fig. 5.23)

5.4 Discussion

The aim of this chapter is to study the permeability of various selected drugs with the help of some kinetics parameters like Apparent Permeability, Exact Permeability on Horse Brain Endothelial cell based Transwell Model of BBB. The objective is to study the role of drug efflux transporters at the level of Horse brain endothelial cells in pumping out the substrate drugs.

In this chapter, the Transwell model of Horse BBB was assessed with a number of selected test drugs. These test drugs were selected based on their chemical and pharmacokinetic properties which were pertinent to the drug compound permeability/transport across the BBB. Drug transport studies were analysed across three time points (30, 60 and 120 minutes) in both apical-to-basal (A-B) and basal-to-apical (B-A) directions. Permeability of individual test drug was assessed using several pharmacokinetic parameters including P_{app}, P_{exact}, P_{app} Efflux Ratio, P_{exact} Efflux Ratio. All these pharmacokinetic parameters permitted comparison of this model of BBB to other related data available from other such studies. During drug transport assays, the transwell plates were not placed on shaking because it was repeatedly observed during the preliminary studies that shaking results in the loss of confluency of HBECs monolayer.

The recovery percentage of most of the test drugs namely camptothecin, etoposide, lamotrigine, methotrexate and loperamide 10X in the Transwell model of Horse BBB for drug transport studies is within the expected range (With 60 to 140%). The recovery values around 100% could be recorded because of the error in the calculation which is mainly based on the straight line regression equation. Lower than expected recovery values are also possible because of the polycarbonate binding (non specific) ability of the drugs as the transwell plate is made of polycarbonate plastic. Another reason of low recovery could be the phenomenon of lysosomal trapping of drugs (Bednarczyk & Sanghvi, 2020).

Recovery values of some of drugs namely chlorpromazine, loperamide and mitoxantrone was more than expected and even several folds higher than expected. This may be due to the fact that in case of all these drugs initial

concentration in the donor compartment was quite low than intended because the working solution was prepared to have concentration of 1000 nanomolar. The lower initial concentration in the donar compartment (like in case of chlorpromazine it was below 100 nanomolar) can result in more statisitical errors because at lower concentrations straight line regression equation is not that correct. This can result into higher than expected recovery percentages in case of these drugs. One reason for lower initial concentration in the donar compartment could be the low solubility of the drug and second reason could be the plastic binding (non-specific) ability of the drug as both stock as well as working solutions were prepared and stored in the plastic tubes. In case of chlorpromazine, loperamide and mitoxantone lower than intended initial concentrations in the donar compartments also effect the Papp, Pexact and the efflux ratio (Bednarczyk & Sanghvi, 2020).

The hypothesis that lower initial concentration in the donar compartment results into higher than expected recovery rates is again bolstered by the fact that as the initial concentration of loperamide was increased in the donar compartment in case of loperamide 10X (i.e.10000 nanomolar) the recovery percentage came within the expected range of 60 to 140% which was more than two folds higher than expected in case of loperamide (i.e.1000 nanomolar).

The comparison of drug transport studies of NCC with HBEC revealed that both P_{app} and P_{exact} were higher for drugs like loperamide, chlorpromazine and mitoxantrone in both A-B and B-A directions in HBECs than NCC. So, it can be hypothesised that there were transporter/carrier molecules in HBECs which were transporting these specific drugs in both directions actively. This hypothesis is further supported by the fact P_{app} and P_{exact} of other drugs (e.g. methotrexate) were similar for NCC and HBEC in both directions. P_{app} Efflux Ratio of chlorpromazine at 120 minute was lower in HBECs than NCC which suggests that might be the efflux transporter molecule for chlorpromazine towards the basal side of the transwell. Likewise, P_{exact} efflux ratio of etoposide was higher in case of HBECs than NCC which indicates that there are transporter molecule/transporting mechanism/transporting forces which is making P_{exact} A-B direction lower than that in B-A direction. LogP value states

the lipophilicity of a drug molecule. A higher LogP value indicates higher lipophilicity, and a lower value indicates affinity towards aqueous phase. It was also observed that loperamide and chlorpromazine have LogP value around 5 while mitoxantrone has a logP value of -3.10 but even then, P_{app} and P_{exact} in both A-B and B-A directions is higher for these drugs in HBECs than NCC. This observation, points in the direction that the transport of these drugs in both directions is facilitated by some process which is not related or dependant on the drugs LogP value/lipophilicity.

For most drugs used in this study, P_{app} the rate of permeability of compounds, was lower than P_{exact}. This is due to two restrictions in the calculation of P_{app}, which is that P_{app} is valid if only 10% of the compound has crossed the membrane and when drug transport is in linear phase (Tran et al., 2004). Whereas P_{exact} also considers the back flow of drug after the linear phase of drug transport has been completed. P_{exact} gives a more precise estimate of the rate of drug permeability, especially at later stages of the experiment, when drug across the membrane is more likely to be getting into equilibrium phase (Tran et al., 2004). Moreover, it was also perceived that for both P_{app} and P_{exact} for many drugs, there was a significant ($P<0.05$) difference in the rate of drug flow between the compartments at different time points in both the directions. While, this was expected with the P_{app}, as its calculation does not consider the backflow of drug present at the later time points. The change in the P_{exact} value at different time points was unexpected. As per Tran et al., 2004, change in P_{exact} with time can be due to the structural changes in the polarised cell membrane. Although, it is possible that this change of P_{exact} with time is due to the slow speed of drug binding in the wells, as P_{exact} calculation only considers the fast non-specific drug binding (Tran et al., 2004). Also, there are chances that the monolayer might have lost confluency during the transport assays because of the effect of the substrate drug on the viability of the cells of the mnolayer. There is a higher rate of efflux of drug from apical-to-basal (A-B) than (B-A) in case of majority of drugs namely loperamide, chlorpromazine, mitoxantrone, camptothecin and etoposide. Data for other two drugs namely, lamotrigine and methotrexate failed to show any efflux on the apical side of the HBEC membrane. Also, loperamide at 10µM failed to

show any efflux on the apical side of HBEC membrane. This was an unexpected outcome, as all drugs are established substrates for efflux transporters. Topiramate at 120 minutes exhibited very high P_{app} and P_{exact} efflux ratio. This should be assessed with caution as there was poor Mass Spectrometry analysis of this drug. Secondly, the standard error of this high efflux ratio is also very high which makes it statistically ($P<0.05$) similar to the efflux ratios at the 30 and 60 minutes.

Results of this study indicate that the efflux ratios neither significantly ($P<0.05$) vary between P_{app} and P_{exact} and nor across time points. Other than that, one important commonality between most compounds is that at all time points efflux ratios remained between 0.5 to 1.5. This implies that for there is no significant active efflux of majority of compounds taking place across the HBEC during this study. Therefore, it was hypothesised that slight differences between A-B and B-A flow of drugs is because of issues like slow rates of drug binding and change in the structure or confluency of the HBEC monolayer. Both P_{app} and P_{exact} efflux ratios of two drugs namely, chlorpromazine and mitoxantrone remained below 0.33 across all the time points of this study. This is because the rate of flow of these drugs in B-A direction is slower than A-B. So, this can be hypothesised that the efflux pumps for which these two drugs are substrates are located on the basal side of the transwell. A good explanation for this phenomenon is that HBEC have disoriented in the transwell insert in such a way that apical surface of the monolayer is facing the basal side of the transwell. As apical surface is the one having the major efflux transporters therefore reverse efflux towards the basal chamber is taking place in the present study. To clarify this, further exploration using confocal microscope is required.

Overall, it can be concluded from the comparison between pharmacokinetic parameters like P_{app} and P_{exact} that for majority of the drugs HBEC monolayer did not reduce the rate of permeability between the two compartments in either direction. This can be partly explained by TEER values being relatively low resulting in high paracellular passive diffusion of drugs. Secondly, this can also be hypothesised that for majority of the drugs the efflux mechanism is not working. This could be due to lack of expression or there is lack of function of

multidrug efflux transporters in the present HBEC model of BBB.Another possible reason could be that the HBEC monolayer might have lost confluency during the transport assays.

Analysis of TEER and permeability parameters showed strong negative correlations for all drugs which means as TEER value increased, the rate of permeability (i.e. P_{app} and P_{exact} value) decreased. So, this suggests that permeability of drugs in the present model was due to paracellular passive diffusion and as the TEER value increases passive diffusion from the intercellular space increases.

Comparison of pharmacokinetic parameters like P_{app}, P_{exact} and Efflux Ratios was also done between loperamide (at 1µM) and loperamide 10x (at 10µM). Lower rate of permeability of more concentrated loperamide (10x) in comparison to loperamide in A-B direction especially initially indicates that loperamide at 10µM was effluxed higher than loperamide at 1µM. This might be that at lower concentrations paracellular passive diffusion is a major part component of the drug's permeability but at higher concentration efflux action has a more major role. Interesting finding is that towards the end of the study permeability rate of both loperamide and loperamide 10x becomes similar in the A-B direction. This may be due to that by this time the efflux transporter molecules might have become saturated.

This study is the first attempt towards establishment of a model of BBB using Horse brain endothelial cells. Therefore, comparable studies in the same species are not available in the literature. However, some studies are there on *in vitro* primary brain endothelial cells Transwell Model in other species. Efflux hypothesis is supported by a similar study on Primary Pig Brain Endothelial Cells (Bentham, 2010) which showed strong efflux took place for drugs like Carbamazepine, Donepezil and Amprenavir. But in the present study, no strong efflux was observed for any of the drugs. Numerous studies have stated that species differences may result in differences in levels, relative abundance, substrate specificity and tissue distribution of transporters (Chu et al., 2013; Verscheijden et al., 2021; W. Zhang et al., 2023; Zou et al., 2021).

Though, many conclusions could be drawn by comparing the present HBEC model of BBB with other Transwell models of BBB developed using various

cell types. For example, Bentham, 2010 reported P_{app} rate of chlorpromazine 56.0 x 10^{-7} $cm.s^{-1}$ in A-B direction and 17.6 x 10^{-7} $cm.s^{-1}$ in B-A direction in Transwell Model of pig brain endothelial cells BBB. Whereas in the present study at the same time point, P_{app} of chlorpromazine was 2.57 x 10^{-4} $cm.s^{-1}$ in A-B direction and 4.64 x 10^{-5} $cm.s^{-1}$ in B-A direction. Likewise, Bentham, 2010 reported P_{exact} of chlorpromazine 91.8 x 10^{-7} $cm.s^{-1}$ in A-B direction and 17.1 x 10^{-7} $cm.s^{-1}$ in B-A direction at 60-minute time point in Transwell Model of pig brain endothelial cells BBB. Whereas in the present study, P_{exact} of chlorpromazine was recorded as 1.93 x 10^{-4} $cm.s^{-1}$ in A-B direction and 4.97 x 10^{-5} $cm.s^{-1}$ in B-A direction at 60-minute time point. This difference in the values of permeability parameters could be attributed to greater TEER values (2000 $\Omega.cm^2$ Bentham, 2010) compared with present study (120-160 $\Omega.cm^2$) and it is evident that P_{app} and P_{exact} have strong negative correlation with TEER values.

Similarly, Whitehouse, 2022 reported a P_{exact} for loperamide as 3.57 x 10^{-5} $cm.s^{-1}$ in A-B direction and 1.61 x 10^{-5} $cm.s^{-1}$ in B-A direction at 60 minutes in porcine BECs. In the present study, P_{exact} for loperamide ws 8.20 x 10^{-5} $cm.s^{-1}$ in A-B direction and 2.00 x 10^{-5} $cm.s^{-1}$ in B-A direction at 60 minute. So, the slightly higher permeability in the present study could be attributed to lower TEER (120-160 vs 150–200 $\Omega.cm^2$). So, this suggests the slight difference in the TEER has been reflected in slight differences permeability parameters like P_{app} and P_{exact}. However, increased permeability across the HBEC monolayer in comparison to brain endothelial cells of other species can be attributed to the species difference. This is quite possible that expression of multidrug efflux transporters in the horse species is distinct from other species.

Some of the results of the present study agree with the findings of the previous studies. Like, P_{app} Efflux ratio and P_{exact} Efflux Ratio recorded for chlorpromazine in this study is 0.18 and 0.26 respectively at 60 minutes. In complete agreement to this, Bentham, 2010 reported a P_{app} Efflux Ratio and P_{exact} Efflux Ratio of 0.3 and 0.2 respectively for chlorpromazine at 60-minute time point in Transwell model of Pig Brain Endothelial Cells. Likewise, P_{app} Efflux ratio and P_{exact} Efflux Ratio recorded for loperamide in this present study was 0.32 and 0.25 respectively at 60-minute time point. Similar P_{app}

Efflux Ratio and P_{exact} Efflux Ratio were recorded by Whitehouse, 2022 for loperamide at 60 minutes in Transwell model of Pig Brain Endothelial Cells. Results of these two drugs along with mitoxantrone provide further evidence that the expression of multidrug efflux transporters were present on the basal side rather than on the apical side of the Transwell HBEC model of BBB.

Though, Horse Brain Endothelial Cells isolated in this study are more restricting than other commonly used cell types for the BBB (MDCK and Hcmec/d3, Bentham, 2010) (rat primary BECs, Veszelka et al., 2018) (human iPSCs, Mantle et al., 2016). The drug permeability data from the transport studies in the present study indicate that the expression of key BBB multidrug efflux transporters (such as MDR1, BCRP and MRP1) are either down regulated or are less functional as other Primary Brain Endothelial Cell transwell models or in MDR1 overexpression cell lines (Bentham, 2010). In the present study, though quantification of these proteins was not performed on the cells in this study. But expression of these genes was observed in the cultured primary HBECs (Chapter 3). Although, there are some indications from the drug transport data that the HBEC transwell model of BBB presented in this study might be expressing the drug efflux transporters on the side facing the basal chamber of the Transwell. Nevertheless, firm conclusions about this cannot be drawn, as high level of paracellular transport of drugs might be masking any efflux transporter function. Further, research on the transport of drugs in the presence of efflux pump inhibitors and confocal microscopy are required to determine the position of the efflux drug transporters in HBECs. It has been shown that transporter properties of an *in vitro* BBB monolayer remain constant above a TEER of 500 $\Omega.cm^2$ (Mantle et al., 2016). In the present study, the highest TEER obtained for HBECs Transwell culture is around 200 $\Omega.cm^2$. Whereas, in a similar culture developed using Pig Brain Endothelial cells with CTX-TNA2 astrocytes was approximately 10-fold higher at 2132±169 $\Omega.cm^2$ (Bentham, 2010). Similarly, in a different study Primary Pig Brain Endothelial cells were used to establish a transwell model with ACM and a mean TEER value of 235±25 $\Omega.cm^2$ was reported (Whitehouse, 2022). However immortalised cell lines, like MDCK and Hcmec/d3 have reported TEER values below 300 $\Omega.cm^2$ (M. K. K. Lee & Dilq, 2014; Rahman et al., 2016). Therefore, this suggests that the present HBEC

transwell model of BBB has a lower TEER than expected but was having resistance and functionality. Hence, the present model of BBB is exhibiting higher than expected paracellular permeability of compounds resulting in lower ability to perceive the effect of drug efflux transporters.

Thus, it was concluded that HBEC model of BBB developed in this present study is expressing the vital BBB tight junction proteins and efflux transporter proteins in molecular techniques but failed to reach the threshold TEER values required to fulfil the criteria for characteristic BBB transwell model for drug transport studies. More research is required to determine how the TEER can be further increased to be closer to other models using brain endothelial cells (Bentham, 2010; Franke et al., 2000). One approach for increasing the TEER values, permeability measurements, expression of multidrug efflux transporters and tight junction marker proteins is by adding the component of shear stress to the *in vitro* model of BBB (Cucullo, Hossain, et al., 2011b; Elbakary & Badhan, 2020; Garcia-Polite et al., 2017a; Kim et al., 2023). One obvious cause in the difference of TEER values may be the species difference because as earlier stated this is the first time that Transwell model of BBB has been established using primary BECs from Horse. Also, the cells used in the study are primary cells from horse and may behave differently to other species. In addition, drug transport studies need to be conducted in presence of inhibitors of multidrug efflux transporters to observe the effect of presence of inhibitors on the pharmacokinetic parameters like P_{app}, P_{exact} and Efflux Ratios.

Chapter 6

Discussion

6.1 Context

The objective of this study was to create a model of Blood-Brain Barrier using Horse brain endothelial cells to study the permeability of selective test drugs across this model. This was the first time that an attempt was made to develop BBB model using horse brain endothelial cells.

Initially, a method was developed to isolate HBECs from horse brains. After isolation, the cells could be preserved in liquid nitrogen and be subsequently thawed and cultured. The cultured cells were then thoroughly characterised to ensure preservation of blood-brain barrier (BBB) phenotype, Also, it was established that in transwell culture that HBECs phenotype can be improved further through the addition of astrocyte conditioned medium. Though, drug transport studies exhibited that the Transwell model of BBB developed using HBECs had a degree of leakiness and had a low level of multidrug efflux. The rate of permeability of most test drugs exhibited negative correlation with the TEER value.

6.2 Junctional Adhesion

The conservation of proteins linked with junctional adhesion at the BBB and the localisation of these proteins at the cell-cell junctions, in HBEC culture has been confirmed many times in this novel study. Earlier similar studies in other species have verified that brain endothelial cells retain expression of tight junction proteins, (e.g. zona occludens-1 (ZO-1), claudin-5 and occludin) and also confirmed that these proteins are present at the cell-cell junction in the brain endothelial cell culture (Cantrill et al., 2012; Gericke et al., 2020; Patabendige et al., 2013; Thomsen et al., 2015). Similarly in the present study, results confirmed that cultured HBECs retain expression of tight junction molecules like ZO-1. Moreover, identification of VE-cadherin in the cultured HBECs verified the presence of adherens junctions. Additionally, the usage of scanning electron microscopy (SEM) revealed the detailed structure of HBECs. SEM showed the definite elevated areas at the cell-cell junction, which are highly likely to be tight junctions. This brings about the fact that tight junctions can be seen/observed using SEM and there is no need of costly and difficult immunostaining techniques to determine this further. Also, the images

of SEM performed in the present study revealed that, addition of puromycin to HBEC culture clearly reduced the number of contaminating cells i.e. astrocytes.

Similar studies in other species have demonstrated that transwell models of Brain Endothelial Cells can achieve high TEER values in monoculture ranging from 370–1650 Ω.cm^2 (Cantrill et al., 2012; Gericke et al., 2020; Patabendige et al., 2013; Thomsen et al., 2015). Whereas in the present study, the maximum TEER reported with HBECs was178 Ω.cm^2. So, it is quite apparent that TEER values stated in the present study are lower than previous studies. The reason may be differences in actual transwell plates used, as incongruities in surface area of the growth surface used can heighten impreciseness in TEER measurements during calculations. A smaller transwell insert, as used in present study, may result in over-confluence, causing reduced cell survival. The differences in TEER values between this study and others maybe due to a residual population of astrocytes and pericytes that survived puromycin purification process. Presence of astrocytes and pericytes in the cultures were also indicated by the presence of mRNA of the biomarker molecules for astrocytes and pericytes by PCR in cultured HBECs. Even though studies have employed puromycin to get pure culture of endothelial cells, the level of astrocytes and pericytes contamination in endothelial cell cultures in these studies is often not fully considered (Gericke et al., 2020; Patabendige et al., 2013; Thomsen et al., 2015). Therefore, straight comparison of TEER values between different but similar studies should be performed with thoughtfulness keeping in mind the fundamental and unanalysed incongruities.

Previous studies have reported that co-culture of Brain Endothelial cells with astrocytes has substantial effect on the expression and function of tight junctions in endothelial cell culture (Nielsen et al., 2017; Thomsen et al., 2015). But in this study astrocyte co-culture failed to increase the TEER levels of HBEC monolayer. Likewise, astrocyte co-culture failed to decrease the permeability of fluorescent marker FITC-dextran. On the contrary, addition of astrocyte conditioned medium (ACM) increased TEER levels of the HBEC monolayer and decreased FITC-dextran permeability of the HBEC monolayer.

The reason behind this difference may be that the astrocyte cell line used in this study (CTX-TNA2) has already undergone several passages and thus might has lost its original phenotype whereas ACM is obtained by conditioning the growth media with primary human astrocytes.

Molecular studies authenticated the expression and localisation of tight junction proteins within the isolated and cultured HBECs however transport studies across transwell monolayer of HBECs exhibited paracellular leakage of test drugs. Undeniably, permeability rates of most test drugs are 10-folds higher for in both directions than those observed in another study (Bentham, 2010). Thus, it is presumed that HBECs are forming a monolayer, but they are not as strongly bound at the cell-cell junctions as other brain endothelial cell cultures (Bentham, 2010).

6.3 Multidrug Efflux Transporters

Different structurally dissimilar substrates of multidrug efflux transporters at the level of BBB, including P-glycoprotein (P-gp), BCP and MRPs, make ATP-Binding Cassette (ABC) transporters a main impediment in the drug development (Rauch, 2011). This is the reason that expression of multidrug efflux transporters by BECs is extensively explored, with P-gp being the most comprehensively characterised BBB transporter. Earlier similar studies have confirmed expression of P-gp and BCRP in brain endothelial cell cultures (Cantrill et al., 2012; Gericke et al., 2020; Patabendige, Skinner, & Abbott, 2013; Thomsen et al., 2015b). Certainly, this present study clearly demonstrated that BECs from horse also expressed both P-gp and BCRP. Additionally, these same cultures also expressed MRP1 which was earlier considered to be expressed at insignificant levels in BECs from other species (Warren et al., 2009).

,In the present study, expression of P-gp was shown using qPCR, though mere presence of mRNA does not directly translate to functionality of transporters. Therefore P-gp function tests are required to authenticate the transporter function in the BBB model. It is also possible that P-gp expression might have decreased during culture and therefore qPCR on HBEC should be conducted on completion of drug transport studies. Also, it is very much possible that

higher levels of paracellular transport could be masking any drug efflux that is taking place. It should be noted that there was slight evidence of reverse active efflux of some drugs (e.g. chlorpromazine and mitoxantrone). Confocal microscopy in combination with immunoflourescent staining for multidrug efflux transporters may prove helpful in localising these transporters on the HBEC monolayer.

Many previous studies have proved that multidrug efflux transporter expression is changed by co-culture with astrocytes or by presence of ACM (Cucullo, Marchi, et al., 2011; Gaillard et al., 2000; Garcia-Polite et al., 2017b; Z. Wang et al., 2018). In the present study, cultured HBECs exhibited elevated mRNA expression of P-gp in the presence of both ACM and puromycin.

6.4 The neurovascular unit (NVU)

Although, often considered a supportive cell type of NVU, pericytes in the pure culture of brain endothelial cells are believed to be a challenging contaminant. The reason is that pericytes can proliferate quicker than BECs *in vitro* and turn out to be the main constituent of the culture. Also, unlike endothelial cells, pericytes do not have tight junctions and thus their contamination in the pure BEC culture would decrease the tightness and increase paracellular permeability (Perrière et al., 2005). Puromycin purification process has been registered to eliminate up to 98% of pericytes from BEC culture (Nielsen et al., 2017b; Perrière et al., 2005)(Nielsen et al., 2017b; Perrière et al., 2005)(Nielsen et al., 2017b; Perrière et al., 2005). Immunofluorescence results of the present study reduced the presence of pericytes in BECs after puromycin exposure for the initial three days. Even then there is possibility of presence of pericytes after addition of puromycin leading to lower level of junctional tightness and TEER. But, as these previous models were developed using endothelial cells from other species and secondly, these studies did not examine the presence of pericytes without puromycin treatment, no solid inferences can be obtained (Cantrill et al., 2012; Patabendige, Skinner, & Abbott, 2013; Thomsen et al., 2015b).

In the preliminary studies, Transwell model of HBEC monolayer exhibited more junctional adhesion with ACM in comparison to astrocyte co-culture using astrocyte cell line i.e. CTX TNA2. Therefore, ACM was used as a substitute for astrocyte co-culture in the drug transport studies. However, other BEC models which exhibited comparatively more junctional tightness employed astrocyte co-culture as standard (Bentham, 2010; Cantrill et al., 2012; Thomsen et al., 2015b). Although, the use of ACM increased junctional tightness of the HBEC Transwell model of BBB, TEER was still below the recommended threshold value for drug transport studies of 500 $\Omega.cm^2$ (Mantle et al., 2016). Therefore, it can be suggested that further modifications to the present Transwell model of BBB is necessary.

The basement membrane is often overlooked as a component of the NVU (Abbott et al., 2006). These basement proteins perform a vital function in controlling gene transcription in endothelial cells (Abbott et al., 2010a). In the present study, proteins such as fibronectin was used to culture HBECS in culture flasks, whereas both fibronectin & collagen were employed to culture HBECs in the Transwell model of Horse BBB.

6.5 Drug transport and quantification

To assess the BBB phenotype of the Transwell model of Horse BBB, few test drugs were selected which were substrates for various multidrug efflux pumps. Drug transport studies across the HBEC monolayer of Transwell model of BBB exhibited higher than anticipated levels of paracellular transport. *In vivo* the level of paracellular transport at BBB is negligible. This elevated level of paracellular transport in the present study made interpretation of other drug transport mechanisms like efflux, uptake and transcellular passive diffusion difficult.

Apparent and Exact permeability coefficients (P_{app} and P_{exact}) were determined for eight selected test drugs to exhibit the rate of transport of these across the HBEC monolayer. It is quite evident from both P_{app} and P_{exact} for some drugs (e.g. chlorpromazine, mitoxantrone and camptothecin) that their rate of transport is higher in apical to basal direction than basal to apical direction. Moreover, both P_{app} and P_{exact} had a higher transport rate of drugs in

comparison to other similar models developed using brain endothelial cells from other species (Bentham, 2010). In the present study, efflux ratios clearly showed that none of the tested drugs experienced significant uptake or efflux across the HBEC monolayer.

6.6 The Transwell Model of Horse BBB

The Transwell model of BBB is frequently used in the drug discovery procedure, and various Transwell models of BBB have been reported in other species (Cantrill et al., 2012; Gericke et al., 2020; Patabendige, Skinner, & Abbott, 2013; Thomsen et al., 2015a). The foremost advantage of the Transwell model system is the comfort of use. This study found that no additional or further cell culture method alterations are required to culture HBECs.. Though, the HBEC Transwell model established in this study lacked some important BBB features which were observed in other Transwell BBB models. This resulted in paracellular permeability of the HBEC monolayer being higher than the other similar previous studies. This made the interpretation of the uptake and efflux of the selected test drugs difficult. Although this might not be the sole reason for the discrepancies. As previously stated, procedural dissimilarities like size of the Transwell insert used, the length of endothelial cell culture time, use of ACM, use and concentration of the stimulation factors and supporting NVU cell types could explain the differences. So, it was concluded that the HBEC Transwell model of BBB developed require modifications.

6.7 Recent developments in the field

Many innovations have taken place with BBB-on-chip like hypoxia induced BBB-on-chip (Park et al., 2019), Neonatal BBB-on-chip (Deosarkar et al., 2015) and induced pluripotent stem cell based BBB-on-chip (Workman & Svendsen, 2020). There are two main BBB-on-chip models commercially available. The two companies marketing these are Synvivo and Mimetas. These products have been used by various research studies on BBB by many researchers (Jagtiani et al., 2022).

6.8 Summary and implications

This is the first time that a BBB model of horse brain endothelial cells has been developed and drug transport studies have been conducted on it. This present study has proved that HBECs show many molecular indicators of the maintenance of the BBB phenotype *in vitro*, like the presence of tight junctions and expression multidrug efflux transporters. Nevertheless, it is obvious that the technical skill needed for the isolation and culture of primary HBEC is a limitation regarding the use of this cell type. Addition to puromycin in the growth media of HBEC cell culture decreased the number of contaminating cells. Addition of ACM to the Transwell model of HBEC cell culture increased TEER and decreased FITC-dextran permeability. Simultaneous, exposure of ACM and puromycin increased the expression level of multidrug efflux transporter, P-glycoprotein. Additionally, the cultured primary HBECs monolayer exhibited lower TEER values and higher permeability of marker molecules and test drugs in comparison to other similar studies done using cells from other species. The reason for this could be linked to the higher leakage of the tight junctions resulting in high paracellular permeability.

6.9 Future directions

The effect of Covid -19 pandemic on this assignment constrained the work that could be undertaken to refine the Transwell model of Horse BBB and develop organ-on-chip model of Horse BBB. Primarily, additional studies into the reason of the lower than anticipated TEER values and higher paracellular permeability of the test drugs are required. This would encompass use of confocal microscopy to image the HBEC culture on the Transwell inserts to observe the presence of cell multi-layering and over-confluency. Confocal microscopy combined with immunoflourescent staining of multidrug efflux transporter proteins like P-gp would enable determination of whether these transporter proteins are present on the apical side of the HBECs. Also, Trypan Blue test (Strober, 2015) would be conducted to examine the cell death on the Transwell inserts, which might have taken place because of over-confluence. Additionally, further enquiry into the presence of pericytes in the HBEC cultures would be required to determine if these cells are the cause of leaky

tight junctions. This would require immunoflourescent co-staining of endothelial cell marker ZO-1 (Tornavaca et al., 2015) and pericytes biomarker αSMA (Skalli et al., 1989). This will help to observe if αSMA-positive cells are incorporated into the HBEC monolayer, where they could cause disruption of integrity of the endothelial cell monolayer. Moreover, the quantitative expression of multidrug efflux transporter proteins must be undertaken after the drug transport studies using qPCR, to confirm that the efflux transporters are downregulated during the drug transport study. Finally, the main difference between the present Transwell model and other previous similar transwell models, is the co-culture with CTX-TNA2 astrocytes (Cantrill et al., 2012). In the present study instead of co-culture with CTX-TNA2 astrocytes, during drug transport studies the endothelial cells were cultured in the presence of ACM. The reason for using ACM instead of CTX-TNA2 is that during preliminary studies endothelial cell monolayer cultured on Transwell insert demonstrated maximum TEER and minimum permeability for FITC-dextran in the presence of ACM. Further, studies need to be conducted in the presence and absence of selective inhibitors of P-gp, MRP1 and BCRP, so that the role of these multidrug efflux pumps in the transport of their substrates can be explained.

Further studies need to be performed to develop a HBEC organ on a chip BBB model (Li et al., 2023). Original plan was to study the effect of shear stress on the phenotype of the HBECs, but time constraints developed due to COVID-19 prevented further investigation. This would include immunofluorescence staining for ZO-1 in the HBEC BBB organ on a chip to envisage the tight junction formation between the endothelial cells cultured on the microfluidic chip. Further studies would include assessment of expression levels of multidrug efflux pumps using qPCR on application of different levels of shear stress. Additional studies include use of confocal microscopy to observe the change in endothelial cell morphology on application of shear stress on a microfluidic chip. Confocal microscopy would also aid in the localisation of the multidrug efflux transporters to the apical side of the endothelial cells. Moreover, the drug transport studies could be repeated on the HBEC BBB organ on a chip model using the same compounds to

compare the permeability and efflux of these drugs between these two models. By this the effect of shear stress on the soundness of the tight junctions (Cucullo et al., 2011) and activity level of multidrug efflux pumps would be elucidated.

Furthermore, the current model of Horse BBB would only be workable for testing drug transport in a healthy brain. Later, this model could be employed to imitate diseases with the addition of astrocytes, microglial cells or diseased patient originated neurons, (e.g. Alzheimer disease, Cerebral Aneurysm, Amyotrophic Lateral Sclerosis, Brain Tumours) (Cui & Cho, 2022). To summarise, if fully authenticated, the microfluidic HBEC BBB organ on a chip model has the capability to be established with the latest advances in the cell culture technology and microfluidic technology to turn out to be more pertinent for pharmacological, physiological and pathological studies than presently available other BBB models.

Bibliography

Bibliography

Abbott, N. J. (2002). Astrocyte-endothelial interactions and blood-brain barrier permeability. In *Journal of Anatomy* (Vol. 200, Issue 6, pp. 629–638). https://doi.org/10.1046/j.1469-7580.2002.00064.x

Abbott, N. J. (2004). Prediction of blood-brain barrier permeation in drug discovery from in vivo, in vitro and in silico models. *Drug Discovery Today: Technologies*, *1*(4), 407–416. https://doi.org/10.1016/J.DDTEC.2004.11.014

Abbott, N. J., Dolman, D. E. M., Drndarski, S., & Fredriksson, S. M. (2012). An improved in vitro blood-brain barrier model: Rat brain endothelial cells co-cultured with astrocytes. *Methods in Molecular Biology*, *814*, 415–430. https://doi.org/10.1007/978-1-61779-452-0_28

Abbott, N. J., Hughes, C. C. W., Revest, P. A., & Greenwood, J. (1992). Development and characterisation of a rat brain capillary endothelial culture: towards an in vitro blood-brain barrier. Journal of Cell Science, 103, 23–37 –

Abbott, N. J., Patabendige, A. A. K., Dolman, D. E. M., Yusof, S. R., & Begley, D. J. (2010a). Structure and function of the blood-brain barrier. *Neurobiology of Disease*, *37*(1), 13–25. https://doi.org/10.1016/j.nbd.2009.07.030

Abbott, N. J., Patabendige, A. A. K., Dolman, D. E. M., Yusof, S. R., & Begley, D. J. (2010b). Structure and function of the blood–brain barrier. *Neurobiology of Disease*, *37*(1), 13–25. https://doi.org/10.1016/J.NBD.2009.07.030

Abbott, N. J., Rönnbäck, L., & Hansson, E. (2006). Astrocyte-endothelial interactions at the blood-brain barrier. *Nature Reviews Neuroscience*, *7*(1), 41–53. https://doi.org/10.1038/NRN1824

Abbott, N. J., Rönnbäck, L., & Hansson, E. (2006). Astrocyte-endothelial interactions at the blood-brain barrier. Nature Reviews Neuroscience, 7(1), 41–53. https://doi.org/10.1038/nrn1824

Alvarez, J. I., Katayama, T., & Prat, A. (2013). Glial influence on the blood brain barrier. In *GLIA* (Vol. 61, Issue 12, pp. 1939–1958). https://doi.org/10.1002/glia.22575

Armulik, A., Genové, G., Mäe, M., Nisancioglu, M. H., Wallgard, E., Niaudet, C., He, L., Norlin, J., Lindblom, P., Strittmatter, K., Johansson, B. R., & Betsholtz, C. (2010). Pericytes regulate the blood-brain barrier. *Nature*, *468*(7323), 557–561. https://doi.org/10.1038/NATURE09522

Baker, D. E. (2007). Loperamide: a pharmacological review. *Reviews in Gastroenterological Disorders*, *7 Suppl 3*, S11-8. http://europepmc.org/abstract/MED/18192961

Ballabh, P., Braun, A., & Nedergaard, M. (2004). The blood-brain barrier: An overview: Structure, regulation, and clinical implications. In *Neurobiology of Disease* (Vol. 16, Issue 1, pp. 1–13). https://doi.org/10.1016/j.nbd.2003.12.016

Barakat, S., Turcotte, S., Demeule, M., Lachambre, M.-P., Régina, A., Baggetto, L. G., & Béliveau, R. (2008). Regulation of brain endothelial cells migration and angiogenesis by P-glycoprotein/caveolin-1 interaction. *Biochemical and Biophysical Research Communications*, *372*(3), 440–446. https://doi.org/10.1016/j.bbrc.2008.05.012

Bates, D. O. (2010). Vascular endothelial growth factors and vascular permeability. *Cardiovascular Research*, *87*(2), 262. https://doi.org/10.1093/CVR/CVQ105

Bazzoni, G. (2006). Endothelial tight junctions: Permeable barriers of the vessel wall. *Thrombosis and Haemostasis*, *95*(1), 36–42. https://doi.org/10.1160/TH05-07-0488

Bednarczyk, D., & Sanghvi, M. V. (2020). The impact of assay recovery on the apparent permeability, a function of lysosomal trapping. *Xenobiotica*, *50*(7), 753–760. https://doi.org/10.1080/00498254.2019.1691284

Begley, D. (2004). ABC Transporters and the Blood-Brain Barrier. *Current Pharmaceutical Design*, *10*(12), 1295–1312. https://doi.org/10.2174/1381612043384844

Begley, D. J. (2006). Structure and function of the blood-brain barrier. *Enhancement in Drug Delivery*, *37*(1), 575–592. https://doi.org/10.1016/j.nbd.2009.07.030

Begley, D. J., & Brightman, M. W. (2003). Structural and functional aspects of the blood-brain barrier. In *Progress in Drug Research* (Vol. 61, pp. 39–78). https://doi.org/10.1007/978-3-0348-8049-7_2

Bentham, L. (2010). The Use of In Vitro Unbound Drug Fraction and Permeability in Predicting Central Nervous System Drug Penetration. University of Manchester, Faculty of Medical & Human Sciences, Doctor of Philosophy.

Berezowski, V., Landry, C., Dehouck, M.-P., Cecchelli, R., & Fenart, L. (2004). Contribution of glial cells and pericytes to the mRNA profiles of P-glycoprotein and multidrug resistance-associated proteins in an in vitro model of the blood-brain barrier. *Brain Research*, *1018*(1), 1–9. https://doi.org/10.1016/j.brainres.2004.05.092

Bernacki, J., Dobrowolska, A., Nierwiñska, K., & Ma3ecki, A. (2008). *Physiology and pharmacological role of the blood-brain barrier*.

Bhatia, S. N., & Ingber, D. E. (2014). Microfluidic organs-on-chips. *Nature Biotechnology*, *32*(8), 760–772. https://doi.org/10.1038/NBT.2989

Bickel, U. (2005). How to measure drug transport across the blood-brain barrier. *NeuroRx*, *2*(1), 15–26. https://doi.org/10.1602/neurorx.2.1.15

Bicker, J., Alves, G., Fortuna, A., & Falcão, A. (2014). Blood-brain barrier models and their relevance for a successful development of CNS drug delivery systems: A review. *European Journal of Pharmaceutics and Biopharmaceutics*, *87*(3), 409–432. https://doi.org/10.1016/j.ejpb.2014.03.012

Booth, R., & Kim, H. (2012). Characterization of a microfluidic in vitro model of the blood-brain barrier (μBBB). *Lab on a Chip*. https://doi.org/10.1039/c2lc40094d

Borst, P., & Schinkel, A. H. (2013). P-glycoprotein abcb1: A major player in drug handling by mammals. *Journal of Clinical Investigation*, *123*(10), 4131–4133. https://doi.org/10.1172/JCI70430

Bowman, P. D., Ennis, S. R., Rarey, K. E., Betz, A. L., & Goldstein, G. W. (1983). Brain microvessel endothelial cells in tissue culture: a model for study of blood-brain barrier permeability. *Annals of Neurology*, *14*(4), 396–402. https://doi.org/10.1002/ana.410140403

Boyer-Di Ponio, J., El-Ayoubi, F., Glacial, F., Ganeshamoorthy, K., Driancourt, C., Godet, M., Perrière, N., Guillevic, O., Olivier Couraud, P., & Uzan, G. (2014). Instruction of circulating endothelial progenitors in vitro towards specialized blood-brain barrier and arterial phenotypes. *PloS One*, *9*(1). https://doi.org/10.1371/JOURNAL.PONE.0084179

Braun, L. D., Cornford, E. M., & Oldendorf, W. H. (1980). Newborn rabbit blood-brain barrier is selectively permeable and differs substantially from the adult. *Journal of Neurochemistry*, *34*(1), 147–152. https://doi.org/10.1111/j.1471-4159.1980.tb04633.x

Brightman, M. W., & Reese, T. S. (1969). Junctions between intimately apposed cell membranes in the vertebrate brain. *The Journal of Cell Biology*, *40*(3), 648–677. https://doi.org/10.1083/jcb.40.3.648

Bussolari, S. R., Dewey, C. F., & Gimbrone, M. A. (1982). Apparatus for subjecting living cells to fluid shear stress. *The Review of Scientific Instruments*, *53*(12), 1851–1854. https://doi.org/10.1063/1.1136909

Butt, A. M., Jones, H. C., & Abbott, N. J. (1990). Electrical resistance across the blood-brain barrier in anaesthetized rats: a developmental study. *The Journal of Physiology*, *429*(1), 47–62. https://doi.org/10.1113/JPHYSIOL.1990.SP018243

Canfield, S. G., Stebbins, M. J., Morales, B. S., Asai, S. W., Vatine, G. D., Svendsen, C. N., Palecek, S. P., & Shusta, E. V. (2017). An isogenic blood-brain barrier model comprising brain endothelial cells, astrocytes, and neurons derived from human induced pluripotent stem cells. *Journal of Neurochemistry*, *140*(6), 874–888. https://doi.org/10.1111/JNC.13923

Cantrill, C. A., Skinner, R. A., Rothwell, N. J., & Penny, J. I. (2012). An immortalised astrocyte cell line maintains the in vivo phenotype of a primary porcine in vitro blood-brain barrier model. *Brain Research*, *1479*, 17–30. https://doi.org/10.1016/J.BRAINRES.2012.08.031

Casbeer, H. C., & Knych, H. K. (2013). Pharmacokinetics and pharmacodynamic effects of tolazoline following intravenous administration to horses. *Veterinary Journal (London, England : 1997)*, *196*(3), 504–509. https://doi.org/10.1016/j.tvjl.2012.12.006

Chen, Y., & Liu, L. (2012). Modern methods for delivery of drugs across the blood-brain barrier. In *Advanced Drug Delivery Reviews* (Vol. 64, Issue 7, pp. 640–665). https://doi.org/10.1016/j.addr.2011.11.010

Cheslow, L., & Alvarez, J. I. (2016). Glial-endothelial crosstalk regulates blood-brain barrier function. *Current Opinion in Pharmacology*, *26*, 39–46. https://doi.org/10.1016/j.coph.2015.09.010

Chong, G. O., Han, H. S., Lee, S. D., & Lee, Y. H. (2020). Improvement in RNA quantity and quality in cervico-vaginal cytology. *Virology Journal*, *17*(1), 8. https://doi.org/10.1186/S12985-020-1282-X

Chu, X., Bleasby, K., & Evers, R. (2013). Species differences in drug transporters and implications for translating preclinical findings to humans. *Expert Opinion on Drug Metabolism and Toxicology*, *9*(3), 237–252. https://doi.org/10.1517/17425255.2013.741589

Circumvention of breast cancer resistance protein (BCRP)-mediated resistance to camptothecins in vitro using non-substrate drugs or the BCRP inhibitor GF120918 - PubMed. (n.d.). Retrieved February 19, 2025, from https://pubmed.ncbi.nlm.nih.gov/11309344/

Clark, D. E. (2003). In silico prediction of blood–brain barrier permeation. *Drug Discovery Today*, *8*(20), 927–933. https://doi.org/10.1016/S1359-6446(03)02827-7

Cohen-Kashi Malina, K., Cooper, I., & Teichberg, V. I. (2009). Closing the gap between the in-vivo and in-vitro blood-brain barrier tightness. *Brain Research*, *1284*, 12–21. https://doi.org/10.1016/j.brainres.2009.05.072

Cole, S. P. C. (2014). Multidrug resistance protein 1 (MRP1, ABCC1), a “multitasking” ATP-binding cassette (ABC) transporter. *The Journal of Biological Chemistry*, *289*(45), 30880–30888. https://doi.org/10.1074/JBC.R114.609248

Crone, C., & Christensen, O. (1981). Electrical resistance of a capillary endothelium. *Journal of General Physiology*, *77*(4), 349–371. https://doi.org/10.1085/jgp.77.4.349

Cucullo, L., Couraud, P. O., Weksler, B., Romero, I. A., Hossain, M., Rapp, E., & Janigro, D. (2008). Immortalized human brain endothelial cells and flow-based vascular modeling: A marriage of convenience for rational

neurovascular studies. *Journal of Cerebral Blood Flow and Metabolism*, *28*(2), 312–328. https://doi.org/10.1038/sj.jcbfm.9600525

Cucullo, L., Hossain, M., Puvenna, V., Marchi, N., & Janigro, D. (2011a). The role of shear stress in Blood-Brain Barrier endothelial physiology. *BMC Neuroscience*, *12*. https://doi.org/10.1186/1471-2202-12-40

Cucullo, L., Hossain, M., Puvenna, V., Marchi, N., & Janigro, D. (2011b). The role of shear stress in Blood-Brain Barrier endothelial physiology. *BMC Neuroscience*, *12*, 40. https://doi.org/10.1186/1471-2202-12-40

Cucullo, L., Marchi, N., Hossain, M., & Janigro, D. (2011). A dynamic in vitro BBB model for the study of immune cell trafficking into the central nervous system. *Journal of Cerebral Blood Flow and Metabolism*, *31*(2), 767–777. https://doi.org/10.1038/jcbfm.2010.162

Czupalla, C. J., Liebner, S., & Devraj, K. (2014). *In Vitro Models of the Blood–Brain Barrier*. 415–437. https://doi.org/10.1007/978-1-4939-0320-7_34

Dahlin, A., Royall, J., Hohmann, J. G., & Wang, J. (2009). Expression profiling of the solute carrier gene family in the mouse brain. *Journal of Pharmacology and Experimental Therapeutics*, *329*(2), 558–570. https://doi.org/10.1124/jpet.108.149831

Dallas, S., Miller, D. S., & Bendayan, R. (2006). Multidrug resistance-associated proteins: Expression and function in the central nervous system. In *Pharmacological Reviews* (Vol. 58, Issue 2, pp. 140–161). https://doi.org/10.1124/pr.58.2.3

Daneman, R., & Prat, A. (2015). The blood–brain barrier. *Cold Spring Harbor Perspectives in Biology*, *7*(1). https://doi.org/10.1101/CSHPERSPECT.A020412

Daneman, R., Zhou, L., Kebede, A. A., & Barres, B. A. (2010). Pericytes are required for blood-brain barrier integrity during embryogenesis. *Nature*, *468*(7323), 562–566. https://doi.org/10.1038/nature09513

Dauchy, S., Dutheil, F., Weaver, R. J., Chassoux, F., Daumas-Duport, C., Couraud, P.-O., Scherrmann, J.-M., De Waziers, I., & Declèves, X. (2008). ABC transporters, cytochromes P450 and their main transcription factors: expression at the human blood-brain barrier. *Journal of Neurochemistry*, *107*(6), 1518–1528. https://doi.org/10.1111/j.1471-4159.2008.05720.x

Dean, M. (2002). *The Human ATP-Binding Cassette (ABC) Transporter Superfamily*.

Dean, M., Rzhetsky, A., & Allikmets, R. (2001). The human ATP-binding cassette (ABC) transporter superfamily. *Genome Research*, *11*(7), 1156–1166. https://doi.org/10.1101/gr.184901

DeBault, L. E., & Cancilla, P. A. (1980). gamma-Glutamyl transpeptidase in isolated brain endothelial cells: induction by glial cells in vitro. *Science (New York, N.Y.)*, *207*(4431), 653–655. https://doi.org/10.1126/science.6101511

DeBault, L. E., Henriquez, E., Hart, M. N., & Cancilla, P. A. (1981). Cerebral microvessels and derived cells in tissue culture - II. Establishment, identification, and preliminary characterization of an endothelial cell line. *In Vitro*, *17*(6), 480–494. https://doi.org/10.1007/BF02633509

DeBault, L. E., Kahn, L. E., Frommes, S. P., & Cancilla, P. A. (1979). Cerebral microvessels and derived cells in tissue culture: Isolation and preliminary characterization. *In Vitro*, *15*(7), 473–487. https://doi.org/10.1007/BF02618149

Decleves, X., Jacob, A., Yousif, S., Shawahna, R., Potin, S., & Scherrmann, J.-M. (2011). Interplay of Drug Metabolizing CYP450 Enzymes and ABC Transporters in the Blood-Brain Barrier. *Current Drug Metabolism*, *12*(8), 732–741. https://doi.org/10.2174/138920011798357024

Deguchi, Y. (2002). Application of In Vivo Brain Microdialysis to the Study of Blood-Brain Barrier Transport of Drugs. *Drug Metabolism and Pharmacokinetics*, *17*(5), 395–407. https://doi.org/10.2133/dmpk.17.395

Dehouck, M. P., Méresse, S., Delorme, P., Fruchart, J. C., & Cecchelli, R. (1990). An easier, reproducible, and mass-production method to study the blood-brain barrier in vitro. *Journal of Neurochemistry*, *54*(5), 1798–1801. https://doi.org/10.1111/j.1471-4159.1990.tb01236.x

Deli, M. A., Ábrahám, C. S., Kataoka, Y., & Niwa, M. (2005). Permeability studies on in vitro blood-brain barrier models: Physiology, pathology, and pharmacology. In *Cellular and Molecular Neurobiology* (Vol. 25, Issue 1, pp. 59–127). https://doi.org/10.1007/s10571-004-1377-8

Deosarkar, S. P., Prabhakarpandian, B., Wang, B., Sheffield, J. B., Krynska, B., & Kiani, M. F. (2015). A novel dynamic neonatal blood-brain barrier on a chip. *PLoS ONE*, *10*(11). https://doi.org/10.1371/JOURNAL.PONE.0142725

Díaz-Castro, B., Robel, S., & Mishra, A. (2023). Astrocyte Endfeet in Brain Function and Pathology: Open Questions. *Annual Review of Neuroscience*, *46*, 101–121. https://doi.org/10.1146/ANNUREV-NEURO-091922-031205

Di, L., & Chang, C. (2015). Methods for Assessing Brain Binding. *Blood-Brain Barrier in Drug Discovery: Optimizing Brain Exposure of CNS Drugs and Minimizing Brain Side Effects for Peripheral Drugs*, 274–283. https://doi.org/10.1002/9781118788523.CH12

Di, L., Kerns, E. H., Bezar, I. F., Petusky, S. L., & Huang, Y. (2009). Comparison of blood-brain barrier permeability assays: In Situ brain

perfusion, MDR1-MDCKII and PAMPA-BBB. *Journal of Pharmaceutical Sciences*, *98*(6), 1980–1991. https://doi.org/10.1002/JPS.21580

Di, L., Kerns, E. H., & Carter, G. T. (2008). Strategies to assess blood-brain barrier penetration. *Expert Opinion on Drug Discovery*, *3*(6), 677–687. https://doi.org/10.1517/17460441.3.6.677

Dohgu, S., Takata, F., Yamauchi, A., Nakagawa, S., Egawa, T., Naito, M., Tsuruo, T., Sawada, Y., Niwa, M., & Kataoka, Y. (2005). Brain pericytes contribute to the induction and up-regulation of blood-brain barrier functions through transforming growth factor-β production. *Brain Research*, *1038*(2), 208–215. https://doi.org/10.1016/j.brainres.2005.01.027

Drin, G., Cottin, S., Blanc, E., Rees, A. R., & Temsamani, J. (2003). Studies on the internalization mechanism of cationic cell-penetrating peptides. *The Journal of Biological Chemistry*, *278*(33), 31192–31201. https://doi.org/10.1074/jbc.M303938200

Elbakary, B., & Badhan, R. K. S. (2020). A dynamic perfusion based blood-brain barrier model for cytotoxicity testing and drug permeation. *Scientific Reports 2020 10:1*, *10*(1), 1–12. https://doi.org/10.1038/s41598-020-60689-w

Erdo, F., & Krajcsi, P. (2019). Age-Related Functional and Expressional Changes in Efflux Pathways at the Blood-Brain Barrier. *Frontiers in Aging Neuroscience*, *11*(JUL). https://doi.org/10.3389/FNAGI.2019.00196

Esser, L., Zhou, F., Pluchino, K. M., Shiloach, J., Ma, J., Tang, W. K., Gutierrez, C., Zhang, A., Shukla, S., Madigan, J. P., Zhou, T., Kwong, P. D., Ambudkar, S. V., Gottesman, M. M., & Xia, D. (2017). Structures of the Multidrug Transporter P-glycoprotein Reveal Asymmetric ATP Binding and the Mechanism of Polyspecificity. *Journal of Biological Chemistry*, *292*(2), 446–461. https://doi.org/10.1074/jbc.M116.755884

Fábián, G., Szabó, C. A., Bozó, B., Greenwood, J., Adamson, P., Deli, M. A., Joó, F., Krizbai, I. A., & Szucs, M. (1998). Expression of G-protein subtypes in cultured cerebral endothelial cells. *Neurochemistry International*, *33*(2), 179–185. https://doi.org/10.1016/S0197-0186(98)00008-4

Förster, C., Burek, M., Romero, I. A., Weksler, B., Couraud, P. O., & Drenckhahn, D. (2008). Differential effects of hydrocortisone and TNFα on tight junction proteins in an in vitro model of the human blood-brain barrier. *Journal of Physiology*, *586*(7), 1937–1949. https://doi.org/10.1113/JPHYSIOL.2007.146852

Förster, F., Volz, A., & Fricker, G. (2008). Compound profiling for ABCC2 (MRP2) using a fluorescent microplate assay system. *European Journal of Pharmaceutics and Biopharmaceutics*, *69*(1), 396–403. https://doi.org/10.1016/j.ejpb.2007.10.003

Franke, H., Galla, H. J., & Beuckmann, C. T. (2000). Primary cultures of brain microvessel endothelial cells: A valid and flexible model to study drug transport through the blood-brain barrier in vitro. *Brain Research Protocols*, *5*(3), 248–256. https://doi.org/10.1016/S1385-299X(00)00020-9

Gaillard, P. J., Van Der Sandt, I. C. J., Voorwinden, L. H., Vu, D., Nielsen, J. L., De Boer, A. G., & Breimer, D. D. (2000). Astrocytes increase the functional expression of P-glycoprotein in an in vitro model of the blood-brain barrier. *Pharmaceutical Research*, *17*(10), 1198–1205. https://doi.org/10.1023/A:1026406528530

Garberg, P., Ball, M., Borg, N., Cecchelli, R., Fenart, L., Hurst, R. D., Lindmark, T., Mabondzo, A., Nilsson, J. E., Raub, T. J., Stanimirovic, D., Terasaki, T., Öberg, J. O., & Österberg, T. (2005). In vitro models for the blood-brain barrier. *Toxicology in Vitro : An International Journal Published in Association with BIBRA*, *19*(3), 299–334. https://doi.org/10.1016/J.TIV.2004.06.011

Garcia-Polite, F., Martorell, J., Del Rey-Puech, P., Melgar-Lesmes, P., O'Brien, C. C., Roquer, J., Ois, A., Principe, A., Edelman, E. R., & Balcells, M. (2017a). Pulsatility and high shear stress deteriorate barrier phenotype in brain microvascular endothelium. *Journal of Cerebral Blood Flow and Metabolism : Official Journal of the International Society of Cerebral Blood Flow and Metabolism*, *37*(7), 2614–2625. https://doi.org/10.1177/0271678X16672482

Garcia-Polite, F., Martorell, J., Del Rey-Puech, P., Melgar-Lesmes, P., O'Brien, C. C., Roquer, J., Ois, A., Principe, A., Edelman, E. R., & Balcells, M. (2017b). Pulsatility and high shear stress deteriorate barrier phenotype in brain microvascular endothelium. *Journal of Cerebral Blood Flow and Metabolism*, *37*(7), 2614–2625. https://doi.org/10.1177/0271678X16672482

Gericke, B., Römermann, K., Noack, A., Noack, S., Kronenberg, J., Blasig, I. E., & Löscher, W. (2020). A face-to-face comparison of claudin-5 transduced human brain endothelial (hCMEC/D3) cells with porcine brain endothelial cells as blood-brain barrier models for drug transport studies. *Fluids and Barriers of the CNS*, *17*(1). https://doi.org/10.1186/S12987-020-00212-5

Ghosh, C., Gonzalez-Martinez, J., Hossain, M., Cucullo, L., Fazio, V., Janigro, D., & Marchi, N. (2010). Pattern of P450 expression at the human blood-brain barrier: Roles of epileptic condition and laminar flow. *Epilepsia*, *51*(8), 1408–1417. https://doi.org/10.1111/J.1528-1167.2009.02428.X

Ghosh, C., Puvenna, V., Gonzalez-Martinez, J., Janigro, D., & Marchi, N. (2011). Blood-Brain Barrier P450 Enzymes and Multidrug Transporters in Drug Resistance: A Synergistic Role in Neurological Diseases. *Current*

Drug Metabolism, *12*(8), 742. https://doi.org/10.2174/13892001 1798357051

Giri, N., Shaik, N., Pan, G., Terasaki, T., Mukai, C., Kitagaki, S., Miyakoshi, N., & Elmquist, W. F. (2008). Investigation of the role of breast cancer resistance protein (Bcrp/Abcg2) on pharmacokinetics and central nervous system penetration of abacavir and zidovudine in the mouse. *Drug Metabolism and Disposition*, *36*(8), 1476–1484. https://doi.org/10.1124/ dmd.108.020974

Gomes, M. J., Mendes, B., Martins, S., & Sarmento, B. (2015). Cell-based in vitro models for studying blood–brain barrier (BBB) permeability. *Concepts and Models for Drug Permeability Studies: Cell and Tissue Based in Vitro Culture Models*, 169–188. https://doi.org/10.1016/B978-0-08-100094-6.00011-0

Gomez-Zepeda, D., Taghi, M., Scherrmann, J. M., Decleves, X., & Menet, M. C. (2020). ABC Transporters at the Blood–Brain Interfaces, Their Study Models, and Drug Delivery Implications in Gliomas. *Pharmaceutics*, *12*(1), 20. https://doi.org/10.3390/PHARMACEUTICS12010020

Greenwood, J., Pryce, G., Devine, L., Male, D. K., Dos Santos, W. L. C., Calder, V. L., & Adamson, P. (1996). SV40 large T immortalised cell lines of the rat blood-brain and blood-retinal barriers retain their phenotypic and immunological characteristics. *Journal of Neuroimmunology*, *71*(1–2), 51–63. https://doi.org/10.1016/S0165-5728(96)00130-0

Griep, L. M., Wolbers, F., De Wagenaar, B., Ter Braak, P. M., Weksler, B. B., Romero, I. A., Couraud, P. O., Vermes, I., Van Der Meer, A. D., & Van Den Berg, A. (2013). BBB on CHIP: Microfluidic platform to mechanically and biochemically modulate blood-brain barrier function. *Biomedical Microdevices*, *15*(1), 145–150. https://doi.org/10.1007/S10544-012-9699-7

Grimsrud, K. N., Ait-Oudhia, S., Durbin-Johnson, B. P., Rocke, D. M., Mama, K. R., Rezende, M. L., Stanley, S. D., & Jusko, W. J. (2015). Pharmacokinetic and pharmacodynamic analysis comparing diverse effects of detomidine, medetomidine, and dexmedetomidine in the horse: A population analysis. *Journal of Veterinary Pharmacology and Therapeutics*, *38*(1), 24–34. https://doi.org/10.1111/jvp.12139

Hamilton, N. B., Attwell, D., & Hall, C. N. (2010). Pericyte-mediated regulation of capillary diameter: a component of neurovascular coupling in health and disease. *Frontiers in Neuroenergetics*, *2*. https://doi.org/10.3389/ fnene.2010.00005

Hamm, S., Dehouck, B., Kraus, J., Wolburg-Buchholz, K., Wolburg, H., Risau, W., Cecchelli, R., Engelhardt, B., & Dehouck, M.-P. (2004). Astrocyte mediated modulation of blood-brain barrier permeability does not correlate with a loss of tight junction proteins from the cellular contacts.

Cell and Tissue Research, *315*(2), 157–166. https://doi.org/10.1007/s00441-003-0825-y

Hawkins, B. T., & Davis, T. P. (2005). The blood-brain barrier/neurovascular unit in health and disease. In *Pharmacological Reviews* (Vol. 57, Issue 2, pp. 173–185). https://doi.org/10.1124/pr.57.2.4

Hayashi, K., Nakao, S., Nakaoke, R., Nakagawa, S., Kitagawa, N., & Niwa, M. (2004). Effects of hypoxia on endothelial/pericytic co-culture model of the blood-brain barrier. *Regulatory Peptides*, *123*(1–3), 77–83. https://doi.org/10.1016/j.regpep.2004.05.023

Hellinger, É., Veszelka, S., Tóth, A. E., Walter, F., Kittel, Á., Bakk, M. L., Tihanyi, K., Háda, V., Nakagawa, S., Dinh Ha Duy, T., Niwa, M., Deli, M. A., & Vastag, M. (2012). Comparison of brain capillary endothelial cell-based and epithelial (MDCK-MDR1, Caco-2, and VB-Caco-2) cell-based surrogate blood-brain barrier penetration models. *European Journal of Pharmaceutics and Biopharmaceutics : Official Journal of Arbeitsgemeinschaft Fur Pharmazeutische Verfahrenstechnik e.V*, *82*(2), 340–351. https://doi.org/10.1016/J.EJPB.2012.07.020

Helms, H. C., Abbott, N. J., Burek, M., Cecchelli, R., Couraud, P. O., Deli, M. A., Förster, C., Galla, H. J., Romero, I. A., Shusta, E. V., Stebbins, M. J., Vandenhaute, E., Weksler, B., & Brodin, B. (2015). In vitro models of the blood-brain barrier: An overview of commonly used brain endothelial cell culture models and guidelines for their use. *Journal of Cerebral Blood Flow and Metabolism*, *36*(5), 862–890. https://doi.org/10.1177/0271678X16630991

Helms, H. C., & Brodin, B. (2014). *Generation of Primary Cultures of Bovine Brain Endothelial Cells and Setup of Cocultures with Rat Astrocytes* (pp. 365–382). https://doi.org/10.1007/978-1-4939-0320-7_30

Heymans, M., Sevin, E., Gosselet, F., Lundquist, S., & Culot, M. (2018). Mimicking brain tissue binding in an in vitro model of the blood-brain barrier illustrates differences between in vitro and in vivo methods for assessing the rate of brain penetration. *European Journal of Pharmaceutics and Biopharmaceutics*, *127*, 453–461. https://doi.org/10.1016/j.ejpb.2018.03.007

He, Y., Yao, Y., Tsirka, S. E., & Cao, Y. (2014). Cell-culture models of the blood-brain barrier. *Stroke*, *45*(8), 2514–2526. https://doi.org/10.1161/STROKEAHA.114.005427

Hori, S., Ohtsuki, S., Hosoya, K. I., Nakashima, E., & Terasaki, T. (2004). A pericyte-derived angiopoietin-1 multimeric complex induces occludin gene expression in brain capillary endothelial cells through Tie-2 activation in vitro. *Journal of Neurochemistry*, *89*(2), 503–513. https://doi.org/10.1111/J.1471-4159.2004.02343.X

Howarth, A. G., Hughes, M. R., & Stevenson, B. R. (1992). Detection of the tight junction-associated protein ZO-1 in astrocytes and other nonepithelial cell types. *American Journal of Physiology - Cell Physiology*, *262*(2 31-2). https://doi.org/10.1152/ AJPCELL.1992.262.2. C461

Hu, C., Tao, L., Cao, X., & Chen, L. (2020). The solute carrier transporters and the brain: Physiological and pharmacological implications. *Asian Journal of Pharmaceutical Sciences*, *15*(2), 131–144. https://doi.org/10.1016/j.ajps.2019.09.002

Hu, J.-G., Wang, X.-F., Zhou, J.-S., Wang, F.-C., Li, X.-W., & Lü, H.-Z. (2010). Activation of PKC-alpha is required for migration of C6 glioma cells. *Acta Neurobiologiae Experimentalis*, *70*(3), 239–245. http://www.ncbi.nlm.nih.gov/pubmed/20871643

Iorio, A. L., Ros, M. da, Fantappiè, O., Lucchesi, M., Facchini, L., Stival, A., Becciani, S., Guidi, M., Favre, C., Martino, M. de, Genitori, L., & Sardi, I. (2016). Blood-Brain Barrier and Breast Cancer Resistance Protein: A Limit to the Therapy of CNS Tumors and Neurodegenerative Diseases. *Anti-Cancer Agents in Medicinal Chemistry*, *16*(7), 810. https://doi.org/10.2174/1871520616666151120121928

Ishizaki, T., Chiba, H., Kojima, T., Fujibe, M., Soma, T., Miyajima, H., Nagasawa, K., Wada, I., & Sawada, N. (2003). Cyclic AMP induces phosphorylation of claudin-5 immunoprecipitates and expression of claudin-5 gene in blood-brain-barrier endothelial cells via protein kinase A-dependent and -independent pathways. *Experimental Cell Research*, *290*(2), 275–288. https://doi.org/10.1016/S0014-4827(03)00354-9

Jagtiani, E., Yeolekar, M., Naik, S., & Patravale, V. (2022). In vitro blood brain barrier models: An overview. *Journal of Controlled Release : Official Journal of the Controlled Release Society*, *343*, 13–30. https://doi.org/10.1016/J.JCONREL.2022.01.011

Janzer, R. C., & Raff, M. C. (1987). Astrocytes induce blood-brain barrier properties in endothelial cells. *Nature*, *325*(6101), 253–257. https://doi.org/10.1038/325253A0

Joó, F., & Karnushina, I. (n.d.). A procedure for the isolation of capillaries from rat brain. *Cytobios*, *8*(29), 41–48. Retrieved October 22, 2019, from http://www.ncbi.nlm.nih.gov/pubmed/4774116

Kamiie, J., Ohtsuki, S., Iwase, R., Ohmine, K., Katsukura, Y., Yanai, K., Sekine, Y., Uchida, Y., Ito, S., & Terasaki, T. (2008). Quantitative atlas of membrane transporter proteins: development and application of a highly sensitive simultaneous LC/MS/MS method combined with novel in-silico peptide selection criteria. *Pharmaceutical Research*, *25*(6), 1469–1483. https://doi.org/10.1007/s11095-008-9532-4

Kawabata, S., Oka, M., Shiozawa, K., Tsukamoto, K., Nakatomi, K., Soda, H., Fukuda, M., Ikegami, Y., Sugahara, K., Yamada, Y., Kamihira, S., Doyle, L. A., Ross, D. D., & Kohno, S. (2001). Breast Cancer Resistance Protein Directly Confers SN-38 Resistance of Lung Cancer Cells. *Biochemical and Biophysical Research Communications*, *280*(5), 1216–1223. https://doi.org/10.1006/BBRC.2001.4267

Kim, J., Shin, S. A., Lee, C. S., & Chung, H. J. (2023). An Improved In Vitro Blood-Brain Barrier Model for the Evaluation of Drug Permeability Using Transwell with Shear Stress. *Pharmaceutics*, *16*(1). https://doi.org/10.3390/PHARMACEUTICS16010048

Kreisl, W. C., Liow, J. S., Kimura, N., Seneca, N., Zoghbi, S. S., Morse, C. L., Herscovitch, P., Pike, V. W., & Innis, R. B. (2010). P-glycoprotein function at the blood-brain barrier in humans can be quantified with the substrate radiotracer 11C-N-desmethyl-loperamide. *Journal of Nuclear Medicine*, *51*(4), 559–566. https://doi.org/10.2967/JNUMED.109.070151

Krizbai, I., Szabó, G., Deli, M., Maderspach, K., Lehel, C., Oláh, Z., Wolff, J. R., & Joó, F. (1995). Expression of Protein Kinase C Family Members in the Cerebral Endothelial Cells. *Journal of Neurochemistry*, *65*(1), 459–462. https://doi.org/10.1046/j.1471-4159.1995.65010459.x

Kuo, Y.-C., & Lu, C.-H. (2011). Effect of human astrocytes on the characteristics of human brain-microvascular endothelial cells in the blood-brain barrier. *Colloids and Surfaces B: Biointerfaces*, *86*, 225–231. https://doi.org/10.1016/j.colsurfb.2011.04.005

Langford, D., Hurford, R., Hashimoto, M., Digicaylioglu, M., & Masliah, E. (2005). Signalling crosstalk in FGF2-mediated protection of endothelial cells from HIV-gp120. *BMC Neuroscience*, *6*, 8. https://doi.org/10.1186/1471-2202-6-8

Laterra, J., Guerin, C., & Goldstein, G. W. (1990). Astrocytes induce neural microvascular endothelial cells to form capillary-like structures in vitro. *Journal of Cellular Physiology*, *144*(2), 204–215. https://doi.org/10.1002/jcp.1041440205

Lee, M. K. K., & Dilq. (2014). Drug Development in Cell Culture: Crosstalk from the Industrial Prospects. *Journal of Bioequivalence & Bioavailability*, *6*(3), 96–114. https://doi.org/10.4172/JBB.10000188

Lee, S. W., Kim, W. J., Choi, Y. K., Song, H. S., Son, M. J., Gelman, I. H., Kim, Y. J., & Kim, K. W. (2003). SSeCKS regulates angiogenesis and tight junction formation in blood-brain barrier. *Nature Medicine*, *9*(7), 900–906. https://doi.org/10.1038/nm889

Liebner, S., & Plate, K. (2010). Differentiation of the brain vasculature: The answer came blowing by the Wnt. *Journal of Angiogenesis Research*, *2*(1). https://doi.org/10.1186/2040-2384-2-1

Lippmann, E. S., Al-Ahmad, A., Palecek, S. P., & Shusta, E. V. (2013). Modeling the blood-brain barrier using stem cell sources. *Fluids and Barriers of the CNS*, *10*(1). https://doi.org/10.1186/2045-8118-10-2

Liu, W. Y., Wang, Z. Bin, Zhang, L. C., Wei, X., & Li, L. (2012). Tight junction in blood-brain barrier: An overview of structure, regulation, and regulator substances. *CNS Neuroscience and Therapeutics*, *18*(8), 609–615. https://doi.org/10.1111/J.1755-5949.2012.00340.X

Locher, K. P. (2016). Mechanistic diversity in ATP-binding cassette (ABC) transporters. *Nature Structural & Molecular Biology*, *23*(6), 487–493. https://doi.org/10.1038/nsmb.3216

Lochhead, J. J., Yang, J., Ronaldson, P. T., & Davis, T. P. (2020). Structure, Function, and Regulation of the Blood-Brain Barrier Tight Junction in Central Nervous System Disorders. *Frontiers in Physiology*, *11*. https://doi.org/10.3389/FPHYS.2020.00914/XML/NLM

Loryan, I., Fridén, M., & Hammarlund-Udenaes, M. (2013). The brain slice method for studying drug distribution in the CNS. *Fluids and Barriers of the CNS*, *10*(1). https://doi.org/10.1186/2045-8118-10-6

Löscher, W., & Potschka, H. (2005). Blood-brain barrier active efflux transporters: ATP-binding cassette gene family. *NeuroRx*, *2*(1), 86–98. https://doi.org/10.1602/NEURORX.2.1.86

Luna-Tortós, C., Rambeck, B., Jürgens, U. H., & Löscher, W. (2009). The antiepileptic drug topiramate is a substrate for human P-glycoprotein but not multidrug resistance proteins. *Pharmaceutical Research*, *26*(11), 2464–2470. https://doi.org/10.1007/S11095-009-9961-8

Lundquist, S., & Renftel, M. (2002). The use of in vitro cell culture models for mechanistic studies and as permeability screens for the blood-brain barrier in the pharmaceutical industry - Background and current status in the drug discovery process. *Vascular Pharmacology*, *38*(6), 355–364. https://doi.org/10.1016/S1537-1891(02)00203-3

Mader, S., & Brimberg, L. (2019). Aquaporin-4 water channel in the brain and its implication for health and disease. *Cells*, *8*(2). https://doi.org/10.3390/CELLS8020090

Mahringer, A., & Fricker, G. (2016). ABC transporters at the blood-brain barrier. *Expert Opinion on Drug Metabolism and Toxicology*, *12*(5), 499–508. https://doi.org/10.1517/17425255.2016.1168804

Mallard, C., Ek, C. J., Vexler, Z. S., Petersen, O., & Bennet, L. (2018). The Journal of Physiology The myth of the immature barrier systems in the developing brain: role in perinatal brain injury. *J Physiol*, *596*, 5655–5664. https://doi.org/10.1113/JP274938

Mantle, J. L., Min, L., & Lee, K. H. (2016). Minimum Transendothelial Electrical Resistance Thresholds for the Study of Small and Large

Molecule Drug Transport in a Human in Vitro Blood-Brain Barrier Model. *Molecular Pharmaceutics*, *13*(12), 4191–4198. https://doi.org/10.1021/ACS.MOLPHARMACEUT.6B00818

Marcos-Contreras, O. A., Martinez de Lizarrondo, S., Bardou, I., Orset, C., Pruvost, M., Anfray, A., Frigout, Y., Hommet, Y., Lebouvier, L., Montaner, J., Vivien, D., & Gauberti, M. (2016). Hyperfibrinolysis increases blood-brain barrier permeability by a plasmin- and bradykinin-dependent mechanism. *Blood*, *128*(20), 2423–2434. https://doi.org/10.1182/blood-2016-03-705384

Mastorakos, P., & McGavern, D. (2019). The anatomy and immunology of vasculature in the central nervous system. *Science Immunology*, *4*(37). https://doi.org/10.1126/SCIIMMUNOL.AAV0492

McDannold, N., Vykhodtseva, N., & Hynynen, K. (2008). Blood-brain barrier disruption induced by focused ultrasound and circulating preformed microbubbles appears to be characterized by the mechanical index. *Ultrasound in Medicine & Biology*, *34*(5), 834–840. https://doi.org/10.1016/j.ultrasmedbio.2007.10.016

Meyer, J., Rauh, J., & Galla, H. -J. (1991). The Susceptibility of Cerebral Endothelial Cells to Astroglial Induction of Blood-Brain Barrier Enzymes Depends on Their Proliferative State. *Journal of Neurochemistry*, *57*(6), 1971–1977. https://doi.org/10.1111/J.1471-4159.1991.TB06411.X

Miller, D. S. (2010). Regulation of P-glycoprotein and other ABC drug transporters at the blood-brain barrier. *Trends in Pharmacological Sciences*, *31*(6), 246–254. https://doi.org/10.1016/J.TIPS.2010.03.003

Mitic, L. L., Van Itallie, C. M., & Anderson, J. M. (2000). Molecular physiology and pathophysiology of tight junctions I. Tight junction structure and function: lessons from mutant animals and proteins. *American Journal of Physiology. Gastrointestinal and Liver Physiology*, *279*(2), G250-4. https://doi.org/10.1152/ajpgi.2000.279.2.G250

Modarres, H. P., Janmaleki, M., Novin, M., Saliba, J., El-Hajj, F., RezayatiCharan, M., Seyfoori, A., Sadabadi, H., Vandal, M., Nguyen, M. D., Hasan, A., & Sanati-Nezhad, A. (2018). In vitro models and systems for evaluating the dynamics of drug delivery to the healthy and diseased brain. In *Journal of Controlled Release* (Vol. 273). https://doi.org/10.1016/j.jconrel.2018.01.024

Molecular cloning of cDNAs which are highly overexpressed in mitoxantrone-resistant cells: demonstration of homology to ABC transport genes - PubMed. (n.d.). Retrieved February 19, 2025, from https://pubmed.ncbi.nlm.nih.gov/9892175/

Morris, M. E., Rodriguez-Cruz, V., & Felmlee, M. A. (2017). SLC and ABC Transporters: Expression, Localization, and Species Differences at the

Blood-Brain and the Blood-Cerebrospinal Fluid Barriers. *AAPS Journal*, *19*(5), 1317–1331. https://doi.org/10.1208/S12248-017-0110-8

Muldoon, L. L., Alvarez, J. I., Begley, D. J., Boado, R. J., Del Zoppo, G. J., Doolittle, N. D., Engelhardt, B., Hallenbeck, J. M., Lonser, R. R., Ohlfest, J. R., Prat, A., Scarpa, M., Smeyne, R. J., Drewes, L. R., & Neuwelt, E. A. (2013). Immunologic privilege in the central nervous system and the blood-brain barrier. *Journal of Cerebral Blood Flow and Metabolism : Official Journal of the International Society of Cerebral Blood Flow and Metabolism*, *33*(1), 13–21. https://doi.org/10.1038/jcbfm.2012.153

Naik, P., & Cucullo, L. (2012). In vitro blood-brain barrier models: current and perspective technologies. *Journal of Pharmaceutical Sciences*, *101*(4), 1337–1354. https://doi.org/10.1002/JPS.23022

Nakagawa, S., Deli, M. A., Kawaguchi, H., Shimizudani, T., Shimono, T., Kittel, A., Tanaka, K., & Niwa, M. (n.d.). A new blood-brain barrier model using primary rat brain endothelial cells, pericytes and astrocytes. *Neurochemistry International*, *54*(3–4), 253–263. https://doi.org/10.1016/j.neuint.2008.12.002

Nazer, B., Hong, S., & Selkoe, D. J. (2008). LRP promotes endocytosis and degradation, but not transcytosis, of the amyloid-beta peptide in a blood-brain barrier in vitro model. *Neurobiology of Disease*, *30*(1), 94–102. https://doi.org/10.1016/j.nbd.2007.12.005

NEUHAUS, J., RISAU, W., & WOLBURG, H. (1991). Induction of Blood-Brain Barrier Characteristics in Bovine Brain Endothelial Cells by Rat Astroglial Cells in Transfilter Coculture. *Annals of the New York Academy of Sciences*, *633*(1), 578–580. https://doi.org/10.1111/j.1749-6632.1991.tb15667.x

Neuhaus, W., Lauer, R., Oelzant, S., Fringeli, U. P., Ecker, G. F., & Noe, C. R. (2006). A novel flow based hollow-fiber blood-brain barrier in vitro model with immortalised cell line PBMEC/C1-2. *Journal of Biotechnology*, *125*(1), 127–141. https://doi.org/10.1016/j.jbiotec.2006.02.019

Nielsen, S. S. E., Siupka, P., Georgian, A., Preston, J. E., Tóth, A. E., Yusof, S. R., Abbott, N. J., & Nielsen, M. S. (2017a). Improved method for the establishment of an in Vitro Blood-Brain barrier model based on porcine brain endothelial cells. *Journal of Visualized Experiments*, *2017*(127). https://doi.org/10.3791/56277

Nielsen, S. S. E., Siupka, P., Georgian, A., Preston, J. E., Tóth, A. E., Yusof, S. R., Abbott, N. J., & Nielsen, M. S. (2017b). Improved method for the establishment of an in Vitro Blood-Brain barrier model based on porcine brain endothelial cells. *Journal of Visualized Experiments*, *2017*(127), 1–13. https://doi.org/10.3791/56277

Nitta, T., Hata, M., Gotoh, S., Seo, Y., Sasaki, H., Hashimoto, N., Furuse, M., & Tsukita, S. (2003). Size-selective loosening of the blood-brain barrier in

claudin-5-deficient mice. *The Journal of Cell Biology*, *161*(3), 653–660. https://doi.org/10.1083/jcb.200302070

Nizet, V., Kim, K. S., Stins, M., Jonas, M., Chi, E. Y., Nguyen, D., & Rubens, C. E. (1997). Invasion of brain microvascular endothelial cells by group B streptococci. *Infection and Immunity*, *65*(12), 5074–5081. https://doi.org/10.1203/00006450-199704001-01351

Oddo, A., Peng, B., Tong, Z., Wei, Y., Tong, W. Y., Thissen, H., & Voelcker, N. H. (2019). Advances in Microfluidic Blood–Brain Barrier (BBB) Models. *Trends in Biotechnology*, *37*(12), 1295–1314. https://doi.org/10.1016/J.TIBTECH.2019.04.006

Oldendorf, W. H., Cornford, M. E., & Brown, W. J. (1977). The large apparent work capability of the blood-brain barrier: A study of the mitochondrial content of capillary endothelial cells in brain and other tissues of the rat. *Annals of Neurology*, *1*(5), 409–417. https://doi.org/10.1002/ana.410010502

Page, S., Patel, R., Raut, S., & Al-Ahmad, A. (2020). Neurological diseases at the blood-brain barrier: Stemming new scientific paradigms using patient-derived induced pluripotent cells. *Biochimica et Biophysica Acta (BBA) - Molecular Basis of Disease*, *1866*(4), 165358. https://doi.org/10.1016/J.BBADIS.2018.12.009

Palumbo, P., Picchini, U., Beck, B., Van Gelder, J., Delbar, N., & DeGaetano, A. (2008). A general approach to the apparent permeability index. *Journal of Pharmacokinetics and Pharmacodynamics*, *35*(2), 235–248. https://doi.org/10.1007/S10928-008-9086-4

Panula, P., Joó, F., & Rechardt, L. (1978). Evidence for the presence of viable endothelial cells in cultures derived from dissociated rat brain. *Experientia*, *34*(1), 95–97. https://doi.org/10.1007/BF01921925

Pan, W., & Kastin, A. J. (2002). TNFalpha transport across the blood-brain barrier is abolished in receptor knockout mice. *Experimental Neurology*, *174*(2), 193–200. https://doi.org/10.1006/exnr.2002.7871

Pardridge, W. M. (1983). Brain metabolism: A perspective from the blood-brain barrier. *Physiological Reviews*, *63*(4), 1481–1535. https://doi.org/10.1152/PHYSREV.1983.63.4.1481

Pardridge, W. M. (2005). The blood-brain barrier: Bottleneck in brain drug development. *NeuroRx*, *2*(1), 3–14. https://doi.org/10.1602/neurorx.2.1.3

Pardridge, W. M. (2007). Blood-brain barrier delivery of protein and non-viral gene therapeutics with molecular Trojan horses. *Journal of Controlled Release*, *122*(3), 345–348. https://doi.org/10.1016/j.jconrel.2007.04.001

Pardridge, W. M. (2012). Drug transport across the blood-brain barrier. *Journal of Cerebral Blood Flow and Metabolism*, *32*(11), 1959–1972. https://doi.org/10.1038/JCBFM.2012.126

Paris-Robidas, S., Emond, V., Tremblay, C., Soulet, D., & Calon, F. (2011). In vivo labeling of brain capillary endothelial cells after intravenous injection of monoclonal antibodies targeting the transferrin receptor. *Molecular Pharmacology*, *80*(1), 32–39. https://doi.org/10.1124/mol.111.071027

Park, T. E., Mustafaoglu, N., Herland, A., Hasselkus, R., Mannix, R., FitzGerald, E. A., Prantil-Baun, R., Watters, A., Henry, O., Benz, M., Sanchez, H., McCrea, H. J., Goumnerova, L. C., Song, H. W., Palecek, S. P., Shusta, E., & Ingber, D. E. (2019). Hypoxia-enhanced Blood-Brain Barrier Chip recapitulates human barrier function and shuttling of drugs and antibodies. *Nature Communications*, *10*(1). https://doi.org/10.1038/s41467-019-10588-0

Patabendige, A., Skinner, R. A., & Abbott, N. J. (2013). Establishment of a simplified in vitro porcine blood-brain barrier model with high transendothelial electrical resistance. *Brain Research*, *1521*, 1–15. https://doi.org/10.1016/j.brainres.2012.06.057

Patabendige, A., Skinner, R. A., Morgan, L., & Joan Abbott, N. (2013). A detailed method for preparation of a functional and flexible blood-brain barrier model using porcine brain endothelial cells. *Brain Research*, *1521*, 16–30. https://doi.org/10.1016/j.brainres.2013.04.006

Perrière, N., Demeuse, P. H., Garcia, E., Regina, A., Debray, M., Andreux, J. P., Couvreur, P., Scherrmann, J. M., Temsamani, J., Couraud, P. O., Deli, M. A., & Roux, F. (2005). Puromycin-based purification of rat brain capillary endothelial cell cultures. Effect on the expression of blood-brain barrier-specific properties. *Journal of Neurochemistry*, *93*(2), 279–289. https://doi.org/10.1111/J.1471-4159.2004.03020.X

Pilorget, A., Demeule, M., Barakat, S., Marvaldi, J., Luis, J., & Béliveau, R. (2007). Modulation of P-glycoprotein function by sphingosine kinase-1 in brain endothelial cells. *Journal of Neurochemistry*, *100*(5), 1203–1210. https://doi.org/10.1111/j.1471-4159.2006.04295.x

Polli, J. W., Olson, K. L., Chism, J. P., John-Williams, L. S., Yeager, R. L., Woodard, S. M., Otto, V., Castellino, S., & Demby, V. E. (2009). An unexpected synergist role of P-glycoprotein and breast cancer resistance protein on the central nervous system penetration of the tyrosine kinase inhibitor lapatinib (N-{3-chloro-4-[(3-fluorobenzyl)oxy]phenyl}-6-[5-({[2-(methylsulfonyl)ethyl]amino}methyl)-2-furyl]-4-quinazolinamine; GW572016). *Drug Metabolism and Disposition: The Biological Fate of Chemicals*, *37*(2), 439–442. https://doi.org/10.1124/dmd.108.024646

Potschka, H., Fedrowitz, M., & Löscher, W. (2002). P-Glycoprotein-mediated efflux of phenobarbital, lamotrigine, and felbamate at the blood-brain barrier: Evidence from microdialysis experiments in rats. *Neuroscience Letters*, *327*(3), 173–176. https://doi.org/10.1016/S0304-3940(02)00423-8

Puech, C., Hodin, S., Forest, V., He, Z., Mismetti, P., Delavenne, X., & Perek, N. (2018). Assessment of HBEC-5i endothelial cell line cultivated in astrocyte conditioned medium as a human blood-brain barrier model for ABC drug transport studies. *International Journal of Pharmaceutics*, *551*(1–2), 281–289. https://doi.org/10.1016/j.ijpharm.2018.09.040

Rahman, N. A., Rasil, A. N. ain H. M., Meyding-Lamade, U., Craemer, E. M., Diah, S., Tuah, A. A., & Muharram, S. H. (2016). Immortalized endothelial cell lines for in vitro blood-brain barrier models: A systematic review. *Brain Research*, *1642*, 532–545. https://doi.org/10.1016/J.BRAINRES.2016.04.024

Rana, P., Kogut, S., Wen, X., Akhlaghi, F., & Aleo, M. D. (2020). Most Influential Physicochemical and In Vitro Assay Descriptors for Hepatotoxicity and Nephrotoxicity Prediction. *Chemical Research in Toxicology*, *33*(7), 1780–1790. https://doi.org/10.1021/ACS.CHEMRESTOX.0C00040

Ransohoff, R. M., & Engelhardt, B. (2012). The anatomical and cellular basis of immune surveillance in the central nervous system. *Nature Reviews. Immunology*, *12*(9), 623–635. https://doi.org/10.1038/nri3265

Rauch, C. (2011). The “Multi” of Drug Resistance Explained by Oscillating Drug Transporters, Drug-Membrane Physical Interactions and Spatial Dimensionality. *Cell Biochemistry and Biophysics*, *61*(1), 103–113. https://doi.org/10.1007/S12013-011-9166-8

Reese, T. S., & Karnovsky, M. J. (1967). Fine structural localization of a blood-brain barrier to exogenous peroxidase. *The Journal of Cell Biology*, *34*(1), 207–217. https://doi.org/10.1083/jcb.34.1.207

Regina, A., Koman, A., Piciotti, M., El Hafny, B., Center, M. S., Bergmann, R., Couraud, P. O., & Roux, F. (1998). Mrp1 multidrug resistance-associated protein and P-glycoprotein expression in rat brain microvessel endothelial cells. *Journal of Neurochemistry*, *71*(2), 705–715. https://doi.org/10.1046/j.1471-4159.1998.71020705.x

Ribatti, D., Nico, B., Crivellato, E., & Artico, M. (2006). Development of the blood-brain barrier: A historical point of view. *Anatomical Record - Part B New Anatomist*, *289*(1), 3–8. https://doi.org/10.1002/AR.B.20087

Roberts, L. M., Black, D. S., Raman, C., Woodford, K., Zhou, M., Haggerty, J. E., Yan, A. T., Cwirla, S. E., & Grindstaff, K. K. (2008). Subcellular localization of transporters along the rat blood-brain barrier and blood-cerebral-spinal fluid barrier by in vivo biotinylation. *Neuroscience*, *155*(2), 423–438. https://doi.org/10.1016/j.neuroscience.2008.06.015

Römermann, K., Fedrowitz, M., Hampel, P., Kaczmarek, E., Töllner, K., Erker, T., Sweet, D. H., & Löscher, W. (2017). Multiple blood-brain barrier transport mechanisms limit bumetanide accumulation, and therapeutic

potential, in the mammalian brain. *Neuropharmacology*, *117*, 182–194. https://doi.org/10.1016/J.NEUROPHARM.2017.02.006

Rosas-Hernandez, H., Cuevas, E., Lantz, S. M., Paule, M. G., & Ali, S. F. (2018). Isolation and culture of brain microvascular endothelial cells for in vitro blood-brain barrier studies. *Methods in Molecular Biology*, *1727*, 315–331. https://doi.org/10.1007/978-1-4939-7571-6_23

Roux, F., Durieu-Trautmann, O., Chaverot, N., Claire, M., Mailly, P., Bourre, J. M., Strosberg, A. D., & Couraud, P. O. (1994). Regulation of gamma-glutamyl transpeptidase and alkaline phosphatase activities in immortalized rat brain microvessel endothelial cells. *Journal of Cellular Physiology*, *159*(1), 101–113. https://doi.org/10.1002/jcp.1041590114

Rubin, L. L., Hall, D. E., Porter, S., Barbu, K., Cannon, C., Horner, H. C., Janatpour, M., Liaw, C. W., Manning, K., & Morales, J. (1991). A cell culture model of the blood-brain barrier. *The Journal of Cell Biology*, *115*(6), 1725–1735. https://doi.org/10.1083/jcb.115.6.1725

Sakamoto, H., Hara, H., Hirano, K., & Adachi, T. (1998). Enhancement of glucuronosyl etoposide transport by glutathione in multidrug resistance-associated protein-overexpressing cells. *Cancer Letters*, *135*(1), 113–119. https://doi.org/10.1016/S0304-3835(98)00285-7

Sakolish, C. M., Esch, M. B., Hickman, J. J., Shuler, M. L., & Mahler, G. J. (2016). Modeling Barrier Tissues In Vitro: Methods, Achievements, and Challenges. *EBioMedicine*, *5*, 30. https://doi.org/10.1016/J.EBIOM.2016.02.023

Sano, Y., Shimizu, F., Abe, M., Maeda, T., Kashiwamura, Y., Ohtsuki, S., Terasaki, T., Obinata, M., Kajiwara, K., Fujii, M., Suzuki, M., & Kanda, T. (2010). Establishment of a new conditionally immortalized human brain microvascular endothelial cell line retaining an in vivo blood-brain barrier function. *Journal of Cellular Physiology*, *225*(2), 519–528. https://doi.org/10.1002/jcp.22232

Sauer, I., Dunay, I. R., Weisgraber, K., Bienert, M., & Dathe, M. (2005). An apolipoprotein E-derived peptide mediates uptake of sterically stabilized liposomes into brain capillary endothelial cells. *Biochemistry*, *44*(6), 2021–2029. https://doi.org/10.1021/bi048080x

Schildge, S., Bohrer, C., Beck, K., & Schachtrup, C. (2013). Isolation and culture of mouse cortical astrocytes. *Journal of Visualized Experiments : JoVE*, *71*. https://doi.org/10.3791/50079

Schmitt, G., Parrott, N., Prinssen, E., & Barrow, P. (2017). The great barrier belief: The blood–brain barrier and considerations for juvenile toxicity studies. *Reproductive Toxicology*, *72*, 129–135. https://doi.org/10.1016/J.REPROTOX.2017.06.043

Scholz, M., Cinatl, J., Schädel-Höpfner, M., & Windolf, J. (2007a). Neutrophils and the blood-brain barrier dysfunction after trauma. In *Medicinal Research Reviews* (Vol. 27, Issue 3, pp. 401–416). https://doi.org/10.1002/med.20064

Scholz, M., Cinatl, J., Schädel-Höpfner, M., & Windolf, J. (2007b). Neutrophils and the blood-brain barrier dysfunction after trauma. In *Medicinal Research Reviews* (Vol. 27, Issue 3, pp. 401–416). https://doi.org/10.1002/med.20064

Schrot, S., Weidenfeller, C., Schärfer, T. E., Robenek, H., & Galla, H. J. (2005). Influence of Hydrocortisone on the Mechanical Properties of the Cerebral Endothelium In Vitro. *Biophysical Journal*, *89*(6), 3904. https://doi.org/10.1529/BIOPHYSJ.104.058750

Seghezzi, G., Patel, S., Ren, C. J., Gualandris, A., Pintucci, G., Robbins, E. S., Shapiro, R. L., Galloway, A. C., Rifkin, D. B., & Mignatti, P. (1998). Fibroblast Growth Factor-2 (FGF-2) Induces Vascular Endothelial Growth Factor (VEGF) Expression in the Endothelial Cells of Forming Capillaries: An Autocrine Mechanism Contributing to Angiogenesis. *The Journal of Cell Biology*, *141*(7), 1659. https://doi.org/10.1083/JCB.141.7.1659

Sharif, Y., Jumah, F., Coplan, L., Krosser, A., Sharif, K., & Tubbs, R. S. (2018). Blood brain barrier: A review of its anatomy and physiology in health and disease. *Clinical Anatomy (New York, N.Y.)*, *31*(6), 812–823. https://doi.org/10.1002/CA.23083

Shayan, G., Choi, Y. S., Shusta, E. V, Shuler, M. L., & Lee, K. H. (2011). Murine in vitro model of the blood-brain barrier for evaluating drug transport. *European Journal of Pharmaceutical Sciences : Official Journal of the European Federation for Pharmaceutical Sciences*, *42*(1–2), 148–155. https://doi.org/10.1016/j.ejps.2010.11.005

Shepro, D., & Morel, N. M. L. (1993). Pericyte physiology. In *FASEB Journal* (Vol. 7, Issue 11, pp. 1031–1038). https://doi.org/10.1096/fasebj.7.11.8370472

Shimizu, F., Sano, Y., Maeda, T., Abe, M.-A., Nakayama, H., Takahashi, R.-I., Ueda, M., Ohtsuki, S., Terasaki, T., Obinata, M., & Kanda, T. (2008). Peripheral nerve pericytes originating from the blood-nerve barrier expresses tight junctional molecules and transporters as barrier-forming cells. *Journal of Cellular Physiology*, *217*(2), 388–399. https://doi.org/10.1002/jcp.21508

Siddharthan, V., Kim, Y. V., Liu, S., & Kim, K. S. (2007). Human astrocytes/astrocyte-conditioned medium and shear stress enhance the barrier properties of human brain microvascular endothelial cells. *Brain Research*, *1147*(1), 39–50. https://doi.org/10.1016/j.brainres.2007.02.029

Sivandzade, F., & Cucullo, L. (2018). In-vitro blood–brain barrier modeling: A review of modern and fast-advancing technologies. *Journal of Cerebral*

Blood Flow and Metabolism, *38*(10), 1667–1681. https://doi.org/10.1177/0271678X18788769

Smith, J. P., & Drewes, L. R. (2006). Modulation of monocarboxylic acid transporter-1 kinetic function by the cAMP signaling pathway in rat brain endothelial cells. *The Journal of Biological Chemistry*, *281*(4), 2053–2060. https://doi.org/10.1074/jbc.M511577200

Sobue, K., Yamamoto, N., Yoneda, K., Hodgson, M. E., Yamashiro, K., Tsuruoka, N., Tsuda, T., Katsuya, H., Miura, Y., Asai, K., & Kato, T. (1999). Induction of blood-brain barrier properties in immortalized bovine brain endothelial cells by astrocytic factors. *Neuroscience Research*, *35*(2), 155–164. https://doi.org/10.1016/s0168-0102(99)00079-6

Srinivasan, B., Kolli, A. R., Esch, M. B., Abaci, H. E., Shuler, M. L., & Hickman, J. J. (2015). TEER Measurement Techniques for In Vitro Barrier Model Systems. *Journal of Laboratory Automation*, *20*(2), 107–126. https://doi.org/10.1177/2211068214561025

Stamatovic, S. M., Johnson, A. M., Keep, R. F., & Andjelkovic, A. V. (2016). Junctional proteins of the blood-brain barrier: New insights into function and dysfunction. *Tissue Barriers*, *4*(1). https://doi.org/10.1080/21688370.2016.1154641

Stamatovic, S. M., Keep, R. F., & Andjelkovic, A. V. (2008). Brain endothelial cell-cell junctions: how to “open” the blood brain barrier. *Current Neuropharmacology*, *6*(3), 179–192. https://doi.org/10.2174/157015908785777210

Stamatovic, S. M., Shakui, P., Keep, R. F., Moore, B. B., Kunkel, S. L., Van Rooijen, N., & Andjelkovic, A. V. (2005). Monocyte chemoattractant protein-1 regulation of blood-brain barrier permeability. *Journal of Cerebral Blood Flow and Metabolism : Official Journal of the International Society of Cerebral Blood Flow and Metabolism*, *25*(5), 593–606. https://doi.org/10.1038/sj.jcbfm.9600055

Stone, N. L., England, T. J., & O’Sullivan, S. E. (2019a). A novel transwell blood brain barrier model using primary human cells. *Frontiers in Cellular Neuroscience*, *13*. https://doi.org/10.3389/FNCEL.2019.00230

Stone, N. L., England, T. J., & O’Sullivan, S. E. (2019b). A Novel Transwell Blood Brain Barrier Model Using Primary Human Cells. *Frontiers in Cellular Neuroscience*, *13*, 230. https://doi.org/10.3389/fncel.2019.00230

Szöllősi, D., Rose-Sperling, D., Hellmich, U. A., & Stockner, T. (2018). Comparison of mechanistic transport cycle models of ABC exporters. *Biochimica et Biophysica Acta. Biomembranes*, *1860*(4), 818–832. https://doi.org/10.1016/j.bbamem.2017.10.028

Tao-Cheng, J.-H., Nagy, Z., & Brightman, M. W. (1987). Tight Junctions of Brain Endothelium in vitro Are Enhanced by Astroglia. *The Journal of Neuroscience*, *7*(10), 32933299.

Tetko, I. V., Gasteiger, J., Todeschini, R., Mauri, A., Livingstone, D., Ertl, P., Palyulin, V. A., Radchenko, E. V., Zefirov, N. S., Makarenko, A. S., Tanchuk, V. Y., & Prokopenko, V. V. (2005). Virtual computational chemistry laboratory--design and description. *Journal of Computer-Aided Molecular Design*, *19*(6), 453–463. https://doi.org/10.1007/S10822-005-8694-Y

Thomsen, L. B., Burkhart, A., & Moos, T. (2015a). A triple culture model of the blood-brain barrier using porcine brain endothelial cells, astrocytes and pericytes. *PLoS ONE*, *10*(8). https://doi.org/10.1371/JOURNAL.PONE.0134765

Thomsen, L. B., Burkhart, A., & Moos, T. (2015b). A Triple Culture Model of the Blood-Brain Barrier Using Porcine Brain Endothelial cells, Astrocytes and Pericytes. *PloS One*, *10*(8), e0134765. https://doi.org/10.1371/journal.pone.0134765

Tietz, S., & Engelhardt, B. (2015). Brain barriers: Crosstalk between complex tight junctions and adherens junctions. In *Journal of Cell Biology* (Vol. 209, Issue 4). https://doi.org/10.1083/jcb.201412147

Toimela, T., Mäenpää, H., Mannerström, M., & Tähti, H. (2004). Development of an in vitro blood-brain barrier model - Cytotoxicity of mercury and aluminum. *Toxicology and Applied Pharmacology*, *195*(1), 73–82. https://doi.org/10.1016/j.taap.2003.11.002

Toth, A. E., Siupka, P., Thomas, T. J., Venø, S. T., Thomsen, L. B., Moos, T., Lohi, H. T., Madsen, P., Lykke-Hartmann, K., & Nielsen, M. S. (2018). The Endo-Lysosomal System of Brain Endothelial Cells Is Influenced by Astrocytes In Vitro. *Molecular Neurobiology*, *55*(11), 8522–8537. https://doi.org/10.1007/S12035-018-0988-X/METRICS

Tran, T. T., Mittal, A., Gales, T., Maleeff, B., Aldinger, T., Polli, J. W., Ayrton, A., Ellens, H., & Bentz, J. (2004). Exact kinetic analysis of passive transport across a polarized confluent MDCK cell monolayer modeled as a single barrier. *Journal of Pharmaceutical Sciences*, *93*(8), 2108–2123. https://doi.org/10.1002/JPS.20105

Tsuji, A. (2005). Small molecular drug transfer across the blood-brain barrier via carrier-mediated transport systems. *NeuroRx*, *2*(1), 54–62. https://doi.org/10.1602/neurorx.2.1.54

Tuma, P. L., & Hubbard, A. L. (2003). Transcytosis: crossing cellular barriers. *Physiological Reviews*, *83*(3), 871–932. https://doi.org/10.1152/physrev.00001.2003

van der Helm, M. W., van der Meer, A. D., Eijkel, J. C. T., van den Berg, A., & Segerink, L. I. (2016). Microfluidic organ-on-chip technology for blood-brain barrier research. *Tissue Barriers*, *4*(1). https://doi.org/10.1080/21688370.2016.1142493

Vastag, M., & Keserű, G. (2009). Current in vitro and in silico models of blood-brain barrier penetration: a practical view. *Current Opinion in Drug Discovery & Development*.

Verscheijden, L. F. M., Koenderink, J. B., de Wildt, S. N., & Russel, F. G. M. (2021). Differences in P-glycoprotein activity in human and rodent blood–brain barrier assessed by mechanistic modelling. *Archives of Toxicology*, *95*(9), 3015–3029. https://doi.org/10.1007/S00204-021-03115-Y/TABLES/2

Veszelka, S., Kittel, Á., & Deli, M. A. (2011). Tools for modelling blood-brain barrier penetrability. *Solubility, Delivery and ADME Problems of Drugs and Drug-Candidates*, 166–188. https://doi.org/10.2174/978160805120511101010166

Veszelka, S., Pásztói, M., Farkas, A. E., Krizbai, I., Ngo, T. K. D., Niwa, M., Abrahám, C. S., & Deli, M. A. (2007). Pentosan polysulfate protects brain endothelial cells against bacterial lipopolysaccharide-induced damages. *Neurochemistry International*, *50*(1), 219–228. https://doi.org/10.1016/j.neuint.2006.08.006

Veszelka, S., Tóth, A., Walter, F. R., Tóth, A. E., Gróf, I., Mészáros, M., Bocsik, A., Hellinger, É., Vastag, M., Rákhely, G., & Deli, M. A. (2018). Comparison of a rat primary cell-based blood-brain barrier model with epithelial and brain endothelial cell lines: Gene expression and drug transport. *Frontiers in Molecular Neuroscience*, *11*. https://doi.org/10.3389/FNMOL.2018.00166

Visser, C. C., Voorwinden, L. H., Crommelin, D. J. A., Danhof, M., & De Boer, A. G. (2004). Characterization and modulation of the transferrin receptor on brain capillary endothelial cells. *Pharmaceutical Research*, *21*(5), 761–769. https://doi.org/10.1023/B:PHAM.0000026425.69874.8e

Wang, J. S., Zhu, H. J., Markowitz, J. S., Donovan, J. L., & DeVane, C. L. (2006). Evaluation of antipsychotic drugs as inhibitors of multidrug resistance transporter P-glycoprotein. *Psychopharmacology*, *187*(4), 415–423. https://doi.org/10.1007/S00213-006-0437-9/METRICS

Wang, Q., Rager, J. D., Weinstein, K., Kardos, P. S., Dobson, G. L., Li, J., & Hidalgo, I. J. (2005). Evaluation of the MDR-MDCK cell line as a permeability screen for the blood-brain barrier. *International Journal of Pharmaceutics*, *288*(2), 349–359. https://doi.org/10.1016/j.ijpharm.2004.10.007

Wang, W., Dentler, W. L., & Borchardt, R. T. (2001). VEGF increases BMEC monolayer permeability by affecting occludin expression and tight

junction assembly. *American Journal of Physiology - Heart and Circulatory Physiology*, *280*(1 49-1). https://doi.org/10.1152/AJPHEART.2001.280.1.H434

Wang, X., Xu, B., Xiang, M., Yang, X., Liu, Y., Liu, X., & Shen, Y. (2020). Advances on fluid shear stress regulating blood-brain barrier. *Microvascular Research*, *128*. https://doi.org/10.1016/j.mvr.2019.103930

Wang, Y. I., Abaci, H. E., & Shuler, M. L. (2017). Microfluidic blood–brain barrier model provides in vivo-like barrier properties for drug permeability screening. *Biotechnology and Bioengineering*, *114*(1), 184–194. https://doi.org/10.1002/BIT.26045

Wang, Z., Yang, H., Wu, Z., Wang, T., Li, W., Tang, Y., & Liu, G. (2018). In Silico Prediction of Blood–Brain Barrier Permeability of Compounds by Machine Learning and Resampling Methods. *ChemMedChem*, *13*(20), 2189–2201. https://doi.org/10.1002/CMDC.201800533

Warren, M. S., Zerangue, N., Woodford, K., Roberts, L. M., Tate, E. H., Feng, B., Li, C., Feuerstein, T. J., Gibbs, J., Smith, B., de Morais, S. M., Dower, W. J., & Koller, K. J. (2009). Comparative gene expression profiles of ABC transporters in brain microvessel endothelial cells and brain in five species including human. *Pharmacological Research*, *59*(6), 404–413. https://doi.org/10.1016/J.PHRS.2009.02.007

Weidman, E. K., Foley, C. P., Kallas, O., Dyke, J. P., Gupta, A., Giambrone, A. E., Ivanidze, J., Baradaran, H., Ballon, D. J., & Sanelli, P. C. (2016). Evaluating permeability surface-area product as a measure of blood-brain barrier permeability in a murine model. *American Journal of Neuroradiology*, *37*(7), 1267–1274. https://doi.org/10.3174/AJNR.A4712

Weksler, B. B., Subileau, E. A., Perrière, N., Charneau, P., Holloway, K., Leveque, M., Tricoire-Leignel, H., Nicotra, A., Bourdoulous, S., Turowski, P., Male, D. K., Roux, F., Greenwood, J., Romero, I. A., & Couraud, P. O. (2005). Blood-brain barrier-specific properties of a human adult brain endothelial cell line. *FASEB Journal*, *19*(13), 1872–1874. https://doi.org/10.1096/fj.04-3458fje

Weksler, B. B., Subileau, E. A., Perrière, N., Charneau, P., Holloway, K., Leveque, M., Tricoire-Leignel, H., Nicotra, A., Bourdoulous, S., Turowski, P., Male, D. K., Roux, F., Greenwood, J., Romero, I. A., & Couraud, P. O. (2005). Blood-brain barrier-specific properties of a human adult brain endothelial cell line. *FASEB Journal : Official Publication of the Federation of American Societies for Experimental Biology*, *19*(13), 1872–1874. https://doi.org/10.1096/FJ.04-3458FJE

Whitehouse, C. A. (2022). *Blood-Brain Barrier on-a-chip model for the study of drug permeability into the brain*.

Wiley, D. T., Webster, P., Gale, A., & Davis, M. E. (2013). Transcytosis and brain uptake of transferrin-containing nanoparticles by tuning avidity to

transferrin receptor. *Proceedings of the National Academy of Sciences of the United States of America*, *110*(21), 8662–8667. https://doi.org/10.1073/pnas.1307152110

Wilhelm, I., Fazakas, C., & Krizbai, I. A. (2011). In vitro models of the blood-brain barrier. *Acta Neurobiologiae Experimentalis*, *71*(1), 113–128. https://doi.org/10.55782/ANE-2011-1828

Wilhelm, I., & Krizbai, I. A. (2014). In vitro models of the blood-brain barrier for the study of drug delivery to the brain. *Molecular Pharmaceutics*, *11*(7), 1949–1963. https://doi.org/10.1021/MP500046F

Wolburg, H., Noell, S., Mack, A., Wolburg-Buchholz, K., & Fallier-Becker, P. (2009). Brain endothelial cells and the glio-vascular complex. *Cell and Tissue Research*, *335*(1), 75–96. https://doi.org/10.1007/s00441-008-0658-9

Wolburg, H., Wolburg-Buchholz, K., Kraus, J., Rascher-Eggstein, G., Liebner, S., Hamm, S., Duffner, F., Grote, E. H., Risau, W., & Engelhardt, B. (2003). Localization of claudin-3 in tight junctions of the blood-brain barrier is selectively lost during experimental autoimmune encephalomyelitis and human glioblastoma multiforme. *Acta Neuropathologica*, *105*(6), 586–592. https://doi.org/10.1007/s00401-003-0688-z

Wolff, A., Antfolk, M., Brodin, B., & Tenje, M. (2015). In Vitro Blood-Brain Barrier Models-An Overview of Established Models and New Microfluidic Approaches. *Journal of Pharmaceutical Sciences*, *104*(9), 2727–2746. https://doi.org/10.1002/JPS.24329

Wong, A. D., Ye, M., Levy, A. F., Rothstein, J. D., Bergles, D. E., & Searson, P. C. (2013). The blood-brain barrier: an engineering perspective. *Frontiers in Neuroengineering*, *6*, 7. https://doi.org/10.3389/fneng.2013.00007

Workman, M. J., & Svendsen, C. N. (2020). Recent advances in human iPSC-derived models of the blood-brain barrier. *Fluids and Barriers of the CNS*, *17*(1), 1–10. https://doi.org/10.1186/S12987-020-00191-7/FIGURES/3

Xiao, G., & Gan, L.-S. (2013). Receptor-mediated endocytosis and brain delivery of therapeutic biologics. *International Journal of Cell Biology*, *2013*, 703545. https://doi.org/10.1155/2013/703545

Yamashita, S., Furubayashi, T., Kataoka, M., Sakane, T., Sezaki, H., & Tokuda, H. (2000). Optimized conditions for prediction of intestinal drug permeability using Caco-2 cells. *European Journal of Pharmaceutical Sciences*, *10*(3), 195–204. https://doi.org/10.1016/S0928-0987(00)00076-2

Yang, L., Froio, R. M., Sciuto, T. E., Dvorak, A. M., Alon, R., & Luscinskas, F. W. (2005). ICAM-1 regulates neutrophil adhesion and transcellular

migration of TNF-α-activated vascular endothelium under flow. *Blood*, *106*(2), 584–592. https://doi.org/10.1182/blood-2004-12-4942

Yeon, J. H., Na, D., Choi, K., Ryu, S. W., Choi, C., & Park, J. K. (2012). Reliable permeability assay system in a microfluidic device mimicking cerebral vasculatures. *Biomedical Microdevices*, *14*(6), 1141–1148. https://doi.org/10.1007/S10544-012-9680-5

Zhang, W., Liu, Q. Y., Haqqani, A. S., Liu, Z., Sodja, C., Leclerc, S., Baumann, E., Delaney, C. E., Brunette, E., & Stanimirovic, D. B. (2023). Differential Expression of ABC Transporter Genes in Brain Vessels vs. Peripheral Tissues and Vessels from Human, Mouse and Rat. *Pharmaceutics*, *15*(5), 1563. https://doi.org/10.3390/PHARMACEUTICS15051563/S1

Zhang, Y., Li, C. S. W., Ye, Y., Johnson, K., Poe, J., Johnson, S., Bobrowski, W., Garrido, R., & Madhu, C. (2006). Porcine brain microvessel endothelial cells as an in vitro model to predict in vivo blood-brain barrier permeability. *Drug Metabolism and Disposition*, *34*(11), 1935–1943. https://doi.org/10.1124/DMD.105.006437

Zhang, Y., Wu, X., He, Y., Kastin, A. J., Hsuchou, H., Rosenblum, C. I., & Pan, W. (2009). Melanocortin potentiates leptin-induced STAT3 signaling via MAPK pathway. *Journal of Neurochemistry*, *110*(1), 390–399. https://doi.org/10.1111/j.1471-4159.2009.06144.x

Zhang, Y. Y., Liu, H., Summerfield, S. G., Luscombe, C. N., & Sahi, J. (2016). Integrating in Silico and in Vitro Approaches to Predict Drug Accessibility to the Central Nervous System. *Molecular Pharmaceutics*, *13*(5), 1540–1550. https://doi.org/10.1021/ACS.MOLPHARMACEUT.6B00031

Zobel, K., Hansen, U., & Galla, H. J. (2016). Blood-brain barrier properties in vitro depend on composition and assembly of endogenous extracellular matrices. *Cell and Tissue Research*, *365*(2), 233–245. https://doi.org/10.1007/S00441-016-2397-7

Zoghbi, S. S., Liow, J. S., Yasuno, F., Hong, J., Tuan, E., Lazarova, N., Gladding, R. L., Pike, V. W., & Innis, R. B. (2008). 11C-Loperamide and Its N-Desmethyl Radiometabolite Are Avid Substrates for Brain Permeability-Glycoprotein Efflux. *Journal of Nuclear Medicine*, *49*(4), 649–656. https://doi.org/10.2967/JNUMED.107.047308

Zonta, M., Angulo, M. C., Gobbo, S., Rosengarten, B., Hossmann, K. A., Pozzan, T., & Carmignoto, G. (2003). Neuron-to-astrocyte signaling is central to the dynamic control of brain microcirculation. *Nature Neuroscience*, *6*(1), 43–50. https://doi.org/10.1038/NN980

Zou, W., Shi, B., Zeng, T., Zhang, Y., Huang, B., Ouyang, B., Cai, Z., & Liu, M. (2021). Drug Transporters in the Kidney: Perspectives on Species Differences, Disease Status, and Molecular Docking. *Frontiers in Pharmacology*, *12*. https://doi.org/10.3389/FPHAR.2021.746208

Zysk, G., Schneider-Wald, B. K., Hwang, J. H., Bejo, L., Kim, K. S., Mitchell, T. J., Hakenbeck, R., & Heinz, H. P. (2001). Pneumolysin is the main inducer of cytotoxicity to brain microvascular endothelial cells caused by Streptococcus pneumoniae. *Infection and Immunity*, *69*(2), 845–852. https://doi.org/10.1128/IAI.69.2.845-852.2001

Appendix 1

Appendix

BLAST gene sequence comparison between humans and horse for key blood-brain barrier transporters namely P-glycoprotein, MRP1, BCRP and GLUT1

Horse vs Human P-glycoprotein

90.16% SEQUENCE IDENTITY

```
Query  1    MDLEGDRNGGAKKKNFFKLNNKSEKDKKEKK-PTVSVFSMFRYSNWLDKLYMVVGTLAAI  59
            MDLEG RN    KKNF K+N +S+KD+K++K PTVS+F+MFRYSNWLDKLYM++GT AAI
Sbjct  1    MDLEGGRNRRRGKKNFLKINEESKKDEKKEKKPTVSIFAMFRYSNWLDKLYMLLGTTAAI  60

Query  60   IHGAGLPLMMLVFGEMTDIFANAGNLEDLMSNITNRSDINDTGFFMNLEEDMTRYAYYYS  119
            IHGAGLPLMMLVFG+MTD FAN GN+     N +  S+ + T F  NLEE+MT+YAYYYS
Sbjct  61   IHGAGLPLMMLVFGQMTDSFANVGNV----GNESYPSNGSPTPF-ENLEEEMTKYAYYYS  115

Query  120  GIGAGVLVAAYIQVSFWCLAAGRQIHKIRKQFFHAIMRQEIGWFDVHDVGELNTRLTDDV  179
            GIGAGVLVAAYIQVSFWCLAAGRQI+KIRKQFFHAIM+QEIGWFD+HDVGELNTRLTDDV
Sbjct  116  GIGAGVLVAAYIQVSFWCLAAGRQIYKIRKQFFHAIMQQEIGWFDMHDVGELNTRLTDDV  175

Query  180  SKINEVIGDKIGMFFQSMATFFTGFIVGFTRGWKLTLVILAISPVLGLSAAVWAKILSSF  239
            SKINE IGDKIGMFFQSMATFFTGFIVGFTRGWKLTLVILAISPVLGLSA +WAKILSSF
Sbjct  176  SKINEGIGDKIGMFFQSMATFFTGFIVGFTRGWKLTLVILAISPVLGLSAGIWAKILSSF  235

Query  240  TDKELLAYAKAGAVAEEVLAAIRTVIAFGGQKKELERYNKNLEEAKRIGIKKAITANISI  299
            TDKELLAYAKAGAVAEEVLAAIRTVIAFGGQKKELERYNKNLEEAKRIGIKKAITANIS+
Sbjct  236  TDKELLAYAKAGAVAEEVLAAIRTVIAFGGQKKELERYNKNLEEAKRIGIKKAITANISM  295

Query  300  GAAFLLIYASYALAFWYGTTLVLSGEYSIGQVLTVFFSVLIGAFSVGQASPSIEAFANAR  359
            GAAFLLIYASYALAFWYGT+LVLSGEYSIGQVLTVFFSVLIGAFSVGQASPSIEAFANAR
Sbjct  296  GAAFLLIYASYALAFWYGTSLVLSGEYSIGQVLTVFFSVLIGAFSVGQASPSIEAFANAR  355

Query  360  GAAYEIFKIIDNKPSIDSYSKSGHKPDNIKGNLEFRNVHFSYPSRKEVKILKGLNLKVQS  419
            GAAYEIFKIIDNKPSIDSYSK+GHKPDNIKGNLEFRNVHFSYPSR EVKILKGLNLKV+S
Sbjct  356  GAAYEIFKIIDNKPSIDSYSKNGHKPDNIKGNLEFRNVHFSYPSRNEVKILKGLNLKVRS  415

Query  420  GQTVALVGNSGCGKSTTVQLMQRLYDPTEGMVSVDGQDIRTINVRFLREIIGVVSQEPVL  479
            GQTVALVGNSGCGKSTTVQLMQRLYDPTEG+VS+DGQDIRTINVR+LREI GVVSQEPVL
Sbjct  416  GQTVALVGNSGCGKSTTVQLMQRLYDPTEGVVSIDGQDIRTINVRYLREITGVVSQEPVL  475

Query  480  FATTIAENIRYGRENVTMDEIEKAVKEANAYDFIMKLPHKFDTLVGERGAQLSGGQKQRI  539
            FATTIAENIRYGRENVTMDEI KAVKEANAYDFIMKLP+KFDTLVGERGAQLSGGQKQRI
Sbjct  476  FATTIAENIRYGRENVTMDEIVKAVKEANAYDFIMKLPNKFDTLVGERGAQLSGGQKQRI  535

Query  540  AIARALVRNPKILLLDEATSALDTESEAVVQVALDKARKGRTTIVIAHRLSTVRNADVIA  599
            AIARALVRNPKILLLDEATSALDTESEAVVQVALDKARKGRTTIVIAHRLSTVRNADVIA
Sbjct  536  AIARALVRNPKILLLDEATSALDTESEAVVQVALDKARKGRTTIVIAHRLSTVRNADVIA  595

Query  600  GFDDGVIVEKGNHDELMKEKGIYFKLVTMQTAGNEVELENAADESKSEIDALEMSSNDSR  659
            G DDGVIVE+GNHDELMKEKGIYFKLVTMQT GNE+ELE+A  ES+SEIDALEMS  DS
Sbjct  596  GLDDGVIVEEGNHDELMKEKGIYFKLVTMQTRGNEIELESAIGESQSEIDALEMSPKDSG  655
```

```
Query  660  SSLIRKRSTRRSVRGSQAQDRKLSTKEALDESIPPVSFWRIMKLNLTEWPYFVVGVFCAI  719
            SSLIR+RSTR+S+R  Q Q+RKLSTKEALDE++PPVSFWRI+KLN+TEWPYFVVG+FCAI
Sbjct  656   SSLIRRRSTRKSIREPQGQERKLSTKEALDENVPPVSFWRILKLNITEWPYFVVGIFCAI  715

Query  720  INGGLQPAFAIIFSKIIGVFTRIDDPETKRQNSNLFSLLFLALGIISFITFFLQGFTFGK  779
            INGGLQPAF+IIFS+IIGVFTR +DPETKRQNSN+FSLLFL LGIISFITFFLQG+TFGK
Sbjct  716  INGGLQPAFSIIFSRIIGVFTRDEDPETKRQNSNMFSLLFLVLGIISFITFFLQGYTFGK  775

Query  780  AGEILTKRLRYMVFRSMLRQDVSWFDDPKNTTGALTTRLANDAAQVKGAIGSRLAVITQN  839
            AGEILTKRLRY+VFRSMLRQDVSWFD+PKNTTGALTTRLANDA QVKGAIGSRLAVITQN
Sbjct  776  AGEILTKRLRYLVFRSMLRQDVSWFDNPKNTTGALTTRLANDAGQVKGAIGSRLAVITQN  835

Query  840  IANLGTGIIISFIYGWQLTLLLLAIVPIIAIAGVVEMKMLSGQALKDKKELEGAGKIATE  899
            IANLGTGIIISFIYGWQLTLLLLAIVPIIAIAGVVEMKMLSGQALKDKK+LEGAGK+ATE
Sbjct  836  IANLGTGIIISFIYGWQLTLLLLAIVPIIAIAGVVEMKMLSGQALKDKKKLEGAGKVATE  895

Query  900  AIENFRTVVSLTQEQKFEHMYAQSLQVPYRNSLRKAHIFGITFSFTQAMMYFSYAGCFRF  959
            AIENFRTVVSLT+EQKFE MYA+ LQVPYRNSLRKAH+FGITFS TQAMMYFSYAGCFRF
Sbjct  896  AIENFRTVVSLTREQKFEDMYAEKLQVPYRNSLRKAHVFGITFSITQAMMYFSYAGCFRF  955

Query  960  GAYLVAHKLMSFEDVLLVFSAVVFGAMAVGQVSSFAPDYAKAKISAAHIIMIIEKTPLID  1019
            GA+LVA +LM+F+DVLLVFSA+VFGAMAVGQVSSFAPDYAKAK+SAAHIIMIIEKTPLID
Sbjct  956  GAFLVARQLMNFQDVLLVFSAIVFGAMAVGQVSSFAPDYAKAKVSAAHIIMIIEKTPLID  1015

Query 1020  SYSTEGLMPNTLEGNVTFGEVVFNYPTRPDIPVLQGLSLEVKKGQTLALVGSSGCGKSTV  1079
            SYSTEGL PNTLEGNV F EVVFNYPTRPDIPVLQGLS+EVKKGQTLALVGSSGCGKST+
Sbjct  1016  SYSTEGLKPNTLEGNVIFNEVVFNYPTRPDIPVLQGLSVEVKKGQTLALVGSSGCGKSTL  1075

Query 1080  VQLLERFYDPLAGKVLLDGKEIKRLNVQWLRAHLGIVSQEPILFDCSIAENIAYGDNSRV  1139
            VQLLERFYDP+AG VLLDG EIK LNVQWLRAHLGIVSQEPILFDCSI ENIAYGDNSRV
Sbjct  1076  VQLLERFYDPMAGTVLLDGTEIKHLNVQWLRAHLGIVSQEPILFDCSIGENIAYGDNSRV  1135

Query 1140   VSQEEIVRAAKEANIHAFIESLPNKYSTKVGDKGTQLSGGQKQRIAIARALVRQPHILLL  1199
            VSQEEIV+AAKEANIH FIE+LP+KY+T+VGDKGTQLSGGQKQRIAIARALVRQP ILLL
Sbjct  1136  VSQEEIVQAAKEANIHPFIETLPDKYNTRVGDKGTQLSGGQKQRIAIARALVRQPQILLL  1195

Query  1200 DEATSALDTESEKVVQEALDKAREGRTCIVIAHRLSTIQNADLIVVFQNGRVKEHGTHQQ  1259
            DEATSALDTESEKVVQEALDKAREGRTCIVIAHRLSTIQNADLIVVFQNG+VKE GTHQQ
Sbjct  1196  DEATSALDTESEKVVQEALDKAREGRTCIVIAHRLSTIQNADLIVVFQNGKVKERGTHQQ  1255

Query  1260 LLAQKGIYFSMVSVQAGTKR  1279
            LLAQKGIYFSMVSVQAG KR
Sbjct  1256  LLAQKGIYFSMVSVQAGAKR  1275
```

Horse vs Human MRP1

86.66% SEQUENCE IDENTITY

```
Query  1    MSRRKPASGGLAASSSAPARQAVLSRFFQSTGSLKSTSSSTGAADQVDPGAAAAAAAAAA  60
            MSRRKPA+GG AA+  APARQAVLSRFFQS GSLKSTSS  GAA++ DP + AAA
Sbjct  1     MSRRKPAAGGAAAAGPAPARQAVLSRFFQSAGSLKSTSSPPGAAEKADPDSDAAA-----  55

Query  61   AAPPAPPAPAFPPQLPPHIATEIDRRKKRPLENDGPVKKKVKKVQQKEGGSDLGMSGNSE  120
            P A +FPP LPP +  E DR KKRPLENDGPVKKK KKVQ+KEG SDL  SGN E
Sbjct  56   -----PLASSFPPPLPPQLVAETDRSKKRPLENDGPVKKKAKKVQEKEGESDLVKSGNPE  110
```

```
Query  121  PKKCLRTRNVSKSLEKLKEFCCDSALPQSRVQTESLQERFAVLPKCTDFDDISLLHAKNA  180
            PKKCLRTR V KSLEKLKEFCCDSA PQ+RVQTE L+ERFAVLPKCTDFDDI LL AKNA
Sbjct  111  PKKCLRTRIVLKSLEKLKEFCCDSAPPQNRVQTEPLKERFAVLPKCTDFDDIDLLRAKNA  170

Query  181  VSSEDSKRQINQKDTTLFDLSQFGSSNTSH-ENLQKTA-SKSANKRSKSIYTPLELQYIE  238
            VSSEDSK Q +QKD T+FD+S+ GSS+    ENLQKT  SK +NKR+KSIYTPLELQYIE
Sbjct  171  VSSEDSKSQTSQKDKTVFDVSRSGSSSLGGCENLQKTCDSKPSNKRTKSIYTPLELQYIE  230

Query  239  MKQQHKDAVLCVECGYKYRFFGEDAEIAARELNIYCHLDHNFMTASIPTHRLFVHVRRLV  298
            MKQQ KDA+LCVECGYKYRFFGEDAEIAARELNIYCHLDHNFMTASIPTHRLFVHVRRLV
Sbjct  231  MKQQQKDAILCVECGYKYRFFGEDAEIAARELNIYCHLDHNFMTASIPTHRLFVHVRRLV  290

Query  299  AKGYKVGVVKQTETAALKAIGDNRSSLFSRKLTALYTKSTLIGEDVNPLIKLDDAVNVDE  358
            AKGYKVGVVKQTETAALKAIGDN+SSLFSRKLTALYTKSTLIGEDVNPL+KLDDAVNVDE
Sbjct  291  AKGYKVGVVKQTETAALKAIGDNKSSLFSRKLTALYTKSTLIGEDVNPLVKLDDAVNVDE  350

Query  359  IMTDTSTSYLLCISENKENVRDKKKGNIFIGIVGVQPATGEVVFDSFQDSASRSELETRM  418
            I+TDTSTSYLLCI ENKENV+DKKKGNIFIG+VGVQPATGEVVFDSFQDSASRSELETR+
Sbjct  351  IITDTSTSYLLCICENKENVKDKKKGNIFIGLVGVQPATGEVVFDSFQDSASRSELETRI  410

Query  419  SSLQPVELLLPSALSEQTEALIHRATSVSVQDDRIRVERMDNIYFEYSHAFQAVTEFYAK  478
            SLQPVELLLPS LSEQTE LI RAT+VSV+DDRIRVERMDN+YFEYSHAFQ VTEFYAK
Sbjct  411  LSLQPVELLLPSTLSEQTELLIRRATAVSVRDDRIRVERMDNMYFEYSHAFQMVTEFYAK  470

Query  479  DTVDIKGSQIISGIVNLEKPVICSLAAIIKYLKEFNLEKMLSKPENFKQLSSKMEFMTIN  538
            D VD+KGS+  SGI+NLEK VICSLAAII+YLK+FNLEK+LSKP+NFKQ S +MEFMTIN
Sbjct  471  DVVDVKGSRSFSGIINLEKAVICSLAAIIRYLKDFNLEKVLSKPKNFKQFSGEMEFMTIN  530

Query  539  GTTLRNLEILQNQTDMKTKGSLLWVLDHTKTSFGRRKLKKWVTQPLLKLREINARLDAVS  598
            GTTLRNLEILQNQTDMKTKGSLLWVLDHTKT+FGRRKLKKWVTQPLLK+R+INARLDAVS
Sbjct  531  GTTLRNLEILQNQTDMKTKGSLLWVLDHTKTAFGRRKLKKWVTQPLLKIRDINARLDAVS  590

Query  599  EVLHSESSVFGQIENHLRKLPDIERGLCSIYHKKCSTQEFFLIVKTLYHLKSEFQAIIPA  658
            EVL+SESSVFGQIENHLRKLPDIERGLCSIYHKKCSTQEFFLIVKTL+HLKSEFQA++PA
Sbjct  591  EVLYSESSVFGQIENHLRKLPDIERGLCSIYHKKCSTQEFFLIVKTLHHLKSEFQALVPA  650

Query  659  VNSHIQSDLLRTVILEIPELLSPVEHYLKILNEQAAKVGDKTELFKDLSDFPLIKKRKDE  718
            VNSH+QSDLLRT ILEIPELLSPVE YLKILNEQAAK+GDKTELFKDLSDFPLIKKRKDE
Sbjct  651  VNSHVQSDLLRTFILEIPELLSPVERYLKILNEQAAKIGDKTELFKDLSDFPLIKKRKDE  710

Query  719  IQGVIDEIRMHLQEIRKILKNPSAQYVTVSGQEFMIEIKNSAVSCIPTDWVKVGSTKAVS  778
            IQ V  I+ HLQEIRKI+KNPSAQYVTVSGQEF+IE+KNSAVSCIPTDWVK+GSTKAVS
Sbjct  711  IQEVTHRIQRHLQEIRKIIKNPSAQYVTVSGQEFLIEVKNSAVSCIPTDWVKIGSTKAVS  770
```

```
Query  779  RFHSPFIVENYRHLNQLREQLVLDCSAEWLDFLEKFSEHYHSLCKAVHHLATVDCIFSLA  838
            RFHSPF+VENYRHLNQLREQLVLDCSAEWL+FLE FSEHYHSLCKAVHHLATVDCIFSLA
Sbjct  771  RFHSPFVVENYRHLNQLREQLVLDCSAEWLEFLENFSEHYHSLCKAVHHLATVDCIFSLA  830

Query  839  KVAKQGDYCRPTVQEERKIVIKNGRHPVIDVLLGEQDQYVPNNTDLSEDSERVMIITGPN  898
            KVAKQGDYCRPT+QEERKI+IKNGRHPVIDVLLGEQDQYVPN+T+LS DSERVMIITGPN
Sbjct  831  KVAKQGDYCRPTLQEERKILIKNGRHPVIDVLLGEQDQYVPNSTNLSGDSERVMIITGPN  890

Query  899  MGGKSSYIKQVALITIMAQIGSYVPAEEATIGIVDGIFTRMGAADNIYKGQSTFMEELTD  958
            MGGKSSYIKQVALIT+MAQIGSYVPAEEATIGIVDGIFTRMGAADNIYKG+STFMEELTD
Sbjct  891  MGGKSSYIKQVALITVMAQIGSYVPAEEATIGIVDGIFTRMGAADNIYKGRSTFMEELTD  950

Query  959  TAEIIRKATSQSLVILDELGRGTSTHDGIAIAYATLEYFIRDVKSLTLFVTHYPPVCELE  1018
            TAEIIRKATSQSLVILDELGRGTSTHDGIAIAYATLE+FIRDVKSLTLFVTHYPPVCELE
Sbjct  951  TAEIIRKATSQSLVILDELGRGTSTHDGIAIAYATLEHFIRDVKSLTLFVTHYPPVCELE  1010

Query 1019  KNYSHQVGNYHMGFLVSEDESKLDPGAAEQVPDFVTFLYQITRGIAARSYGLNVAKLADV  1078
            ++YS QVGNYHMGFLV+ED+SK D G  EQVPDFVTFLYQIT+GIAARSYGLNVAKLADV
Sbjct  1011  RSYSQQVGNYHMGFLVNEDDSKPDQGEEEQVPDFVTFLYQITKGIAARSYGLNVAKLADV  1070

Query  1079 PGEILKKAAHKSKELEGLINTKRKRLKYFAKLWTMHNAQDLQKWTEEFNMEE  1130
            PGEILKKAA KSKELEGL+N KRKRLK FAKLWT+++A+DL+K T+EF MEE
Sbjct  1071 PGEILKKAASKSKELEGLVNMKRKRLKCFAKLWTINDAEDLRKRTDEFEMEE  1122
```

Horse vs Human BCRP

86.13% SEQUENCE IDENTITY

```
Query  1    MSSSNVEVFIPVSQGNTNGFPATASNDLKAFTEGAVLSFHNICYRVKLKSGFLPCRKPVE  60
            MSSSN +V IP+SQ NTNG P      +KAFTEGAVLSFHNICYRVK KSGFL CRK VE
Sbjct  22   MSSSNDQVSIPMSQRNTNGLPKKTPKGVKAFTEGAVLSFHNICYRVKEKSGFLLCRKTVE  81

Query  61   KEILSNINGIMKPGLNAILGPTGGGKSSLLDVLAARKDPSGLSGDVLINGAPRPANFKCN  120
            KEILSNINGIM+PGLNAILGPTGGGKSSLLDVLAARKDP GLSGDVLINGA RPANFKC+
Sbjct  82   KEILSNINGIMRPGLNAILGPTGGGKSSLLDVLAARKDPHGLSGDVLINGATRPANFKCS  141

Query  121  SGYVVQDDVVMGTLTVRENLQFSAALRLATTMTNHEKNERINRVIQELGLDKVADSKVGT  180
            SGYVVQDDVVMGTLTVRENLQFSAALRL TTM NHEKNERINR+IQELGL+KVADSK+GT
Sbjct  142  SGYVVQDDVVMGTLTVRENLQFSAALRLPTTMRNHEKNERINRIIQELGLEKVADSKIGT  201

Query  181  QFIRGVSGGERKRTSIGMELITDPSILFLDEPTTGLDSSTANAVLLLLKRMSKQGRTIIF  240
            QFIRGVSGGERKRTSIGMELITDPSILFLDEPTTGLDSSTANAVLLLLKRMSKQGRTIIF
Sbjct  202  QFIRGVSGGERKRTSIGMELITDPSILFLDEPTTGLDSSTANAVLLLLKRMSKQGRTIIF  261

Query  241  SIHQPRYSIFKLFDSLTLLASGRLMFHGPAQEALGYFESAGYHCEAYNNPADFFLDIING  300
            SIHQPRYSIFKLFDSLTLLASG+LMFHGPAQEALGYF SAGYHCE YNNPADFFLD+ING
Sbjct  262  SIHQPRYSIFKLFDSLTLLASGKLMFHGPAQEALGYFASAGYHCEPYNNPADFFLDVING  321
```

```
Query  301  DSTAVALNREE-DFKATEIIEPSKQDKPLIEKLAEIYVNSSFYKETKAELHQLSGGEKKK  359
            DS+AV LNRE+ + +A E  EPS++D  L+EKLAE Y NS+F++ETKAEL QLSG +K K
Sbjct  322  DSSAVLLNREDPEGEARETEEPSQRDLSLLEKLAEFYGNSTFFRETKAELDQLSGAQKSK  381

Query  360  KITVFKEISYTTSFCHQLRWVSKRSFKNLLGNPQASIAQIIVTVVLGLVIGAIYFGLKND  419
            K  FKEI+Y +SF HQL+W+SKRSFKNLLGNPQASIAQII+T +LGLVIGAI++ LK D
Sbjct  382  KSIAFKEITYVSSFFHQLKWISKRSFKNLLGNPQASIAQIIITAILGLVIGAIFYDLKMD  441

Query  420  STGIQNRAGVLFFLTTNQCFSSVSAVELFVVEKKLFIHEYISGYYRVSSYFLGKLLSDLL  479
            S GIQNRAGVLFFLTTNQCFSSVSAVELFVVEKKLFIHEYISGYYRVSSYFLGKLLSDLL
Sbjct  442  SAGIQNRAGVLFFLTTNQCFSSVSAVELFVVEKKLFIHEYISGYYRVSSYFLGKLLSDLL  501

Query  480  PMRMLPSIIFTCIVYFMLGLKPKADAFFVMMFTLMMVAYSASSMALAIAAGQSVVSVATL  539
            PMRMLPSIIFTCI YF+LGLKPK +AFF+MMFTLMMVAYSASSMALAIAAGQSVVS+ATL
Sbjct  502  PMRMLPSIIFTCITYFLLGLKPKVEAFFIMMFTLMMVAYSASSMALAIAAGQSVVSIATL  561

Query  540  LMTICFVFMMIFSGLLVNLTTIASWLSWLQYFSIPRYGFTALQHNEFLGQNFCPGLNATG  599
            LMTICFVFMMIFSGLLVNL T+ +WLSWLQYFSIPRYG+ ALQHNEFLGQNFCPGLN T
Sbjct  562  LMTICFVFMMIFSGLLVNLRTVVAWLSWLQYFSIPRYGYAALQHNEFLGQNFCPGLNVTA  621

Query  600  NNPCNYATCTGEEYLVKQGIDLSPWGLWKNHVALACMIVIFLTIAYLKLLFLKKYS  655
            N+ C+YATCTGEE+L  QGIDLSPWGLW+NHVALACMIVIFLTIAYLKLLFLKKYS
Sbjct  622  NDTCSYATCTGEEFLENQGIDLSPWGLWRNHVALACMIVIFLTIAYLKLLFLKKYS  677
```

Horse vs Human GLUT1

93.09% SEQUENCE IDENTITY

```
Query  1    MEPSSKKLTGRLMLAVGGAVLGSLQFGYNTGVINAPQKVIEEFYNQTWVHRYGESILPTT  60
            M+PSSKKLTGRLMLAVGGAVLGSLQ+GYNTGVINAPQKVIEEFYN+TW+HRYGE ILP+T
Sbjct  1    MDPSSKKLTGRLMLAVGGAVLGSLQYGYNTGVINAPQKVIEEFYNETWIHRYGEPILPST  60

Query  61   LTTLWSLSVAIFSVGGMIGSFSVGLFVNRFGRRNSMLMMNLLAFVSAVLMGFSKLGKSFE  120
            LTTLWSLSVAIFS+GGM+G+FSVGLFVNRFGRRNSMLM+NLLAFV+AVLMGFSKLGKSFE
Sbjct  61   LTTLWSLSVAIFSIGGMLGAFSVGLFVNRFGRRNSMLMVNLLAFVAAVLMGFSKLGKSFE  120

Query  121  MLILGRFIIGVYCGLTTGFVPMYVGEVSPTALRGALGTLHQLGIVVGILIAQVFGLDSIM  180
            MLILGRFIIGVY GL+TGFVPMYVGEVSPTALRGALGTLHQL +V+GILIAQVFGLDSIM
Sbjct  121  MLILGRFIIGVYSGLSTGFVPMYVGEVSPTALRGALGTLHQLSVVIGILIAQVFGLDSIM  180

Query  181  GNKDLWPLLLSIIFIPALLQCIVLPFCPESPRFLLINRNEENRAKSVLKKLRGTADVTHD  240
            GN++LWPLLLSI F+PA++QC++LPFCPESPRFLLINRNEENRAKSVLKKLRGTADVT D
Sbjct  181  GNEELWPLLLSITFLPAVVQCVLLPFCPESPRFLLINRNEENRAKSVLKKLRGTADVTRD  240
```

```
Query  241  LQEMKEESRQMMREKKVTILELFRSPAYRQPILIAVVLQLSQQLSGINAVFYYSTSIFEK  300
            LQEMKEESRQMMREKKVTILELFRSP YRQPILIAV+LQLSQQLSGINAVFYYSTSIFEK
Sbjct  241  LQEMKEESRQMMREKKVTILELFRSPTYRQPILIAVMLQLSQQLSGINAVFYYSTSIFEK  300

Query  301  AGVQQPVYATIGSGIVNTAFTVVSLFVVERAGRRTLHLIGLAGMAGCAILMTIALALLEQ  360
            AGVQQPVYATIG+GIVNTAFTVVSLFVVERAGRRTLHLIGL GMAGCA+LMTIA+ALLEQ
Sbjct  301  AGVQQPVYATIGAGIVNTAFTVVSLFVVERAGRRTLHLIGLGGMAGCAVLMTIAVALLEQ  360

Query  361  LPWMSYLSIVAIFGFVAFFEVGPGPIPWFIVAELFSQGPRPAAIAVAGFSNWTSNFIVGM  420
            LPWMSYLSIVAIFGFVAFFEVGPGPIPWFIVAELFSQGPRPAAIAV+GFSNW SNF+VGM
Sbjct  361  LPWMSYLSIVAIFGFVAFFEVGPGPIPWFIVAELFSQGPRPAAIAVSGFSNWASNFLVGM  420

Query  421  CFQYVEQLCGPYVFIIFTVLLVLFFIFTYFKVPETKGRTFDEIASGFRQGGASQSDKTPE  480
            CFQYVEQLCGPYVFIIFTVLLVLFFIFTYFKVPETKGRTFDEIASGFRQGGASQSDKTPE
Sbjct  421  CFQYVEQLCGPYVFIIFTVLLVLFFIFTYFKVPETKGRTFDEIASGFRQGGASQSDKTPE  480

Query  481  ELFHPLGADSQV  492
            ELFHPLGADSQV
Sbjct  481  ELFHPLGADSQV  492
```

Appendix 2

Standard curves were developed from calibration line concentrations and measured response (ratio of area of drug peak to internal standard peak). This standard curve was used to generate sample concentration of each test drug. The standard curve of each drug as calculated is listed below.

Fig. A2.1: loperamide

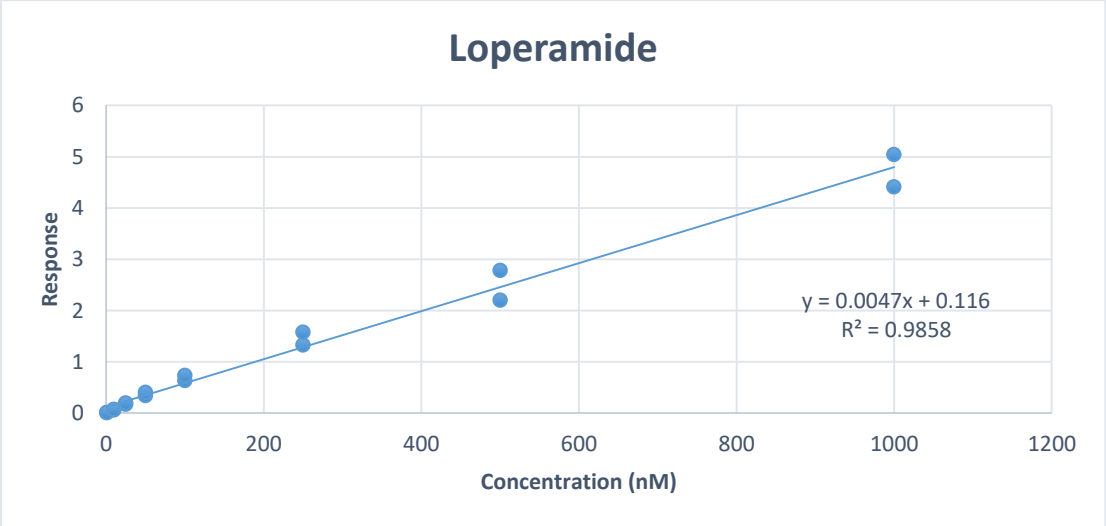

Fig. A2.1: Standard curve fit of loperamide calibration values for drug transport study. Sample concentration is shown on X axis and response is shown on Y axis. The graph shows the linear line of best fit equation used to calculate projected concentrations.

Fig. A2.2: chlorpromazine

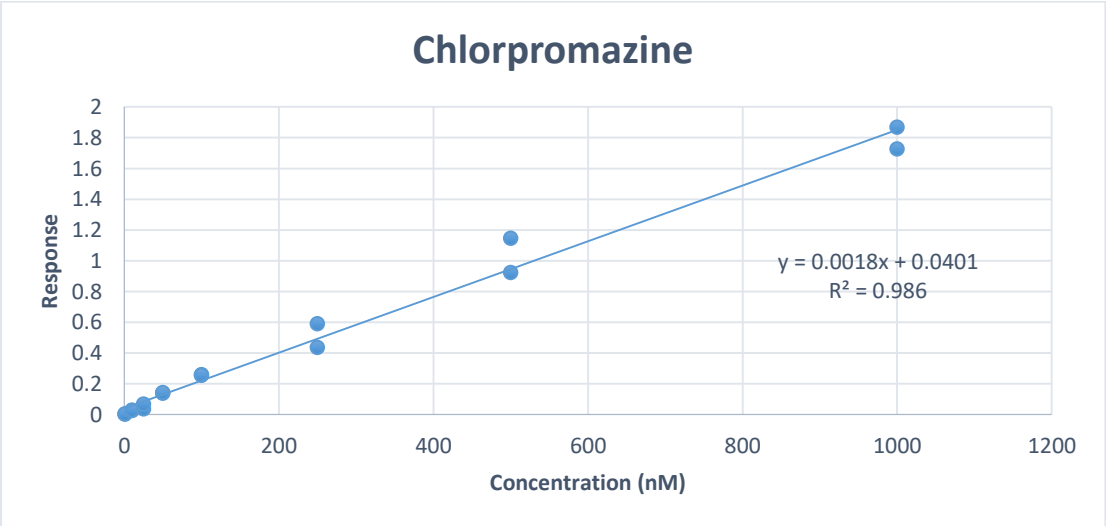

Fig. A2.2: Standard curve fit of chlorpromazine calibration values for drug transport study. Sample concentration is shown on X axis and response is shown on Y axis. The graph shows the linear line of best fit equation used to calculate projected concentrations.

Fig. A2.3: lamotrigine

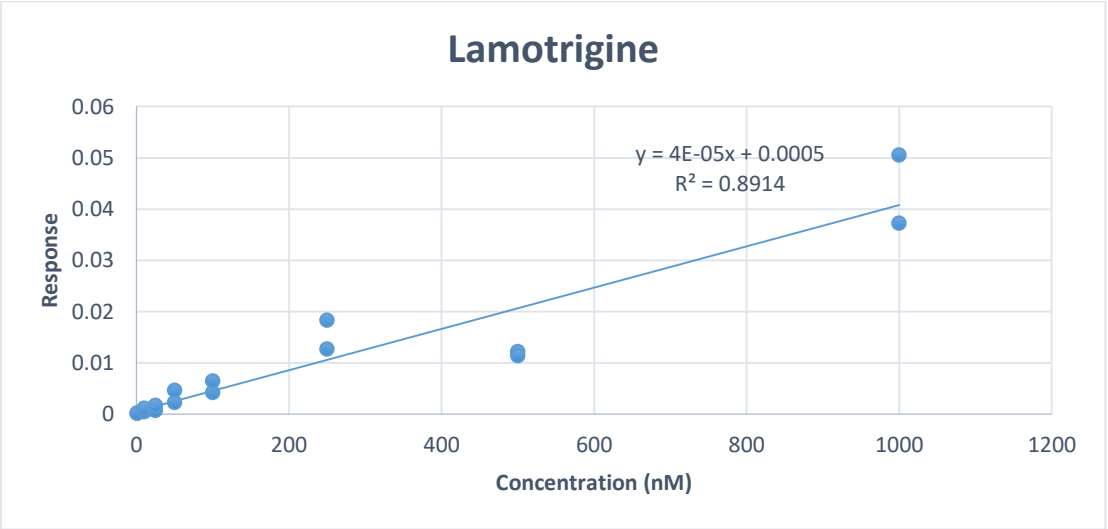

Fig. A2.3: Standard curve fit of lamotrigine calibration values for drug transport study. Sample concentration is shown on X axis and response is shown on Y axis. The graph shows the linear line of best fit equation used to calculate projected concentrations.

Fig. A2.4: topiramate

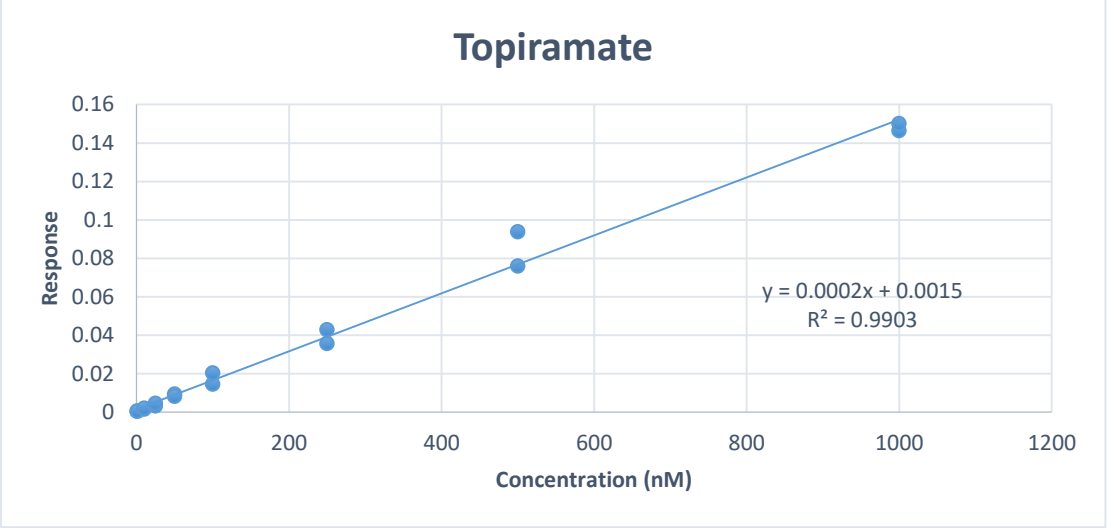

Fig. A2.4: Standard curve fit of topiramate calibration values for drug transport study. Sample concentration is shown on X axis and response is shown on Y axis. The graph shows the linear line of best fit equation used to calculate projected concentrations.

Fig. A2.5: mitoxantrone

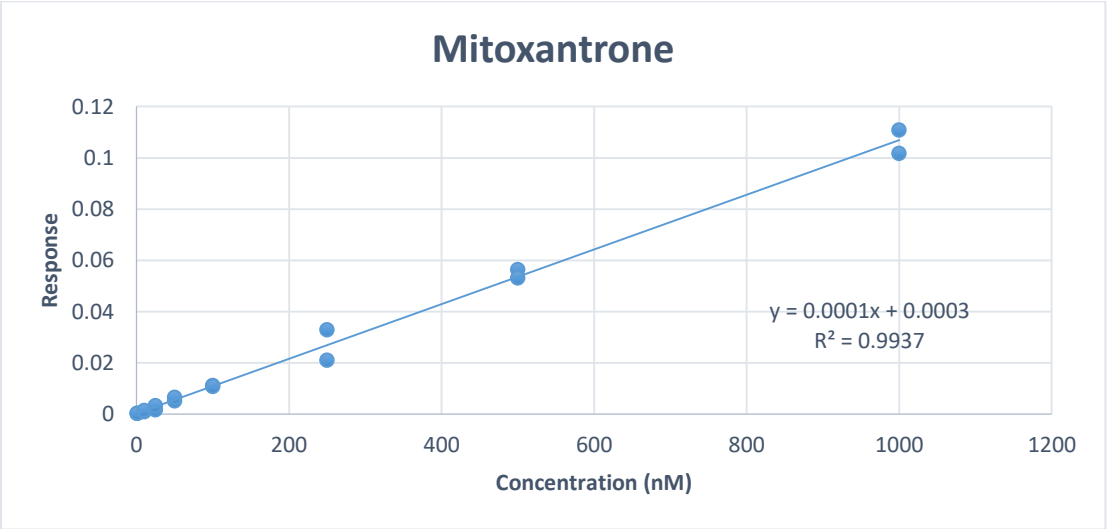

Fig. A2.5: Standard curve fit of mitoxantrone calibration values for drug transport study. Sample concentration is shown on X axis and response is shown on Y axis. The graph shows the linear line of best fit equation used to calculate projected concentrations.

Fig. A2.6: camptothecin

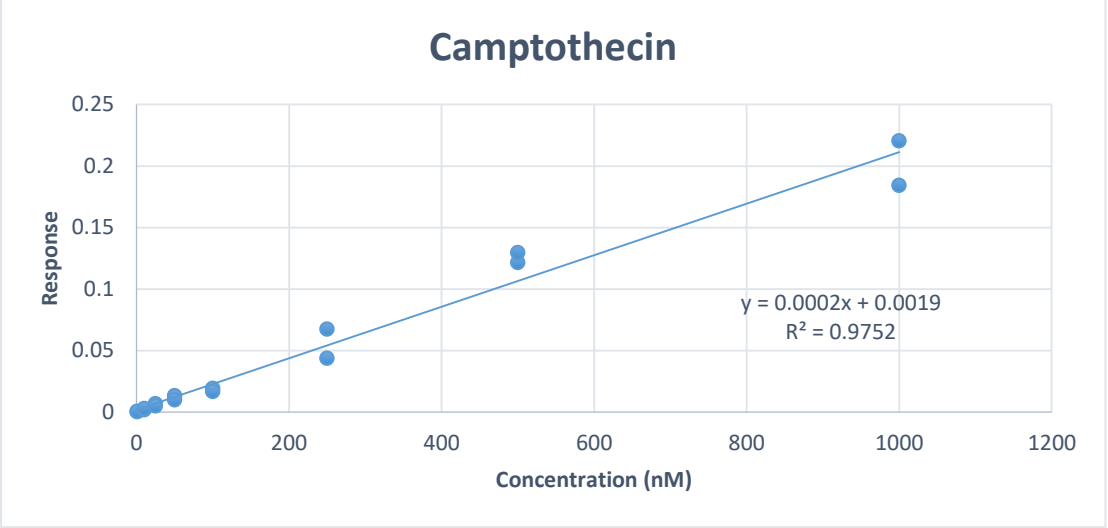

Fig. A2.6: Standard curve fit of camptothecin calibration values for drug transport study. Sample concentration is shown on X axis and response is shown on Y axis. The graph shows the linear line of best fit equation used to calculate projected concentrations.

Fig. A2.7: methotrexate

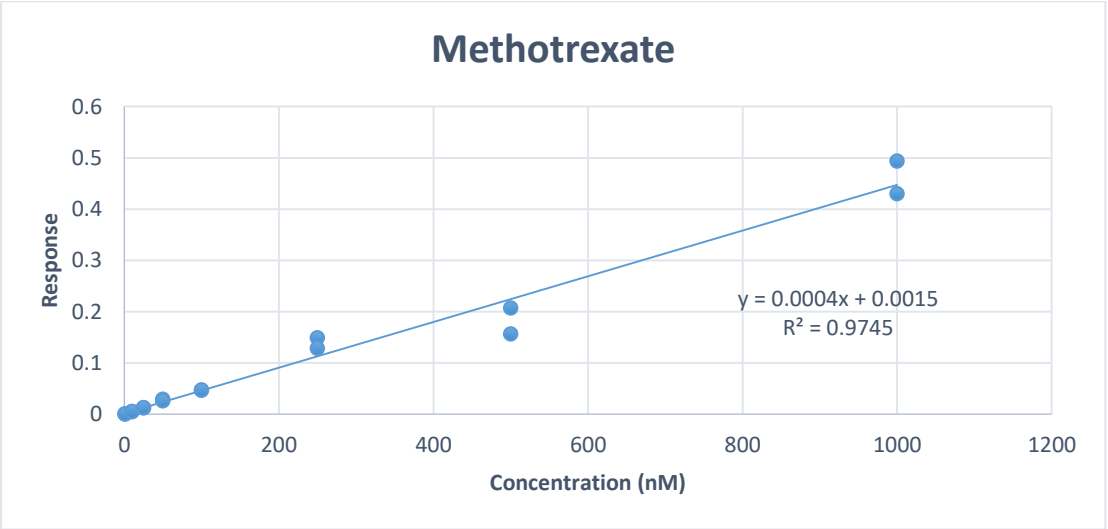

Fig. A2.7: Standard curve fit of methotrexate calibration values for drug transport study. Sample concentration is shown on X axis and response is shown on Y axis. The graph shows the linear line of best fit equation used to calculate projected concentrations.

Fig. A2.8: etoposide

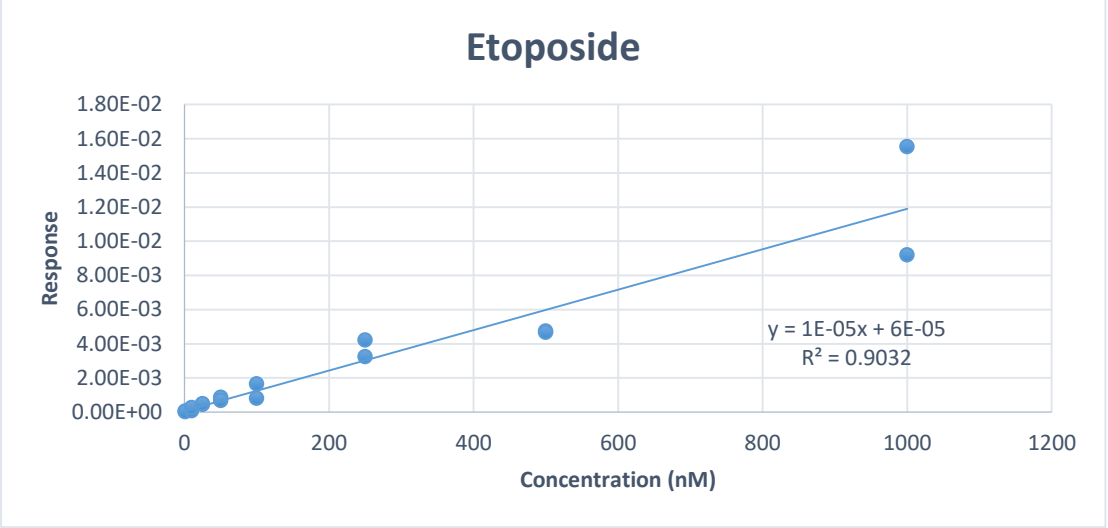

Fig. A2.8: Standard curve fit of etoposide calibration values for drug transport study. Sample concentration is shown on X axis and response is shown on Y axis. The graph shows the linear line of best fit equation used to calculate projected concentrations

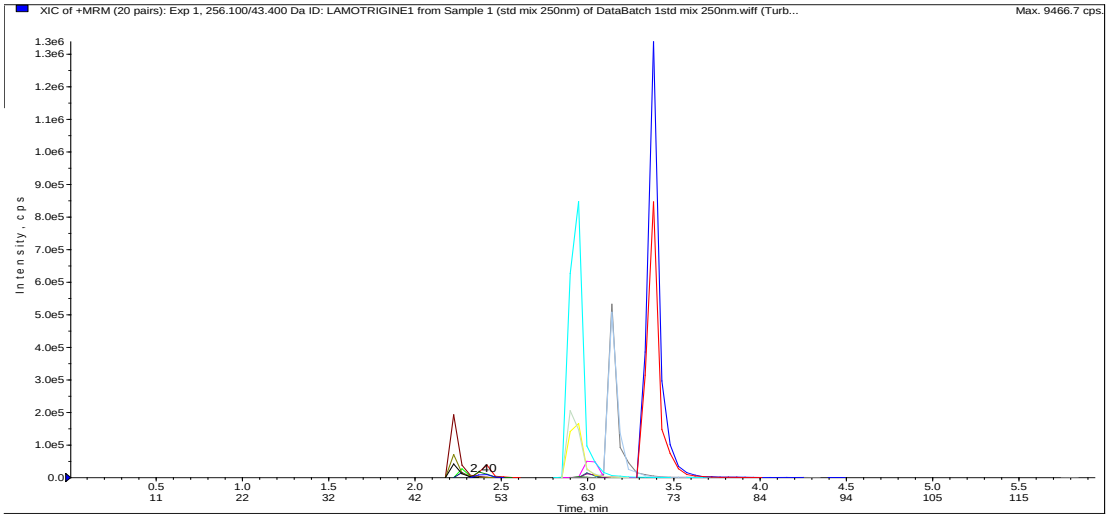

Fig. A2.9: Chromatograms produced by seven test drugs namely loperamide, chlorpromazine, lamotrigine, mitoxantrone, camptothecin, methotrexate and etoposide for drug transport studies. Percentage response is shown on Y axis and retention time (in minutes) is shown on X axis. All these drugs were run in positive MRM. This chromatogram is produced by 250nM standard mixture of drugs.

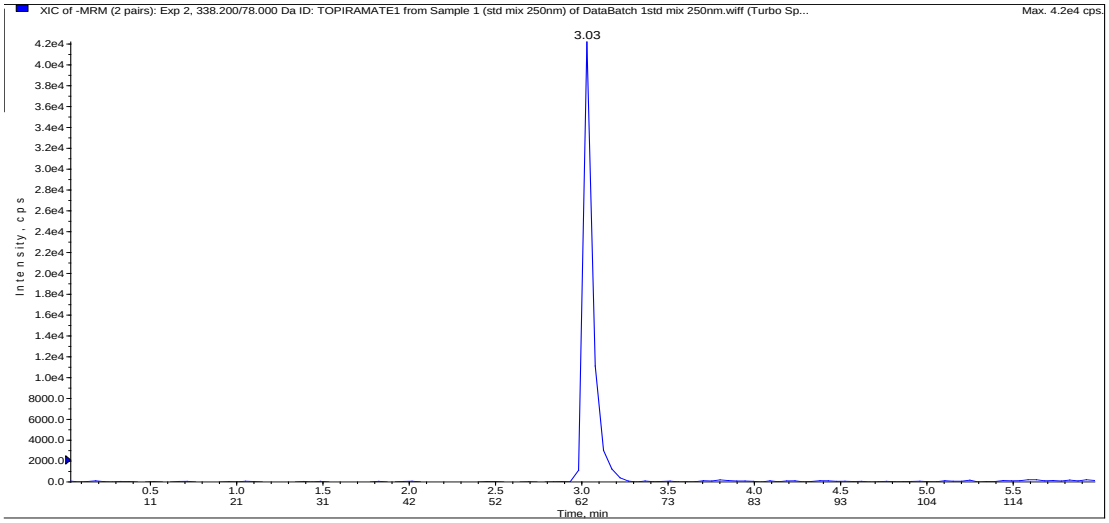

Fig. A2.10: Chromatograms produced by test drug topiramate for drug transport studies. Percentage response is shown on Y axis and retention time (minutes) is shown on X axis. This drug was run in negative MRM. This chromatogram is produced by 250nM standard mixture of drugs.

Appendix 3

Additional data from LC-MS/MS analysis of no cell control (NCC) studies on Transwell

Table A3.1: Recovery percentage of camptothecin in no cell control (NCC) studies on transwell in both apical-to-basal (A-B) and basal-to-apical (B-A) direction in six replicates at 30 minutes time point

Drug	Conc apical start (nM)	conc apical end (nM)	Conc basolateral start (nM)	Conc basolateral end (nM)	amount apical start (nmol)	amount apical end (nmol)	amount basolateral start (nmol)	amount basolateral end (nmol)	Total in well start (nmol)	Total in well end (nmol)	Recovery (%)
camptothecin 1 A-B	900.8	919.33	0	36.05	0.090	0.092	0.000	0.022	0.090	0.114	126
camptothecin 1 B-A	0	171.55	900.8	810.708	0.000	0.017	0.540	0.486	0.540	0.504	93
camptothecin 2 A-B	900.8	1006.48	0	36.15	0.090	0.101	0.000	0.022	0.090	0.122	136
camptothecin 2 B-A	0	157.54	900.8	775.029	0.000	0.016	0.540	0.465	0.540	0.481	89
camptothecin 3 A-B	900.8	1035.2	0	39.17	0.090	0.104	0.000	0.024	0.090	0.127	141
camptothecin 3 B-A	0	96.26	900.8	970.25	0.000	0.010	0.540	0.582	0.540	0.592	109
camptothecin 4 A-B	900.8	812.28	0	43.51	0.090	0.081	0.000	0.026	0.090	0.107	119
camptothecin 4 B-A	0	128.046	900.8	690.893	0.000	0.013	0.540	0.415	0.540	0.427	79
camptothecin 5 A-B	900.8	820.038	0	29.8	0.090	0.082	0.000	0.018	0.090	0.100	111
camptothecin 5 B-A	0	97.33	900.8	697.72	0.000	0.010	0.540	0.419	0.540	0.428	79
camptothecin 6 A-B	900.8	878.85	0	29.375	0.090	0.088	0.000	0.018	0.090	0.106	117
camptothecin 6 B-A	0	89.92	900.8	728.21	0.000	0.009	0.540	0.437	0.540	0.446	83

Table A3.2: Recovery percentage of chlorpromazine in no cell control (NCC) studies on transwell in both apical-to-basal (A-B) and basal-to-apical (B-A) direction in six replicates at 30 minutes time point

Drug	Conc apical start (nM)	conc apical end (nM)	Conc basolateral start (nM)	Conc basolateral end (nM)	amount apical start (nmol)	amount apical end (nmol)	amount basolateral start (nmol)	amount basolateral end (nmol)	Total in well start (nmol)	Total in well end (nmol)	Recovery (%)
chlorpromazine 1 A-B	60.76667	209.33	0	1.06	0.006	0.021	0.000	0.001	0.006	0.022	355
chlorpromazine 1 B-A	0	2.86	60.76667	447.75	0.000	0.000	0.036	0.269	0.036	0.269	738
chlorpromazine 2 A-B	60.76667	152.58	0	0.94	0.006	0.015	0.000	0.001	0.006	0.016	260
chlorpromazine 2 B-A	0	1.72	60.76667	517.9	0.000	0.000	0.036	0.311	0.036	0.311	853
chlorpromazine 3 A-B	60.76667	181.88	0	0.98	0.006	0.018	0.000	0.001	0.006	0.019	309
chlorpromazine 3 B-A	0	2.05	60.76667	474.41	0.000	0.000	0.036	0.285	0.036	0.285	781
chlorpromazine 4 A-B	60.76667	343.18	0	1.53	0.006	0.034	0.000	0.001	0.006	0.035	580
chlorpromazine 4 B-A	0	2.25	60.76667	440.42	0.000	0.000	0.036	0.264	0.036	0.264	725
chlorpromazine 5 A-B	60.76667	272.63	0	1.11	0.006	0.027	0.000	0.001	0.006	0.028	460
chlorpromazine 5 B-A	0	1.99	60.76667	462.25	0.000	0.000	0.036	0.277	0.036	0.278	761
chlorpromazine 6 A-B	60.76667	249.85	0	1.16	0.006	0.025	0.000	0.001	0.006	0.026	423
chlorpromazine 6 B-A	0	2.32	60.76667	518.12	0.000	0.000	0.036	0.311	0.036	0.311	853

Table A3.3: Recovery percentage of loperamide in no cell control (NCC) studies on transwell in both apical-to-basal (A-B) and basal-to-apical (B-A) direction in six replicates at 30 minutes time point

Drug	Conc apical start (nM)	conc apical end (nM)	Conc basolateral start (nM)	Conc basolateral end (nM)	amount apical start (nmol)	amount apical end (nmol)	amount basolateral start (nmol)	amount basolateral end (nmol)	Total in well start (nmol)	Total in well end (nmol)	Recovery (%)
loperamide 1 A-B	194.4333	181.015	0	0.684	0.019	0.018	0.000	0.000	0.019	0.019	95
loperamide 1 B-A	0	1.552	194.4333	414.139	0.000	0.000	0.117	0.248	0.117	0.249	213
loperamide 2 A-B	194.4333	175.324	0	0.649	0.019	0.018	0.000	0.000	0.019	0.018	92
loperamide 2 B-A	0	1.105	194.4333	445.97	0.000	0.000	0.117	0.268	0.117	0.268	229
loperamide 3 A-B	194.4333	112.289	0	0.674	0.019	0.011	0.000	0.000	0.019	0.012	60
loperamide 3 B-A	0	1.171	194.4333	437.336	0.000	0.000	0.117	0.262	0.117	0.263	225
loperamide 4 A-B	194.4333	421.579	0	1.106	0.019	0.042	0.000	0.001	0.019	0.043	220
loperamide 4 B-A	0	2.306	194.4333	503.754	0.000	0.000	0.117	0.302	0.117	0.302	259
loperamide 5 A-B	194.4333	378.165	0	0.641	0.019	0.038	0.000	0.000	0.019	0.038	196
loperamide 5 B-A	0	1.693	194.4333	479.174	0.000	0.000	0.117	0.288	0.117	0.288	247
loperamide 6 A-B	194.4333	310.678	0	0.679	0.019	0.031	0.000	0.000	0.019	0.031	162
loperamide 6 B-A	0	1.671	194.4333	568.099	0.000	0.000	0.117	0.341	0.117	0.341	292

Table A3.4: Recovery percentage of etoposide in no cell control (NCC) studies on transwell in both apical-to-basal (A-B) and basal-to-apical (B-A) direction in six replicates at 30 minutes time point

Drug	Conc apical start (nM)	conc apical end (nM)	Conc basolateral start (nM)	Conc basolateral end (nM)	amount apical start (nmol)	amount apical end (nmol)	amount basolateral start (nmol)	amount basolateral end (nmol)	Total in well start (nmol)	Total in well end (nmol)	Recovery (%)
etoposide 1 A-B	489.08	438.02	0	56.21	0.049	0.044	0.000	0.034	0.049	0.078	159
etoposide 1 B-A	0	100	489.08	697.03	0.000	0.010	0.293	0.418	0.293	0.428	146
etoposide 2 A-B	489.08	533.24	0	54.46	0.049	0.053	0.000	0.033	0.049	0.086	176
etoposide 2 B-A	0	114.55	489.08	527.37	0.000	0.011	0.293	0.316	0.293	0.328	112
etoposide 3 A-B	489.08	431.98	0	33.91	0.049	0.043	0.000	0.020	0.049	0.064	130
etoposide 3 B-A	0	91.19	489.08	580.25	0.000	0.009	0.293	0.348	0.293	0.357	122
etoposide 4 A-B	489.08	659.84	0	53.22	0.049	0.066	0.000	0.032	0.049	0.098	200
etoposide 4 B-A	0	57.06	489.08	679.57	0.000	0.006	0.293	0.408	0.293	0.413	141
etoposide 5 A-B	489.08	611.19	0	51.55	0.049	0.061	0.000	0.031	0.049	0.092	188
etoposide 5 B-A	0	81.17	489.08	647.97	0.000	0.008	0.293	0.389	0.293	0.397	135
etoposide 6 A-B	489.08	534.31	0	52.26	0.049	0.053	0.000	0.031	0.049	0.085	173
etoposide 6 B-A	0	81.25	489.08	893.1	0.000	0.008	0.293	0.536	0.293	0.544	185

Table A3.5: Recovery percentage of lamotrigine in no cell control (NCC) studies on transwell in both apical-to-basal (A-B) and basal-to-apical (B-A) direction in six replicates at 30 minutes time point

Drug	Conc apical start (nM)	conc apical end (nM)	Conc basolateral start (nM)	Conc basolateral end (nM)	amount apical start (nmol)	amount apical end (nmol)	amount basolateral start (nmol)	amount basolateral end (nmol)	Total in well start (nmol)	Total in well end (nmol)	Recovery (%)
lamotrigine 1 A-B	753.9533	983.84	0	1	0.075	0.098	0.000	0.001	0.075	0.099	131
lamotrigine 1 B-A	0	139.25	753.9533	1473.58	0.000	0.014	0.452	0.884	0.452	0.898	199
lamotrigine 2 A-B	753.9533	1031.4	0	15.24	0.075	0.103	0.000	0.009	0.075	0.112	149
lamotrigine 2 B-A	0	145.52	753.9533	1069.42	0.000	0.015	0.452	0.642	0.452	0.656	145
lamotrigine 3 A-B	753.9533	1357.8	0	27.33	0.075	0.136	0.000	0.016	0.075	0.152	202
lamotrigine 3 B-A	0	184.87	753.9533	1147.85	0.000	0.018	0.452	0.689	0.452	0.707	156
lamotrigine 4 A-B	753.9533	1190.4	0	28.13	0.075	0.119	0.000	0.017	0.075	0.136	180
lamotrigine 4 B-A	0	145.21	753.9533	1214.23	0.000	0.015	0.452	0.729	0.452	0.743	164
lamotrigine 5 A-B	753.9533	1382.14	0	1.14	0.075	0.138	0.000	0.001	0.075	0.139	184
lamotrigine 5 B-A	0	225.14	753.9533	1124.77	0.000	0.023	0.452	0.675	0.452	0.697	154
lamotrigine 6 A-B	753.9533	1337.34	0	6.31	0.075	0.134	0.000	0.004	0.075	0.138	182
lamotrigine 6 B-A	0	162.12	753.9533	1276.46	0.000	0.016	0.452	0.766	0.452	0.782	173

Table A3.6: Recovery percentage of methotrexate in no cell control (NCC) studies on transwell in both apical-to-basal (A-B) and basal-to-apical (B-A) direction in six replicates at 30 minutes time point

Drug	Conc apical start (nM)	conc apical end (nM)	Conc basolateral start (nM)	Conc basolateral end (nM)	amount apical start (nmol)	amount apical end (nmol)	amount basolateral start (nmol)	amount basolateral end (nmol)	Total in well start (nmol)	Total in well end (nmol)	Recovery (%)
methotrexate 1 A-B	974.0233	1340.61	0	15.01	0.097	0.134	0.000	0.009	0.097	0.143	147
methotrexate 1 B-A	0	106.04	974.0233	1134.56	0.000	0.011	0.584	0.681	0.584	0.691	118
methotrexate 2 A-B	974.0233	1065.41	0	25.17	0.097	0.107	0.000	0.015	0.097	0.122	125
methotrexate 2 B-A	0	145.12	974.0233	898.92	0.000	0.015	0.584	0.539	0.584	0.554	95
methotrexate 3 A-B	974.0233	1203.63	0	20.68	0.097	0.120	0.000	0.012	0.097	0.133	136
methotrexate 3 B-A	0	104.99	974.0233	1105.35	0.000	0.010	0.584	0.663	0.584	0.674	115
methotrexate 4 A-B	974.0233	1152.16	0	15.38	0.097	0.115	0.000	0.009	0.097	0.124	128
methotrexate 4 B-A	0	90.81	974.0233	883.59	0.000	0.009	0.584	0.530	0.584	0.539	92
methotrexate 5 A-B	974.0233	1185.62	0	12.88	0.097	0.119	0.000	0.008	0.097	0.126	130
methotrexate 5 B-A	0	107.19	974.0233	881.63	0.000	0.011	0.584	0.529	0.584	0.540	92
methotrexate 6 A-B	974.0233	1203.95	0	14.23	0.097	0.120	0.000	0.009	0.097	0.129	132
methotrexate 6 B-A	0	92.94	974.0233	929.97	0.000	0.009	0.584	0.558	0.584	0.567	97

Table A3.7: Recovery percentage of topiramate in no cell control (NCC) studies on transwell in both apical-to-basal (A-B) and basal-to-apical (B-A) direction in six replicates at 30 minutes time point

Drug	Conc apical start (nM)	conc apical end (nM)	Conc basolateral start (nM)	Conc basolateral end (nM)	amount apical start (nmol)	amount apical end (nmol)	amount basolateral start (nmol)	amount basolateral end (nmol)	Total in well start (nmol)	Total in well end (nmol)	Recovery (%)
topiramate 1 A-B	967.61	1043.49	0	11.86	0.097	0.104	0.000	0.007	0.097	0.111	115
topiramate 1 B-A	0	134.65	967.61	883.12	0.000	0.013	0.581	0.530	0.581	0.543	94
topiramate 2 A-B	967.61	1059.91	0	17.52	0.097	0.106	0.000	0.011	0.097	0.117	120
topiramate 2 B-A	0	135.22	967.61	960.37	0.000	0.014	0.581	0.576	0.581	0.590	102
topiramate 3 A-B	967.61	911.15	0	28.97	0.097	0.091	0.000	0.017	0.097	0.108	112
topiramate 3 B-A	0	140.88	967.61	1178.05	0.000	0.014	0.581	0.707	0.581	0.721	124
topiramate 4 A-B	967.61	1190.39	0	21.49	0.097	0.119	0.000	0.013	0.097	0.132	136
topiramate 4 B-A	0	97.04	967.61	1140.26	0.000	0.010	0.581	0.684	0.581	0.694	120
topiramate 5 A-B	967.61	1060.45	0	20.69	0.097	0.106	0.000	0.012	0.097	0.118	122
topiramate 5 B-A	0	130.81	967.61	1271.02	0.000	0.013	0.581	0.763	0.581	0.776	134
topiramate 6 A-B	967.61	1178.6	0	14.27	0.097	0.118	0.000	0.009	0.097	0.126	131
topiramate 6 B-A	0	118.43	967.61	1371.96	0.000	0.012	0.581	0.823	0.581	0.835	144

Table A3.8: Recovery percentage of mitoxantrone in no cell control (NCC) studies on transwell in both apical-to-basal (A-B) and basal-to-apical (B-A) direction in six replicates at 30 minutes time point

Drug	Conc apical start (nM)	conc apical end (nM)	Conc basolateral start (nM)	Conc basolateral end (nM)	amount apical start (nmol)	amount apical end (nmol)	amount basolateral start (nmol)	amount basolateral end (nmol)	Total in well start (nmol)	Total in well end (nmol)	Recovery (%)
mitoxantrone 1 A-B	103.0167	107.25	0	0.396	0.010	0.011	0.000	0.000	0.010	0.011	106
mitoxantrone 1 B-A	0	0.43	103.0167	81.16	0.000	0.000	0.062	0.049	0.062	0.049	79
mitoxantrone 2 A-B	103.0167	156.96	0	0.59	0.010	0.016	0.000	0.000	0.010	0.016	156
mitoxantrone 2 B-A	0	1.21	103.0167	94.72	0.000	0.000	0.062	0.057	0.062	0.057	92
mitoxantrone 3 A-B	103.0167	89.35	0	0.86	0.010	0.009	0.000	0.001	0.010	0.009	92
mitoxantrone 3 B-A	0	4.4	103.0167	98.12	0.000	0.000	0.062	0.059	0.062	0.059	96
mitoxantrone 4 A-B	103.0167	242.75	0	0.71	0.010	0.024	0.000	0.000	0.010	0.025	240
mitoxantrone 4 B-A	0	1.09	103.0167	121.03	0.000	0.000	0.062	0.073	0.062	0.073	118
mitoxantrone 5 A-B	103.0167	197.12	0	1	0.010	0.020	0.000	0.001	0.010	0.020	197
mitoxantrone 5 B-A	0	0.43	103.0167	169.87	0.000	0.000	0.062	0.102	0.062	0.102	165
mitoxantrone 6 A-B	103.0167	145.76	0	0.53	0.010	0.015	0.000	0.000	0.010	0.015	145
mitoxantrone 6 B-A	0	0.25	103.0167	164.41	0.000	0.000	0.062	0.099	0.062	0.099	160

Table A3.9: Recovery percentage of camptothecin in no cell control (NCC) studies on transwell in both apical-to-basal (A-B) and basal-to-apical (B-A) direction in six replicates at 60 minutes time point

Drug	Conc apical start (nM)	conc apical end (nM)	Conc basolateral start (nM)	Conc basolateral end (nM)	amount apical start (nmol)	amount apical end (nmol)	amount basolateral start (nmol)	amount basolateral end (nmol)	Total in well start (nmol)	Total in well end (nmol)	Recovery (%)
camptothecin 1 A-B	1008.427	870.26	0	110.86	0.101	0.087	0.000	0.067	0.101	0.154	152
camptothecin 1 B-A	0	229.19	1008.427	767.04	0.000	0.023	0.605	0.460	0.605	0.483	80
camptothecin 2 A-B	1008.427	969.85	0	50.88	0.101	0.097	0.000	0.031	0.101	0.128	126
camptothecin 2 B-A	0	163.53	1008.427	816.6	0.000	0.016	0.605	0.490	0.605	0.506	84
camptothecin 3 A-B	1008.427	885.06	0	49.12	0.101	0.089	0.000	0.029	0.101	0.118	117
camptothecin 3 B-A	0	197.66	1008.427	800.74	0.000	0.020	0.605	0.480	0.605	0.500	83
camptothecin 4 A-B	1008.427	687.38	0	94.6	0.101	0.069	0.000	0.057	0.101	0.125	124
camptothecin 4 B-A	0	184.53	1008.427	621.7	0.000	0.018	0.605	0.373	0.605	0.391	65
camptothecin 5 A-B	1008.427	835.86	0	45.71	0.101	0.084	0.000	0.027	0.101	0.111	110
camptothecin 5 B-A	0	174.99	1008.427	787.43	0.000	0.017	0.605	0.472	0.605	0.490	81
camptothecin 6 A-B	1008.427	814.67	0	44.31	0.101	0.081	0.000	0.027	0.101	0.108	107
camptothecin 6 B-A	0	173.83	1008.427	693.05	0.000	0.017	0.605	0.416	0.605	0.433	72

Table A3.10: Recovery percentage of chlorpromazine in no cell control (NCC) studies on transwell in both apical-to-basal (A-B) and basal-to-apical (B-A) direction in six replicates at 60 minutes time point

Drug	Conc apical start (nM)	conc apical end (nM)	Conc basolateral start (nM)	Conc basolateral end (nM)	amount apical start (nmol)	amount apical end (nmol)	amount basolateral start (nmol)	amount basolateral end (nmol)	Total in well start (nmol)	Total in well end (nmol)	Recovery (%)
chlorpromazine 1 A-B	57.95667	210.77	0	1.96	0.006	0.021	0.000	0.001	0.006	0.022	384
chlorpromazine 1 B-A	0	2.86	57.95667	339.86	0.000	0.000	0.035	0.204	0.035	0.204	587
chlorpromazine 2 A-B	57.95667	172.62	0	1.47	0.006	0.017	0.000	0.001	0.006	0.018	313
chlorpromazine 2 B-A	0	2.53	57.95667	380.61	0.000	0.000	0.035	0.228	0.035	0.229	657
chlorpromazine 3 A-B	57.95667	210.55	0	1.15	0.006	0.021	0.000	0.001	0.006	0.022	375
chlorpromazine 3 B-A	0	2.96	57.95667	395.41	0.000	0.000	0.035	0.237	0.035	0.238	683
chlorpromazine 4 A-B	57.95667	208.1	0	3.27	0.006	0.021	0.000	0.002	0.006	0.023	393
chlorpromazine 4 B-A	0	3.49	57.95667	426.94	0.000	0.000	0.035	0.256	0.035	0.257	738
chlorpromazine 5 A-B	57.95667	280.92	0	1.93	0.006	0.028	0.000	0.001	0.006	0.029	505
chlorpromazine 5 B-A	0	3.99	57.95667	432.32	0.000	0.000	0.035	0.259	0.035	0.260	747
chlorpromazine 6 A-B	57.95667	221.6	0	2.35	0.006	0.022	0.000	0.001	0.006	0.024	407
chlorpromazine 6 B-A	0	4.29	57.95667	396.24	0.000	0.000	0.035	0.238	0.035	0.238	685

Table A3.11: Recovery percentage of loperamide in no cell control (NCC) studies on transwell in both apical-to-basal (A-B) and basal-to-apical (B-A) direction in six replicates at 60 minutes time point

Drug	Conc apical start (nM)	conc apical end (nM)	Conc basolateral start (nM)	Conc basolateral end (nM)	amount apical start (nmol)	amount apical end (nmol)	amount basolateral start (nmol)	amount basolateral end (nmol)	Total in well start (nmol)	Total in well end (nmol)	Recovery (%)
loperamide 1 A-B	183.8867	172.07	0	1.3	0.018	0.017	0.000	0.001	0.018	0.018	98
loperamide 1 B-A	0	1.91	183.8867	276.15	0.000	0.000	0.110	0.166	0.110	0.166	150
loperamide 2 A-B	183.8867	135.69	0	0.83	0.018	0.014	0.000	0.000	0.018	0.014	76
loperamide 2 B-A	0	1.48	183.8867	329.36	0.000	0.000	0.110	0.198	0.110	0.198	179
loperamide 3 A-B	183.8867	180.92	0	0.65	0.018	0.018	0.000	0.000	0.018	0.018	101
loperamide 3 B-A	0	2.26	183.8867	345.79	0.000	0.000	0.110	0.207	0.110	0.208	188
loperamide 4 A-B	183.8867	298.65	0	3.36	0.018	0.030	0.000	0.002	0.018	0.032	173
loperamide 4 B-A	0	4.06	183.8867	483.78	0.000	0.000	0.110	0.290	0.110	0.291	263
loperamide 5 A-B	183.8867	364.01	0	1.83	0.018	0.036	0.000	0.001	0.018	0.037	204
loperamide 5 B-A	0	4.37	183.8867	463.64	0.000	0.000	0.110	0.278	0.110	0.279	253
loperamide 6 A-B	183.8867	326.55	0	1.73	0.018	0.033	0.000	0.001	0.018	0.034	183
loperamide 6 B-A	0	4.41	183.8867	468.75	0.000	0.000	0.110	0.281	0.110	0.282	255

Table A3.12: Recovery percentage of etoposide in no cell control (NCC) studies on transwell in both apical-to-basal (A-B) and basal-to-apical (B-A) direction in six replicates at 60 minutes time point

Drug	Conc apical start (nM)	conc apical end (nM)	Conc basolateral start (nM)	Conc basolateral end (nM)	amount apical start (nmol)	amount apical end (nmol)	amount basolateral start (nmol)	amount basolateral end (nmol)	Total in well start (nmol)	Total in well end (nmol)	Recovery (%)
etoposide 1 A-B	611.8933	495.33	0	76.26	0.061	0.050	0.000	0.046	0.061	0.095	156
etoposide 1 B-A	0	104.01	611.8933	531.68	0.000	0.010	0.367	0.319	0.367	0.329	90
etoposide 2 A-B	611.8933	581.81	0	69.89	0.061	0.058	0.000	0.042	0.061	0.100	164
etoposide 2 B-A	0	100.81	611.8933	692.3	0.000	0.010	0.367	0.415	0.367	0.425	116
etoposide 3 A-B	611.8933	421.25	0	60.79	0.061	0.042	0.000	0.036	0.061	0.079	128
etoposide 3 B-A	0	126.58	611.8933	542.49	0.000	0.013	0.367	0.325	0.367	0.338	92
etoposide 4 A-B	611.8933	520.3	0	53.55	0.061	0.052	0.000	0.032	0.061	0.084	138
etoposide 4 B-A	0	130	611.8933	732.03	0.000	0.013	0.367	0.439	0.367	0.452	123
etoposide 5 A-B	611.8933	549.11	0	56.56	0.061	0.055	0.000	0.034	0.061	0.089	145
etoposide 5 B-A	0	139.16	611.8933	767.05	0.000	0.014	0.367	0.460	0.367	0.474	129
etoposide 6 A-B	611.8933	657.43	0	73.41	0.061	0.066	0.000	0.044	0.061	0.110	179
etoposide 6 B-A	0	95.72	611.8933	825.52	0.000	0.010	0.367	0.495	0.367	0.505	138

Table A3.13: Recovery percentage of lamotrigine in no cell control (NCC) studies on transwell in both apical-to-basal (A-B) and basal-to-apical (B-A) direction in six replicates at 60 minutes time point

Drug	Conc apical start (nM)	conc apical end (nM)	Conc basolateral start (nM)	Conc basolateral end (nM)	amount apical start (nmol)	amount apical end (nmol)	amount basolateral start (nmol)	amount basolateral end (nmol)	Total in well start (nmol)	Total in well end (nmol)	Recovery (%)
lamotrigine 1 A-B	928.6067	1000.96	0	57.54	0.093	0.100	0.000	0.035	0.093	0.135	145
lamotrigine 1 B-A	0	293.04	928.6067	1144.8	0.000	0.029	0.557	0.687	0.557	0.716	129
lamotrigine 2 A-B	928.6067	826.08	0	57.48	0.093	0.083	0.000	0.034	0.093	0.117	126
lamotrigine 2 B-A	0	272.83	928.6067	1132.4	0.000	0.027	0.557	0.679	0.557	0.707	127
lamotrigine 3 A-B	928.6067	1112.57	0	39.1	0.093	0.111	0.000	0.023	0.093	0.135	145
lamotrigine 3 B-A	0	347.69	928.6067	1052.65	0.000	0.035	0.557	0.632	0.557	0.666	120
lamotrigine 4 A-B	928.6067	867.41	0	47.12	0.093	0.087	0.000	0.028	0.093	0.115	124
lamotrigine 4 B-A	0	292.69	928.6067	1040.39	0.000	0.029	0.557	0.624	0.557	0.654	117
lamotrigine 5 A-B	928.6067	1142.21	0	35.89	0.093	0.114	0.000	0.022	0.093	0.136	146
lamotrigine 5 B-A	0	357.86	928.6067	1333.53	0.000	0.036	0.557	0.800	0.557	0.836	150
lamotrigine 6 A-B	928.6067	1278.69	0	40.53	0.093	0.128	0.000	0.024	0.093	0.152	164
lamotrigine 6 B-A	0	367.49	928.6067	1148.62	0.000	0.037	0.557	0.689	0.557	0.726	130

Table A3.14: Recovery percentage of methotrexate in no cell control (NCC) studies on transwell in both apical-to-basal (A-B) and basal-to-apical (B-A) direction in six replicates at 60 minutes time point

Drug	Conc apical start (nM)	conc apical end (nM)	Conc basolateral start (nM)	Conc basolateral end (nM)	amount apical start (nmol)	amount apical end (nmol)	amount basolateral start (nmol)	amount basolateral end (nmol)	Total in well start (nmol)	Total in well end (nmol)	Recovery (%)
methotrexate 1 A-B	934.2767	1230.19	0	31.29	0.093	0.123	0.000	0.019	0.093	0.142	152
methotrexate 1 B-A	0	172.07	934.2767	901.75	0.000	0.017	0.561	0.541	0.561	0.558	100
methotrexate 2 A-B	934.2767	1055.42	0	34.55	0.093	0.106	0.000	0.021	0.093	0.126	135
methotrexate 2 B-A	0	148.69	934.2767	958.67	0.000	0.015	0.561	0.575	0.561	0.590	105
methotrexate 3 A-B	934.2767	1304.72	0	31.31	0.093	0.130	0.000	0.019	0.093	0.149	160
methotrexate 3 B-A	0	209.11	934.2767	1100.21	0.000	0.021	0.561	0.660	0.561	0.681	121
methotrexate 4 A-B	934.2767	835.76	0	35.88	0.093	0.084	0.000	0.022	0.093	0.105	112
methotrexate 4 B-A	0	170.17	934.2767	865.97	0.000	0.017	0.561	0.520	0.561	0.537	96
methotrexate 5 A-B	934.2767	1132.11	0	42.21	0.093	0.113	0.000	0.025	0.093	0.139	148
methotrexate 5 B-A	0	190.3	934.2767	924.9	0.000	0.019	0.561	0.555	0.561	0.574	102
methotrexate 6 A-B	934.2767	909.59	0	32.73	0.093	0.091	0.000	0.020	0.093	0.111	118
methotrexate 6 B-A	0	184.01	934.2767	802.26	0.000	0.018	0.561	0.481	0.561	0.500	89

Table A3.15: Recovery percentage of topiramate in no cell control (NCC) studies on transwell in both apical-to-basal (A-B) and basal-to-apical (B-A) direction in six replicates at 60 minutes time point

Drug	Conc apical start (nM)	conc apical end (nM)	Conc basolateral start (nM)	Conc basolateral end (nM)	amount apical start (nmol)	amount apical end (nmol)	amount basolateral start (nmol)	amount basolateral end (nmol)	Total in well start (nmol)	Total in well end (nmol)	Recovery (%)
topiramate 1 A-B	1837.513	1000.11	0	36.46	0.184	0.100	0.000	0.022	0.184	0.122	66
topiramate 1 B-A	0	247.96	1837.513	1132.33	0.000	0.025	1.103	0.679	1.103	0.704	64
topiramate 2 A-B	1837.513	849.33	0	47.54	0.184	0.085	0.000	0.029	0.184	0.113	62
topiramate 2 B-A	0	268.77	1837.513	1162.69	0.000	0.027	1.103	0.698	1.103	0.724	66
topiramate 3 A-B	1837.513	861.02	0	41.53	0.184	0.086	0.000	0.025	0.184	0.111	60
topiramate 3 B-A	0	189.83	1837.513	861.71	0.000	0.019	1.103	0.517	1.103	0.536	49
topiramate 4 A-B	1837.513	1163.93	0	38.92	0.184	0.116	0.000	0.023	0.184	0.140	76
topiramate 4 B-A	0	274.34	1837.513	1022.31	0.000	0.027	1.103	0.613	1.103	0.641	58
topiramate 5 A-B	1837.513	1148.49	0	36.17	0.184	0.115	0.000	0.022	0.184	0.137	74
topiramate 5 B-A	0	282.26	1837.513	1226.92	0.000	0.028	1.103	0.736	1.103	0.764	69
topiramate 6 A-B	1837.513	1053.28	0	41.72	0.184	0.105	0.000	0.025	0.184	0.130	71
topiramate 6 B-A	0	245.3	1837.513	1174.2	0.000	0.025	1.103	0.705	1.103	0.729	66

Table A3.16: Recovery percentage of mitoxantrone in no cell control (NCC) studies on transwell in both apical-to-basal (A-B) and basal-to-apical (B-A) direction in six replicates at 60 minutes time point

Drug	Conc apical start (nM)	conc apical end (nM)	Conc basolateral start (nM)	Conc basolateral end (nM)	amount apical start (nmol)	amount apical end (nmol)	amount basolateral start (nmol)	amount basolateral end (nmol)	Total in well start (nmol)	Total in well end (nmol)	Recovery (%)
mitoxantrone 1 A-B	106.18	69.09	0	0.28	0.011	0.007	0.000	0.000	0.011	0.007	67
mitoxantrone 1 B-A	0	1.79	106.18	66.65	0.000	0.000	0.064	0.040	0.064	0.040	63
mitoxantrone 2 A-B	106.18	79.35	0	0.16	0.011	0.008	0.000	0.000	0.011	0.008	76
mitoxantrone 2 B-A	0	1.04	106.18	82.66	0.000	0.000	0.064	0.050	0.064	0.050	78
mitoxantrone 3 A-B	106.18	60.18	0	1.45	0.011	0.006	0.000	0.001	0.011	0.007	65
mitoxantrone 3 B-A	0	0.5	106.18	69.86	0.000	0.000	0.064	0.042	0.064	0.042	66
mitoxantrone 4 A-B	106.18	111.65	0	0.07	0.011	0.011	0.000	0.000	0.011	0.011	106
mitoxantrone 4 B-A	0	0.26	106.18	130.9	0.000	0.000	0.064	0.079	0.064	0.079	123
mitoxantrone 5 A-B	106.18	147.29	0	3.22	0.011	0.015	0.000	0.002	0.011	0.017	157
mitoxantrone 5 B-A	0	1.45	106.18	105.98	0.000	0.000	0.064	0.064	0.064	0.064	100
mitoxantrone 6 A-B	106.18	96.79	0	0.65	0.011	0.010	0.000	0.000	0.011	0.010	95
mitoxantrone 6 B-A	0	0.45	106.18	101.96	0.000	0.000	0.064	0.061	0.064	0.061	96

Table A3.17: Recovery percentage of camptothecin in no cell control (NCC) studies on transwell in both apical-to-basal (A-B) and basal-to-apical (B-A) direction in six replicates at 120 minutes time point

Drug	Conc apical start (nM)	conc apical end (nM)	Conc basolateral start (nM)	Conc basolateral end (nM)	amount apical start (nmol)	amount apical end (nmol)	amount basolateral start (nmol)	amount basolateral end (nmol)	Total in well start (nmol)	Total in well end (nmol)	Recovery (%)
camptothecin 1 A-B	960.54	591.69	0	112.24	0.096	0.059	0.000	0.067	0.096	0.127	132
camptothecin 1 B-A	0	498.21	960.54	801.68	0.000	0.050	0.576	0.481	0.576	0.531	92
camptothecin 2 A-B	960.54	697.85	0	76.62	0.096	0.070	0.000	0.046	0.096	0.116	121
camptothecin 2 B-A	0	474.46	960.54	805.93	0.000	0.047	0.576	0.484	0.576	0.531	92
camptothecin 3 A-B	960.54	753.55	0	86.07	0.096	0.075	0.000	0.052	0.096	0.127	132
camptothecin 3 B-A	0	400.53	960.54	707.85	0.000	0.040	0.576	0.425	0.576	0.465	81
camptothecin 4 A-B	960.54	611.69	0	123.83	0.096	0.061	0.000	0.074	0.096	0.135	141
camptothecin 4 B-A	0	338.17	960.54	834.66	0.000	0.034	0.576	0.501	0.576	0.535	93
camptothecin 5 A-B	960.54	542.71	0	79.36	0.096	0.054	0.000	0.048	0.096	0.102	106
camptothecin 5 B-A	0	288.05	960.54	792.35	0.000	0.029	0.576	0.475	0.576	0.504	87
camptothecin 6 A-B	960.54	594.29	0	67.28	0.096	0.059	0.000	0.040	0.096	0.100	104
camptothecin 6 B-A	0	316.34	960.54	710.75	0.000	0.032	0.576	0.426	0.576	0.458	79

Table A3.18: Recovery percentage of chlorpromazine in no cell control (NCC) studies on transwell in both apical-to-basal (A-B) and basal-to-apical (B-A) direction in six replicates at 120 minutes time point

Drug	Conc apical start (nM)	conc apical end (nM)	Conc basolateral start (nM)	Conc basolateral end (nM)	amount apical start (nmol)	amount apical end (nmol)	amount basolateral start (nmol)	amount basolateral end (nmol)	Total in well start (nmol)	Total in well end (nmol)	Recovery (%)
chlorpromazine 1 A-B	58.67333	103.17	0	3.04	0.006	0.010	0.000	0.002	0.006	0.012	207
chlorpromazine 1 B-A	0	10.27	58.67333	331.21	0.000	0.001	0.035	0.199	0.035	0.200	567
chlorpromazine 2 A-B	58.67333	152.24	0	2.99	0.006	0.015	0.000	0.002	0.006	0.017	290
chlorpromazine 2 B-A	0	12.09	58.67333	310.25	0.000	0.001	0.035	0.186	0.035	0.187	532
chlorpromazine 3 A-B	58.67333	158.3	0	2.72	0.006	0.016	0.000	0.002	0.006	0.017	298
chlorpromazine 3 B-A	0	12.57	58.67333	338.32	0.000	0.001	0.035	0.203	0.035	0.204	580
chlorpromazine 4 A-B	58.67333	149.19	0	4.55	0.006	0.015	0.000	0.003	0.006	0.018	301
chlorpromazine 4 B-A	0	16.88	58.67333	390.88	0.000	0.002	0.035	0.235	0.035	0.236	671
chlorpromazine 5 A-B	58.67333	140.97	0	3.35	0.006	0.014	0.000	0.002	0.006	0.016	275
chlorpromazine 5 B-A	0	15.99	58.67333	372.49	0.000	0.002	0.035	0.223	0.035	0.225	639
chlorpromazine 6 A-B	58.67333	145.45	0	2.81	0.006	0.015	0.000	0.002	0.006	0.016	277
chlorpromazine 6 B-A	0	15.63	58.67333	331.92	0.000	0.002	0.035	0.199	0.035	0.201	570

Table A3.19: Recovery percentage of loperamide in no cell control (NCC) studies on transwell in both apical-to-basal (A-B) and basal-to-apical (B-A) direction in six replicates at 120 minutes time point

Drug	Conc apical start (nM)	conc apical end (nM)	Conc basolateral start (nM)	Conc basolateral end (nM)	amount apical start (nmol)	amount apical end (nmol)	amount basolateral start (nmol)	amount basolateral end (nmol)	Total in well start (nmol)	Total in well end (nmol)	Recovery (%)
loperamide 1 A-B	168.5733	61.18	0	1.78	0.017	0.006	0.000	0.001	0.017	0.007	43
loperamide 1 B-A	0	6.93	168.5733	263.39	0.000	0.001	0.101	0.158	0.101	0.159	157
loperamide 2 A-B	168.5733	141.57	0	2.31	0.017	0.014	0.000	0.001	0.017	0.016	92
loperamide 2 B-A	0	7.5	168.5733	307.83	0.000	0.001	0.101	0.185	0.101	0.185	183
loperamide 3 A-B	168.5733	141.05	0	1.79	0.017	0.014	0.000	0.001	0.017	0.015	90
loperamide 3 B-A	0	11.38	168.5733	268.64	0.000	0.001	0.101	0.161	0.101	0.162	160
loperamide 4 A-B	168.5733	140.15	0	3.15	0.017	0.014	0.000	0.002	0.017	0.016	94
loperamide 4 B-A	0	14.18	168.5733	385.92	0.000	0.001	0.101	0.232	0.101	0.233	230
loperamide 5 A-B	168.5733	142.83	0	2.34	0.017	0.014	0.000	0.001	0.017	0.016	93
loperamide 5 B-A	0	11.94	168.5733	384.23	0.000	0.001	0.101	0.231	0.101	0.232	229
loperamide 6 A-B	168.5733	125.6	0	2.02	0.017	0.013	0.000	0.001	0.017	0.014	82
loperamide 6 B-A	0	14.17	168.5733	323.55	0.000	0.001	0.101	0.194	0.101	0.196	193

Table A3.20: Recovery percentage of etoposide in no cell control (NCC) studies on transwell in both apical-to-basal (A-B) and basal-to-apical (B-A) direction in six replicates at 120 minutes time point

Drug	Conc apical start (nM)	conc apical end (nM)	Conc basolateral start (nM)	Conc basolateral end (nM)	amount apical start (nmol)	amount apical end (nmol)	amount basolateral start (nmol)	amount basolateral end (nmol)	Total in well start (nmol)	Total in well end (nmol)	Recovery (%)
etoposide 1 A-B	559.3267	348.85	0	60.68	0.056	0.035	0.000	0.036	0.056	0.071	127
etoposide 1 B-A	0	240.76	559.3267	688.59	0.000	0.024	0.336	0.413	0.336	0.437	130
etoposide 2 A-B	559.3267	470.43	0	75.04	0.056	0.047	0.000	0.045	0.056	0.092	165
etoposide 2 B-A	0	227.27	559.3267	592.95	0.000	0.023	0.336	0.356	0.336	0.378	113
etoposide 3 A-B	559.3267	461.89	0	87.53	0.056	0.046	0.000	0.053	0.056	0.099	176
etoposide 3 B-A	0	231.57	559.3267	557.67	0.000	0.023	0.336	0.335	0.336	0.358	107
etoposide 4 A-B	559.3267	516.36	0	92.51	0.056	0.052	0.000	0.056	0.056	0.107	192
etoposide 4 B-A	0	175.77	559.3267	921.35	0.000	0.018	0.336	0.553	0.336	0.570	170
etoposide 5 A-B	559.3267	510.86	0	91.19	0.056	0.051	0.000	0.055	0.056	0.106	189
etoposide 5 B-A	0	204.11	559.3267	827.81	0.000	0.020	0.336	0.497	0.336	0.517	154
etoposide 6 A-B	559.3267	485.97	0	88.77	0.056	0.049	0.000	0.053	0.056	0.102	182
etoposide 6 B-A	0	204	559.3267	688.63	0.000	0.020	0.336	0.413	0.336	0.434	129

Table A3.21: Recovery percentage of lamotrigine in no cell control (NCC) studies on transwell in both apical-to-basal (A-B) and basal-to-apical (B-A) direction in six replicates at 120 minutes time point

Drug	Conc apical start (nM)	conc apical end (nM)	Conc basolateral start (nM)	Conc basolateral end (nM)	amount apical start (nmol)	amount apical end (nmol)	amount basolateral start (nmol)	amount basolateral end (nmol)	Total in well start (nmol)	Total in well end (nmol)	Recovery (%)
lamotrigine 1 A-B	951.33	653.83	0	86.95	0.095	0.065	0.000	0.052	0.095	0.118	124
lamotrigine 1 B-A	0	683.8	951.33	1220.38	0.000	0.068	0.571	0.732	0.571	0.801	140
lamotrigine 2 A-B	951.33	801.15	0	76.23	0.095	0.080	0.000	0.046	0.095	0.126	132
lamotrigine 2 B-A	0	572.55	951.33	1404.83	0.000	0.057	0.571	0.843	0.571	0.900	158
lamotrigine 3 A-B	951.33	794.57	0	98.04	0.095	0.079	0.000	0.059	0.095	0.138	145
lamotrigine 3 B-A	0	713.87	951.33	984.71	0.000	0.071	0.571	0.591	0.571	0.662	116
lamotrigine 4 A-B	951.33	816.8	0	98.05	0.095	0.082	0.000	0.059	0.095	0.141	148
lamotrigine 4 B-A	0	580.3	951.33	1295.56	0.000	0.058	0.571	0.777	0.571	0.835	146
lamotrigine 5 A-B	951.33	760.45	0	104.7	0.095	0.076	0.000	0.063	0.095	0.139	146
lamotrigine 5 B-A	0	539.12	951.33	1070.11	0.000	0.054	0.571	0.642	0.571	0.696	122
lamotrigine 6 A-B	951.33	844.87	0	65.02	0.095	0.084	0.000	0.039	0.095	0.123	130
lamotrigine 6 B-A	0	663.07	951.33	1183.41	0.000	0.066	0.571	0.710	0.571	0.776	136

Table A3.22: Recovery percentage of methotrexate in no cell control (NCC) studies on transwell in both apical-to-basal (A-B) and basal-to-apical (B-A) direction in six replicates at 120 minutes time point

Drug	Conc apical start (nM)	conc apical end (nM)	Conc basolateral start (nM)	Conc basolateral end (nM)	amount apical start (nmol)	amount apical end (nmol)	amount basolateral start (nmol)	amount basolateral end (nmol)	Total in well start (nmol)	Total in well end (nmol)	Recovery (%)
methotrexate 1 A-B	1188.107	876.41	0	68.02	0.119	0.088	0.000	0.041	0.119	0.128	108
methotrexate 1 B-A	0	406.71	1188.107	1226.05	0.000	0.041	0.713	0.736	0.713	0.776	109
methotrexate 2 A-B	1188.107	884.76	0	49.41	0.119	0.088	0.000	0.030	0.119	0.118	99
methotrexate 2 B-A	0	410.94	1188.107	1085.19	0.000	0.041	0.713	0.651	0.713	0.692	97
methotrexate 3 A-B	1188.107	890.97	0	71.74	0.119	0.089	0.000	0.043	0.119	0.132	111
methotrexate 3 B-A	0	414.98	1188.107	855.95	0.000	0.041	0.713	0.514	0.713	0.555	78
methotrexate 4 A-B	1188.107	806.83	0	74.57	0.119	0.081	0.000	0.045	0.119	0.125	106
methotrexate 4 B-A	0	366.9	1188.107	1034.56	0.000	0.037	0.713	0.621	0.713	0.657	92
methotrexate 5 A-B	1188.107	653.79	0	67.17	0.119	0.065	0.000	0.040	0.119	0.106	89
methotrexate 5 B-A	0	282.85	1188.107	809.28	0.000	0.028	0.713	0.486	0.713	0.514	72
methotrexate 6 A-B	1188.107	779.93	0	62.16	0.119	0.078	0.000	0.037	0.119	0.115	97
methotrexate 6 B-A	0	379.39	1188.107	1001	0.000	0.038	0.713	0.601	0.713	0.639	90

Table A3.23: Recovery percentage of topiramate in no cell control (NCC) studies on transwell in both apical-to-basal (A-B) and basal-to-apical (B-A) direction in six replicates at 120 minutes time point

Drug	Conc apical start (nM)	conc apical end (nM)	Conc basolateral start (nM)	Conc basolateral end (nM)	amount apical start (nmol)	amount apical end (nmol)	amount basolateral start (nmol)	amount basolateral end (nmol)	Total in well start (nmol)	Total in well end (nmol)	Recovery (%)
topiramate 1 A-B	1448.43	854.74	0	98.03	0.145	0.085	0.000	0.059	0.145	0.144	100
topiramate 1 B-A	0	557.72	1448.43	1023.21	0.000	0.056	0.869	0.614	0.869	0.670	77
topiramate 2 A-B	1448.43	710.24	0	98.12	0.145	0.071	0.000	0.059	0.145	0.130	90
topiramate 2 B-A	0	461.67	1448.43	1262.32	0.000	0.046	0.869	0.757	0.869	0.804	92
topiramate 3 A-B	1448.43	666.04	0	84.51	0.145	0.067	0.000	0.051	0.145	0.117	81
topiramate 3 B-A	0	449.7	1448.43	1070.71	0.000	0.045	0.869	0.642	0.869	0.687	79
topiramate 4 A-B	1448.43	917.77	0	72.5	0.145	0.092	0.000	0.044	0.145	0.135	93
topiramate 4 B-A	0	454.32	1448.43	1445.86	0.000	0.045	0.869	0.868	0.869	0.913	105
topiramate 5 A-B	1448.43	800.5	0	84.23	0.145	0.080	0.000	0.051	0.145	0.131	90
topiramate 5 B-A	0	467.47	1448.43	1005.1	0.000	0.047	0.869	0.603	0.869	0.650	75
topiramate 6 A-B	1448.43	819.27	0	77.45	0.145	0.082	0.000	0.046	0.145	0.128	89
topiramate 6 B-A	0	440.97	1448.43	1141.29	0.000	0.044	0.869	0.685	0.869	0.729	84

Table A3.24: Recovery percentage of mitoxantrone in no cell control (NCC) studies on transwell in both apical-to-basal (A-B) and basal-to-apical (B-A) direction in six replicates at 120 minutes time point

Drug	Conc apical start (nM)	conc apical end (nM)	Conc basolateral start (nM)	Conc basolateral end (nM)	amount apical start (nmol)	amount apical end (nmol)	amount basolateral start (nmol)	amount basolateral end (nmol)	Total in well start (nmol)	Total in well end (nmol)	Recovery (%)
mitoxantrone 1 A-B	103.3833	40.42	0	2.45	0.010	0.004	0.000	0.001	0.010	0.006	53
mitoxantrone 1 B-A	0	1.92	103.3833	76.76	0.000	0.000	0.062	0.046	0.062	0.046	75
mitoxantrone 2 A-B	103.3833	46.32	0	0.25	0.010	0.005	0.000	0.000	0.010	0.005	46
mitoxantrone 2 B-A	0	0.55	103.3833	79.72	0.000	0.000	0.062	0.048	0.062	0.048	77
mitoxantrone 3 A-B	103.3833	49.42	0	0.39	0.010	0.005	0.000	0.000	0.010	0.005	50
mitoxantrone 3 B-A	0	0.45	103.3833	69.02	0.000	0.000	0.062	0.041	0.062	0.041	67
mitoxantrone 4 A-B	103.3833	48.09	0	1.25	0.010	0.005	0.000	0.001	0.010	0.006	54
mitoxantrone 4 B-A	0	1.1	103.3833	97.71	0.000	0.000	0.062	0.059	0.062	0.059	95
mitoxantrone 5 A-B	103.3833	52.98	0	0.86	0.010	0.005	0.000	0.001	0.010	0.006	56
mitoxantrone 5 B-A	0	1.95	103.3833	108.9	0.000	0.000	0.062	0.065	0.062	0.066	106
mitoxantrone 6 A-B	103.3833	65.65	0	0.95	0.010	0.007	0.000	0.001	0.010	0.007	69
mitoxantrone 6 B-A	0	0.79	103.3833	68.37	0.000	0.000	0.062	0.041	0.062	0.041	66

Table A3.25: Apparent Permeabilty (Papp), Exact Permeabiltiy (Pexact), Papp Efflux Ratio and Pexact Efflux Ratio of camptothecin in no cell control (NCC) studies on transwell in six replicates at 30 minutes time point

Drug	initial concentration in donor (uM)	Change in time (s)	Growth area (cm2)	Final concentration in donor (uM)	Change in concentration (uM)	Papp (cm/s)	Efflux ratio (B-A/A-B)	Vd (cm3)	Vr (cm3)	Ct	Pexact	Efflux Ratio (B-A/A-B)
camptothecin 1 A-B	0.9008	1800	0.33	0.91933	-0.01853	4.04E-05		0.1	0.6	162.2329	3.63E-05	1.084025
camptothecin 1 B-A	0.9008	1800	0.33	0.810708	0.090092	3.21E-05	0.793111	0.6	0.1	719.3997	3.93E-05	
camptothecin 2 A-B	0.9008	1800	0.33	1.00648	-0.10568	4.05E-05		0.1	0.6	174.7686	3.34E-05	1.124364
camptothecin 2 B-A	0.9008	1800	0.33	0.775029	0.125771	2.94E-05	0.726325	0.6	0.1	686.8163	3.76E-05	
camptothecin 3 A-B	0.9008	1800	0.33	1.0352	-0.1344	4.39E-05		0.1	0.6	181.46	3.51E-05	0.497125
camptothecin 3 B-A	0.9008	1800	0.33	0.97025	-0.06945	1.80E-05	0.409582	0.6	0.1	845.3943	1.74E-05	
camptothecin 4 A-B	0.9008	1800	0.33	0.81228	0.08852	4.88E-05		0.1	0.6	153.3343	4.82E-05	0.705338
camptothecin 4 B-A	0.9008	1800	0.33	0.690893	0.209907	2.39E-05	0.490485	0.6	0.1	610.4863	3.4E-05	
camptothecin 5 A-B	0.9008	1800	0.33	0.820038	0.080762	3.34E-05		0.1	0.6	142.6911	3.38E-05	0.739447
camptothecin 5 B-A	0.9008	1800	0.33	0.69772	0.20308	1.82E-05	0.544351	0.6	0.1	611.95	2.5E-05	
camptothecin 6 A-B	0.9008	1800	0.33	0.87885	0.02195	3.29E-05		0.1	0.6	150.7286	3.13E-05	0.701971
camptothecin 6 B-A	0.9008	1800	0.33	0.72821	0.17259	1.68E-05	0.510184	0.6	0.1	637.0257	2.2E-05	

Table A3.26: Apparent Permeabilty (Papp), Exact Permeabiltiy (Pexact), Papp Efflux Ratio and Pexact Efflux Ratio of chlorpromazine in no cell control (NCC) studies on transwell in six replicates at 30 minutes time point

Drug	initial concentration in donor (uM)	Change in time (s)	Growth area (cm2)	Final concentration in donor (uM)	Change in concentration (uM)	Papp (cm/s)	Efflux ratio (B-A/A-B)	Vd (cm3)	Vr (cm3)	Ct	Pexact	Efflux Ratio (B-A/A-B)
chlorpromazine 1 A-B	0.060767	1800	0.33	0.20933	-0.14856	1.76E-05		0.1	0.6	30.81286	5.05E-06	0.213444
chlorpromazine 1 B-A	0.060767	1800	0.33	0.44775	-0.38698	7.92E-06	0.449686	0.6	0.1	384.1943	1.08E-06	
chlorpromazine 2 A-B	0.060767	1800	0.33	0.15258	-0.09181	1.56E-05		0.1	0.6	22.60286	6.13E-06	0.091343
chlorpromazine 2 B-A	0.060767	1800	0.33	0.5179	-0.45713	4.77E-06	0.304965	0.6	0.1	444.16	5.6E-07	
chlorpromazine 3 A-B	0.060767	1800	0.33	0.18188	-0.12111	1.63E-05		0.1	0.6	26.82286	5.37E-06	0.135691
chlorpromazine 3 B-A	0.060767	1800	0.33	0.47441	-0.41364	5.68E-06	0.348639	0.6	0.1	406.93	7.29E-07	
chlorpromazine 4 A-B	0.060767	1800	0.33	0.34318	-0.28241	2.54E-05		0.1	0.6	50.33714	4.45E-06	0.193509
chlorpromazine 4 B-A	0.060767	1800	0.33	0.44042	-0.37965	6.23E-06	0.245098	0.6	0.1	377.8243	8.62E-07	
chlorpromazine 5 A-B	0.060767	1800	0.33	0.27263	-0.21186	1.85E-05		0.1	0.6	39.89857	4.07E-06	0.17833
chlorpromazine 5 B-A	0.060767	1800	0.33	0.46225	-0.40148	5.51E-06	0.298799	0.6	0.1	396.4986	7.26E-07	
chlorpromazine 6 A-B	0.060767	1800	0.33	0.24985	-0.18908	1.93E-05		0.1	0.6	36.68714	4.64E-06	0.162897
chlorpromazine 6 B-A	0.060767	1800	0.33	0.51812	-0.45735	6.43E-06	0.333333	0.6	0.1	444.4343	7.55E-07	

Table A3.27: Apparent Permeabilty (Papp), Exact Permeabiltiy (Pexact), Papp Efflux Ratio and Pexact Efflux Ratio of loperamide in no cell control (NCC) studies on transwell in six replicates at 30 minutes time point

Drug	initial concentration in donor (uM)	Change in time (s)	Growth area (cm2)	Final concentration in donor (uM)	Change in concentration (uM)	Papp (cm/s)	Efflux ratio (B-A/A-B)	Vd (cm3)	Vr (cm3)	Ct	Pexact	Efflux Ratio (B-A/A-B)
loperamide 1 A-B	0.194433	1800	0.33	0.181015	0.013418	3.55E-06		0.1	0.6	26.44557	3.78E-06	0.167105
loperamide 1 B-A	0.194433	1800	0.33	0.414139	-0.21971	1.34E-06	0.378168	0.6	0.1	355.198	6.32E-07	
loperamide 2 A-B	0.194433	1800	0.33	0.175324	0.019109	3.37E-06		0.1	0.6	25.60257	3.71E-06	0.112701
loperamide 2 B-A	0.194433	1800	0.33	0.44597	-0.25154	9.57E-07	0.28377	0.6	0.1	382.4179	4.18E-07	
loperamide 3 A-B	0.194433	1800	0.33	0.112289	0.082144	3.50E-06		0.1	0.6	16.619	5.97E-06	0.075537
loperamide 3 B-A	0.194433	1800	0.33	0.437336	-0.2429	1.01E-06	0.289565	0.6	0.1	375.0267	4.51E-07	
loperamide 4 A-B	0.194433	1800	0.33	0.421579	-0.22715	5.75E-06		0.1	0.6	61.17357	2.63E-06	0.293272
loperamide 4 B-A	0.194433	1800	0.33	0.503754	-0.30932	2.00E-06	0.347498	0.6	0.1	432.1186	7.72E-07	
loperamide 5 A-B	0.194433	1800	0.33	0.378165	-0.18373	3.33E-06		0.1	0.6	54.573	1.7E-06	0.349388
loperamide 5 B-A	0.194433	1800	0.33	0.479174	-0.28474	1.47E-06	0.440198	0.6	0.1	410.9624	5.96E-07	
loperamide 6 A-B	0.194433	1800	0.33	0.310678	-0.11624	3.53E-06		0.1	0.6	44.96457	2.2E-06	0.225805
loperamide 6 B-A	0.194433	1800	0.33	0.568099	-0.37367	1.45E-06	0.410162	0.6	0.1	487.1807	4.96E-07	

Table A3.28: Apparent Permeabilty (Papp), Exact Permeabiltiy (Pexact), Papp Efflux Ratio and Pexact Efflux Ratio of etoposide in no cell control (NCC) studies on transwell in six replicates at 30 minutes time point

Drug	initial concentration in donor (uM)	Change in time (s)	Growth area (cm2)	Final concentration in donor (uM)	Change in concentration (uM)	Papp (cm/s)	Efflux ratio (B-A/A-B)	Vd (cm3)	Vr (cm3)	Ct	Pexact	Efflux Ratio (B-A/A-B)
etoposide 1 A-B	0.48908	1800	0.33	0.43802	0.05106	1.16E-04		0.1	0.6	110.7543	0.000102	0.251998
etoposide 1 B-A	0.48908	1800	0.33	0.69703	-0.20795	3.44E-05	0.296507	0.6	0.1	611.74	2.58E-05	
etoposide 2 A-B	0.48908	1800	0.33	0.53324	-0.04416	1.12E-04		0.1	0.6	122.8571	8.45E-05	0.47884
etoposide 2 B-A	0.48908	1800	0.33	0.52737	-0.03829	3.94E-05	0.350563	0.6	0.1	468.3957	4.05E-05	
etoposide 3 A-B	0.48908	1800	0.33	0.43198	0.0571	7.00E-05		0.1	0.6	90.77714	6.75E-05	0.420855
etoposide 3 B-A	0.48908	1800	0.33	0.58025	-0.09117	3.14E-05	0.448196	0.6	0.1	510.3843	2.84E-05	
etoposide 4 A-B	0.48908	1800	0.33	0.65984	-0.17076	1.10E-04		0.1	0.6	139.88	6.91E-05	0.212196
etoposide 4 B-A	0.48908	1800	0.33	0.67957	-0.19049	1.96E-05	0.178692	0.6	0.1	590.64	1.47E-05	
etoposide 5 A-B	0.48908	1800	0.33	0.61119	-0.12211	1.06E-04		0.1	0.6	131.4986	7.18E-05	0.310485
etoposide 5 B-A	0.48908	1800	0.33	0.64797	-0.15889	2.79E-05	0.262431	0.6	0.1	566.9986	2.23E-05	
etoposide 6 A-B	0.48908	1800	0.33	0.53431	-0.04523	1.08E-04		0.1	0.6	121.1243	8.15E-05	0.195565
etoposide 6 B-A	0.48908	1800	0.33	0.8931	-0.40402	2.80E-05	0.259121	0.6	0.1	777.1214	1.59E-05	

Table A3.29: Apparent Permeabilty (Papp), Exact Permeabiltiy (Pexact), Papp Efflux Ratio and Pexact Efflux Ratio of lamotrigine in no cell control (NCC) studies on transwell in six replicates at 30 minutes time point

Drug	initial concentration in donor (uM)	Change in time (s)	Growth area (cm2)	Final concentration in donor (uM)	Change in concentration (uM)	Papp (cm/s)	Efflux ratio (B-A/A-B)	Vd (cm3)	Vr (cm3)	Ct	Pexact	Efflux Ratio (B-A/A-B)
lamotrigine 1 A-B	0.753953	1800	0.33	0.98384	-0.22989	1.34E-06		0.1	0.6	141.4057	1.02E-06	16.18893
lamotrigine 1 B-A	0.753953	1800	0.33	1.47358	-0.71963	3.11E-05	23.20833	0.6	0.1	1282.961	1.66E-05	
lamotrigine 2 A-B	0.753953	1800	0.33	1.0314	-0.27745	2.04E-05		0.1	0.6	160.4057	1.44E-05	1.689801
lamotrigine 2 B-A	0.753953	1800	0.33	1.06942	-0.31547	3.25E-05	1.591426	0.6	0.1	937.4343	2.43E-05	
lamotrigine 3 A-B	0.753953	1800	0.33	1.3578	-0.60385	3.66E-05		0.1	0.6	217.3971	1.94E-05	1.504314
lamotrigine 3 B-A	0.753953	1800	0.33	1.14785	-0.3939	4.13E-05	1.127394	0.6	0.1	1010.281	2.92E-05	
lamotrigine 4 A-B	0.753953	1800	0.33	1.1904	-0.43645	3.77E-05		0.1	0.6	194.1686	2.26E-05	0.939919
lamotrigine 4 B-A	0.753953	1800	0.33	1.21423	-0.46028	3.24E-05	0.860351	0.6	0.1	1061.513	2.12E-05	
lamotrigine 5 A-B	0.753953	1800	0.33	1.38214	-0.62819	1.53E-06		0.1	0.6	198.4257	8.31E-07	44.45958
lamotrigine 5 B-A	0.753953	1800	0.33	1.12477	-0.37082	5.03E-05	32.9152	0.6	0.1	996.2514	3.7E-05	
lamotrigine 6 A-B	0.753953	1800	0.33	1.33734	-0.58339	8.45E-06		0.1	0.6	196.4571	4.71E-06	4.802268
lamotrigine 6 B-A	0.753953	1800	0.33	1.27646	-0.52251	3.62E-05	4.282092	0.6	0.1	1117.269	2.26E-05	

Table A3.30: Apparent Permeabilty (Papp), Exact Permeabiltiy (Pexact), Papp Efflux Ratio and Pexact Efflux Ratio of methotrexate in no cell control (NCC) studies on transwell in six replicates at 30 minutes time point

Drug	initial concentration in donor (uM)	Change in time (s)	Growth area (cm2)	Final concentration in donor (uM)	Change in concentration (uM)	Papp (cm/s)	Efflux ratio (B-A/A-B)	Vd (cm3)	Vr (cm3)	Ct	Pexact	Efflux Ratio (B-A/A-B)
methotrexate 1 A-B	0.974023	1800	0.33	1.34061	-0.36659	1.56E-05		0.1	0.6	204.3814	1.1E-05	1.489049
methotrexate 1 B-A	0.974023	1800	0.33	1.13456	-0.16054	1.83E-05	1.177437	0.6	0.1	987.6286	1.64E-05	
methotrexate 2 A-B	0.974023	1800	0.33	1.06541	-0.09139	2.61E-05		0.1	0.6	173.7757	2.26E-05	1.294939
methotrexate 2 B-A	0.974023	1800	0.33	0.89892	0.075103	2.51E-05	0.960932	0.6	0.1	791.2343	2.92E-05	
methotrexate 3 A-B	0.974023	1800	0.33	1.20363	-0.22961	2.14E-05		0.1	0.6	189.6729	1.67E-05	1.000557
methotrexate 3 B-A	0.974023	1800	0.33	1.10535	-0.13133	1.81E-05	0.846148	0.6	0.1	962.4414	1.67E-05	
methotrexate 4 A-B	0.974023	1800	0.33	1.15216	-0.17814	1.59E-05		0.1	0.6	177.7771	1.31E-05	1.386197
methotrexate 4 B-A	0.974023	1800	0.33	0.88359	0.090433	1.57E-05	0.98407	0.6	0.1	770.3357	1.81E-05	
methotrexate 5 A-B	0.974023	1800	0.33	1.18562	-0.2116	1.34E-05		0.1	0.6	180.4143	1.07E-05	2.021032
methotrexate 5 B-A	0.974023	1800	0.33	0.88163	0.092393	1.85E-05	1.387034	0.6	0.1	770.9957	2.16E-05	
methotrexate 6 A-B	0.974023	1800	0.33	1.20395	-0.22993	1.48E-05		0.1	0.6	184.19	1.16E-05	1.514982
methotrexate 6 B-A	0.974023	1800	0.33	0.92997	0.044053	1.61E-05	1.088545	0.6	0.1	810.3943	1.76E-05	

Table A3.31: Apparent Permeabilty (Papp), Exact Permeabiltiy (Pexact), Papp Efflux Ratio and Pexact Efflux Ratio of topiramate in no cell control (NCC) studies on transwell in six replicates at 30 minutes time point

Drug	Initial concentration in donor (uM)	Change in time (s)	Growth area (cm2)	Final concentration in donor (uM)	Change in concentration (uM)	Papp (cm/s)	Efflux ratio (B-A/A-B)	Vd (cm3)	Vr (cm3)	Ct	Pexact	Efflux Ratio (B-A/A-B)
topiramate 1 A-B	0.96761	1800	0.33	1.04349	-0.07588	1.24E-05		0.1	0.6	159.2357	1.12E-05	2.461542
topiramate 1 B-A	0.96761	1800	0.33	0.88312	0.08449	2.34E-05	1.892215	0.6	0.1	776.1957	2.75E-05	
topiramate 2 A-B	0.96761	1800	0.33	1.05991	-0.0923	1.83E-05		0.1	0.6	166.4329	1.61E-05	1.572848
topiramate 2 B-A	0.96761	1800	0.33	0.96037	0.00724	2.35E-05	1.286339	0.6	0.1	842.4914	2.52E-05	
topiramate 3 A-B	0.96761	1800	0.33	0.91115	0.05646	3.02E-05		0.1	0.6	154.9957	2.99E-05	0.710931
topiramate 3 B-A	0.96761	1800	0.33	1.17805	-0.21044	2.45E-05	0.810494	0.6	0.1	1029.883	2.12E-05	
topiramate 4 A-B	0.96761	1800	0.33	1.19039	-0.22278	2.24E-05		0.1	0.6	188.4757	1.75E-05	0.851047
topiramate 4 B-A	0.96761	1800	0.33	1.14026	-0.17265	1.69E-05	0.752598	0.6	0.1	991.2286	1.49E-05	
topiramate 5 A-B	0.96761	1800	0.33	1.06045	-0.09284	2.16E-05		0.1	0.6	169.2271	1.88E-05	0.963253
topiramate 5 B-A	0.96761	1800	0.33	1.27102	-0.30341	2.28E-05	1.05373	0.6	0.1	1108.133	1.81E-05	
topiramate 6 A-B	0.96761	1800	0.33	1.1786	-0.21099	1.49E-05		0.1	0.6	180.6029	1.19E-05	1.270342
topiramate 6 B-A	0.96761	1800	0.33	1.37196	-0.40435	2.06E-05	1.383205	0.6	0.1	1192.884	1.51E-05	

Table A3.32: Apparent Permeabilty (Papp), Exact Permeabiltiy (Pexact), Papp Efflux Ratio and Pexact Efflux Ratio of mitoxantrone in no cell control (NCC) studies on transwell in six replicates at 30 minutes time point

Drug	initial concentration in donor (uM)	Change in time (s)	Growth area (cm2)	Final concentration in donor (uM)	Change in concentration (uM)	Papp (cm/s)	Efflux ratio (B-A/A-B)	Vd (cm3)	Vr (cm3)	Ct	Pexact	Efflux Ratio (B-A/A-B)
mitoxantrone 1 A-B	0.103017	1800	0.33	0.10725	-0.00423	3.88E-06		0.1	0.6	15.66086	3.7E-06	0.241883
mitoxantrone 1 B-A	0.103017	1800	0.33	0.08116	0.021857	7.03E-07	0.180976	0.6	0.1	69.62714	8.94E-07	
mitoxantrone 2 A-B	0.103017	1800	0.33	0.15696	-0.05394	5.79E-06		0.1	0.6	22.92857	3.76E-06	0.574768
mitoxantrone 2 B-A	0.103017	1800	0.33	0.09472	0.008297	1.98E-06	0.341808	0.6	0.1	81.36143	2.16E-06	
mitoxantrone 3 A-B	0.103017	1800	0.33	0.08935	0.013667	8.43E-06		0.1	0.6	13.50143	9.5E-06	0.810222
mitoxantrone 3 B-A	0.103017	1800	0.33	0.09812	0.004897	7.19E-06	0.852713	0.6	0.1	84.73143	7.69E-06	
mitoxantrone 4 A-B	0.103017	1800	0.33	0.24275	-0.13973	6.96E-06		0.1	0.6	35.28714	2.93E-06	0.518882
mitoxantrone 4 B-A	0.103017	1800	0.33	0.12103	-0.01801	1.78E-06	0.255869	0.6	0.1	103.8957	1.52E-06	
mitoxantrone 5 A-B	0.103017	1800	0.33	0.19712	-0.0941	9.81E-06		0.1	0.6	29.01714	5.06E-06	0.084298
mitoxantrone 5 B-A	0.103017	1800	0.33	0.16987	-0.06685	7.03E-07	0.071667	0.6	0.1	145.6643	4.27E-07	
mitoxantrone 6 A-B	0.103017	1800	0.33	0.14576	-0.04274	5.20E-06		0.1	0.6	21.27714	3.64E-06	0.070373
mitoxantrone 6 B-A	0.103017	1800	0.33	0.16441	-0.06139	4.09E-07	0.078616	0.6	0.1	140.9586	2.56E-07	

Table A3.33: Apparent Permeabilty (Papp), Exact Permeabiltiy (Pexact), Papp Efflux Ratio and Pexact Efflux Ratio of camptothecin in no cell control (NCC) studies on transwell in six replicates at 60 minutes time point

Drug	initial concentration in donor (uM)	Change in time (s)	Growth area (cm2)	Final concentration in donor (uM)	Change in concentration (uM)	Papp (cm/s)	Efflux ratio (B-A/A-B)	Vd (cm3)	Vr (cm3)	Ct	Pexact	Efflux Ratio (B-A/A-B)
camptothecin 1 A-B	1.008427	3600	0.33	0.87026	0.138167	5.55E-05		0.1	0.6	219.3457	5.08E-05	0.573212
camptothecin 1 B-A	1.008427	3600	0.33	0.76704	0.241387	1.91E-05	0.344564	0.6	0.1	690.2043	2.91E-05	
camptothecin 2 A-B	1.008427	3600	0.33	0.96985	0.038577	2.55E-05		0.1	0.6	182.1614	2.36E-05	0.782465
camptothecin 2 B-A	1.008427	3600	0.33	0.8166	0.191827	1.37E-05	0.535672	0.6	0.1	723.3043	1.85E-05	
camptothecin 3 A-B	1.008427	3600	0.33	0.88506	0.123367	2.46E-05		0.1	0.6	168.54	2.49E-05	0.939852
camptothecin 3 B-A	1.008427	3600	0.33	0.80074	0.207687	1.65E-05	0.67067	0.6	0.1	714.5857	2.34E-05	
camptothecin 4 A-B	1.008427	3600	0.33	0.68738	0.321047	4.74E-05		0.1	0.6	179.2829	5.41E-05	0.533857
camptothecin 4 B-A	1.008427	3600	0.33	0.6217	0.386727	1.54E-05	0.325106	0.6	0.1	559.2471	2.89E-05	
camptothecin 5 A-B	1.008427	3600	0.33	0.83586	0.172567	2.29E-05		0.1	0.6	158.5886	2.45E-05	0.846152
camptothecin 5 B-A	1.008427	3600	0.33	0.78743	0.220997	1.46E-05	0.638044	0.6	0.1	699.9386	2.08E-05	
camptothecin 6 A-B	1.008427	3600	0.33	0.81467	0.193757	2.22E-05		0.1	0.6	154.3614	2.44E-05	0.974519
camptothecin 6 B-A	1.008427	3600	0.33	0.69305	0.315377	1.45E-05	0.65384	0.6	0.1	618.8757	2.38E-05	

Table A3.34: Apparent Permeabilty (Papp), Exact Permeabiltiy (Pexact), Papp Efflux Ratio and Pexact Efflux Ratio of chlorpromazine in no cell control (NCC) studies on transwell in six replicates at 60 minutes time point

Drug	initial concentration in donor (uM)	Change in time (s)	Growth area (cm2)	Final concentration in donor (uM)	Change in concentration (uM)	Papp (cm/s)	Efflux ratio (B-A/A-B)	Vd (cm3)	Vr (cm3)	Ct	Pexact	Efflux Ratio (B-A/A-B)
chlorpromazine 1 A-B	0.057957	3600	0.33	0.21077	-0.15281	1.71E-05		0.1	0.6	31.79	4.59E-06	0.154821
chlorpromazine 1 B-A	0.057957	3600	0.33	0.33986	-0.2819	4.15E-06	0.243197	0.6	0.1	291.7171	7.11E-07	
chlorpromazine 2 A-B	0.057957	3600	0.33	0.17262	-0.11466	1.28E-05		0.1	0.6	25.92	4.21E-06	0.133197
chlorpromazine 2 B-A	0.057957	3600	0.33	0.38061	-0.32265	3.67E-06	0.286848	0.6	0.1	326.5986	5.61E-07	
chlorpromazine 3 A-B	0.057957	3600	0.33	0.21055	-0.15259	1.00E-05		0.1	0.6	31.06429	2.72E-06	0.232246
chlorpromazine 3 B-A	0.057957	3600	0.33	0.39541	-0.33745	4.30E-06	0.428986	0.6	0.1	339.3457	6.32E-07	
chlorpromazine 4 A-B	0.057957	3600	0.33	0.2081	-0.15014	2.85E-05		0.1	0.6	32.53143	7.64E-06	0.090333
chlorpromazine 4 B-A	0.057957	3600	0.33	0.42694	-0.36898	5.07E-06	0.17788	0.6	0.1	366.4471	6.9E-07	
chlorpromazine 5 A-B	0.057957	3600	0.33	0.28092	-0.22296	1.68E-05		0.1	0.6	41.78571	3.41E-06	0.228578
chlorpromazine 5 B-A	0.057957	3600	0.33	0.43232	-0.37436	5.79E-06	0.34456	0.6	0.1	371.13	7.8E-07	
chlorpromazine 6 A-B	0.057957	3600	0.33	0.2216	-0.16364	2.05E-05		0.1	0.6	33.67143	5.22E-06	0.175385
chlorpromazine 6 B-A	0.057957	3600	0.33	0.39624	-0.33828	6.23E-06	0.304255	0.6	0.1	340.2471	9.15E-07	

Table A3.35: Apparent Permeabilty (Papp), Exact Permeabiltiy (Pexact), Papp Efflux Ratio and Pexact Efflux Ratio of loperamide in no cell control (NCC) studies on transwell in six replicates at 60 minutes time point

Drug	Initial concentration in donor (uM)	Change in time (s)	Growth area (cm2)	Final concentration in donor (uM)	Change in concentration (uM)	Papp (cm/s)	Efflux ratio (B-A/A-B)	Vd (cm3)	Vr (cm3)	Ct	Pexact	Efflux Ratio (B-A/A-B)
loperamide 1 A-B	0.183887	3600	0.33	0.17207	0.011817	3.57E-06		0.1	0.6	25.69571	3.75E-06	0.155877
loperamide 1 B-A	0.183887	3600	0.33	0.27615	-0.09226	8.74E-07	0.244872	0.6	0.1	236.9729	5.84E-07	
loperamide 2 A-B	0.183887	3600	0.33	0.13569	0.048197	2.28E-06		0.1	0.6	20.09571	3.04E-06	0.124523
loperamide 2 B-A	0.183887	3600	0.33	0.32936	-0.14547	6.77E-07	0.297189	0.6	0.1	282.52	3.79E-07	
loperamide 3 A-B	0.183887	3600	0.33	0.18092	0.002967	1.79E-06		0.1	0.6	26.40286	1.8E-06	0.306736
loperamide 3 B-A	0.183887	3600	0.33	0.34579	-0.1619	1.03E-06	0.579487	0.6	0.1	296.7143	5.52E-07	
loperamide 4 A-B	0.183887	3600	0.33	0.29865	-0.11476	9.23E-06		0.1	0.6	45.54429	5.53E-06	0.128206
loperamide 4 B-A	0.183887	3600	0.33	0.48378	-0.29989	1.86E-06	0.201389	0.6	0.1	415.2486	7.09E-07	
loperamide 5 A-B	0.183887	3600	0.33	0.36401	-0.18012	5.03E-06		0.1	0.6	53.57	2.51E-06	0.317618
loperamide 5 B-A	0.183887	3600	0.33	0.46364	-0.27975	2.00E-06	0.397996	0.6	0.1	398.03	7.97E-07	
loperamide 6 A-B	0.183887	3600	0.33	0.32655	-0.14266	4.75E-06		0.1	0.6	48.13286	2.64E-06	0.301041
loperamide 6 B-A	0.183887	3600	0.33	0.46875	-0.28486	2.02E-06	0.424855	0.6	0.1	402.4157	7.95E-07	

Table A3.36: Apparent Permeabilty (Papp), Exact Permeabiltiy (Pexact), Papp Efflux Ratio and Pexact Efflux Ratio of etoposide in no cell control (NCC) studies on transwell in six replicates at 60 minutes time point

Drug	initial concentration in donor (uM)	Change in time (s)	Growth area (cm2)	Final concentration in donor (uM)	Change in concentration (uM)	Papp (cm/s)	Efflux ratio (B-A/A-B)	Vd (cm3)	Vr (cm3)	Ct	Pexact	Efflux Ratio (B-A/A-B)
etoposide 1 A-B	0.611893	3600	0.33	0.49533	0.116563	6.29E-05		0.1	0.6	136.1271	5.93E-05	0.30406
etoposide 1 B-A	0.611893	3600	0.33	0.53168	0.080213	1.43E-05	0.227314	0.6	0.1	470.5843	1.8E-05	
etoposide 2 A-B	0.611893	3600	0.33	0.58181	0.030083	5.77E-05		0.1	0.6	143.0214	4.84E-05	0.270381
etoposide 2 B-A	0.611893	3600	0.33	0.6923	-0.08041	1.39E-05	0.240402	0.6	0.1	607.8014	1.31E-05	
etoposide 3 A-B	0.611893	3600	0.33	0.42125	0.190643	5.02E-05		0.1	0.6	112.2843	5.62E-05	0.389772
etoposide 3 B-A	0.611893	3600	0.33	0.54249	0.069403	1.74E-05	0.347042	0.6	0.1	483.0743	2.19E-05	
etoposide 4 A-B	0.611893	3600	0.33	0.5203	0.091593	4.42E-05		0.1	0.6	120.2286	4.25E-05	0.381134
etoposide 4 B-A	0.611893	3600	0.33	0.73203	-0.12014	1.79E-05	0.404606	0.6	0.1	646.0257	1.62E-05	
etoposide 5 A-B	0.611893	3600	0.33	0.54911	0.062783	4.67E-05		0.1	0.6	126.9243	4.26E-05	0.389853
etoposide 5 B-A	0.611893	3600	0.33	0.76705	-0.15516	1.91E-05	0.410066	0.6	0.1	677.3514	1.66E-05	
etoposide 6 A-B	0.611893	3600	0.33	0.65743	-0.04554	6.06E-05		0.1	0.6	156.8414	4.55E-05	0.225573
etoposide 6 B-A	0.611893	3600	0.33	0.82552	-0.21363	1.32E-05	0.217318	0.6	0.1	721.2629	1.03E-05	

Table A3.37: Apparent Permeabilty (Papp), Exact Permeabiltiy (Pexact), Papp Efflux Ratio and Pexact Efflux Ratio of lamotrigine in no cell control (NCC) studies on transwell in six replicates at 60 minutes time point

Drug	initial concentration in donor (uM)	Change in time (s)	Growth area (cm2)	Final concentration in donor (uM)	Change in concentration (uM)	Papp (cm/s)	Efflux ratio (B-A/A-B)	Vd (cm3)	Vr (cm3)	Ct	Pexact	Efflux Ratio (B-A/A-B)
lamotrigine 1 A-B	0.928607	3600	0.33	1.00096	-0.07235	3.13E-05		0.1	0.6	192.3143	2.57E-05	0.94917
lamotrigine 1 B-A	0.928607	3600	0.33	1.1448	-0.21619	2.66E-05	0.848801	0.6	0.1	1023.12	2.43E-05	
lamotrigine 2 A-B	0.928607	3600	0.33	0.82608	0.102527	3.13E-05		0.1	0.6	167.28	3.04E-05	0.74828
lamotrigine 2 B-A	0.928607	3600	0.33	1.1324	-0.20379	2.47E-05	0.791087	0.6	0.1	1009.604	2.27E-05	
lamotrigine 3 A-B	0.928607	3600	0.33	1.11257	-0.18396	2.13E-05		0.1	0.6	192.4529	1.64E-05	2.001293
lamotrigine 3 B-A	0.928607	3600	0.33	1.05265	-0.12404	3.15E-05	1.482055	0.6	0.1	951.9414	3.28E-05	
lamotrigine 4 A-B	0.928607	3600	0.33	0.86741	0.061197	2.56E-05		0.1	0.6	164.3043	2.44E-05	1.113023
lamotrigine 4 B-A	0.928607	3600	0.33	1.04039	-0.11178	2.65E-05	1.035265	0.6	0.1	933.5757	2.71E-05	
lamotrigine 5 A-B	0.928607	3600	0.33	1.14221	-0.2136	1.95E-05		0.1	0.6	193.9357	1.48E-05	1.74067
lamotrigine 5 B-A	0.928607	3600	0.33	1.33353	-0.40492	3.24E-05	1.661837	0.6	0.1	1194.149	2.57E-05	
lamotrigine 6 A-B	0.928607	3600	0.33	1.27869	-0.35008	2.20E-05		0.1	0.6	217.41	1.49E-05	2.120682
lamotrigine 6 B-A	0.928607	3600	0.33	1.14862	-0.22001	3.33E-05	1.511185	0.6	0.1	1037.03	3.16E-05	

Table A3.38: Apparent Permeabilty (Papp), Exact Permeabiltiy (Pexact), Papp Efflux Ratio and Pexact Efflux Ratio of methotrexate in no cell control (NCC) studies on transwell in six replicates at 60 minutes time point

Drug	initial concentration in donor (uM)	Change in time (s)	Growth area (cm2)	Final concentration in donor (uM)	Change in concentration (uM)	Papp (cm/s)	Efflux ratio (B-A/A-B)	Vd (cm3)	Vr (cm3)	Ct	Pexact	Efflux Ratio (B-A/A-B)
methotrexate 1 A-B	0.934277	3600	0.33	1.23019	-0.29591	1.69E-05		0.1	0.6	202.5614	1.21E-05	1.44844
methotrexate 1 B-A	0.934277	3600	0.33	0.90175	0.032527	1.55E-05	0.916534	0.6	0.1	797.51	1.75E-05	
methotrexate 2 A-B	0.934277	3600	0.33	1.05542	-0.12114	1.87E-05		0.1	0.6	180.3886	1.53E-05	0.912734
methotrexate 2 B-A	0.934277	3600	0.33	0.95867	-0.02439	1.34E-05	0.71727	0.6	0.1	842.9586	1.4E-05	
methotrexate 3 A-B	0.934277	3600	0.33	1.30472	-0.37044	1.69E-05		0.1	0.6	213.2257	1.15E-05	1.523764
methotrexate 3 B-A	0.934277	3600	0.33	1.10021	-0.16593	1.88E-05	1.113116	0.6	0.1	972.91	1.75E-05	
methotrexate 4 A-B	0.934277	3600	0.33	0.83576	0.098517	1.94E-05		0.1	0.6	150.1486	1.97E-05	0.919219
methotrexate 4 B-A	0.934277	3600	0.33	0.86597	0.068307	1.53E-05	0.790459	0.6	0.1	766.57	1.81E-05	
methotrexate 5 A-B	0.934277	3600	0.33	1.13211	-0.19783	2.28E-05		0.1	0.6	197.91	1.73E-05	1.100864
methotrexate 5 B-A	0.934277	3600	0.33	0.9249	0.009377	1.71E-05	0.751402	0.6	0.1	819.9571	1.91E-05	
methotrexate 6 A-B	0.934277	3600	0.33	0.90959	0.024687	1.77E-05		0.1	0.6	157.9957	1.67E-05	1.283995
methotrexate 6 B-A	0.934277	3600	0.33	0.80226	0.132017	1.66E-05	0.93701	0.6	0.1	713.9386	2.15E-05	

Table A3.39: Apparent Permeabilty (Papp), Exact Permeabiltiy (Pexact), Papp Efflux Ratio and Pexact Efflux Ratio of topiramate in no cell control (NCC) studies on transwell in six replicates at 60 minutes time point

Drug	Initial concentration in donor (uM)	Change in time (s)	Growth area (cm2)	Final concentration in donor (uM)	Change in concentration (uM)	Papp (cm/s)	Efflux ratio (B-A/A-B)	Vd (cm3)	Vr (cm3)	Ct	Pexact	Efflux Ratio (B-A/A-B)
topiramate 1 A-B	1.837513	3600	0.33	1.00011	0.837403	1.00E-05		0.1	0.6	174.1243	1.7E-05	1.204522
topiramate 1 B-A	1.837513	3600	0.33	1.13233	0.705183	1.14E-05	1.13348	0.6	0.1	1005.991	2.04E-05	
topiramate 2 A-B	1.837513	3600	0.33	0.84933	0.988183	1.31E-05		0.1	0.6	162.0814	2.5E-05	0.866104
topiramate 2 B-A	1.837513	3600	0.33	1.16269	0.674823	1.23E-05	0.942259	0.6	0.1	1034.987	2.17E-05	
topiramate 3 A-B	1.837513	3600	0.33	0.86102	0.976493	1.14E-05		0.1	0.6	158.6	2.19E-05	0.938354
topiramate 3 B-A	1.837513	3600	0.33	0.86171	0.975803	8.70E-06	0.761819	0.6	0.1	765.7271	2.06E-05	
topiramate 4 A-B	1.837513	3600	0.33	1.16393	0.673583	1.07E-05		0.1	0.6	199.6357	1.56E-05	1.642608
topiramate 4 B-A	1.837513	3600	0.33	1.02231	0.815203	1.26E-05	1.174803	0.6	0.1	915.4571	2.57E-05	
topiramate 5 A-B	1.837513	3600	0.33	1.14849	0.689023	9.94E-06		0.1	0.6	195.0729	1.48E-05	1.458274
topiramate 5 B-A	1.837513	3600	0.33	1.22692	0.610593	1.29E-05	1.300617	0.6	0.1	1091.969	2.16E-05	
topiramate 6 A-B	1.837513	3600	0.33	1.05328	0.784233	1.15E-05		0.1	0.6	186.2286	1.83E-05	1.058867
topiramate 6 B-A	1.837513	3600	0.33	1.1742	0.663313	1.12E-05	0.979946	0.6	0.1	1041.5	1.94E-05	

Table A3.40: Apparent Permeabilty (Papp), Exact Permeabiltiy (Pexact), Papp Efflux Ratio and Pexact Efflux Ratio of mitoxantrone in no cell control (NCC) studies on transwell in six replicates at 60 minutes time point

Drug	Initial concentration in donor (uM)	Change in time (s)	Growth area (cm2)	Final concentration in donor (uM)	Change in concentration (uM)	Papp (cm/s)	Efflux ratio (B-A/A-B)	Vd (cm3)	Vr (cm3)	Ct	Pexact	Efflux Ratio (B-A/A-B)
mitoxantrone 1 A-B	0.10618	3600	0.33	0.06909	0.03709	1.33E-06		0.1	0.6	10.11	2.03E-06	1.128319
mitoxantrone 1 B-A	0.10618	3600	0.33	0.06665	0.03953	1.42E-06	1.065476	0.6	0.1	57.38429	2.29E-06	
mitoxantrone 2 A-B	0.10618	3600	0.33	0.07935	0.02683	7.61E-07		0.1	0.6	11.47286	1.01E-06	1.050705
mitoxantrone 2 B-A	0.10618	3600	0.33	0.08266	0.02352	8.24E-07	1.083333	0.6	0.1	71	1.06E-06	
mitoxantrone 3 A-B	0.10618	3600	0.33	0.06018	0.046	6.90E-06		0.1	0.6	9.84	1.15E-05	0.052536
mitoxantrone 3 B-A	0.10618	3600	0.33	0.06986	0.03632	3.96E-07	0.057471	0.6	0.1	59.95143	6.04E-07	
mitoxantrone 4 A-B	0.10618	3600	0.33	0.11165	-0.00547	3.33E-07		0.1	0.6	16.01	3.16E-07	0.529276
mitoxantrone 4 B-A	0.10618	3600	0.33	0.1309	-0.02472	2.06E-07	0.619048	0.6	0.1	112.2371	1.67E-07	
mitoxantrone 5 A-B	0.10618	3600	0.33	0.14729	-0.04111	1.53E-05		0.1	0.6	23.80143	1.05E-05	0.110446
mitoxantrone 5 B-A	0.10618	3600	0.33	0.10598	0.0002	1.15E-06	0.075052	0.6	0.1	91.04714	1.16E-06	
mitoxantrone 6 A-B	0.10618	3600	0.33	0.09679	0.00939	3.09E-06		0.1	0.6	14.38429	3.34E-06	0.111558
mitoxantrone 6 B-A	0.10618	3600	0.33	0.10196	0.00422	3.57E-07	0.115385	0.6	0.1	87.45857	3.72E-07	

Table A3.41: Apparent Permeabilty (Papp), Exact Permeabiltiy (Pexact), Papp Efflux Ratio and Pexact Efflux Ratio of camptothecin in no cell control (NCC) studies on transwell in six replicates at 120 minutes time point

Drug	Initial concentration in donor (uM)	Change in time (s)	Growth area (cm2)	Final concentration in donor (uM)	Change in concentration (uM)	Papp (cm/s)	Efflux ratio (B-A/A-B)	Vd (cm3)	Vr (cm3)	Ct	Pexact	Efflux Ratio (B-A/A-B)
camptothecin 1 A-B	0.96054	7200	0.33	0.59169	0.36885	2.95E-05		0.1	0.6	180.7329	3.5E-05	1.102745
camptothecin 1 B-A	0.96054	7200	0.33	0.80168	0.15886	2.18E-05	0.739799	0.6	0.1	758.3271	3.86E-05	
camptothecin 2 A-B	0.96054	7200	0.33	0.69785	0.26269	2.01E-05		0.1	0.6	165.3671	2.25E-05	1.577915
camptothecin 2 B-A	0.96054	7200	0.33	0.80593	0.15461	2.08E-05	1.032063	0.6	0.1	758.5771	3.54E-05	
camptothecin 3 A-B	0.96054	7200	0.33	0.75355	0.20699	2.26E-05		0.1	0.6	181.4243	2.32E-05	1.437201
camptothecin 3 B-A	0.96054	7200	0.33	0.70785	0.25269	1.75E-05	0.77559	0.6	0.1	663.9471	3.34E-05	
camptothecin 4 A-B	0.96054	7200	0.33	0.61169	0.34885	3.26E-05		0.1	0.6	193.5243	3.68E-05	0.572617
camptothecin 4 B-A	0.96054	7200	0.33	0.83466	0.12588	1.48E-05	0.455154	0.6	0.1	763.7329	2.11E-05	
camptothecin 5 A-B	0.96054	7200	0.33	0.54271	0.41783	2.09E-05		0.1	0.6	145.5529	2.84E-05	0.648069
camptothecin 5 B-A	0.96054	7200	0.33	0.79235	0.16819	1.26E-05	0.604944	0.6	0.1	720.3071	1.84E-05	
camptothecin 6 A-B	0.96054	7200	0.33	0.59429	0.36625	1.77E-05		0.1	0.6	142.5671	2.3E-05	1.03443
camptothecin 6 B-A	0.96054	7200	0.33	0.71075	0.24979	1.39E-05	0.783641	0.6	0.1	654.4057	2.38E-05	

Table A3.42: Apparent Permeabilty (Papp), Exact Permeabiltiy (Pexact), Papp Efflux Ratio and Pexact Efflux Ratio of chlorpromazine in no cell control (NCC) studies on transwell in six replicates at 120 minutes time point

Drug	initial concentration in donor (uM)	Change in time (s)	Growth area (cm2)	Final concentration in donor (uM)	Change in concentration (uM)	Papp (cm/s)	Efflux ratio (B-A/A-B)	Vd (cm3)	Vr (cm3)	Ct	Pexact	Efflux Ratio (B-A/A-B)
chlorpromazine 1 A-B	0.058673	7200	0.33	0.10317	-0.0445	1.31E-05		0.1	0.6	17.34429	6.95E-06	0.190204
chlorpromazine 1 B-A	0.058673	7200	0.33	0.33121	-0.27254	7.37E-06	0.563048	0.6	0.1	285.3614	1.32E-06	
chlorpromazine 2 A-B	0.058673	7200	0.33	0.15224	-0.09357	1.29E-05		0.1	0.6	24.31143	4.73E-06	0.35221
chlorpromazine 2 B-A	0.058673	7200	0.33	0.31025	-0.25158	8.67E-06	0.673913	0.6	0.1	267.6557	1.67E-06	
chlorpromazine 3 A-B	0.058673	7200	0.33	0.1583	-0.09963	1.17E-05		0.1	0.6	24.94571	4.16E-06	0.381416
chlorpromazine 3 B-A	0.058673	7200	0.33	0.33832	-0.27965	9.02E-06	0.770221	0.6	0.1	291.7843	1.59E-06	
chlorpromazine 4 A-B	0.058673	7200	0.33	0.14919	-0.09052	1.96E-05		0.1	0.6	25.21286	7.18E-06	0.257851
chlorpromazine 4 B-A	0.058673	7200	0.33	0.39088	-0.33221	1.21E-05	0.618315	0.6	0.1	337.4514	1.85E-06	
chlorpromazine 5 A-B	0.058673	7200	0.33	0.14097	-0.0823	1.44E-05		0.1	0.6	23.01	5.68E-06	0.324165
chlorpromazine 5 B-A	0.058673	7200	0.33	0.37249	-0.31382	1.15E-05	0.795522	0.6	0.1	321.5614	1.84E-06	
chlorpromazine 6 A-B	0.058673	7200	0.33	0.14545	-0.08678	1.21E-05		0.1	0.6	23.18714	4.66E-06	0.433893
chlorpromazine 6 B-A	0.058673	7200	0.33	0.33192	-0.27325	1.12E-05	0.927046	0.6	0.1	286.7357	2.02E-06	

Table A3.43: Apparent Permeabilty (Papp), Exact Permeabiltiy (Pexact), Papp Efflux Ratio and Pexact Efflux Ratio of loperamide in no cell control (NCC) studies on transwell in six replicates at 120 minutes time point

Drug	Initial concentration in donor (uM)	Change in time (s)	Growth area (cm2)	Final concentration in donor (uM)	Change in concentration (uM)	Papp (cm/s)	Efflux ratio (B-A/A-B)	Vd (cm3)	Vr (cm3)	Ct	Pexact	Efflux Ratio (B-A/A-B)
loperamide 1 A-B	0.168573	7200	0.33	0.06118	0.107393	2.67E-06		0.1	0.6	10.26571	6.87E-06	0.162996
loperamide 1 B-A	0.168573	7200	0.33	0.26339	-0.09482	1.73E-06	0.648876	0.6	0.1	226.7529	1.12E-06	
loperamide 2 A-B	0.168573	7200	0.33	0.14157	0.027003	3.46E-06		0.1	0.6	22.20429	3.96E-06	0.261425
loperamide 2 B-A	0.168573	7200	0.33	0.30783	-0.13926	1.87E-06	0.541126	0.6	0.1	264.9257	1.04E-06	
loperamide 3 A-B	0.168573	7200	0.33	0.14105	0.027523	2.68E-06		0.1	0.6	21.68429	3.11E-06	0.584066
loperamide 3 B-A	0.168573	7200	0.33	0.26864	-0.10007	2.84E-06	1.05959	0.6	0.1	231.8886	1.82E-06	
loperamide 4 A-B	0.168573	7200	0.33	0.14015	0.028423	4.72E-06		0.1	0.6	22.72143	5.38E-06	0.291754
loperamide 4 B-A	0.168573	7200	0.33	0.38592	-0.21735	3.54E-06	0.750265	0.6	0.1	332.8143	1.57E-06	
loperamide 5 A-B	0.168573	7200	0.33	0.14283	0.025743	3.51E-06		0.1	0.6	22.41	3.98E-06	0.333094
loperamide 5 B-A	0.168573	7200	0.33	0.38423	-0.21566	2.98E-06	0.850427	0.6	0.1	331.0457	1.33E-06	
loperamide 6 A-B	0.168573	7200	0.33	0.1256	0.042973	3.03E-06		0.1	0.6	19.67429	3.91E-06	0.480515
loperamide 6 B-A	0.168573	7200	0.33	0.32355	-0.15498	3.54E-06	1.169142	0.6	0.1	279.3529	1.88E-06	

Table A3.44: Apparent Permeabilty (Papp), Exact Permeabiltiy (Pexact), Papp Efflux Ratio and Pexact Efflux Ratio of etoposide in no cell control (NCC) studies on transwell in six replicates at 120 minutes time point

Drug	Initial concentration in donor (uM)	Change in time (s)	Growth area (cm2)	Final concentration in donor (uM)	Change in concentration (uM)	Papp (cm/s)	Efflux ratio (B-A/A-B)	Vd (cm3)	Vr (cm3)	Ct	Pexact	Efflux Ratio (B-A/A-B)
etoposide 1 A-B	0.559327	7200	0.33	0.34885	0.210477	2.74E-05		0.1	0.6	101.8471	3.27E-05	0.537485
etoposide 1 B-A	0.559327	7200	0.33	0.68859	-0.12926	1.81E-05	0.661283	0.6	0.1	624.6143	1.76E-05	
etoposide 2 A-B	0.559327	7200	0.33	0.47043	0.088897	3.39E-05		0.1	0.6	131.5243	3.05E-05	0.645121
etoposide 2 B-A	0.559327	7200	0.33	0.59295	-0.03362	1.71E-05	0.504775	0.6	0.1	540.71	1.97E-05	
etoposide 3 A-B	0.559327	7200	0.33	0.46189	0.097437	3.95E-05		0.1	0.6	141.01	3.5E-05	0.622452
etoposide 3 B-A	0.559327	7200	0.33	0.55767	0.001657	1.74E-05	0.440935	0.6	0.1	511.0843	2.18E-05	
etoposide 4 A-B	0.559327	7200	0.33	0.51636	0.042967	4.18E-05		0.1	0.6	153.06	3.35E-05	0.262011
etoposide 4 B-A	0.559327	7200	0.33	0.92135	-0.36202	1.32E-05	0.316668	0.6	0.1	814.8386	8.77E-06	
etoposide 5 A-B	0.559327	7200	0.33	0.51086	0.048467	4.12E-05		0.1	0.6	151.1429	3.34E-05	0.349733
etoposide 5 B-A	0.559327	7200	0.33	0.82781	-0.26848	1.54E-05	0.373049	0.6	0.1	738.71	1.17E-05	
etoposide 6 A-B	0.559327	7200	0.33	0.48597	0.073357	4.01E-05		0.1	0.6	145.5129	3.4E-05	0.424229
etoposide 6 B-A	0.559327	7200	0.33	0.68863	-0.1293	1.54E-05	0.383012	0.6	0.1	619.3971	1.44E-05	

Table A3.45: Apparent Permeabilty (Papp), Exact Permeabiltiy (Pexact), Papp Efflux Ratio and Pexact Efflux Ratio of lamotrigine in no cell control (NCC) studies on transwell in six replicates at 120 minutes time point

Drug	Initial concentration in donor (uM)	Change in time (s)	Growth area (cm2)	Final concentration in donor (uM)	Change in concentration (uM)	Papp (cm/s)	Efflux ratio (B-A/A-B)	Vd (cm3)	Vr (cm3)	Ct	Pexact	Efflux Ratio (B-A/A-B)
lamotrigine 1 A-B	0.95133	7200	0.33	0.65383	0.2975	2.31E-05		0.1	0.6	167.9329	2.63E-05	1.249072
lamotrigine 1 B-A	0.95133	7200	0.33	1.22038	-0.26905	3.03E-05	1.310715	0.6	0.1	1143.726	3.29E-05	
lamotrigine 2 A-B	0.95133	7200	0.33	0.80115	0.15018	2.02E-05		0.1	0.6	179.79	1.99E-05	1.06813
lamotrigine 2 B-A	0.95133	7200	0.33	1.40483	-0.4535	2.53E-05	1.251804	0.6	0.1	1285.933	2.13E-05	
lamotrigine 3 A-B	0.95133	7200	0.33	0.79457	0.15676	2.60E-05		0.1	0.6	197.5443	2.47E-05	2.048647
lamotrigine 3 B-A	0.95133	7200	0.33	0.98471	-0.03338	3.16E-05	1.213569	0.6	0.1	946.0186	5.07E-05	
lamotrigine 4 A-B	0.95133	7200	0.33	0.8168	0.13453	2.60E-05		0.1	0.6	200.7286	2.42E-05	0.993584
lamotrigine 4 B-A	0.95133	7200	0.33	1.29556	-0.34423	2.57E-05	0.986401	0.6	0.1	1193.38	2.4E-05	
lamotrigine 5 A-B	0.95133	7200	0.33	0.76045	0.19088	2.78E-05		0.1	0.6	198.3786	2.71E-05	1.04144
lamotrigine 5 B-A	0.95133	7200	0.33	1.07011	-0.11878	2.39E-05	0.858198	0.6	0.1	994.2543	2.82E-05	
lamotrigine 6 A-B	0.95133	7200	0.33	0.84487	0.10646	1.73E-05		0.1	0.6	176.4271	1.66E-05	1.981548
lamotrigine 6 B-A	0.95133	7200	0.33	1.18341	-0.23208	2.93E-05	1.699657	0.6	0.1	1109.076	3.29E-05	

Table A3.46: Apparent Permeabilty (Papp), Exact Permeabiltiy (Pexact), Papp Efflux Ratio and Pexact Efflux Ratio of methotrexate in no cell control (NCC) studies on transwell in six replicates at 120 minutes time point

Drug	Initial concentration in donor (uM)	Change in time (s)	Growth area (cm2)	Final concentration in donor (uM)	Change in concentration (uM)	Papp (cm/s)	Efflux ratio (B-A/A-B)	Vd (cm3)	Vr (cm3)	Ct	Pexact	Efflux Ratio (B-A/A-B)
methotrexate 1 A-B	1.188107	7200	0.33	0.87641	0.311697	1.45E-05		0.1	0.6	183.5043	1.67E-05	0.986533
methotrexate 1 B-A	1.188107	7200	0.33	1.22605	-0.03794	1.44E-05	0.996545	0.6	0.1	1109.001	1.65E-05	
methotrexate 2 A-B	1.188107	7200	0.33	0.88476	0.303347	1.05E-05		0.1	0.6	168.7457	1.25E-05	1.550318
methotrexate 2 B-A	1.188107	7200	0.33	1.08519	0.102917	1.46E-05	1.386157	0.6	0.1	988.8686	1.94E-05	
methotrexate 3 A-B	1.188107	7200	0.33	0.89097	0.297137	1.52E-05		0.1	0.6	188.7729	1.72E-05	1.549791
methotrexate 3 B-A	1.188107	7200	0.33	0.85595	0.332157	1.47E-05	0.964083	0.6	0.1	792.9543	2.67E-05	
methotrexate 4 A-B	1.188107	7200	0.33	0.80683	0.381277	1.58E-05		0.1	0.6	179.1786	1.94E-05	0.920509
methotrexate 4 B-A	1.188107	7200	0.33	1.03456	0.153547	1.30E-05	0.820035	0.6	0.1	939.18	1.79E-05	
methotrexate 5 A-B	1.188107	7200	0.33	0.65379	0.534317	1.43E-05		0.1	0.6	150.9729	2.12E-05	0.826737
methotrexate 5 B-A	1.188107	7200	0.33	0.80928	0.378827	1.00E-05	0.701826	0.6	0.1	734.0757	1.76E-05	
methotrexate 6 A-B	1.188107	7200	0.33	0.77993	0.408177	1.32E-05		0.1	0.6	164.6986	1.71E-05	1.134671
methotrexate 6 B-A	1.188107	7200	0.33	1.001	0.187107	1.34E-05	1.01724	0.6	0.1	912.1986	1.94E-05	

Table A3.47: Apparent Permeabilty (Papp), Exact Permeabiltiy (Pexact), Papp Efflux Ratio and Pexact Efflux Ratio of topiramate in no cell control (NCC) studies on transwell in six replicates at 120 minutes time point

Drug	Initial concentration in donor (uM)	Change in time (s)	Growth area (cm2)	Final concentration in donor (uM)	Change in concentration (uM)	Papp (cm/s)	Efflux ratio (B-A/A-B)	Vd (cm3)	Vr (cm3)	Ct	Pexact	Efflux Ratio (B-A/A-B)
topiramate 1 A-B	1.44843	7200	0.33	0.85474	0.59369	1.71E-05		0.1	0.6	206.1314	2.33E-05	1.354977
topiramate 1 B-A	1.44843	7200	0.33	1.02321	0.42522	1.62E-05	0.948213	0.6	0.1	956.7114	3.15E-05	
topiramate 2 A-B	1.44843	7200	0.33	0.71024	0.73819	1.71E-05		0.1	0.6	185.5657	2.71E-05	0.683757
topiramate 2 B-A	1.44843	7200	0.33	1.26232	0.18611	1.34E-05	0.784193	0.6	0.1	1147.941	1.86E-05	
topiramate 3 A-B	1.44843	7200	0.33	0.66604	0.78239	1.47E-05		0.1	0.6	167.5857	2.53E-05	0.872669
topiramate 3 B-A	1.44843	7200	0.33	1.07071	0.37772	1.31E-05	0.886877	0.6	0.1	981.9943	2.21E-05	
topiramate 4 A-B	1.44843	7200	0.33	0.91777	0.53066	1.26E-05		0.1	0.6	193.2529	1.7E-05	0.910669
topiramate 4 B-A	1.44843	7200	0.33	1.44586	0.00257	1.32E-05	1.044414	0.6	0.1	1304.211	1.54E-05	
topiramate 5 A-B	1.44843	7200	0.33	0.8005	0.64793	1.47E-05		0.1	0.6	186.5543	2.17E-05	1.166099
topiramate 5 B-A	1.44843	7200	0.33	1.0051	0.44333	1.36E-05	0.924987	0.6	0.1	928.2957	2.53E-05	
topiramate 6 A-B	1.44843	7200	0.33	0.81927	0.62916	1.35E-05		0.1	0.6	183.4243	1.98E-05	1.003973
topiramate 6 B-A	1.44843	7200	0.33	1.14129	0.30714	1.28E-05	0.948935	0.6	0.1	1041.244	1.99E-05	

Table A3.48: Apparent Permeabilty (Papp), Exact Permeabiltiy (Pexact), Papp Efflux Ratio and Pexact Efflux Ratio of mitoxantrone in no cell control (NCC) studies on transwell in six replicates at 120 minutes time point

Drug	Initial concentration in donor (uM)	Change in time (s)	Growth area (cm2)	Final concentration in donor (uM)	Change in concentration (uM)	Papp (cm/s)	Efflux ratio (B-A/A-B)	Vd (cm3)	Vr (cm3)	Ct	Pexact	Efflux Ratio (B-A/A-B)
mitoxantrone 1 A-B	0.103383	7200	0.33	0.04042	0.062963	5.98E-06		0.1	0.6	7.874286	1.34E-05	0.079125
mitoxantrone 1 B-A	0.103383	7200	0.33	0.07676	0.026623	7.82E-07	0.130612	0.6	0.1	66.06857	1.06E-06	
mitoxantrone 2 A-B	0.103383	7200	0.33	0.04632	0.057063	6.11E-07		0.1	0.6	6.831429	1.34E-06	0.216519
mitoxantrone 2 B-A	0.103383	7200	0.33	0.07972	0.023663	2.24E-07	0.366667	0.6	0.1	68.41	2.91E-07	
mitoxantrone 3 A-B	0.103383	7200	0.33	0.04942	0.053963	9.53E-07		0.1	0.6	7.394286	1.95E-06	0.140762
mitoxantrone 3 B-A	0.103383	7200	0.33	0.06902	0.034363	1.83E-07	0.192308	0.6	0.1	59.22429	2.75E-07	
mitoxantrone 4 A-B	0.103383	7200	0.33	0.04809	0.055293	3.05E-06		0.1	0.6	7.941429	6.18E-06	0.077051
mitoxantrone 4 B-A	0.103383	7200	0.33	0.09771	0.005673	4.48E-07	0.146667	0.6	0.1	83.90857	4.76E-07	
mitoxantrone 5 A-B	0.103383	7200	0.33	0.05298	0.050403	2.10E-06		0.1	0.6	8.305714	3.94E-06	0.192567
mitoxantrone 5 B-A	0.103383	7200	0.33	0.1089	-0.00552	7.94E-07	0.377907	0.6	0.1	93.62143	7.59E-07	
mitoxantrone 6 A-B	0.103383	7200	0.33	0.06565	0.037733	2.32E-06		0.1	0.6	10.19286	3.53E-06	0.138456
mitoxantrone 6 B-A	0.103383	7200	0.33	0.06837	0.035013	3.22E-07	0.138596	0.6	0.1	58.71571	4.89E-07	

Table A3.49: Average recovery percentage of test drugs in no cell control (NCC) studies in apical-to-basal (A-B) and basal-to-apical (B-A) direction on transwell in six replicates at 30 minutes time point

Drug	Rep 1	Rep 2	Rep 3	Rep 4	Rep 5	Rep 6	Average	Std.Dev.	Std Error
camptothecin A-B	126.0690	135.8104	141.0102	119.1541	110.8834	117.1292	125.0094	11.57355	4.725
camptothecin B-A	93.1727	88.9527	109.4908	79.0668	79.2564	82.5041	88.74058	11.59902	4.735
chlorpromazine A-B	354.94789	260.37301	308.98519	579.85738	459.61053	422.61657	397.7318	115.0581	46.97
chlorpromazine B-A	737.61931	852.74822	781.26988	725.38947	761.24246	853.27482	785.2574	55.90627	22.82
loperamide A-B	95.209498	92.174524	59.831819	220.23744	196.47403	161.88171	137.6348	64.48722	26.33
loperamide B-A	213.13098	229.46383	225.02889	259.28596	246.59155	292.32513	244.3044	28.63298	11.69
etoposide A-B	158.51803	175.84035	129.92557	200.20447	188.20847	173.36019	171.0095	24.58023	10.03
etoposide B-A	145.92637	111.73257	121.74866	140.89311	135.25361	185.37697	140.1552	25.49326	10.41
lamotrigine A-B	131.28664	148.92699	201.84008	180.27376	184.22626	182.39856	171.492	26.09556	10.65
lamotrigine B-A	198.52533	145.05849	156.33085	164.2584	154.15985	172.88603	165.2032	18.85082	7.696
methotrexate A-B	146.88252	124.88715	136.31193	127.76285	129.65808	132.37157	132.979	7.854933	3.207
methotrexate B-A	118.29628	94.772541	115.27941	92.26935	92.348404	97.06749	101.6722	11.88	4.85
topiramate A-B	115.19621	120.40285	112.12885	136.34936	122.42432	130.65388	122.8592	9.195933	3.754
topiramate B-A	93.587465	101.58087	124.17503	119.5144	133.60979	143.82844	119.3827	19.00151	7.757
mitoxantrone A-B	106.41579	155.80003	91.742436	239.77674	197.17198	144.57855	155.9143	55.55492	22.68
mitoxantrone B-A	78.852936	92.142048	95.958583	117.66219	164.96522	159.63598	118.2028	36.40358	14.86

Table A3.50: Average recovery percentage of test drugs in no cell control (NCC) studies in apical-to-basal (A-B) and basal-to-apical (B-A) direction on transwell in six replicates at 60 minutes time point

Drug	Rep 1	Rep 2	Rep 3	Rep 4	Rep 5	Rep 6	Average	Std.Dev.	Std Error
camptothecin A-B	152.25896	126.44747	116.99215	124.44931	110.08436	107.15008	122.8971	16.27352	6.644
camptothecin B-A	79.850956	83.680354	82.671687	64.700292	80.977133	71.598827	77.24654	7.494418	3.06
chlorpromazine A-B	383.95928	313.06148	375.19411	392.91425	504.68741	406.68315	396.0833	62.27877	25.43
chlorpromazine B-A	587.22609	657.44234	683.10232	737.65745	747.08403	684.91689	682.9049	58.17846	23.75
loperamide A-B	97.815684	76.498205	100.50756	173.37309	203.92452	183.22699	139.2243	53.73401	21.94
loperamide B-A	150.34713	179.24446	188.25001	263.45394	252.52964	255.31215	214.8562	48.07331	19.63
etoposide A-B	155.72812	163.61512	128.45213	137.54031	145.20014	179.42506	151.6601	18.49364	7.55
etoposide B-A	89.723971	115.88648	92.105378	123.17452	129.14724	137.51961	114.5929	19.68214	8.035
lamotrigine A-B	144.96988	126.0986	145.07434	123.85545	146.19214	163.88747	141.6796	14.80791	6.045
lamotrigine B-A	128.54097	126.8429	119.59836	117.29096	150.02836	130.28857	128.765	11.60928	4.739
methotrexate A-B	151.76768	135.15483	159.75782	112.49773	148.28263	118.37714	137.6396	19.03377	7.771
methotrexate B-A	99.588095	105.26343	121.49096	95.7245	102.39115	89.152214	102.2684	10.95932	4.474
topiramate A-B	66.33258	61.744858	60.418609	76.051149	74.31293	70.943703	68.30064	6.514319	2.659
topiramate B-A	63.872008	65.712993	48.617244	58.123841	69.330835	66.126504	61.9639	7.512321	3.067
mitoxantrone A-B	66.65097	75.635713	64.870974	105.54718	156.91279	94.829535	94.07453	34.71521	14.17
mitoxantrone B-A	63.051736	78.012181	65.872418	123.32203	100.03924	96.096252	87.73231	23.10632	9.433

Table A3.51: Average recovery percentage of test drugs in no cell control (NCC) studies in apical-to-basal (A-B) and basal-to-apical (B-A) direction on transwell in six replicates at 120 minutes time point

Drug	Rep 1	Rep 2	Rep 3	Rep 4	Rep 5	Rep 6	Average	Std.Dev.	Std Error
camptothecin A-B	131.71029	120.51242	132.21417	141.03213	106.07263	103.89677	122.5731	15.11616	6.171
camptothecin B-A	92.106003	92.136368	80.642659	92.762578	87.488114	79.483763	87.43658	6.027688	2.461
chlorpromazine A-B	206.92535	290.04659	297.61391	300.80105	274.51994	276.63334	274.4234	34.7521	14.19
chlorpromazine B-A	567.41563	532.20941	580.18691	670.99193	639.39609	570.14828	593.3914	51.51864	21.03
loperamide A-B	42.628332	92.203195	90.043898	94.350629	93.057423	81.697382	82.33014	19.96587	8.151
loperamide B-A	156.9317	183.35047	160.48604	230.33497	229.11097	193.33524	192.2582	32.08086	13.1
etoposide A-B	127.46219	164.60327	176.47469	191.55532	189.15601	182.11004	171.8936	23.82115	9.725
etoposide B-A	130.28463	112.78353	106.60407	169.9624	154.08318	129.19641	133.819	24.2239	9.889
lamotrigine A-B	123.56701	132.29163	145.35545	147.69849	145.96933	129.8172	137.4499	10.17558	4.154
lamotrigine B-A	140.26118	157.7008	116.0153	146.35055	121.9307	136.01186	136.3784	15.44468	6.305
methotrexate A-B	108.11571	99.420366	111.21981	105.56712	88.949084	97.0359	101.718	8.200942	3.348
methotrexate B-A	108.89889	97.102393	77.864502	92.223201	72.082894	89.573748	89.62427	13.26787	5.417
topiramate A-B	99.619588	89.680551	80.991142	93.395608	90.158309	88.645637	90.41514	6.101697	2.491
topiramate B-A	77.060219	92.463219	79.096677	105.0503	74.771419	83.869086	85.38515	11.49449	4.693
mitoxantrone A-B	53.316137	46.255038	50.066097	53.770756	56.237305	69.014993	54.77672	7.782236	3.177
mitoxantrone B-A	74.557472	77.199742	66.83379	94.689666	105.65049	66.259874	80.86517	15.93013	6.503

Table A3.52: Average Apparent permeability (Papp) of test drugs in no cell control (NCC) studies in apical-to-basal (A-B) and basal-to-apical (B-A) direction on transwell in six replicates at 30 minutes time point

Drug	Rep 1	Rep 2	Rep 3	Rep 4	Rep 5	Rep 6	Average	std. dev.	std error
camptothecin A-B	4.04242E-05	4.05364E-05	4.39228E-05	4.87894E-05	3.34159E-05	3.29393E-05	4.00E-05	6.10E-06	2.49E-06
camptothecin B-A	3.20609E-05	2.94426E-05	1.799E-05	2.39305E-05	1.819E-05	1.68051E-05	2.31E-05	6.50E-06	2.65E-06
chlorpromazine A-B	1.762E-05	1.56253E-05	1.62902E-05	2.54326E-05	1.84511E-05	1.92822E-05	1.88E-05	3.52E-06	1.44E-06
chlorpromazine B-A	7.92345E-06	4.76515E-06	5.67939E-06	6.23348E-06	5.51317E-06	6.42741E-06	6.09E-06	1.07E-06	4.38E-07
loperamide A-B	3.55345E-06	3.37162E-06	3.5015E-06	5.74578E-06	3.33006E-06	3.52747E-06	3.84E-06	9.39E-07	3.83E-07
loperamide B-A	1.3438E-06	9.56765E-07	1.01391E-06	1.99665E-06	1.46588E-06	1.44684E-06	1.37E-06	3.76E-07	1.53E-07
etoposide A-B	0.000116091	0.000112477	7.00346E-05	0.000109916	0.000106467	0.000107933	1.04E-04	1.69E-05	6.90E-06
etoposide B-A	3.44218E-05	3.94302E-05	3.13892E-05	1.96411E-05	2.79402E-05	2.79677E-05	3.01E-05	6.72E-06	2.74E-06
lamotrigine A-B	1.33974E-06	2.04176E-05	3.66151E-05	3.76869E-05	1.5273E-06	8.45376E-06	1.77E-05	1.66E-05	6.78E-06
lamotrigine B-A	3.10931E-05	3.24931E-05	4.12796E-05	3.24239E-05	5.02715E-05	3.61998E-05	3.73E-05	7.36E-06	3.00E-06
methotrexate A-B	1.5566E-05	2.61023E-05	2.1446E-05	1.59497E-05	1.33571E-05	1.47571E-05	1.79E-05	4.89E-06	2.00E-06
methotrexate B-A	1.8328E-05	2.50825E-05	1.81465E-05	1.56956E-05	1.85267E-05	1.60637E-05	1.86E-05	3.38E-06	1.38E-06
topiramate A-B	1.23808E-05	1.82894E-05	3.02422E-05	2.24337E-05	2.15986E-05	1.48966E-05	2.00E-05	6.33E-06	2.58E-06
topiramate B-A	2.34272E-05	2.35263E-05	2.45111E-05	1.68836E-05	2.27591E-05	2.06051E-05	2.20E-05	2.81E-06	1.15E-06
mitoxantrone A-B	3.88287E-06	5.78508E-06	8.43249E-06	6.96171E-06	9.80522E-06	5.19677E-06	6.68E-06	2.18E-06	8.90E-07
mitoxantrone B-A	7.02707E-07	1.97739E-06	7.19049E-06	1.78128E-06	7.02707E-07	4.08551E-07	2.13E-06	2.56E-06	1.05E-06

Table A3.53: Average Apparent permeability (Papp) of test drugs in no cell control (NCC) studies in apical-to-basal (A-B) and basal-to-apical (B-A) direction on transwell in six replicates at 60 minutes time point

Drug	Rep 1	Rep 2	Rep 3	Rep 4	Rep 5	Rep 6	Average	std dev	std error
camptothecin A-B	5.5522E-05	2.54822E-05	2.46008E-05	4.73785E-05	2.28929E-05	2.21918E-05	3.30E-05	1.46E-05	5.94E-06
camptothecin B-A	1.91309E-05	1.36501E-05	1.6499E-05	1.5403E-05	1.46067E-05	1.45099E-05	1.56E-05	1.96E-06	8.02E-07
chlorpromazine A-B	1.708E-05	1.281E-05	1.00214E-05	2.84957E-05	1.68186E-05	2.04786E-05	1.76E-05	6.45E-06	2.63E-06
chlorpromazine B-A	4.15381E-06	3.67452E-06	4.29904E-06	5.06881E-06	5.79499E-06	6.23071E-06	4.87E-06	1.00E-06	4.09E-07
loperamide A-B	3.57049E-06	2.27962E-06	1.78525E-06	9.22835E-06	5.02615E-06	4.7515E-06	4.44E-06	2.68E-06	1.09E-06
loperamide B-A	8.74312E-07	6.77478E-07	1.03453E-06	1.85849E-06	2.00039E-06	2.0187E-06	1.41E-06	6.14E-07	2.51E-07
etoposide A-B	6.29442E-05	5.76865E-05	5.01754E-05	4.41996E-05	4.6684E-05	6.05919E-05	5.37E-05	7.76E-06	3.17E-06
etoposide B-A	1.43081E-05	1.38679E-05	1.7413E-05	1.78834E-05	1.91435E-05	1.31677E-05	1.60E-05	2.48E-06	1.01E-06
lamotrigine A-B	3.12948E-05	3.12622E-05	2.12657E-05	2.56276E-05	1.95198E-05	2.20435E-05	2.52E-05	5.13E-06	2.10E-06
lamotrigine B-A	2.65631E-05	2.47311E-05	3.15169E-05	2.65314E-05	3.24388E-05	3.33117E-05	2.92E-05	3.66E-06	1.49E-06
methotrexate A-B	1.69147E-05	1.8677E-05	1.69255E-05	1.9396E-05	2.28178E-05	1.76932E-05	1.87E-05	2.23E-06	9.09E-07
methotrexate B-A	1.55029E-05	1.33965E-05	1.88401E-05	1.53317E-05	1.71454E-05	1.65787E-05	1.61E-05	1.85E-06	7.55E-07
topiramate A-B	1.00212E-05	1.30666E-05	1.14147E-05	1.06974E-05	9.94152E-06	1.1467E-05	1.11E-05	1.16E-06	4.75E-07
topiramate B-A	1.13589E-05	1.23121E-05	8.69597E-06	1.25673E-05	1.29301E-05	1.1237E-05	1.15E-05	1.54E-06	6.27E-07
mitoxantrone A-B	1.33183E-06	7.61048E-07	6.897E-06	3.32959E-07	1.53161E-05	3.09176E-06	4.62E-06	5.76E-06	2.35E-06
mitoxantrone B-A	1.41904E-06	8.24469E-07	3.96379E-07	2.06117E-07	1.1495E-06	3.56741E-07	7.25E-07	4.87E-07	1.99E-07

Table A3.54: Average Apparent permeability (Papp) of test drugs in no cell control (NCC) studies in apical-to-basal (A-B) and basal-to-apical (B-A) direction on transwell in six replicates at 120 minutes time point

Drug	Rep 1	Rep 2	Rep 3	Rep 4	Rep 5	Rep 6	Average	std dev	std error
camptothecin A-B	2.95078E-05	2.01433E-05	2.26277E-05	3.25548E-05	2.08637E-05	1.76879E-05	2.39E-05	5.83E-06	2.38E-06
camptothecin B-A	2.18298E-05	2.07892E-05	1.75498E-05	1.48174E-05	1.26214E-05	1.38609E-05	1.69E-05	3.79E-06	1.55E-06
chlorpromazine A-B	1.30839E-05	1.28687E-05	1.17067E-05	1.95828E-05	1.44181E-05	1.2094E-05	1.40E-05	2.91E-06	1.19E-06
chlorpromazine B-A	7.36687E-06	8.6724E-06	9.01671E-06	1.21084E-05	1.14699E-05	1.12117E-05	9.97E-06	1.88E-06	7.69E-07
loperamide A-B	2.66647E-06	3.46041E-06	2.68145E-06	4.71874E-06	3.50535E-06	3.02599E-06	3.34E-06	7.65E-07	3.12E-07
loperamide B-A	1.73021E-06	1.87252E-06	2.84123E-06	3.54031E-06	2.98105E-06	3.53781E-06	2.75E-06	7.90E-07	3.22E-07
etoposide A-B	2.73959E-05	3.38791E-05	3.95181E-05	4.17665E-05	4.11705E-05	4.0078E-05	3.73E-05	5.61E-06	2.29E-06
etoposide B-A	1.81164E-05	1.71013E-05	1.74249E-05	1.32261E-05	1.53586E-05	1.53503E-05	1.61E-05	1.80E-06	7.35E-07
lamotrigine A-B	2.30804E-05	2.02348E-05	2.60242E-05	2.60268E-05	2.7792E-05	1.72592E-05	2.34E-05	4.02E-06	1.64E-06
lamotrigine B-A	3.02518E-05	2.533E-05	3.15821E-05	2.56729E-05	2.38511E-05	2.93347E-05	2.77E-05	3.12E-06	1.28E-06
methotrexate A-B	1.44573E-05	1.05018E-05	1.52479E-05	1.58494E-05	1.42766E-05	1.32118E-05	1.39E-05	1.90E-06	7.76E-07
methotrexate B-A	1.44073E-05	1.45572E-05	1.47003E-05	1.29971E-05	1.00197E-05	1.34395E-05	1.34E-05	1.77E-06	7.22E-07
topiramate A-B	1.7091E-05	1.71066E-05	1.47338E-05	1.26399E-05	1.4685E-05	1.3503E-05	1.50E-05	1.83E-06	7.48E-07
topiramate B-A	1.62059E-05	1.34149E-05	1.30671E-05	1.32013E-05	1.35834E-05	1.28134E-05	1.37E-05	1.25E-06	5.10E-07
mitoxantrone A-B	5.9844E-06	6.10653E-07	9.52618E-07	3.05326E-06	2.10065E-06	2.32048E-06	2.50E-06	1.93E-06	7.87E-07
mitoxantrone B-A	7.81635E-07	2.23906E-07	1.83196E-07	4.47812E-07	7.93849E-07	3.2161E-07	4.59E-07	2.71E-07	1.11E-07

Table A3.55: Average Exact permeability (Pexact) of test drugs in no cell control (NCC) studies in apical-to-basal (A-B) and basal-to-apical (B-A) direction on transwell in six replicates at 30 minutes time point

Drug	Rep 1	Rep 2	Rep 3	Rep 4	Rep 5	Rep 6	Average	Std. Dev.	Std Error
camptothecin A-B	3.62627E-05	3.34396E-05	3.50892E-05	4.81585E-05	3.38035E-05	3.13E-05	3.63E-05	6.02819E-06	2.461E-06
camptothecin B-A	3.93097E-05	3.75983E-05	1.74437E-05	3.39681E-05	2.49959E-05	2.2E-05	2.92E-05	8.9867E-06	3.66881E-06
chlorpromazine A-B	5.0515E-06	6.12946E-06	5.37087E-06	4.45405E-06	4.07141E-06	4.64E-06	4.95E-06	7.34146E-07	2.99714E-07
chlorpromazine B-A	1.07821E-06	5.59884E-07	7.28781E-07	8.61898E-07	7.26056E-07	7.55E-07	7.85E-07	1.73253E-07	7.07303E-08
loperamide A-B	3.78136E-06	3.70503E-06	5.97422E-06	2.63278E-06	1.70494E-06	2.2E-06	3.33E-06	1.53296E-06	6.25829E-07
loperamide B-A	6.31886E-07	4.1756E-07	4.51274E-07	7.7212E-07	5.95686E-07	4.96E-07	5.61E-07	1.32413E-07	5.40573E-08
etoposide A-B	0.000102208	8.45153E-05	6.74877E-05	6.90898E-05	7.18055E-05	8.15E-05	7.94E-05	1.30888E-05	5.34348E-06
etoposide B-A	2.57562E-05	4.04693E-05	2.84025E-05	1.46606E-05	2.22945E-05	1.59E-05	2.46E-05	9.4532E-06	3.85925E-06
lamotrigine A-B	1.02409E-06	1.44055E-05	1.93865E-05	2.25839E-05	8.31427E-07	4.71E-06	1.05E-05	9.56067E-06	3.90313E-06
lamotrigine B-A	1.6579E-05	2.43425E-05	2.91634E-05	2.1227E-05	3.69649E-05	2.26E-05	2.51E-05	7.09352E-06	2.89592E-06
methotrexate A-B	1.10069E-05	2.25785E-05	1.66586E-05	1.30571E-05	1.0688E-05	1.16E-05	1.43E-05	4.62173E-06	1.88682E-06
methotrexate B-A	1.63898E-05	2.92378E-05	1.66679E-05	1.80998E-05	2.16008E-05	1.76E-05	1.99E-05	4.92919E-06	2.01233E-06
topiramate A-B	1.11689E-05	1.60506E-05	2.98574E-05	1.74691E-05	1.88177E-05	1.19E-05	1.75E-05	6.75619E-06	2.7582E-06
topiramate B-A	2.74927E-05	2.52452E-05	2.12265E-05	1.4867E-05	1.81262E-05	1.51E-05	2.03E-05	5.262E-06	2.1482E-06
mitoxantrone A-B	3.69569E-06	3.76175E-06	9.49727E-06	2.93302E-06	5.06064E-06	3.64E-06	4.76E-06	2.41883E-06	9.87482E-07
mitoxantrone B-A	8.93925E-07	2.16214E-06	7.6949E-06	1.52189E-06	4.26603E-07	2.56E-07	2.16E-06	2.80266E-06	1.14418E-06

Table A3.56: Average Exact permeability (Pexact) of test drugs in no cell control (NCC) studies in apical-to-basal (A-B) and basal-to-apical (B-A) direction on transwell in six replicates at 60 minutes time point

Drug	Rep 1	Rep 2	Rep 3	Rep 4	Rep 5	Rep 6	Average	Std. Dev.	Std Error
camptothecin A-B	5.07959E-05	2.36328E-05	2.48576E-05	5.41163E-05	2.45311E-05	2.44E-05	3.37E-05	1.45531E-05	5.94128E-06
camptothecin B-A	2.91168E-05	1.84918E-05	2.33625E-05	2.88903E-05	2.0757E-05	2.38E-05	2.41E-05	4.27497E-06	1.74525E-06
chlorpromazine A-B	4.59143E-06	4.21246E-06	2.72169E-06	7.64332E-06	3.41189E-06	5.22E-06	4.63E-06	1.71635E-06	7.00696E-07
chlorpromazine B-A	7.10851E-07	5.61088E-07	6.32102E-07	6.90442E-07	7.79882E-07	9.15E-07	7.15E-07	1.22952E-07	5.01949E-08
loperamide A-B	3.7458E-06	3.04326E-06	1.79846E-06	5.52939E-06	2.50779E-06	2.64E-06	3.21E-06	1.30413E-06	5.32409E-07
loperamide B-A	5.83885E-07	3.78956E-07	5.51653E-07	7.08902E-07	7.96521E-07	7.95E-07	6.36E-07	1.62652E-07	6.64024E-08
etoposide A-B	5.92685E-05	4.83937E-05	5.62455E-05	4.25333E-05	4.25617E-05	4.55E-05	4.91E-05	7.12022E-06	2.90682E-06
etoposide B-A	1.80212E-05	1.30847E-05	2.1923E-05	1.62109E-05	1.65928E-05	1.03E-05	1.60E-05	4.0214E-06	1.64173E-06
lamotrigine A-B	2.56515E-05	3.03758E-05	1.6386E-05	2.43847E-05	1.4765E-05	1.49E-05	2.11E-05	6.61084E-06	2.69887E-06
lamotrigine B-A	2.43476E-05	2.27296E-05	3.27932E-05	2.71408E-05	2.57009E-05	3.16E-05	2.74E-05	4.01336E-06	1.63845E-06
methotrexate A-B	1.21063E-05	1.534E-05	1.1458E-05	1.97023E-05	1.73075E-05	1.67E-05	1.54E-05	3.17319E-06	1.29545E-06
methotrexate B-A	1.75353E-05	1.40014E-05	1.74593E-05	1.81107E-05	1.90531E-05	2.15E-05	1.79E-05	2.4447E-06	9.98043E-07
topiramate A-B	1.69518E-05	2.50478E-05	2.19057E-05	1.56463E-05	1.47965E-05	1.83E-05	1.88E-05	3.95768E-06	1.61572E-06
topiramate B-A	2.04188E-05	2.1694E-05	2.05553E-05	2.57007E-05	2.15774E-05	1.94E-05	2.16E-05	2.20182E-06	8.98888E-07
mitoxantrone A-B	2.02641E-06	1.01328E-06	1.15018E-05	3.16151E-07	1.04875E-05	3.34E-06	4.78E-06	4.93029E-06	2.01278E-06
mitoxantrone B-A	2.28644E-06	1.06466E-06	6.04261E-07	1.67331E-07	1.1583E-06	3.72E-07	9.42E-07	7.62655E-07	3.11353E-07

Table A3.57: Average Exact permeability (Pexact) of test drugs in no cell control (NCC) studies in apical-to-basal (A-B) and basal-to-apical (B-A) direction on transwell in six replicates at 120 minutes time point

Drug	Rep 1	Rep 2	Rep 3	Rep 4	Rep 5	Rep 6	Average	Std. Dev.	Std Error
camptothecin A-B	3.50033E-05	2.24523E-05	2.32049E-05	3.68429E-05	2.84259E-05	2.3E-05	2.82E-05	6.41405E-06	2.61853E-06
camptothecin B-A	3.85997E-05	3.54278E-05	3.33501E-05	2.10969E-05	1.8422E-05	2.38E-05	2.85E-05	8.38709E-06	3.42402E-06
chlorpromazine A-B	6.9518E-06	4.73427E-06	4.16494E-06	7.17952E-06	5.67615E-06	4.66E-06	5.56E-06	1.26577E-06	5.16749E-07
chlorpromazine B-A	1.32226E-06	1.66746E-06	1.58857E-06	1.85124E-06	1.84001E-06	2.02E-06	1.72E-06	2.45348E-07	1.00163E-07
loperamide A-B	6.86961E-06	3.96294E-06	3.10806E-06	5.38376E-06	3.9784E-06	3.91E-06	4.54E-06	1.35919E-06	5.54886E-07
loperamide B-A	1.11972E-06	1.03601E-06	1.81531E-06	1.57073E-06	1.32518E-06	1.88E-06	1.46E-06	3.54079E-07	1.44552E-07
etoposide A-B	3.26779E-05	3.04917E-05	3.49756E-05	3.34546E-05	3.33574E-05	3.4E-05	3.32E-05	1.51231E-06	6.17399E-07
etoposide B-A	1.75639E-05	1.96708E-05	2.17706E-05	8.76545E-06	1.16662E-05	1.44E-05	1.56E-05	4.94147E-06	2.01735E-06
lamotrigine A-B	2.63105E-05	1.99004E-05	2.47389E-05	2.41829E-05	2.70674E-05	1.66E-05	2.31E-05	4.06429E-06	1.65924E-06
lamotrigine B-A	3.28637E-05	2.12562E-05	5.06813E-05	2.40278E-05	2.81891E-05	3.29E-05	3.16E-05	1.04234E-05	4.25535E-06
methotrexate A-B	1.67065E-05	1.24983E-05	1.72471E-05	1.9414E-05	2.1235E-05	1.71E-05	1.74E-05	2.94552E-06	1.2025E-06
methotrexate B-A	1.64815E-05	1.93763E-05	2.67294E-05	1.78708E-05	1.75557E-05	1.94E-05	1.96E-05	3.68261E-06	1.50342E-06
topiramate A-B	2.32844E-05	2.71425E-05	2.53154E-05	1.69644E-05	2.16658E-05	1.98E-05	2.24E-05	3.70556E-06	1.51279E-06
topiramate B-A	3.15499E-05	1.85589E-05	2.2092E-05	1.5449E-05	2.52644E-05	1.99E-05	2.21E-05	5.67553E-06	2.31703E-06
mitoxantrone A-B	1.34458E-05	1.34495E-06	1.95474E-06	6.17842E-06	3.94319E-06	3.53E-06	5.07E-06	4.44085E-06	1.81297E-06
mitoxantrone B-A	1.0639E-06	2.91207E-07	2.75153E-07	4.76053E-07	7.59327E-07	4.89E-07	5.59E-07	3.03039E-07	1.23715E-07

Table A3.58: Average Apparent permeability Efflux Ratio of test drugs in no cell control (NCC) studies on transwell in six replicates at 30 minutes time point

Drug	Rep 1	Rep 2	Rep 3	Rep 4	Rep 5	Rep 6	Average	std dev	std error
camptothecin	0.793111	0.726325	0.409582	0.490485	0.544351	0.510184	0.579007	0.148339	0.060559
chlorpromazine	0.449686	0.304965	0.348639	0.245098	0.298799	0.333333	0.330087	0.068545	0.027983
loperamide	0.378168	0.28377	0.289565	0.347498	0.440198	0.410162	0.358227	0.063541	0.025941
etoposide	0.296507	0.350563	0.448196	0.178692	0.262431	0.259121	0.299252	0.092006	0.037561
lamotrigine	23.20833	1.591426	1.127394	0.860351	32.9152	4.282092	10.66413	13.87498	5.664436
methotrexate	1.177437	0.960932	0.846148	0.98407	1.387034	1.088545	1.074028	0.190625	0.077822
topiramate	1.892215	1.286339	0.810494	0.752598	1.05373	1.383205	1.19643	0.422701	0.172567
mitoxantrone	0.180976	0.341808	0.852713	0.255869	0.071667	0.078616	0.296942	0.291357	0.118946

Table A3.59: Average Apparent permeability Efflux Ratio of test drugs in no cell control (NCC) studies on transwell in six replicates at 60 minutes time point

Drug	Rep 1	Rep 2	Rep 3	Rep 4	Rep 5	Rep 6	Average	std dev	std error
camptothecin	0.344564	0.535672	0.67067	0.325106	0.638044	0.65384	0.527983	0.156955	0.064077
chlorpromazine	0.243197	0.286848	0.428986	0.17788	0.34456	0.304255	0.297621	0.08593	0.035081
loperamide	0.244872	0.297189	0.579487	0.201389	0.397996	0.424855	0.357631	0.138671	0.056612
etoposide	0.227314	0.240402	0.347042	0.404606	0.410066	0.217318	0.307791	0.090086	0.036777
lamotrigine	0.848801	0.791087	1.482055	1.035265	1.661837	1.511185	1.221705	0.375379	0.153248
methotrexate	0.916534	0.71727	1.113116	0.790459	0.751402	0.93701	0.870965	0.147969	0.060408
topiramate	1.13348	0.942259	0.761819	1.174803	1.300617	0.979946	1.048821	0.192307	0.078509
mitoxantrone	1.065476	1.083333	0.057471	0.619048	0.075052	0.115385	0.502627	0.489594	0.199876

Table A3.60: Average Apparent permeability Efflux Ratio of test drugs in no cell control (NCC) studies on transwell in six replicates at 120 minutes time point

Drug	Rep 1	Rep 2	Rep 3	Rep 4	Rep 5	Rep 6	Average	std dev	std error
camptothecin	0.739799	1.032063	0.77559	0.455154	0.604944	0.783641	0.731865	0.193625	0.079047
chlorpromazine	0.563048	0.673913	0.770221	0.618315	0.795522	0.927046	0.724678	0.13271	0.054179
loperamide	0.648876	0.541126	1.05959	0.750265	0.850427	1.169142	0.836571	0.241039	0.098404
etoposide	0.661283	0.504775	0.440935	0.316668	0.373049	0.383012	0.44662	0.123159	0.050279
lamotrigine	1.310715	1.251804	1.213569	0.986401	0.858198	1.699657	1.220057	0.291486	0.118999
methotrexate	0.996545	1.386157	0.964083	0.820035	0.701826	1.01724	0.980981	0.232311	0.09484
topiramate	0.948213	0.784193	0.886877	1.044414	0.924987	0.948935	0.922936	0.085587	0.034941
mitoxantrone	0.130612	0.366667	0.192308	0.146667	0.377907	0.138596	0.225459	0.115783	0.047268

Table A3.61: Average Exact Permeability Efflux Ratio of test drugs in no cell control (NCC) studies on transwell in six replicates at 30 minutes time point

Drug	Rep 1	Rep 2	Rep 3	Rep 4	Rep 5	Rep 6	Average	std dev	std error
camptothecin	1.084025	1.124364	0.497125	0.705338	0.739447	0.701971	0.808712	0.244703	0.099899
chlorpromazine	0.213444	0.091343	0.135691	0.193509	0.17833	0.162897	0.162536	0.043794	0.017879
loperamide	0.167105	0.112701	0.075537	0.293272	0.349388	0.225805	0.203968	0.105624	0.043121
etoposide	0.251998	0.47884	0.420855	0.212196	0.310485	0.195565	0.311656	0.11559	0.047189
lamotrigine	16.18893	1.689801	1.504314	0.939919	44.45958	4.802268	11.59747	17.09264	6.978041
methotrexate	1.489049	1.294939	1.000557	1.386197	2.021032	1.514982	1.451126	0.33524	0.136861
topiramate	2.461542	1.572848	0.710931	0.851047	0.963253	1.270342	1.304994	0.645959	0.263712
mitoxantrone	0.241883	0.574768	0.810222	0.518882	0.084298	0.070373	0.383405	0.298204	0.121741

Table A3.62: Average Exact Permeability Efflux Ratio of test drugs in no cell control (NCC) studies on transwell in six replicates at 60 minutes time point

Drug	Rep 1	Rep 2	Rep 3	Rep 4	Rep 5	Rep 6	Average	std dev	std error
camptothecin	0.573212	0.782465	0.939852	0.533857	0.846152	0.974519	0.775009	0.184917	0.075492
chlorpromazine	0.154821	0.133197	0.232246	0.090333	0.228578	0.175385	0.169093	0.055248	0.022555
loperamide	0.155877	0.124523	0.306736	0.128206	0.317618	0.301041	0.222334	0.095122	0.038833
etoposide	0.30406	0.270381	0.389772	0.381134	0.389853	0.225573	0.326795	0.070485	0.028775
lamotrigine	0.94917	0.74828	2.001293	1.113023	1.74067	2.120682	1.44552	0.58222	0.237691
methotrexate	1.44844	0.912734	1.523764	0.919219	1.100864	1.283995	1.198169	0.26259	0.107202
topiramate	1.204522	0.866104	0.938354	1.642608	1.458274	1.058867	1.194788	0.304082	0.124141
mitoxantrone	1.128319	1.050705	0.052536	0.529276	0.110446	0.111558	0.49714	0.490251	0.200144

Table A3.63: Average Exact Permeability Efflux Ratio of test drugs in no cell control (NCC) studies on transwell in six replicates at 120 minutes time point

Drug	Rep 1	Rep 2	Rep 3	Rep 4	Rep 5	Rep 6	Average	std dev	std error
camptothecin	1.102745	1.577915	1.437201	0.572617	0.648069	1.03443	1.062163	0.405018	0.165348
chlorpromazine	0.190204	0.35221	0.381416	0.257851	0.324165	0.433893	0.32329	0.087685	0.035797
loperamide	0.162996	0.261425	0.584066	0.291754	0.333094	0.480515	0.352308	0.153807	0.062792
etoposide	0.537485	0.645121	0.622452	0.262011	0.349733	0.424229	0.473505	0.153758	0.062772
lamotrigine	1.249072	1.06813	2.048647	0.993584	1.04144	1.981548	1.39707	0.486939	0.198792
methotrexate	0.986533	1.550318	1.549791	0.920509	0.826737	1.134671	1.161426	0.317309	0.129541
topiramate	1.354977	0.683757	0.872669	0.910669	1.166099	1.003973	0.998691	0.235714	0.09623
mitoxantrone	0.079125	0.216519	0.140762	0.077051	0.192567	0.138456	0.140747	0.057072	0.0233

Appendix 4

Additional data from LC-MS/MS analysis on Transwell model of Horse BBB for drug transport studies

Table A4.1: Recovery percentage of camptothecin and chlorpromazine in Transwell model of Horse BBB for drug transport studies in both apical-to-basal (A-B) and basal-to-apical (B-A) direction in three replicates at 30 minutes time point

Drug	Conc apical start (nM)	conc apical end (nM)	Conc basolateral start (nM)	Conc basolateral end (nM)	amount apical start (nmol)	amount apical end (nmol)	amount basolateral start (nmol)	amount basolateral end (nmol)	Total in well start (nmol)	Total in well end (nmol)	Recovery (%)
camptothecin 1 A-B	956.46	565.25	0	76.96	0.096	0.057	0.000	0.046	0.096	0.103	107
camptothecin 1 B-A	0	205.9	956.46	792.11	0.000	0.021	0.574	0.475	0.574	0.496	86
camptothecin 2 A-B	1013.55	782.53	0	88.63	0.101	0.078	0.000	0.053	0.101	0.131	130
camptothecin 2 B-A	0	234.36	1013.55	894.12	0.000	0.023	0.608	0.536	0.608	0.560	92
camptothecin 3 A-B	732.39	801.55	0	62.58	0.073	0.080	0.000	0.038	0.073	0.118	161
camptothecin 3 B-A	0	73.81	732.39	736.24	0.000	0.007	0.439	0.442	0.439	0.449	102
chlorpromazine 1 A-B	68.69	54.04	0	32.65	0.007	0.005	0.000	0.020	0.007	0.025	364
chlorpromazine 1 B-A	0	34.89	68.69	76.95	0.000	0.003	0.041	0.046	0.041	0.050	120
chlorpromazine 2 A-B	59.75	42.39	0	27.71	0.006	0.004	0.000	0.017	0.006	0.021	349
chlorpromazine 2 B-A	0	30.88	59.75	59.65	0.000	0.003	0.036	0.036	0.036	0.039	108
chlorpromazine 3 A-B	53.86	37.19	0	27.32	0.005	0.004	0.000	0.016	0.005	0.020	373
chlorpromazine 3 B-A	0	27.11	53.86	57.58	0.000	0.003	0.032	0.035	0.032	0.037	115

Table A4.2: Recovery percentage of loperamide and etoposide in Transwell model of Horse BBB for drug transport studies in both apical-to-basal (A-B) and basal-to-apical (B-A) direction in three replicates at 30 minutes time point

Drug	Conc apical start (nM)	conc apical end (nM)	Conc basolateral start (nM)	Conc basolateral end (nM)	amount apical start (nmol)	amount apical end (nmol)	amount basolateral start (nmol)	amount basolateral end (nmol)	Total in well start (nmol)	Total in well end (nmol)	Recovery (%)
loperamide 1 A-B	209.22	186.7	0	43.09	0.021	0.019	0.000	0.026	0.021	0.045	213
loperamide 1 B-A	0	58.09	209.22	257.05	0.000	0.006	0.126	0.154	0.126	0.160	127
loperamide 2 A-B	149.37	264.07	0	32.65	0.015	0.026	0.000	0.020	0.015	0.046	308
loperamide 2 B-A	0	109.05	149.37	217.27	0.000	0.011	0.090	0.130	0.090	0.141	158
loperamide 3 A-B	224.71	149.64	0	30.76	0.022	0.015	0.000	0.018	0.022	0.033	149
loperamide 3 B-A	0	35.49	224.71	261.75	0.000	0.004	0.135	0.157	0.135	0.161	119
etoposide 1 A-B	688.37	594.65	0	45.06	0.069	0.059	0.000	0.027	0.069	0.087	126
etoposide 1 B-A	0	156.69	688.37	635.6	0.000	0.016	0.413	0.381	0.413	0.397	96
etoposide 2 A-B	517.57	268.07	0	34.38	0.052	0.027	0.000	0.021	0.052	0.047	92
etoposide 2 B-A	0	87.85	517.57	338.18	0.000	0.009	0.311	0.203	0.311	0.212	68
etoposide 3 A-B	261.3	239.68	0	34.13	0.026	0.024	0.000	0.020	0.026	0.044	170
etoposide 3 B-A	0	42.28	261.3	283.2	0.000	0.004	0.157	0.170	0.157	0.174	111

Table A4.3: Recovery percentage of lamotrigine and methotrexate in Transwell model of Horse BBB for drug transport studies in both apical-to-basal (A-B) and basal-to-apical (B-A) direction in three replicates at 30 minutes time point

Drug	Conc apical start (nM)	conc apical end (nM)	Conc basolateral start (nM)	Conc basolateral end (nM)	amount apical start (nmol)	amount apical end (nmol)	amount basolateral start (nmol)	amount basolateral end (nmol)	Total in well start (nmol)	Total in well end (nmol)	Recovery (%)
lamotrigine 1 A-B	675.54	400.48	0	41.64	0.068	0.040	0.000	0.025	0.068	0.065	96
lamotrigine 1 B-A	0	197.43	675.54	803.99	0.000	0.020	0.405	0.482	0.405	0.502	124
lamotrigine 2 A-B	858.36	577.41	0	21.27	0.086	0.058	0.000	0.013	0.086	0.071	82
lamotrigine 2 B-A	0	205.33	858.36	790.36	0.000	0.021	0.515	0.474	0.515	0.495	96
lamotrigine 3 A-B	727.96	606.61	0	20.9	0.073	0.061	0.000	0.013	0.073	0.073	101
lamotrigine 3 B-A	0	117.93	727.96	848.65	0.000	0.012	0.437	0.509	0.437	0.521	119
methotrexate 1 A-B	581.33	840.81	0	27.02	0.058	0.084	0.000	0.016	0.058	0.100	173
methotrexate 1 B-A	0	150.33	581.33	755.65	0.000	0.015	0.349	0.453	0.349	0.468	134
methotrexate 2 A-B	1544.93	1094.7	0	35.36	0.154	0.109	0.000	0.021	0.154	0.131	85
methotrexate 2 B-A	0	241.75	1544.93	1460.68	0.000	0.024	0.927	0.876	0.927	0.901	97
methotrexate 3 A-B	795.81	674.72	0	4.11	0.080	0.067	0.000	0.002	0.080	0.070	88
methotrexate 3 B-A	0	40.31	795.81	753.33	0.000	0.004	0.477	0.452	0.477	0.456	96

Table A4.4: Recovery percentage of topiramate, mitoxantrone and loperamide 10x in Transwell model of Horse BBB for drug transport studies in both apical-to-basal (A-B) and basal-to-apical (B-A) direction in three replicates at 30 minutes time point

Drug	Conc apical start (nM)	conc apical end (nM)	Conc basolateral start (nM)	Conc basolateral end (nM)	amount apical start (nmol)	amount apical end (nmol)	amount basolateral start (nmol)	amount basolateral end (nmol)	Total in well start (nmol)	Total in well end (nmol)	Recovery (%)
topiramate 1 A-B	686.18	1219.87	0	9.9	0.069	0.122	0.000	0.006	0.069	0.128	186
topiramate 1 B-A	0	1	686.18	1465.69	0.000	0.000	0.412	0.879	0.412	0.880	214
topiramate 2 A-B	2140.91	1506.47	0	1	0.214	0.151	0.000	0.001	0.214	0.151	71
topiramate 2 B-A	0	1	2140.91	888.175	0.000	0.000	1.285	0.533	1.285	0.533	41
topiramate 3 A-B	75.74	2052.49	0	209.21	0.008	0.205	0.000	0.126	0.008	0.331	4367
topiramate 3 B-A	0	1942.92	75.74	874.66	0.000	0.194	0.045	0.525	0.045	0.719	1582
mitoxantrone 1 A-B	77.54	143.72	0	39.7	0.008	0.014	0.000	0.024	0.008	0.038	493
mitoxantrone 1 B-A	0	42.86	77.54	233.15	0.000	0.004	0.047	0.140	0.047	0.144	310
mitoxantrone 2 A-B	139.7	120.87	0	41.45	0.014	0.012	0.000	0.025	0.014	0.037	265
mitoxantrone 2 B-A	0	41.38	139.7	110.98	0.000	0.004	0.084	0.067	0.084	0.071	84
mitoxantrone 3 A-B	91.81	219.79	0	42.71	0.009	0.022	0.000	0.026	0.009	0.048	519
mitoxantrone 3 B-A	0	41.3	91.81	156.77	0.000	0.004	0.055	0.094	0.055	0.098	178
loperamide 10x 1 A-B	4319.02	3018.26	0	183.28	0.432	0.302	0.000	0.110	0.432	0.412	95
loperamide 10x 1 B-A	0	1593.31	4319.02	3938.82	0.000	0.159	2.591	2.363	2.591	2.523	97
loperamide 10x 2 A-B	3230.87	2330.28	0	76.76	0.323	0.233	0.000	0.046	0.323	0.279	86
loperamide 10x 2 B-A	0	250.43	3230.87	3448.88	0.000	0.025	1.939	2.069	1.939	2.094	108

Table A4.5: Recovery percentage of camptothecin and chlorpromazine in Transwell model of Horse BBB for drug transport studies in both apical-to-basal (A-B) and basal-to-apical (B-A) direction in three replicates at 60 minutes time point

Drug	Conc apical start (nM)	conc apical end (nM)	Conc basolateral start (nM)	Conc basolateral end (nM)	amount apical start (nmol)	amount apical end (nmol)	amount basolateral start (nmol)	amount basolateral end (nmol)	Total in well start (nmol)	Total in well end (nmol)	Recovery (%)
camptothecin 1 A-B	837.2	668.29	0	79.38	0.084	0.067	0.000	0.048	0.084	0.114	137
camptothecin 1 B-A	0	316.24	837.2	1198.17	0.000	0.032	0.502	0.719	0.502	0.751	149
camptothecin 2 A-B	1187.03	921.23	0	80.31	0.119	0.092	0.000	0.048	0.119	0.140	118
camptothecin 2 B-A	0	127.8	1187.03	814.39	0.000	0.013	0.712	0.489	0.712	0.501	70
camptothecin 3 A-B	1001.05	837.44	0	74.87	0.100	0.084	0.000	0.045	0.100	0.129	129
camptothecin 3 B-A	0	224.14	1001.05	812.18	0.000	0.022	0.601	0.487	0.601	0.510	85
chlorpromazine 1 A-B	57.46	52.03	0	33.52	0.006	0.005	0.000	0.020	0.006	0.025	441
chlorpromazine 1 B-A	0	37.01	57.46	74.91	0.000	0.004	0.034	0.045	0.034	0.049	141
chlorpromazine 2 A-B	54.61	36.97	0	27.27	0.005	0.004	0.000	0.016	0.005	0.020	367
chlorpromazine 2 B-A	0	29.64	54.61	66.74	0.000	0.003	0.033	0.040	0.033	0.043	131
chlorpromazine 3 A-B	61.8	46.69	0	27.46	0.006	0.005	0.000	0.016	0.006	0.021	342
chlorpromazine 3 B-A	0	28.77	61.8	65.64	0.000	0.003	0.037	0.039	0.037	0.042	114

Table A4.6: Recovery percentage of loperamide and etoposide in Transwell model of Horse BBB for drug transport studies in both apical-to-basal (A-B) and basal-to-apical (B-A) direction in three replicates at 60 minutes time point

Drug	Conc apical start (nM)	conc apical end (nM)	Conc basolateral start (nM)	Conc basolateral end (nM)	amount apical start (nmol)	amount apical end (nmol)	amount basolateral start (nmol)	amount basolateral end (nmol)	Total in well start (nmol)	Total in well end (nmol)	Recovery (%)
loperamide 1 A-B	175.72	162.26	0	44.92	0.018	0.016	0.000	0.027	0.018	0.043	246
loperamide 1 B-A	0	72.63	175.72	278.05	0.000	0.007	0.105	0.167	0.105	0.174	165
loperamide 2 A-B	145.84	111.92	0	30.95	0.015	0.011	0.000	0.019	0.015	0.030	204
loperamide 2 B-A	0	49.53	145.84	277.29	0.000	0.005	0.088	0.166	0.088	0.171	196
loperamide 3 A-B	230.1	231.32	0	34.72	0.023	0.023	0.000	0.021	0.023	0.044	191
loperamide 3 B-A	0	86.67	230.1	427.97	0.000	0.009	0.138	0.257	0.138	0.265	192
etoposide 1 A-B	1108.85	664.98	0	59.8	0.111	0.066	0.000	0.036	0.111	0.102	92
etoposide 1 B-A	0	315.92	1108.85	609.93	0.000	0.032	0.665	0.366	0.665	0.398	60
etoposide 2 A-B	382.06	243.41	0	36.01	0.038	0.024	0.000	0.022	0.038	0.046	120
etoposide 2 B-A	0	65.17	382.06	333.53	0.000	0.007	0.229	0.200	0.229	0.207	90
etoposide 3 A-B	344.77	254.09	0	44.39	0.034	0.025	0.000	0.027	0.034	0.052	151
etoposide 3 B-A	0	105.25	344.77	302.77	0.000	0.011	0.207	0.182	0.207	0.192	93

Table A4.7: Recovery percentage of lamotrigine and methotrexate in Transwell model of Horse BBB for drug transport studies in both apical-to-basal (A-B) and basal-to-apical (B-A) direction in three replicates at 60 minutes time point

Drug	Conc apical start (nM)	conc apical end (nM)	Conc basolateral start (nM)	Conc basolateral end (nM)	amount apical start (nmol)	amount apical end (nmol)	amount basolateral start (nmol)	amount basolateral end (nmol)	Total in well start (nmol)	Total in well end (nmol)	Recovery (%)
lamotrigine 1 A-B	689.41	543	0	48.53	0.069	0.054	0.000	0.029	0.069	0.083	121
lamotrigine 1 B-A	0	395.41	689.41	895.37	0.000	0.040	0.414	0.537	0.414	0.577	139
lamotrigine 2 A-B	1041.3	361.3	0	34.07	0.104	0.036	0.000	0.020	0.104	0.057	54
lamotrigine 2 B-A	0	185.81	1041.3	701.44	0.000	0.019	0.625	0.421	0.625	0.439	70
lamotrigine 3 A-B	1055.11	807.35	0	64.74	0.106	0.081	0.000	0.039	0.106	0.120	113
lamotrigine 3 B-A	0	430.12	1055.11	897.2	0.000	0.043	0.633	0.538	0.633	0.581	92
methotrexate 1 A-B	629.08	688.56	0	36.54	0.063	0.069	0.000	0.022	0.063	0.091	144
methotrexate 1 B-A	0	288.95	629.08	684.86	0.000	0.029	0.377	0.411	0.377	0.440	117
methotrexate 2 A-B	1227.65	761.67	0	9.55	0.123	0.076	0.000	0.006	0.123	0.082	67
methotrexate 2 B-A	0	71.6	1227.65	1129.4	0.000	0.007	0.737	0.678	0.737	0.685	93
methotrexate 3 A-B	946.1	1307.47	0	33.31	0.095	0.131	0.000	0.020	0.095	0.151	159
methotrexate 3 B-A	0	120.54	946.1	933.77	0.000	0.012	0.568	0.560	0.568	0.572	101

Table A4.8: Recovery percentage of topiramate, mitoxantrone and loperamide 10x in Transwell model of Horse BBB for drug transport studies in both apical-to-basal (A-B) and basal-to-apical (B-A) direction in three replicates at 60 minutes time point

Drug	Conc apical start (nM)	conc apical end (nM)	Conc basolateral start (nM)	Conc basolateral end (nM)	amount apical start (nmol)	amount apical end (nmol)	amount basolateral start (nmol)	amount basolateral end (nmol)	Total in well start (nmol)	Total in well end (nmol)	Recovery (%)
topiramate 1 A-B	1173.52	369.11	0	1	0.117	0.037	0.000	0.001	0.117	0.038	32
topiramate 1 B-A	0	1	1173.52	79.2	0.000	0.000	0.704	0.048	0.704	0.048	7
topiramate 2 A-B	3792.96	1	0	1	0.379	0.000	0.000	0.001	0.379	0.001	0
topiramate 2 B-A	0	1	3792.96	1022.34	0.000	0.000	2.276	0.613	2.276	0.614	27
topiramate 3 A-B	546.06	1539.97	0	361.13	0.055	0.154	0.000	0.217	0.055	0.371	679
topiramate 3 B-A	0	1	546.06	326.98	0.000	0.000	0.328	0.196	0.328	0.196	60
mitoxantrone 1 A-B	89.27	106.58	0	39.24	0.009	0.011	0.000	0.024	0.009	0.034	383
mitoxantrone 1 B-A	0	41.73	89.27	133	0.000	0.004	0.054	0.080	0.054	0.084	157
mitoxantrone 2 A-B	116.84	173.45	0	41.75	0.012	0.017	0.000	0.025	0.012	0.042	363
mitoxantrone 2 B-A	0	42.8	116.84	167.95	0.000	0.004	0.070	0.101	0.070	0.105	150
mitoxantrone 3 A-B	112.43	135.5	0	42.89	0.011	0.014	0.000	0.026	0.011	0.039	349
mitoxantrone 3 B-A	0	41.37	112.43	128.19	0.000	0.004	0.067	0.077	0.067	0.081	120
loperamide 10x 1 A-B	4150.71	1785.86	0	96.56	0.415	0.179	0.000	0.058	0.415	0.237	57
loperamide 10x 1 B-A	0	838.77	4150.71	3654.33	0.000	0.084	2.490	2.193	2.490	2.276	91
loperamide 10x 2 A-B	3898.38	2805.97	0	364.34	0.390	0.281	0.000	0.219	0.390	0.499	128
loperamide 10x 2 B-A	0	1391.31	3898.38	3927.12	0.000	0.139	2.339	2.356	2.339	2.495	107

Table A4.9: Recovery percentage of camptothecin, chlorpromazine and loperamide in Transwell model of Horse BBB for drug transport studies in both apical-to-basal (A-B) and basal-to-apical (B-A) direction in three replicates at 120 minutes time point

Drug	Conc apical start (nM)	conc apical end (nM)	Conc basolateral start (nM)	Conc basolateral end (nM)	amount apical start (nmol)	amount apical end (nmol)	amount basolateral start (nmol)	amount basolateral end (nmol)	Total in well start (nmol)	Total in well end (nmol)	Recovery (%)
camptothecin 1 A-B	883.11	615.98	0	83.2	0.088	0.062	0.000	0.050	0.088	0.112	126
camptothecin 1 B-A	0	279.71	883.11	820.15	0.000	0.028	0.530	0.492	0.530	0.520	98
camptothecin 2 A-B	1135.32	687.28	0	143.53	0.114	0.069	0.000	0.086	0.114	0.155	136
camptothecin 2 B-A	0	502.24	1135.32	1031.73	0.000	0.050	0.681	0.619	0.681	0.669	98
camptothecin 3 A-B	863.19	571.22	0	98.59	0.086	0.057	0.000	0.059	0.086	0.116	135
camptothecin 3 B-A	0	402.36	863.19	62.18	0.000	0.040	0.518	0.037	0.518	0.078	15
chlorpromazine 1 A-B	49.74	41.89	0	33.44	0.005	0.004	0.000	0.020	0.005	0.024	488
chlorpromazine 1 B-A	0	33.7	49.74	63.86	0.000	0.003	0.030	0.038	0.030	0.042	140
chlorpromazine 2 A-B	62.32	37.87	0	27.91	0.006	0.004	0.000	0.017	0.006	0.021	329
chlorpromazine 2 B-A	0	35.42	62.32	59.75	0.000	0.004	0.037	0.036	0.037	0.039	105
chlorpromazine 3 A-B	63.96	48.02	0	28.73	0.006	0.005	0.000	0.017	0.006	0.022	345
chlorpromazine 3 B-A	0	37.63	63.96	75.44	0.000	0.004	0.038	0.045	0.038	0.049	128
loperamide 1 A-B	136.2	102.74	0	45.1	0.014	0.010	0.000	0.027	0.014	0.037	274
loperamide 1 B-A	0	96.59	136.2	245.49	0.000	0.010	0.082	0.147	0.082	0.157	192
loperamide 2 A-B	142.59	200.187	0	42.47	0.014	0.020	0.000	0.025	0.014	0.046	319
loperamide 2 B-A	0	148.43	142.59	447.14	0.000	0.015	0.086	0.268	0.086	0.283	331
loperamide 3 A-B	226.93	292.04	0	35.9	0.023	0.029	0.000	0.022	0.023	0.051	224
loperamide 3 B-A	0	162.89	226.93	408.3	0.000	0.016	0.136	0.245	0.136	0.261	192

Table A4.10: Recovery percentage of etoposide, lamotrigine and methotrexate in Transwell model of Horse BBB for drug transport studies in both apical-to-basal (A-B) and basal-to-apical (B-A) direction in three replicates at 120 minutes time point

Drug	Conc apical start (nM)	conc apical end (nM)	Conc basolateral start (nM)	Conc basolateral end (nM)	amount apical start (nmol)	amount apical end (nmol)	amount basolateral start (nmol)	amount basolateral end (nmol)	Total in well start (nmol)	Total in well end (nmol)	Recovery (%)
etoposide 1 A-B	575.94	473.56	0	38.3	0.058	0.047	0.000	0.023	0.058	0.070	122
etoposide 1 B-A	0	242.99	575.94	656.38	0.000	0.024	0.346	0.394	0.346	0.418	121
etoposide 2 A-B	745.27	354.71	0	48.48	0.075	0.035	0.000	0.029	0.075	0.065	87
etoposide 2 B-A	0	207.92	745.27	387.57	0.000	0.021	0.447	0.233	0.447	0.253	57
etoposide 3 A-B	356.77	315.41	0	56.92	0.036	0.032	0.000	0.034	0.036	0.066	184
etoposide 3 B-A	0	169.6	356.77	325.99	0.000	0.017	0.214	0.196	0.214	0.213	99
lamotrigine 1 A-B	801.35	256.48	0	73.37	0.080	0.026	0.000	0.044	0.080	0.070	87
lamotrigine 1 B-A	0	484.18	801.35	556.85	0.000	0.048	0.481	0.334	0.481	0.383	80
lamotrigine 2 A-B	985.68	289.41	0	64.34	0.099	0.029	0.000	0.039	0.099	0.068	69
lamotrigine 2 B-A	0	423.37	985.68	743.07	0.000	0.042	0.591	0.446	0.591	0.488	83
lamotrigine 3 A-B	1066.96	586.84	0	99.35	0.107	0.059	0.000	0.060	0.107	0.118	111
lamotrigine 3 B-A	0	619.86	1066.96	1013.7	0.000	0.062	0.640	0.608	0.640	0.670	105
methotrexate 1 A-B	1031.43	734.27	0	48.97	0.103	0.073	0.000	0.029	0.103	0.103	100
methotrexate 1 B-A	0	220.52	1031.43	842.33	0.000	0.022	0.619	0.505	0.619	0.527	85
methotrexate 2 A-B	1486.04	776.12	0	44.38	0.149	0.078	0.000	0.027	0.149	0.104	70
methotrexate 2 B-A	0	761.16	1486.04	1427.87	0.000	0.076	0.892	0.857	0.892	0.933	105
methotrexate 3 A-B	1046.85	516.98	0	59.45	0.105	0.052	0.000	0.036	0.105	0.087	83
methotrexate 3 B-A	0	354.42	1046.85	997.85	0.000	0.035	0.628	0.599	0.628	0.634	101

Table A4.11: Recovery percentage of topiramate, mitoxantrone and loperamide 10x in Transwell model of Horse BBB for drug transport studies in both apical-to-basal (A-B) and basal-to-apical (B-A) direction in three replicates at 120 minutes time point

Drug	Conc apical start (nM)	conc apical end (nM)	Conc basolateral start (nM)	Conc basolateral end (nM)	amount apical start (nmol)	amount apical end (nmol)	amount basolateral start (nmol)	amount basolateral end (nmol)	Total in well start (nmol)	Total in well end (nmol)	Recovery (%)
topiramate 1 A-B	1856.41	1805.86	0	1	0.186	0.181	0.000	0.001	0.186	0.181	98
topiramate 1 B-A	0	1	1856.41	21.82	0.000	0.000	1.114	0.013	1.114	0.013	1
topiramate 2 A-B	1140.14	1320.47	0	218.39	0.114	0.132	0.000	0.131	0.114	0.263	231
topiramate 2 B-A	0	965.05	1140.14	5004.64	0.000	0.097	0.684	3.003	0.684	3.099	453
topiramate 3 A-B	1348.74	953.127	0	1	0.135	0.095	0.000	0.001	0.135	0.096	71
topiramate 3 B-A	0	422.48	1348.74	1030.31	0.000	0.042	0.809	0.618	0.809	0.660	82
mitoxantrone 1 A-B	110.75	137.33	0	42.54	0.011	0.014	0.000	0.026	0.011	0.039	354
mitoxantrone 1 B-A	0	39.76	110.75	101.37	0.000	0.004	0.066	0.061	0.066	0.065	98
mitoxantrone 2 A-B	98.96	119.91	0	43.06	0.010	0.012	0.000	0.026	0.010	0.038	382
mitoxantrone 2 B-A	0	42.95	98.96	116.19	0.000	0.004	0.059	0.070	0.059	0.074	125
mitoxantrone 3 A-B	100.44	99.45	0	42.28	0.010	0.010	0.000	0.025	0.010	0.035	352
mitoxantrone 3 B-A	0	43.45	100.44	181.55	0.000	0.004	0.060	0.109	0.060	0.113	188
loperamide 10x 1 A-B	4344.46	2505.2	0	562.14	0.434	0.251	0.000	0.337	0.434	0.588	135
loperamide 10x 1 B-A	0	2745.76	4344.46	3838.72	0.000	0.275	2.607	2.303	2.607	2.578	99
loperamide 10x 2 A-B	4681.24	2855.93	0	519.71	0.468	0.286	0.000	0.312	0.468	0.597	128
loperamide 10x 2 B-A	0	2292.82	4681.24	3422.73	0.000	0.229	2.809	2.054	2.809	2.283	81

Table A4.12: Apparent Permeability (Papp), Exact Permeability (Pexact), Papp Efflux Ratio and Pexact Efflux Ratio of camptothecin, chlorpromazine and loperamide in Transwell model of Horse BBB for drug transport studies in three replicates at 30 minutes time point

Drug	initial concentration in donor (uM)	Change in time (s)	Growth area (cm2)	Final concentration in donor (uM)	Change in concentration (uM)	Papp (cm/s)	Efflux ratio (B-A/A-B)	Vd (cm3)	Vr (cm3)	Ct	Pexact	Efflux Ratio (B-A/A-B)
camptothecin 1 A-B	0.95646	1800	0.33	0.56525	0.39121	8.13E-05		0.1	0.6	146.7157	0.000107	0.461916
camptothecin 1 B-A	0.95646	1800	0.33	0.79211	0.16435	3.62E-05	0.445903	0.6	0.1	708.3657	4.96E-05	
camptothecin 2 A-B	1.01355	1800	0.33	0.78253	0.23102	8.83E-05		0.1	0.6	187.7586	9.22E-05	0.542822
camptothecin 2 B-A	1.01355	1800	0.33	0.89412	0.11943	3.89E-05	0.440709	0.6	0.1	799.8686	5E-05	
camptothecin 3 A-B	0.73239	1800	0.33	0.80155	-0.06916	8.63E-05		0.1	0.6	168.1471	6.72E-05	0.262544
camptothecin 3 B-A	0.73239	1800	0.33	0.73624	-0.00385	1.70E-05	0.196575	0.6	0.1	641.6071	1.76E-05	
chlorpromazine 1 A-B	0.06869	1800	0.33	0.05404	0.01465	4.80E-04		0.1	0.6	35.70571	0.000355	0.275356
chlorpromazine 1 B-A	0.06869	1800	0.33	0.07695	-0.00826	8.55E-05	0.178101	0.6	0.1	70.94143	9.77E-05	
chlorpromazine 2 A-B	0.05975	1800	0.33	0.04239	0.01736	4.68E-04		0.1	0.6	29.80714	0.000383	0.305904
chlorpromazine 2 B-A	0.05975	1800	0.33	0.05965	1E-04	8.70E-05	0.185733	0.6	0.1	55.54	0.000117	
chlorpromazine 3 A-B	0.05386	1800	0.33	0.03719	0.01667	5.12E-04		0.1	0.6	28.73	0.000435	0.236196
chlorpromazine 3 B-A	0.05386	1800	0.33	0.05758	-0.00372	8.47E-05	0.165386	0.6	0.1	53.22714	0.000103	
loperamide 1 A-B	0.20922	1800	0.33	0.1867	0.02252	2.08E-04		0.1	0.6	63.60571	0.000163	0.259069
loperamide 1 B-A	0.20922	1800	0.33	0.25705	-0.04783	4.67E-05	0.224685	0.6	0.1	228.6271	4.23E-05	
loperamide 2 A-B	0.14937	1800	0.33	0.26407	-0.1147	2.21E-04		0.1	0.6	65.71	9.91E-05	1.131577
loperamide 2 B-A	0.14937	1800	0.33	0.21727	-0.0679	1.23E-04	0.556662	0.6	0.1	201.81	0.000112	
loperamide 3 A-B	0.22471	1800	0.33	0.14964	0.07507	1.38E-04		0.1	0.6	47.74286	0.000149	0.162585
loperamide 3 B-A	0.22471	1800	0.33	0.26175	-0.03704	2.66E-05	0.192295	0.6	0.1	229.4271	2.42E-05	

Table A4.13: Apparent Permeability (Papp), Exact Permeability (Pexact), Papp Efflux Ratio and Pexact Efflux Ratio of etoposide, lamotrigine and methotrexate in Transwell model of Horse BBB for drug transport studies in three replicates at 30 minutes time point

Drug	initial concentration in donor (uM)	Change in time (s)	Growth area (cm2)	Final concentration in donor (uM)	Change in concentration (uM)	Papp (cm/s)	Efflux ratio (B-A/A-B)	Vd (cm3)	Vr (cm3)	Ct	Pexact	Efflux Ratio (B-A/A-B)
etoposide 1 A-B	0.68837	1800	0.33	0.59465	0.09372	6.61E-05		0.1	0.6	123.5729	6.55E-05	0.712841
etoposide 1 B-A	0.68837	1800	0.33	0.6356	0.05277	3.83E-05	0.579561	0.6	0.1	567.1843	4.67E-05	
etoposide 2 A-B	0.51757	1800	0.33	0.26807	0.2495	6.71E-05		0.1	0.6	67.76429	0.000102	0.484756
etoposide 2 B-A	0.51757	1800	0.33	0.33818	0.17939	2.86E-05	0.425877	0.6	0.1	302.4186	4.95E-05	
etoposide 3 A-B	0.2613	1800	0.33	0.23968	0.02162	1.32E-04		0.1	0.6	63.49429	0.000111	0.241537
etoposide 3 B-A	0.2613	1800	0.33	0.2832	-0.0219	2.72E-05	0.206465	0.6	0.1	248.7829	2.69E-05	
lamotrigine 1 A-B	0.67554	1800	0.33	0.40048	0.27506	6.23E-05		0.1	0.6	92.90286	8.58E-05	0.541375
lamotrigine 1 B-A	0.67554	1800	0.33	0.80399	-0.12845	4.92E-05	0.790226	0.6	0.1	717.3386	4.64E-05	
lamotrigine 2 A-B	0.85836	1800	0.33	0.57741	0.28095	2.50E-05		0.1	0.6	100.7186	3.42E-05	1.446812
lamotrigine 2 B-A	0.85836	1800	0.33	0.79036	0.068	4.03E-05	1.608917	0.6	0.1	706.7843	4.95E-05	
lamotrigine 3 A-B	0.72796	1800	0.33	0.60661	0.12135	2.90E-05		0.1	0.6	104.5729	3.22E-05	0.773706
lamotrigine 3 B-A	0.72796	1800	0.33	0.84865	-0.12069	2.73E-05	0.940431	0.6	0.1	744.2614	2.49E-05	
methotrexate 1 A-B	0.58133	1800	0.33	0.84081	-0.25948	4.69E-05		0.1	0.6	143.2757	3.02E-05	1.217541
methotrexate 1 B-A	0.58133	1800	0.33	0.75565	-0.17432	4.35E-05	0.927276	0.6	0.1	669.1757	3.67E-05	
methotrexate 2 A-B	1.54493	1800	0.33	1.0947	0.45023	2.31E-05		0.1	0.6	186.6943	3.03E-05	0.991228
methotrexate 2 B-A	1.54493	1800	0.33	1.46068	0.08425	2.63E-05	1.13947	0.6	0.1	1286.547	3E-05	
methotrexate 3 A-B	0.79581	1800	0.33	0.67472	0.12109	5.22E-06		0.1	0.6	99.91143	6.06E-06	1.52054
methotrexate 3 B-A	0.79581	1800	0.33	0.75333	0.04248	8.53E-06	1.634631	0.6	0.1	651.47	9.22E-06	

Table A4.14: Apparent Permeability (Papp), Exact Permeability (Pexact), Papp Efflux Ratio and Pexact Efflux Ratio of topiramate, mitoxantrone and loperamide 10x in Transwell model of Horse BBB for drug transport studies in three replicates at 30 minutes time point

Drug	initial concentration in donor (uM)	Change in time (s)	Growth area (cm2)	Final concentration in donor (uM)	Change in concentration (uM)	Papp (cm/s)	Efflux ratio (B-A/A-B)	Vd (cm3)	Vr (cm3)	Ct	Pexact	Efflux Ratio (B-A/A-B)
topiramate 1 A-B	0.68618	1800	0.33	1.21987	-0.53369	1.46E-05		0.1	0.6	182.7529	8.04E-06	0.014296
topiramate 1 B-A	0.68618	1800	0.33	1.46569	-0.77951	2.45E-07	0.016835	0.6	0.1	1256.449	1.15E-07	
topiramate 2 A-B	2.14091	1800	0.33	1.50647	0.63444	4.72E-07		0.1	0.6	216.0671	6.69E-07	0.283292
topiramate 2 B-A	2.14091	1800	0.33	0.888175	1.252735	7.86E-08	0.166667	0.6	0.1	761.4357	1.9E-07	
topiramate 3 A-B	0.07574	1800	0.33	2.05249	-1.97675	2.79E-03		0.1	0.6	472.5357	8.44E-05	#NUM!
topiramate 3 B-A	0.07574	1800	0.33	0.87466	-0.79892	4.32E-03	1.547823	0.6	0.1	1027.269	#NUM!	
mitoxantrone 1 A-B	0.07754	1800	0.33	0.14372	-0.06618	5.17E-04		0.1	0.6	54.56	0.000188	0.179383
mitoxantrone 1 B-A	0.07754	1800	0.33	0.23315	-0.15561	9.31E-05	0.179933	0.6	0.1	205.9657	3.37E-05	
mitoxantrone 2 A-B	0.1397	1800	0.33	0.12087	0.01883	3.00E-04		0.1	0.6	52.79571	0.000222	0.342662
mitoxantrone 2 B-A	0.1397	1800	0.33	0.11098	0.02872	4.99E-05	0.166385	0.6	0.1	101.0371	7.6E-05	
mitoxantrone 3 A-B	0.09181	1800	0.33	0.21979	-0.12798	4.70E-04		0.1	0.6	68.00714	0.000143	0.352646
mitoxantrone 3 B-A	0.09181	1800	0.33	0.15677	-0.06496	7.57E-05	0.161164	0.6	0.1	140.2743	5.03E-05	
loperamide 10x 1 A-B	4.31902	1800	0.33	3.01826	1.30076	4.29E-05		0.1	0.6	588.2771	5.39E-05	1.563337
loperamide 10x 1 B-A	4.31902	1800	0.33	3.93882	0.3802	6.21E-05	1.448885	0.6	0.1	3603.747	8.42E-05	
loperamide 10x 2 A-B	3.23087	1800	0.33	2.33028	0.90059	2.40E-05		0.1	0.6	398.6914	3.09E-05	0.408758
loperamide 10x 2 B-A	3.23087	1800	0.33	3.44888	-0.21801	1.30E-05	0.543751	0.6	0.1	2991.959	1.26E-05	

Table A4.15: Apparent Permeability (Papp), Exact Permeability (Pexact), Papp Efflux Ratio and Pexact Efflux Ratio of camptothecin, chlorpromazine and loperamide in Transwell model of Horse BBB for drug transport studies in three replicates at 60 minutes time point

Drug	initial concentration in donor (uM)	Change in time (s)	Growth area (cm2)	Final concentration in donor (uM)	Change in concentration (uM)	Papp (cm/s)	Efflux ratio (B-A/A-B)	Vd (cm3)	Vr (cm3)	Ct	Pexact	Efflux Ratio (B-A/A-B)
camptothecin 1 A-B	0.8372	3600	0.33	0.66829	0.16891	4.79E-05		0.1	0.6	163.51	4.79E-05	0.525932
camptothecin 1 B-A	0.8372	3600	0.33	1.19817	-0.36097	3.18E-05	0.663979	0.6	0.1	1072.18	2.52E-05	
camptothecin 2 A-B	1.18703	3600	0.33	0.92123	0.2658	3.42E-05		0.1	0.6	200.4414	3.69E-05	0.383877
camptothecin 2 B-A	1.18703	3600	0.33	0.81439	0.37264	9.06E-06	0.265222	0.6	0.1	716.3057	1.42E-05	
camptothecin 3 A-B	1.00105	3600	0.33	0.83744	0.16361	3.78E-05		0.1	0.6	183.8086	3.77E-05	0.703285
camptothecin 3 B-A	1.00105	3600	0.33	0.81218	0.18887	1.88E-05	0.498954	0.6	0.1	728.1743	2.65E-05	
chlorpromazine 1 A-B	0.05746	3600	0.33	0.05203	0.00543	2.95E-04		0.1	0.6	36.16429	0.000189	0.290734
chlorpromazine 1 B-A	0.05746	3600	0.33	0.07491	-0.01745	5.42E-05	0.184019	0.6	0.1	69.49571	5.49E-05	
chlorpromazine 2 A-B	0.05461	3600	0.33	0.03697	0.01764	2.52E-04		0.1	0.6	28.65571	0.000219	0.21742
chlorpromazine 2 B-A	0.05461	3600	0.33	0.06674	-0.01213	4.57E-05	0.181151	0.6	0.1	61.44	4.75E-05	
chlorpromazine 3 A-B	0.0618	3600	0.33	0.04669	0.01511	2.24E-04		0.1	0.6	30.20714	0.000173	0.269984
chlorpromazine 3 B-A	0.0618	3600	0.33	0.06564	-0.00384	3.92E-05	0.174618	0.6	0.1	60.37286	4.67E-05	
loperamide 1 A-B	0.17572	3600	0.33	0.16226	0.01346	1.29E-04		0.1	0.6	61.68286	9.4E-05	0.265081
loperamide 1 B-A	0.17572	3600	0.33	0.27805	-0.10233	3.48E-05	0.269479	0.6	0.1	248.7043	2.49E-05	
loperamide 2 A-B	0.14584	3600	0.33	0.11192	0.03392	1.07E-04		0.1	0.6	42.51714	9.39E-05	0.173696
loperamide 2 B-A	0.14584	3600	0.33	0.27729	-0.13145	2.86E-05	0.266721	0.6	0.1	244.7529	1.63E-05	
loperamide 3 A-B	0.2301	3600	0.33	0.23132	-0.00122	7.62E-05		0.1	0.6	62.80571	5.81E-05	0.32243
loperamide 3 B-A	0.2301	3600	0.33	0.42797	-0.19787	3.17E-05	0.416043	0.6	0.1	379.2129	1.87E-05	

Table A4.16: Apparent Permeability (Papp), Exact Permeability (Pexact), Papp Efflux Ratio and Pexact Efflux Ratio of etoposide, lamotrigine and methotrexate in Transwell model of Horse BBB for drug transport studies in three replicates at 60 minutes time point

Drug	initial concentration in donor (uM)	Change in time (s)	Growth area (cm2)	Final concentration in donor (uM)	Change in concentration (uM)	Papp (cm/s)	Efflux ratio (B-A/A-B)	Vd (cm3)	Vr (cm3)	Ct	Pexact	Efflux Ratio (B-A/A-B)
etoposide 1 A-B	1.10885	3600	0.33	0.66498	0.44387	2.72E-05		0.1	0.6	146.2543	3.79E-05	1.545529
etoposide 1 B-A	1.10885	3600	0.33	0.60993	0.49892	2.40E-05	0.880491	0.6	0.1	567.9286	5.86E-05	
etoposide 2 A-B	0.38206	3600	0.33	0.24341	0.13865	4.76E-05		0.1	0.6	65.63857	5.74E-05	0.313606
etoposide 2 B-A	0.38206	3600	0.33	0.33353	0.04853	1.44E-05	0.301629	0.6	0.1	295.1929	1.8E-05	
etoposide 3 A-B	0.34477	3600	0.33	0.25409	0.09068	6.50E-05		0.1	0.6	74.34714	6.56E-05	0.531866
etoposide 3 B-A	0.34477	3600	0.33	0.30277	0.042	2.57E-05	0.395172	0.6	0.1	274.5529	3.49E-05	
lamotrigine 1 A-B	0.68941	3600	0.33	0.543	0.14641	3.56E-05		0.1	0.6	119.1686	3.77E-05	1.250049
lamotrigine 1 B-A	0.68941	3600	0.33	0.89537	-0.20596	4.83E-05	1.357957	0.6	0.1	823.9471	4.72E-05	
lamotrigine 2 A-B	1.0413	3600	0.33	0.3613	0.68	1.65E-05		0.1	0.6	80.81714	3.95E-05	0.641077
lamotrigine 2 B-A	1.0413	3600	0.33	0.70144	0.33986	1.50E-05	0.908962	0.6	0.1	627.7786	2.53E-05	
lamotrigine 3 A-B	1.05511	3600	0.33	0.80735	0.24776	3.10E-05		0.1	0.6	170.8271	3.44E-05	1.531613
lamotrigine 3 B-A	1.05511	3600	0.33	0.8972	0.15791	3.43E-05	1.107301	0.6	0.1	830.4743	5.26E-05	
methotrexate 1 A-B	0.62908	3600	0.33	0.68856	-0.05948	2.93E-05		0.1	0.6	129.6857	2.39E-05	1.861266
methotrexate 1 B-A	0.62908	3600	0.33	0.68486	-0.05578	3.87E-05	1.317962	0.6	0.1	628.3014	4.44E-05	
methotrexate 2 A-B	1.22765	3600	0.33	0.76167	0.46598	3.93E-06		0.1	0.6	116.9957	6.14E-06	0.892595
methotrexate 2 B-A	1.22765	3600	0.33	1.1294	0.09825	4.91E-06	1.249564	0.6	0.1	978.2857	5.48E-06	
methotrexate 3 A-B	0.9461	3600	0.33	1.30747	-0.36137	1.78E-05		0.1	0.6	215.3329	1.21E-05	0.949124
methotrexate 3 B-A	0.9461	3600	0.33	0.93377	0.01233	1.07E-05	0.603122	0.6	0.1	817.5943	1.15E-05	

Table A4.17: Apparent Permeability (Papp), Exact Permeability (Pexact), Papp Efflux Ratio and Pexact Efflux Ratio of topiramate, mitoxantrone and loperamide 10x in Transwell model of Horse BBB for drug transport studies in three replicates at 60 minutes time point

Drug	Initial concentration in donor (uM)	Change in time (s)	Growth area (cm2)	Final concentration in donor (uM)	Change in concentration (uM)	Papp (cm/s)	Efflux ratio (B-A/A-B)	Vd (cm3)	Vr (cm3)	Ct	Pexact	Efflux Ratio (B-A/A-B)
topiramate 1 A-B	1.17352	3600	0.33	0.36911	0.80441	4.30E-07		0.1	0.6	53.58714	1.36E-06	0.786135
topiramate 1 B-A	1.17352	3600	0.33	0.0792	1.09432	7.17E-08	0.166667	0.6	0.1	68.02857	1.07E-06	
topiramate 2 A-B	3.79296	3600	0.33	0.001	3.79196	1.33E-07		0.1	0.6	1	#NUM!	#NUM!
topiramate 2 B-A	3.79296	3600	0.33	1.02234	2.77062	2.22E-08	0.166667	0.6	0.1	876.4343	8.24E-08	
topiramate 3 A-B	0.54606	3600	0.33	1.53997	-0.99391	3.34E-04		0.1	0.6	529.5357	8.27E-05	0.003118
topiramate 3 B-A	0.54606	3600	0.33	0.32698	0.21908	1.54E-07	0.000462	0.6	0.1	280.4114	2.58E-07	
mitoxantrone 1 A-B	0.08927	3600	0.33	0.10658	-0.01731	2.22E-04		0.1	0.6	48.86	0.000117	0.263058
mitoxantrone 1 B-A	0.08927	3600	0.33	0.133	-0.04373	3.93E-05	0.177243	0.6	0.1	119.9614	3.08E-05	
mitoxantrone 2 A-B	0.11684	3600	0.33	0.17345	-0.05661	1.80E-04		0.1	0.6	60.56429	8.43E-05	0.287189
mitoxantrone 2 B-A	0.11684	3600	0.33	0.16795	-0.05111	3.08E-05	0.170858	0.6	0.1	150.0714	2.42E-05	
mitoxantrone 3 A-B	0.11243	3600	0.33	0.1355	-0.02307	1.93E-04		0.1	0.6	56.12	0.000104	0.305928
mitoxantrone 3 B-A	0.11243	3600	0.33	0.12819	-0.01576	3.10E-05	0.16076	0.6	0.1	115.7871	3.19E-05	
loperamide 10x 1 A-B	4.15071	3600	0.33	1.78586	2.36485	1.17E-05		0.1	0.6	337.8886	2.43E-05	0.886307
loperamide 10x 1 B-A	4.15071	3600	0.33	3.65433	0.49638	1.70E-05	1.447753	0.6	0.1	3252.107	2.15E-05	
loperamide 10x 2 A-B	3.89838	3600	0.33	2.80597	1.09241	4.72E-05		0.1	0.6	713.1443	5.16E-05	0.691809
loperamide 10x 2 B-A	3.89838	3600	0.33	3.92712	-0.02874	3.00E-05	0.636452	0.6	0.1	3564.861	3.57E-05	

Table A4.18: Apparent Permeability (Papp), Exact Permeability (Pexact), Papp Efflux Ratio and Pexact Efflux Ratio of camptothecin, chlorpromazine and loperamide in Transwell model of Horse BBB for drug transport studies in three replicates at 120 minutes time point

Drug	Initial concentration in donor (uM)	Change in time (s)	Growth area (cm2)	Final concentration in donor (uM)	Change in concentration (uM)	Papp (cm/s)	Efflux ratio (B-A/A-B)	Vd (cm3)	Vr (cm3)	Ct	Pexact	Efflux Ratio (B-A/A-B)
camptothecin 1 A-B	0.88311	7200	0.33	0.61598	0.26713	2.38E-05		0.1	0.6	159.3114	2.66E-05	0.639518
camptothecin 1 B-A	0.88311	7200	0.33	0.82015	0.06296	1.33E-05	0.560317	0.6	0.1	742.9443	1.7E-05	
camptothecin 2 A-B	1.13532	7200	0.33	0.68728	0.44804	3.19E-05		0.1	0.6	221.2086	3.78E-05	0.711962
camptothecin 2 B-A	1.13532	7200	0.33	1.03173	0.10359	1.86E-05	0.5832	0.6	0.1	956.0886	2.69E-05	
camptothecin 3 A-B	0.86319	7200	0.33	0.57122	0.29197	2.88E-05		0.1	0.6	166.1086	3.25E-05	#NUM!
camptothecin 3 B-A	0.86319	7200	0.33	0.06218	0.80101	1.96E-05	0.680191	0.6	0.1	110.7771	#NUM!	
chlorpromazine 1 A-B	0.04974	7200	0.33	0.04189	0.00785	1.70E-04		0.1	0.6	34.64714	0.000121	0.24858
chlorpromazine 1 B-A	0.04974	7200	0.33	0.06386	-0.01412	2.85E-05	0.167963	0.6	0.1	59.55143	3.01E-05	
chlorpromazine 2 A-B	0.06232	7200	0.33	0.03787	0.02445	1.13E-04		0.1	0.6	29.33286	0.000109	0.328045
chlorpromazine 2 B-A	0.06232	7200	0.33	0.05975	0.00257	2.39E-05	0.211513	0.6	0.1	56.27429	3.58E-05	
chlorpromazine 3 A-B	0.06396	7200	0.33	0.04802	0.01594	1.13E-04		0.1	0.6	31.48571	8.79E-05	0.316366
chlorpromazine 3 B-A	0.06396	7200	0.33	0.07544	-0.01148	2.48E-05	0.218297	0.6	0.1	70.03857	2.78E-05	
loperamide 1 A-B	0.1362	7200	0.33	0.10274	0.03346	8.36E-05		0.1	0.6	53.33429	6.74E-05	0.301614
loperamide 1 B-A	0.1362	7200	0.33	0.24549	-0.10929	2.98E-05	0.356948	0.6	0.1	224.2186	2.03E-05	
loperamide 2 A-B	0.14259	7200	0.33	0.200187	-0.0576	7.52E-05		0.1	0.6	65.001	3.82E-05	0.431565
loperamide 2 B-A	0.14259	7200	0.33	0.44714	-0.30455	4.38E-05	0.58249	0.6	0.1	404.4671	1.65E-05	
loperamide 3 A-B	0.22693	7200	0.33	0.29204	-0.06511	3.99E-05		0.1	0.6	72.49143	2.47E-05	0.838795
loperamide 3 B-A	0.22693	7200	0.33	0.4083	-0.18137	3.02E-05	0.756221	0.6	0.1	373.2414	2.07E-05	

Table A4.19: Apparent Permeability (Papp), Exact Permeability (Pexact), Papp Efflux Ratio and Pexact Efflux Ratio of etoposide, lamotrigine and methotrexate in Transwell model of Horse BBB for drug transport studies in three replicates at 120 minutes time point

Drug	initial concentration in donor (uM)	Change in time (s)	Growth area (cm2)	Final concentration in donor (uM)	Change in concentration (uM)	Papp (cm/s)	Efflux ratio (B-A/A-B)	Vd (cm3)	Vr (cm3)	Ct	Pexact	Efflux Ratio (B-A/A-B)
etoposide 1 A-B	0.57594	7200	0.33	0.47356	0.10238	1.68E-05		0.1	0.6	100.48	1.73E-05	1.088126
etoposide 1 B-A	0.57594	7200	0.33	0.65638	-0.08044	1.78E-05	1.057398	0.6	0.1	597.3243	1.88E-05	
etoposide 2 A-B	0.74527	7200	0.33	0.35471	0.39056	1.64E-05		0.1	0.6	92.22714	2.69E-05	1.145738
etoposide 2 B-A	0.74527	7200	0.33	0.38757	0.3577	1.17E-05	0.714796	0.6	0.1	361.9057	3.08E-05	
etoposide 3 A-B	0.35677	7200	0.33	0.31541	0.04136	4.03E-05		0.1	0.6	93.84714	3.36E-05	0.876649
etoposide 3 B-A	0.35677	7200	0.33	0.32599	0.03078	2.00E-05	0.496603	0.6	0.1	303.6486	2.95E-05	
lamotrigine 1 A-B	0.80135	7200	0.33	0.25648	0.54487	2.31E-05		0.1	0.6	99.52857	4.82E-05	1.625197
lamotrigine 1 B-A	0.80135	7200	0.33	0.55685	0.2445	2.54E-05	1.099859	0.6	0.1	546.4686	7.83E-05	
lamotrigine 2 A-B	0.98568	7200	0.33	0.28941	0.69627	1.65E-05		0.1	0.6	96.49286	3.96E-05	0.850002
lamotrigine 2 B-A	0.98568	7200	0.33	0.74307	0.24261	1.81E-05	1.0967	0.6	0.1	697.3986	3.37E-05	
lamotrigine 3 A-B	1.06696	7200	0.33	0.58684	0.48012	2.35E-05		0.1	0.6	168.9914	3.2E-05	1.17595
lamotrigine 3 B-A	1.06696	7200	0.33	1.0137	0.05326	2.45E-05	1.039859	0.6	0.1	957.4371	3.76E-05	
methotrexate 1 A-B	1.03143	7200	0.33	0.73427	0.29716	1.20E-05		0.1	0.6	146.87	1.46E-05	0.853659
methotrexate 1 B-A	1.03143	7200	0.33	0.84233	0.1891	9.00E-06	0.750528	0.6	0.1	753.5	1.25E-05	
methotrexate 2 A-B	1.48604	7200	0.33	0.77612	0.70992	7.54E-06		0.1	0.6	148.9143	1.28E-05	2.392788
methotrexate 2 B-A	1.48604	7200	0.33	1.42787	0.05817	2.16E-05	2.858495	0.6	0.1	1332.626	3.05E-05	
methotrexate 3 A-B	1.04685	7200	0.33	0.51698	0.52987	1.43E-05		0.1	0.6	124.8114	2.33E-05	0.767233
methotrexate 3 B-A	1.04685	7200	0.33	0.99785	0.049	1.42E-05	0.993608	0.6	0.1	905.9314	1.79E-05	

Table A4.20: Apparent Permeability (Papp), Exact Permeability (Pexact), Papp Efflux Ratio and Pexact Efflux Ratio of topiramate, mitoxantrone and loperamide 10x in Transwell model of Horse BBB for drug transport studies in three replicates at 120 minutes time point

Drug	initial concentration in donor (uM)	Change in time (s)	Growth area (cm2)	Final concentration in donor (uM)	Change in concentration (uM)	Papp (cm/s)	Efflux ratio (B-A/A-B)	Vd (cm3)	Vr (cm3)	Ct	Pexact	Efflux Ratio (B-A/A-B)
topiramate 1 A-B	1.85641	7200	0.33	1.80586	0.05055	1.36E-07		0.1	0.6	258.8371	1.4E-07	14.08508
topiramate 1 B-A	1.85641	7200	0.33	0.02182	1.83459	2.27E-08	0.166667	0.6	0.1	18.84571	1.97E-06	
topiramate 2 A-B	1.14014	7200	0.33	1.32047	-0.18033	4.84E-05		0.1	0.6	375.83	3.14E-05	0.282562
topiramate 2 B-A	1.14014	7200	0.33	5.00464	-3.8645	3.56E-05	0.736488	0.6	0.1	4427.556	8.87E-06	
topiramate 3 A-B	1.34874	7200	0.33	0.953127	0.395613	1.87E-07		0.1	0.6	137.0181	2.64E-07	81.06788
topiramate 3 B-A	1.34874	7200	0.33	1.03031	0.31843	1.32E-05	70.41333	0.6	0.1	943.4771	2.14E-05	
mitoxantrone 1 A-B	0.11075	7200	0.33	0.13733	-0.02658	9.70E-05		0.1	0.6	56.08143	5.13E-05	0.394973
mitoxantrone 1 B-A	0.11075	7200	0.33	0.10137	0.00938	1.51E-05	0.155775	0.6	0.1	92.56857	2.02E-05	
mitoxantrone 2 A-B	0.09896	7200	0.33	0.11991	-0.02095	1.10E-04		0.1	0.6	54.03857	5.75E-05	0.327071
mitoxantrone 2 B-A	0.09896	7200	0.33	0.11619	-0.01723	1.83E-05	0.166241	0.6	0.1	105.7271	1.88E-05	
mitoxantrone 3 A-B	0.10044	7200	0.33	0.09945	0.00099	1.06E-04		0.1	0.6	50.44714	6.57E-05	0.171718
mitoxantrone 3 B-A	0.10044	7200	0.33	0.18155	-0.08111	1.82E-05	0.171279	0.6	0.1	161.8214	1.13E-05	
loperamide 10x 1 A-B	4.34446	7200	0.33	2.5052	1.83926	3.27E-05		0.1	0.6	839.72	3.99E-05	1.236609
loperamide 10x 1 B-A	4.34446	7200	0.33	3.83872	0.50574	2.66E-05	0.81408	0.6	0.1	3682.583	4.94E-05	
loperamide 10x 2 A-B	4.68124	7200	0.33	2.85593	1.82531	2.80E-05		0.1	0.6	853.4557	3.39E-05	1.293135
loperamide 10x 2 B-A	4.68124	7200	0.33	3.42273	1.25851	2.06E-05	0.735288	0.6	0.1	3261.314	4.38E-05	

Table A4.21: Average recovery percentage of test drugs in Transwell model of Horse BBB for drug transport studies in three replicates at 30 minutes time point

Drug	Rep 1	Rep 2	Rep 3	Average	SD	SEM
camptothecin A-B	107.3762	129.6739	160.7108	132.587	26.7864	15.46513
camptothecin B-A	86.40473	92.07045	102.2053	93.56017	8.004953	4.621662
chlorpromazine A-B	363.8666	349.205	373.394	362.1552	12.18496	7.03499
chlorpromazine B-A	120.4906	108.4463	115.2958	114.7442	6.041068	3.487812
loperamide A-B	212.8095	307.94	148.725	223.1582	80.11039	46.25176
loperamide B-A	127.4886	157.6254	119.1157	134.7432	20.25388	11.69358
etoposide A-B	125.6606	91.64944	170.0957	129.1352	39.33838	22.71202
etoposide B-A	96.12781	68.16888	111.0779	91.79154	21.78071	12.5751
lamotrigine A-B	96.26669	82.13687	100.5563	92.98664	9.637864	5.564423
lamotrigine B-A	123.8853	96.06478	119.2792	113.0764	14.91146	8.609135
methotrexate A-B	172.5234	84.70675	87.88279	115.0376	49.80942	28.75748
methotrexate B-A	134.2964	97.15467	95.50626	108.9858	21.93511	12.66424
topiramate A-B	186.4336	70.64613		128.5399	81.8741	47.27003
topiramate B-A	213.6257	41.49365		127.5597	121.7157	70.27261
mitoxantrone A-B	492.5458	264.5455	518.5165	425.2026	139.7378	80.67766
mitoxantrone B-A	309.896	84.37843	178.2522	190.8422	113.2847	65.40495
loperamide 10x A-B	95.34431	86.38045		90.86238	6.33841	3.659483
loperamide 10x B-A	97.3455	108.0396		102.6925	7.561855	4.365839

Table A4.22: Average recovery percentage of test drugs in Transwell model of Horse BBB for drug transport studies in three replicates at 60 minutes time point

Drug	Rep 1	Rep 2	Rep 3	Average	SD	SEM
camptothecin A-B	136.714	118.2017	128.531	127.8156	9.276872	5.356004
camptothecin B-A	149.4119	70.40176	84.86456	101.5594	42.06769	24.28779
chlorpromazine A-B	440.5674	367.3137	342.1521	383.3444	51.12854	29.51908
chlorpromazine B-A	141.104	131.258	113.9725	128.7782	13.73468	7.92972
loperamide A-B	245.7205	204.073	191.0648	213.6194	28.55105	16.48396
loperamide B-A	165.1235	195.7933	192.2708	184.3959	16.78304	9.68969
etoposide A-B	92.32809	120.2612	150.9499	121.1797	29.3217	16.92889
etoposide B-A	59.7541	90.14073	92.9059	80.93358	18.394	10.61978
lamotrigine A-B	120.9991	54.32824	113.3332	96.22019	36.4814	21.06255
lamotrigine B-A	139.434	70.33596	91.82802	100.5326	35.36186	20.41618
methotrexate A-B	144.306	66.71038	159.3204	123.4456	49.70432	28.6968
methotrexate B-A	116.5223	92.96895	100.8202	103.4371	11.99275	6.924017
topiramate A-B	31.96452	0.184552	678.8173	236.9888	382.9645	221.1047
topiramate B-A	6.763129	26.95801	59.91039	31.21051	26.82761	15.48893
mitoxantrone A-B	383.1298	362.8466	349.4085	365.1283	16.97605	9.801127
mitoxantrone B-A	156.7772	149.8488	120.8352	142.4871	19.06839	11.00914
loperamide 10x A-B	56.9835	128.0534		92.51848	50.25404	29.01418
loperamide 10x B-A	91.40906	106.6855		99.04726	10.80205	6.236568

Table A4.23: Average recovery percentage of test drugs in Transwell model of Horse BBB for drug transport studies in three replicates at 120 minutes time point

Drug	Rep 1	Rep 2	Rep 3	Average	SD	SEM
camptothecin A-B	126.2787	136.3897	134.705	132.4578	5.417151	3.127594
camptothecin B-A	98.15519	98.24866	14.97237	70.45874	48.05263	27.7432
chlorpromazine A-B	487.5955	329.4769	344.5904	387.2209	87.25478	50.37657
chlorpromazine B-A	139.6797	105.3487	127.7543	124.2609	17.43004	10.06324
loperamide A-B	274.1116	319.1016	223.6108	272.2747	47.7719	27.58112
loperamide B-A	192.0619	330.9337	189.383	237.4595	80.96207	46.74347
etoposide A-B	122.1238	86.62498	184.1326	130.9605	49.35079	28.49269
etoposide B-A	120.9984	56.65374	99.29553	92.3159	32.73524	18.8997
lamotrigine A-B	86.94079	68.5263	110.8701	88.77907	21.23169	12.25812
lamotrigine B-A	79.55908	82.54521	104.6909	88.93173	13.72927	7.926596
methotrexate A-B	99.67618	70.14616	83.45799	84.42678	14.78883	8.538333
methotrexate B-A	85.22957	104.6224	100.9619	96.93795	10.30361	5.948791
topiramate A-B	97.60021	230.7445	71.11282	133.1525	85.54847	49.39143
topiramate B-A	1.184365	453.0568	81.61123	178.6175	241.0494	139.17
mitoxantrone A-B	354.465	382.2454	351.583	362.7645	16.93237	9.775908
mitoxantrone B-A	97.51392	124.6446	187.9646	136.7077	46.41628	26.79845
loperamide 10x A-B	135.2997	127.6198		131.4597	5.430474	3.135286
loperamide 10x B-A	98.89254	81.27903		90.08579	12.45463	7.190682

Table A4.24: Average Apparent Permeability (Papp) of test drugs in Transwell model of Horse BBB for drug transport studies in three replicates at 30 minutes time point

Drug	Rep 1	Rep 2	Rep 3	Average	SD	SEM
camptothecin A-B	8.13E-05	8.83E-05	8.63E-05	8.53E-05	3.63E-06	2.10E-06
camptothecin B-A	3.62E-05	3.89E-05	1.70E-05	3.07E-05	1.20E-05	6.92E-06
chlorpromazine A-B	4.80E-04	0.000468	0.000512	4.87E-04	2.27E-05	1.31E-05
chlorpromazine B-A	8.55E-05	8.70E-05	8.47E-05	8.58E-05	1.15E-06	6.66E-07
loperamide A-B	2.08E-04	2.21E-04	1.38E-04	1.89E-04	4.44E-05	2.56E-05
loperamide B-A	4.67E-05	1.23E-04	2.66E-05	6.54E-05	5.08E-05	2.93E-05
etoposide A-B	6.61E-05	6.71E-05	1.32E-04	8.84E-05	3.77E-05	2.18E-05
etoposide B-A	3.83E-05	2.86E-05	2.72E-05	3.14E-05	6.05E-06	3.49E-06
lamotrigine A-B	6.23E-05	2.50E-05	2.90E-05	3.88E-05	2.04E-05	1.18E-05
lamotrigine B-A	4.92E-05	4.03E-05	2.73E-05	3.89E-05	1.10E-05	6.37E-06
methotrexate A-B	4.69E-05	2.33E-05	5.22E-06	2.52E-05	2.09E-05	1.21E-05
methotrexate B-A	4.35E-05	2.63E-05	8.53E-06	2.61E-05	1.75E-05	1.01E-05
topiramate A-B	1.46E-05	4.72E-07	2.79E-03	9.35E-04	1.61E-03	9.28E-04
topiramate B-A	2.45E-07	7.86E-08	4.32E-03	1.44E-03	2.49E-03	1.44E-03
mitoxantrone A-B	0.000517	3.00E-04	4.70E-04	4.29E-04	1.14E-04	6.60E-05
mitoxantrone B-A	9.31E-05	4.99E-05	7.57E-05	7.29E-05	2.17E-05	1.25E-05
loperamide 10x A-B	4.29E-05	2.40E-05		3.34E-05	1.33E-05	7.70E-06
loperamide 10x B-A	6.21E-05	1.30E-05		3.76E-05	3.47E-05	2.00E-05

Table A4.25: Average Apparent Permeability (Papp) of test drugs in Transwell model of Horse BBB for drug transport studies in three replicates at 60 minutes time point

Drug	Rep 1	Rep 2	Rep 3	Average	SD	SEM
camptothecin A-B	4.79E-05	3.42E-05	3.78E-05	3.99E-05	7.11E-06	4.11E-06
camptothecin B-A	3.18E-05	9.06E-06	1.88E-05	1.99E-05	1.14E-05	6.58E-06
chlorpromazine A-B	2.95E-04	2.52E-04	2.24E-04	2.57E-04	3.54E-05	2.04E-05
chlorpromazine B-A	5.42E-05	4.57E-05	3.92E-05	4.64E-05	7.54E-06	4.35E-06
loperamide A-B	1.29E-04	1.07E-04	7.62E-05	1.04E-04	2.66E-05	1.53E-05
loperamide B-A	3.48E-05	2.86E-05	3.17E-05	3.17E-05	3.10E-06	1.79E-06
etoposide A-B	2.72E-05	4.76E-05	6.50E-05	4.66E-05	1.89E-05	1.09E-05
etoposide B-A	2.40E-05	1.44E-05	2.57E-05	2.13E-05	6.11E-06	3.53E-06
lamotrigine A-B	3.56E-05	1.65E-05	3.10E-05	2.77E-05	9.93E-06	5.74E-06
lamotrigine B-A	4.83E-05	1.50E-05	3.43E-05	3.25E-05	1.67E-05	9.64E-06
methotrexate A-B	2.93E-05	3.93E-06	1.78E-05	1.70E-05	1.27E-05	7.34E-06
methotrexate B-A	3.87E-05	4.91E-06	1.07E-05	1.81E-05	1.80E-05	1.04E-05
topiramate A-B	4.30E-07	1.33E-07	3.34E-04	1.12E-04	1.93E-04	1.11E-04
topiramate B-A	7.17E-08	2.22E-08	1.54E-07	8.27E-08	6.67E-08	3.85E-08
mitoxantrone A-B	2.22E-04	1.80E-04	1.93E-04	1.98E-04	2.13E-05	1.23E-05
mitoxantrone B-A	3.93E-05	3.08E-05	3.10E-05	3.37E-05	4.88E-06	2.82E-06
loperamide 10x A-B	1.17E-05	4.72E-05		2.95E-05	2.51E-05	1.45E-05
loperamide 10x B-A	1.70E-05	3.00E-05		2.35E-05	9.21E-06	5.32E-06

Table A4.26: Average Apparent Permeability (Papp) of test drugs in Transwell model of Horse BBB for drug transport studies in three replicates at 120 minutes time point

Drug	Rep 1	Rep 2	Rep 3	Average	SD	SEM
camptothecin A-B	2.38E-05	3.19E-05	2.88E-05	2.82E-05	4.11E-06	2.37E-06
camptothecin B-A	1.33E-05	1.86E-05	1.96E-05	1.72E-05	3.38E-06	1.95E-06
chlorpromazine A-B	1.70E-04	1.13E-04	1.13E-04	1.32E-04	3.26E-05	1.88E-05
chlorpromazine B-A	2.85E-05	2.39E-05	2.48E-05	2.57E-05	2.45E-06	1.41E-06
loperamide A-B	8.36E-05	7.52E-05	3.99E-05	6.63E-05	2.32E-05	1.34E-05
loperamide B-A	2.98E-05	4.38E-05	2.98E-05	3.45E-05	8.07E-06	4.66E-06
etoposide A-B	1.68E-05	1.64E-05	4.03E-05	2.45E-05	1.37E-05	7.89E-06
etoposide B-A	1.78E-05	1.17E-05	2.00E-05	1.65E-05	4.27E-06	2.47E-06
lamotrigine A-B	2.31E-05	1.65E-05	2.35E-05	2.10E-05	3.95E-06	2.28E-06
lamotrigine B-A	2.54E-05	1.81E-05	2.45E-05	2.27E-05	3.99E-06	2.30E-06
methotrexate A-B	1.20E-05	7.54E-06	1.43E-05	1.13E-05	3.45E-06	1.99E-06
methotrexate B-A	9.00E-06	2.16E-05	1.42E-05	1.49E-05	6.31E-06	3.64E-06
topiramate A-B	1.36E-07	4.84E-05	1.87E-07	1.62E-05	2.78E-05	1.61E-05
topiramate B-A	2.27E-08	3.56E-05	1.32E-05	1.63E-05	1.80E-05	1.04E-05
mitoxantrone A-B	9.70E-05	1.10E-04	1.06E-04	1.04E-04	6.65E-06	3.84E-06
mitoxantrone B-A	1.51E-05	1.83E-05	1.82E-05	1.72E-05	1.81E-06	1.04E-06
loperamide 10x A-B	3.27E-05	2.80E-05		3.04E-05	3.28E-06	1.89E-06
loperamide 10x B-A	2.66E-05	2.06E-05		2.36E-05	4.23E-06	2.44E-06

Table A4.27: Average Exact Permeability (Pexact) of test drugs in Transwell model of Horse BBB for drug transport studies in three replicates at 30 minutes time point

Drug	Rep 1	Rep 2	Rep 3	Average	SD	SEM
camptothecin A-B	0.000107	9.22E-05	6.72E-05	8.89E-05	2.03E-05	1.17E-05
camptothecin B-A	4.96E-05	5E-05	1.76E-05	3.91E-05	1.86E-05	1.07E-05
chlorpromazine A-B	0.000355	0.000383	0.000435	3.91E-04	4.07E-05	2.35E-05
chlorpromazine B-A	9.77E-05	0.000117	0.000103	1.06E-04	1.01E-05	5.84E-06
loperamide A-B	0.000163	9.91E-05	0.000149	1.37E-04	3.37E-05	1.95E-05
loperamide B-A	4.23E-05	0.000112	2.42E-05	5.96E-05	4.64E-05	2.68E-05
etoposide A-B	6.55E-05	0.000102	0.000111	9.30E-05	2.43E-05	1.4E-05
etoposide B-A	4.67E-05	4.95E-05	2.69E-05	4.10E-05	1.23E-05	7.12E-06
lamotrigine A-B	8.58E-05	3.42E-05	3.22E-05	5.07E-05	3.04E-05	1.75E-05
lamotrigine B-A	4.64E-05	4.95E-05	2.49E-05	4.03E-05	1.34E-05	7.75E-06
methotrexate A-B	3.02E-05	3.05E-05	6.06E-06	2.23E-05	1.4E-05	8.1E-06
methotrexate B-A	3.67E-05	3E-05	9.22E-06	2.53E-05	1.43E-05	8.28E-06
topiramate A-B	8.04E-06	6.69E-07	8.44E-05	3.10E-05	4.63E-05	2.68E-05
topiramate B-A	1.15E-07	1.9E-07	0.000275	9.18E-05	0.000159	9.17E-05
mitoxantrone A-B	0.000188	0.000222	0.000143	1.84E-04	3.97E-05	2.29E-05
mitoxantrone B-A	3.37E-05	7.6E-05	5.03E-05	5.33E-05	2.13E-05	1.23E-05
loperamide 10x A-B	5.39E-05	3.09E-05		4.24E-05	1.63E-05	9.39E-06
loperamide 10x B-A	8.42E-05	1.26E-05		4.84E-05	5.06E-05	2.92E-05

Table A4.28: Average Exact Permeability (Pexact) of test drugs in Transwell model of Horse BBB for drug transport studies in three replicates at 60 minutes time point

Drug	Rep 1	Rep 2	Rep 3	Average	SD	SEM
camptothecin A-B	4.79E-05	3.69E-05	3.77E-05	4.09E-05	6.14E-06	3.54E-06
camptothecin B-A	2.52E-05	1.42E-05	2.65E-05	2.20E-05	6.79E-06	3.92E-06
chlorpromazine A-B	1.89E-04	2.19E-04	1.73E-04	1.93E-04	2.31E-05	1.34E-05
chlorpromazine B-A	5.49E-05	4.75E-05	4.67E-05	4.97E-05	4.5E-06	2.6E-06
loperamide A-B	9.40E-05	9.39E-05	5.81E-05	8.20E-05	2.07E-05	1.2E-05
loperamide B-A	2.49E-05	1.63E-05	1.87E-05	2.00E-05	4.44E-06	2.56E-06
etoposide A-B	3.79E-05	5.74E-05	6.56E-05	5.36E-05	1.42E-05	8.2E-06
etoposide B-A	5.86E-05	1.80E-05	3.49E-05	3.72E-05	2.04E-05	1.18E-05
lamotrigine A-B	3.77E-05	3.95E-05	3.44E-05	3.72E-05	2.6E-06	1.5E-06
lamotrigine B-A	4.72E-05	2.53E-05	5.26E-05	4.17E-05	1.45E-05	8.35E-06
methotrexate A-B	2.39E-05	6.14E-06	1.21E-05	1.40E-05	9.02E-06	5.21E-06
methotrexate B-A	4.44E-05	5.48E-06	1.15E-05	2.05E-05	2.1E-05	1.21E-05
topiramate A-B	1.36E-06	8.27E-05		4.20E-05	5.75E-05	3.32E-05
topiramate B-A	1.07E-06	8.24E-08	2.58E-07	4.70E-07	5.26E-07	3.04E-07
mitoxantrone A-B	1.17E-04	8.43E-05	1.04E-04	1.02E-04	1.66E-05	9.57E-06
mitoxantrone B-A	3.08E-05	2.42E-05	3.17E-05	2.89E-05	4.08E-06	2.36E-06
loperamide 10x A-B	2.43E-05	5.16E-05		3.79E-05	1.93E-05	1.12E-05
loperamide 10x B-A	2.15E-05	3.57E-05		2.86E-05	1E-05	5.79E-06

Table A4.29: Average Exact Permeability (Pexact) of test drugs in Transwell model of Horse BBB for drug transport studies in three replicates at 120 minutes time point

Drug	Rep 1	Rep 2	Rep 3	Average	SD	SEM
camptothecin A-B	2.66E-05	3.78E-05	3.25E-05	3.23E-05	5.56E-06	3.21E-06
camptothecin B-A	1.70E-05	2.69E-05	2.97E-05	2.45E-05	6.66E-06	3.84E-06
chlorpromazine A-B	1.21E-04	1.09E-04	8.79E-05	1.06E-04	1.68E-05	9.72E-06
chlorpromazine B-A	3.01E-05	3.58E-05	2.78E-05	3.12E-05	4.12E-06	2.38E-06
loperamide A-B	6.74E-05	3.82E-05	2.47E-05	4.34E-05	2.18E-05	1.26E-05
loperamide B-A	2.03E-05	1.65E-05	2.07E-05	1.92E-05	2.32E-06	1.34E-06
etoposide A-B	1.73E-05	2.69E-05	3.36E-05	2.60E-05	8.21E-06	4.74E-06
etoposide B-A	1.88E-05	3.08E-05	2.95E-05	2.64E-05	6.57E-06	3.79E-06
lamotrigine A-B	4.82E-05	3.96E-05	3.20E-05	3.99E-05	8.12E-06	4.69E-06
lamotrigine B-A	7.83E-05	3.37E-05	3.76E-05	4.99E-05	2.47E-05	1.43E-05
methotrexate A-B	1.46E-05	1.28E-05	2.33E-05	1.69E-05	5.64E-06	3.26E-06
methotrexate B-A	1.25E-05	3.05E-05	1.79E-05	2.03E-05	9.26E-06	5.35E-06
topiramate A-B	1.40E-07	3.14E-05	2.64E-07	1.06E-05	1.8E-05	1.04E-05
topiramate B-A	1.97E-06	8.87E-06	2.14E-05	1.08E-05	9.86E-06	5.69E-06
mitoxantrone A-B	5.13E-05	5.75E-05	6.57E-05	5.81E-05	7.23E-06	4.18E-06
mitoxantrone B-A	2.02E-05	1.88E-05	1.13E-05	1.68E-05	4.82E-06	2.78E-06
loperamide 10x A-B	3.99E-05	3.39E-05		3.69E-05	4.29E-06	2.47E-06
loperamide 10x B-A	4.94E-05	4.38E-05		4.66E-05	3.95E-06	2.28E-06

Table A4.30: Papp Efflux Ratio of test drugs in Transwell model of Horse BBB for drug transport studies in three replicates at 30 minutes time point

Drug	Rep 1	Rep 2	Rep 3	Average	SD	SEM
camptothecin	0.445903	0.440709	0.196575	0.3611	0.14247	0.0823
chlorpromazine	0.178101	0.185733	0.165386	0.1764	0.01028	0.0059
loperamide	0.224685	0.556662	0.192295	0.3245	0.20167	0.1164
etoposide	0.579561	0.425877	0.206465	0.404	0.18751	0.1083
lamotrigine	0.790226	1.608917	0.940431	1.1132	0.43583	0.2516
methotrexate	0.927276	1.129884	1.634631	1.2306	0.36427	0.2103
topiramate	0.016835	0.166667	1.547823	0.5771	0.84399	0.4873
mitoxantrone	0.179933	0.166385	0.161164	0.1692	0.00969	0.0056
loperamide 10x	1.448885	0.543751		0.9963	0.64003	0.3695

Table A4.31: Papp Efflux Ratio of test drugs in Transwell model of Horse BBB for drug transport studies in three replicates at 60 minutes time point

Drug	Rep 1	Rep 2	Rep 3	Average	SD	SEM
camptothecin	0.663979	0.265222	0.498954	0.4761	0.20036	0.1157
chlorpromazine	0.184019	0.181151	0.174618	0.1799	0.00482	0.0028
loperamide	0.269479	0.266721	0.416043	0.3174	0.08543	0.0493
etoposide	0.880491	0.301629	0.395172	0.5258	0.31074	0.1794
lamotrigine	1.357957	0.908962	1.107301	1.1247	0.22501	0.1299
methotrexate	1.317962	1.249564	0.603122	1.0569	0.39445	0.2277
topiramate	0.166667	0.166667	0.000462	0.1113	0.09596	0.0554
mitoxantrone	0.177243	0.170858	0.16076	0.1696	0.00831	0.0048
loperamide 10x	1.447753	0.636452		1.0421	0.57368	0.3312

Table A4.32: Papp Efflux Ratio of test drugs in Transwell model of Horse BBB for drug transport studies in three replicates at 120 minutes time point

Drug	Rep 1	Rep 2	Rep 3	Average	SD	SEM
camptothecin	0.560317	0.5832	0.680191	0.6079	0.06364	0.0367
chlorpromazine	0.167963	0.211513	0.218297	0.1993	0.02731	0.0158
loperamide	0.356948	0.58249	0.746354	0.5619	0.19552	0.1129
etoposide	1.057398	0.714796	0.496603	0.7563	0.28269	0.1632
lamotrigine	1.099859	1.0967	1.039859	1.0788	0.03377	0.0195
methotrexate	0.750528	2.858495	0.993608	1.5342	1.15329	0.6659
topiramate	0.166667	0.736488	70.41333	23.772	40.3934	23.321
mitoxantrone	0.155775	0.166241	0.171279	0.1644	0.00791	0.0046
loperamide 10x	0.81408	0.735288		0.7747	0.05571	0.0322

Table A4.33: Pexact Efflux Ratio of test drugs in Transwell model of Horse BBB for drug transport studies in three replicates at 30 minutes time point

Drug	Rep 1	Rep 2	Rep 3	Average	SD	SEM
camptothecin	0.461916	0.542822	0.262544	0.42243	0.144252	0.083284
chlorpromazine	0.275356	0.305904	0.236196	0.27249	0.034943	0.020174
loperamide	0.259069	1.131577	0.162585	0.51774	0.53378	0.308178
etoposide	0.712841	0.484756	0.241537	0.47971	0.235693	0.136077
lamotrigine	0.541375	1.446812	0.773706	0.92063	0.47026	0.271505
methotrexate	1.217541	0.983455	1.52054	1.24051	0.269279	0.155468
topiramate	0.014296	0.283292	3.261009	1.1862	1.801865	1.040307
mitoxantrone	0.179383	0.342662	0.352646	0.29156	0.097279	0.056164
loperamide 10x	1.563337	0.408758		0.98605	0.81641	0.471355

Table A4.34: Pexact Efflux Ratio of test drugs in Transwell model of Horse BBB for drug transport studies in three replicates at 60 minutes time point

Drug	Rep 1	Rep 2	Rep 3	Average	SD	SEM
camptothecin	0.525932	0.383877	0.703285	0.5377	0.160029	0.092393
chlorpromazine	0.290734	0.21742	0.269984	0.25938	0.03779	0.021818
loperamide	0.265081	0.173696	0.32243	0.25374	0.075013	0.043309
etoposide	1.545529	0.313606	0.531866	0.797	0.657366	0.379531
lamotrigine	1.250049	0.641077	1.531613	1.14091	0.455188	0.262803
methotrexate	1.861266	0.892595	0.949124	1.23433	0.543679	0.313893
topiramate	0.786135	0.003118		0.39463	0.553676	0.319665
mitoxantrone	0.263058	0.287189	0.303751	0.28467	0.020464	0.011815
loperamide 10x	0.886307	0.691809		0.78906	0.137531	0.079404

Table A4.35: Pexact Efflux Ratio of test drugs in Transwell model of Horse BBB for drug transport studies in three replicates at 120 minutes time point

Drug	Rep 1	Rep 2	Rep 3	Average	SD	SEM
camptothecin	0.639471	0.711962	0.915263	0.75557	0.142973	0.082546
chlorpromazine	0.24858	0.328045	0.316366	0.29766	0.042907	0.024772
loperamide	0.301614	0.431565	0.838795	0.52399	0.280264	0.16181
etoposide	1.088126	1.145738	0.876649	1.03684	0.141687	0.081803
lamotrigine	1.625197	0.850002	1.17595	1.21705	0.389228	0.224721
methotrexate	0.853659	2.392788	0.767233	1.33789	0.914587	0.528037
topiramate	14.08508	0.282562	81.06788	31.8118	43.21163	24.94825
mitoxantrone	0.394973	0.327071	0.171718	0.29792	0.114446	0.066076
loperamide 10x	1.236609	1.293135		1.26487	0.03997	0.023077

Appendix 5

Table A5.1: Apparent permeability (P_{app}) values of drug compounds from the no cell control studies in apical-to-basal (A-B) and basal-to-apical (B-A) directions carried out on transwell plates at 30-minute, 60 minute and 120 minute time points (values are reported as x 10^{-6}).

S. no.	Compound	Apparent Permeability (P_{app}) (cm/s)		
		30 minutes	60 minutes	120 minutes
1.	loperamide A-B	3.84 ± 0.38	4.44 ± 1.09	3.34 ± 0.31
2.	loperamide B-A	1.37 ± 0.15[a]	1.41 ± 0.25[a]	2.75 ± 0.32[b]
3.	chlorpromazine A-B	18.80 ± 1.44	17.60 ± 2.63	14.00 ± 1.19
4.	chlorpromazine B-A	6.09 ± 0.44[a]	4.87 ± 0.41[a]	9.97 ± 0.77[b]
5.	lamotrigine A-B	17.70 ± 6.78	25.20 ± 2.10	23.40 ± 1.64
6.	lamotrigine B-A	37.30 ± 3.00[a]	29.20 ± 1.49[b]	27.70 ± 1.28[b]
7.	topiramate A-B	20.00 ± 2.58[a]	11.10 ± 0.48[b]	15.00 ± 0.75[a,b]
8.	topiramate B-A	22.00 ± 1.15[a]	11.50 ± 0.627[b]	13.70 ± 0.51[b]
9.	mitoxantrone A-B	6.68 ± 0.89	4.62 ± 2.35	2.50 ± 0.79
10.	mitoxantrone B-A	2.13 ± 1.05	0.73 ± 0.20	0.46 ± 0.11
11.	camptothecin A-B	40.00 ± 2.49[a]	33.00 ± 5.94[a,b]	23.90 ± 2.38[b]
12.	camptothecin B-A	23.10 ± 2.65[a]	15.60 ± 0.80[b]	16.90 ± 1.55[a,b]
13.	methotrexate A-B	17.90 ± 2.00	18.70 ± 0.91	13.90 ± 0.78
14.	methotrexate B-A	18.60 ± 1.38[a]	16.10 ± 0.76[a,b]	13.40 ± 0.72[b]
15.	etoposide A-B	104.00 ± 6.90[a]	53.70 ± 3.17[b]	37.30 ± 2.29[b]
16.	etoposide B-A	30.10 ± 2.74[a]	16.00 ± 1.01[b]	16.10 ± 0.74[b]

Data shown are mean ± SEM for n=6 replicates for each drug and time point.Six replicates mean six different wells were used. Values bearing different superscript in a row differ significantly (P<0.05) in one-way ANOVA followed by Tukey's multiple comparison post-hoc test. Further Apparent permeability calculations and concentrations of no cell control studies can be found in detail in Appendix 3.

Table A5.2: Exact permeability (P_{exact}) of drug compounds from the no cell control studies in A-B and B-A directions conducted on transwell plates at 30, 60 and 120 minutes (values are reported as x 10^{-6}).

S. no.	Compound	Exact Permeability (P_{exact}) (cm/s)		
		30 minutes	**60 minutes**	**120 minutes**
1.	loperamide A-B	3.33 ± 0.63	3.21 ± 0.53	4.54 ± 0.56
2.	loperamide B-A	0.56 ± 0.05[a]	0.64 ± 0.07[a]	1.46 ± 0.15[b]
3.	chlorpromazine A-B	4.95 ± 0.30	4.63 ± 0.70	5.56 ± 0.52
4.	chlorpromazine B-A	0.79 ± 0.07[a]	0.72 ± 0.05[a]	1.72 ± 0.10[b]
5.	lamotrigine A-B	10.50 ± 3.90[a]	21.10 ± 2.70[a,b]	23.10 ± 1.66[b]
6.	lamotrigine B-A	25.10 ± 2.90	27.40 ± 1.64	31.60 ± 4.26
7.	topiramate A-B	17.50 ± 2.76	18.80 ± 1.62	22.40 ± 1.51
8.	topiramate B-A	20.30 ± 2.15	21.60 ± 0.90	22.10 ± 2.32
9.	mitoxantrone A-B	4.76 ± 1.00	4.78 ± 2.01	5.07 ± 1.81
10.	mitoxantrone B-A	2.16 ± 1.14	0.94 ± 0.31	0.56 ± 0.12
11.	camptothecin A-B	36.30 ± 2.46	33.70 ± 5.94	28.20 ± 2.62
12.	camptothecin B-A	29.20 ± 3.67	20.30 ± 3.11	28.50 ± 3.42
13.	methotrexate A-B	14.30 ± 1.89	15.40 ± 1.30	17.40 ± 1.20
14.	methotrexate B-A	19.90 ± 2.01	17.90 ± 9.98	19.60 ± 1.50
15.	etoposide A-B	79.40 ± 5.34[a]	49.10 ± 2.91[b]	33.20 ± 0.62[c]
16.	etoposide B-A	24.60 ± 3.86	16.00 ± 1.64	15.60 ± 2.02

Data shown are mean ± SEM for n=6 replicates for each drug and time point. Six replicates mean six different wells were used. Values bearing different superscript in a row differ significantly (P<0.05) in one-way ANOVA followed by Tukey's multiple comparison post-hoc test. Further Exact permeability calculations and concentrations of no cell control studies can be found in detail in Appendix 3.

Table A5.3: Efflux ratio from apparent permeability (P_{app}) of selected test drugs from the no cell control studies in A-B and B-A directions conducted on transwell plates at 30, 60 and 120 minutes.

S.no.	Compound	P_{app} Efflux ratio (B-A/A-B)		
		30 minutes	**60 minutes**	**120 minutes**
1.	loperamide	0.358 ± 0.026^{a}	0.357 ± 0.057^{a}	0.836 ± 0.098^{b}
2.	chlorpromazine	0.330 ± 0.028^{a}	0.297 ± 0.035^{a}	0.724 ± 0.054^{b}
3.	lamotrigine	10.664 ± 5.664	1.221 ± 0.153	1.220 ± 0.119
4.	topiramate	1.196 ± 0.173	1.048 ± 0.079	0.922 ± 0.035
5.	mitoxantrone	0.296 ± 0.119	0.502 ± 0.200	0.225 ± 0.047
6.	camptothecin	0.579 ± 0.061	0.527 ± 0.064	0.731 ± 0.079
7.	methotrexate	1.074 ± 0.078	0.870 ± 0.060	0.980 ± 0.095
8.	etoposide	0.299 ± 0.038	0.307 ± 0.037	0.446 ± 0.050

Data shown are mean ± SEM for n=6 replicates for each drug and time point. Six replicates mean six different wells were used. Values bearing different superscript in a row differ significantly (P<0.05) in one-way ANOVA followed by Tukey's multiple comparison post-hoc test. Further Efflux ratio from apparent permeability (P_{app}) calculations of no cell control studies can be found in detail in Appendix 3.

Table A5.4: Efflux ratio from Exact permeability (P_{exact}) of selected test drugs from the no cell control studies in A-B and B-A directions conducted on transwell plates at 30-minute, 60 minute and 120-minute time points.

S. no.	Compound	P_{exact} Efflux ratio (B-A/A-B)		
		30 minutes	60 minutes	120 minutes
1	loperamide	0.203 ± 0.043	0.222 ± 0.039	0.352 ± 0.063
2.	chlorpromazine	0.162 ± 0.018[a]	0.1690 ± 0.023[a]	0.323 ± 0.036[b]
3.	lamotrigine	11.597 ± 6.978	1.445 ± 0.238	1.397 ± 0.199
4.	topiramate	1.304 ± 0.264	1.194 ± 0.124	0.998 ± 0.096
5.	mitoxantrone	0.383 ± 0.122	0.497 ± 0.200	0.140 ± 0.023
6.	camptothecin	0.808 ± 0.100	0.775 ± 0.075	1.062 ± 0.165
7.	methotrexate	1.451 ± 0.137	1.198 ± 0.107	1.161 ± 0.130
8.	etoposide	0.311 ± 0.047	0.326 ± 0.029	0.473 ± 0.063

Data shown are mean ± SEM for n=6 replicates for each drug and time point. Six replicates mean six different wells were used. Values bearing different superscript in a row differ significantly ($P<0.05$) in one-way ANOVA followed by Tukey's multiple comparison post-hoc test. Further Efflux ratio from Exact permeability (P_{exact}) calculations of no cell control studies can be found in detail in Appendix 3.

Table A5.5: Apparent permeability (P_{app}) of individual selected test drugs from drug transport studies in A-B and B-A directions conducted on transwell model of horse BBB at 30-minute, 60 minute and 120-minute time points (values are reported as x 10^{-6}).

S. no.	Compound	Apparent Permeability (P_{app}) (cm/s)		
		30 minutes	60 minutes	120 minutes
1.	loperamide A-B	189.00 ± 25.60[a]	104.00 ± 15.30[b]	66.30 ± 13.40[b]
2.	loperamide B-A	65.40 ± 29.30	31.70 ± 1.79	34.50 ± 4.66
3.	chlorpromazine A-B	487.00 ± 13.10[a]	257.00 ± 20.40[b]	132.00 ± 18.80[c]
4.	chlorpromazine B-A	85.80 ± 0.67[a]	46.40 ± 4.35[b]	25.70 ± 1.41[c]
5.	lamotrigine A-B	38.80 ± 11.80	27.70 ± 5.74	21.00 ± 2.28
6.	lamotrigine B-A	38.90 ± 6.37	32.50 ± 9.64	22.70 ± 2.30
7.	topiramate A-B	935.00 ± 928.00	112.00 ± 111.00	16.20 ± 16.10
8.	topiramate B-A	1440.00 ± 1440	0.08 ± 0.03	16.30 ± 10.40
9.	mitoxantrone A-B	429.00 ± 66.00[a]	198.00 ± 12.30[b]	104.00 ± 3.84[b]
10.	mitoxantrone B-A	72.90 ± 12.50[a]	33.70 ± 2.8[b]	17.20 ± 1.04[b]
11.	camptothecin A-B	85.30 ± 2.10	39.90 ± 4.11	28.20 ± 2.37
12.	camptothecin B-A	30.70 ± 6.92	19.90 ± 6.58	17.20 ± 1.95
13.	methotrexate A-B	25.20 ± 12.10	17.00 ± 7.34	11.30 ± 1.99
14.	methotrexate B-A	26.10 ± 10.10	18.10 ± 10.40	14.90 ± 3.64
15.	etoposide A-B	88.40 ± 21.80	46.60 ± 10.90	24.50 ± 7.89
16.	etoposide B-A	31.40 ± 3.49[a]	21.30 ± 3.53[a,b]	16.50 ± 2.47[b]
17.	loperamide 10x A-B	33.40 ± 7.70	29.50 ± 14.50	30.40 ± 1.89
18.	loperamide 10x B-A	37.60 ± 20.00	23.50 ± 5.32	23.60 ± 2.44

Data shown are mean ± SEM for n=3 replicates for each drug and time point. Three replicates mean three independent experiments were carried out with three different animals. Values bearing different superscript in a row differ significantly (P<0.05) in one-way ANOVA followed by Tukey's multiple comparison post-hoc test. Further Apparent permeability (P_{app}) calculations and concentrations of drug transport studies conducted on transwell model of horse BBB can be found in detail in Appendix 4.

Table A5.6: Exact permeability (P_{exact}) of individual selected test drugs from drug transport studies in A-B and B-A directions conducted on transwell model of horse BBB at 30-minute, 60 minute and 120-minute time points (values are reported as x 10^{-6}).

S. no.	Compound	Exact Permeability (P_{exact}) (cm/s)		
		30 minutes	60 minutes	120 minutes
1.	loperamide A-B	137.00 ± 19.50[a]	82.00 ± 12.00[a,b]	43.40 ± 12.60[b]
2.	loperamide B-A	59.60 ± 26.80	20.00 ± 2.56	19.20 ± 1.34
3.	chlorpromazine A-B	391.00 ± 23.50[a]	193.00 ± 13.40[b]	106.00 ± 9.72[c]
4.	chlorpromazine B-A	106.00 ± 5.84[a]	49.70 ± 2.6[b]	31.20 ± 2.38[c]
5.	lamotrigine A-B	50.70 ± 17.50	37.20 ± 1.50	39.90 ± 4.69
6.	lamotrigine B-A	40.30 ± 7.75	41.70 ± 8.35	49.90 ± 14.30
7.	topiramate A-B	31.00 ± 26.80	42.00 ± 33.20	10.60 ± 10.40
8.	topiramate B-A	91.80 ± 91.70	0.47 ± 0.30	10.80 ± 5.69
9.	mitoxantrone A-B	184.00 ± 22.90[a]	102.00 ± 9.57[b]	58.10 ± 4.18[b]
10.	mitoxantrone B-A	53.30 ± 12.30[a]	28.90 ± 2.36[a,b]	16.80 ± 2.78[b]
11.	camptothecin A-B	88.90 ± 11.70[a]	40.90 ± 3.54[b]	32.30 ± 3.21[b]
12.	camptothecin B-A	39.10 ± 10.70	22.00 ± 3.92	24.50 ± 3.84
13.	methotrexate A-B	22.30 ± 8.10	14.00 ± 5.21	16.90 ± 3.26
14.	methotrexate B-A	25.30 ± 8.28	20.50 ± 12.10	20.30 ± 5.35
15.	etoposide A-B	93.00 ± 14.00[a]	53.60 ± 8.20[a,b]	26.00 ± 4.74[b]
16.	etoposide B-A	41.00 ± 7.12	37.20 ± 11.80	26.40 ± 3.79
17.	loperamide 10x A-B	42.40 ± 9.39	37.90 ± 11.20	36.90 ± 2.47
18.	loperamide 10x B-A	48.40 ± 29.20	28.60 ± 5.79	46.60 ± 2.28

Data shown are mean ± SEM for n=3 replicates for each drug and time point. Three replicates mean three independent experiments were carried out with three different animals. Values bearing different superscript in a row differ significantly (P<0.05) in one-way ANOVA followed by Tukey's multiple comparison post-hoc test. Further Exact permeability (P_{exact}) calculations and concentrations of drug transport studies in A-B and B-A directions conducted on transwell model of horse BBB can be found in detail in Appendix 4.

Table A5.7: Efflux ratio from apparent permeability (P_{app}) of selected test drugs from drug transport studies in A-B and B-A directions conducted on transwell model of horse BBB at 30-minute, 60 minute and 120-minute time points.

S. no.	Compound	P_{app} Efflux ratio (B-A/A-B)		
		30 minutes	60 minutes	120 minutes
1.	loperamide	0.32 ± 0.12	0.32 ± 0.05	0.56 ± 0.11
2.	chlorpromazine	0.18 ± 0.01	0.18 ± 0.00	0.20 ± 0.02
3.	lamotrigine	1.11 ± 0.25	1.12 ± 0.13	1.08 ± 0.02
4.	topiramate	0.58 ± 0.49	0.11 ± 0.06	23.77 ± 23.32
5.	mitoxantrone	0.17 ± 0.01	0.17 ± 0.00	0.16 ± 0.00
6.	camptothecin	0.36 ± 0.08	0.48 ± 0.12	0.61 ± 0.04
7.	methotrexate	1.23 ± 0.21	1.06 ± 0.23	1.53 ± 0.67
8.	etoposide	0.40 ± 0.11	0.53 ± 0.18	0.76 ± 0.16
9.	loperamide 10x	1.00 ± 0.37	1.04 ± 0.33	0.77 ± 0.03

Data shown are mean ± SEM for n=3 replicates for each drug and time point. Three replicates mean three independent experiments were carried out with three different animals. Values bearing different superscript in a row differ significantly (P<0.05) in one-way ANOVA followed by Tukey's multiple comparison post-hoc test. Further Efflux ratio from apparent permeability (P_{app}) calculations of drug transport studies conducted on transwell model of horse BBB can be found in detail in Appendix 4.

Table A5.8: Efflux ratio from Exact permeability (P_{exact}) of selected test from drug transport studies in A-B and B-A directions conducted on transwell model of horse BBB at 30, 60 and 120 minutes.

S. no.	Compound	P_{exact} Efflux ratio (B-A/A-B)		
		30 minutes	60 minutes	120 minutes
1	loperamide	0.52 ± 0.31	0.25 ± 0.04	0.52 ± 0.16
2.	chlorpromazine	0.27 ± 0.02	0.26 ± 0.02	0.30 ± 0.02
3.	lamotrigine	0.92 ± 0.27	1.14 ± 0.26	1.22 ± 0.22
4.	topiramate	1.19 ± 1.04	0.39 ± 0.32	31.8 ± 24.9
5.	mitoxantrone	0.29 ± 0.06	0.28 ± 0.01	0.30 ± 0.07
6.	camptothecin	0.42 ± 0.08	0.54 ± 0.09	0.76 ± 0.08
7.	methotrexate	1.24 ± 0.16	1.23 ± 0.31	1.34 ± 0.53
8.	etoposide	0.48 ± 0.14	0.80 ± 0.38	1.04 ± 0.08
9.	loperamide 10x	0.99 ± 0.47	0.79 ± 0.08	1.26 ± 0.02

Data shown are mean ± SEM for n=3 replicates for each drug and time point. Three replicates mean three independent experiments were carried out with three different animals. Values bearing same superscript in a row do not differ significantly (P<0.05) in one-way ANOVA followed by Tukey's multiple comparison post-hoc test. Further Efflux ratio from Exact permeability (P_{exact}) calculations of drug transport studies conducted on transwell model of horse BBB can be found in detail in Appendix 4.